2014-03-28

FUS/TLS in Stress Response - Implications for Amyotrophic Lateral Sclerosis: A Dissertation

Reddy Ranjith Kumar Sama
University of Massachusetts Medical School

FUS/TLS IN STRESS RESPONSE

– IMPLICATIONS FOR AMYOTROPHIC LATERAL SCLEROSIS

A Dissertation Presented

By

REDDY RANJITH KUMAR SAMA

Submitted to the faculty of the

University of Massachusetts Graduate School of Biomedical Sciences, Worcester

In partial fulfillment of the requirement for the degree of

DOCTOR OF PHILOSOPHY

March 28, 2014

CELL AND DEVELOPMENTAL BIOLOGY

FUS/TLS IN STRESS RESPONSE
– IMPLICATIONS FOR AMYOTROPHIC LATERAL SCLEROSIS

A Dissertation Presented
By
Reddy Ranjith Kumar Sama
The signatures of the Dissertation Defense Committee signify
Completion and approval as to style and content of the Dissertation

_____
Daryl A. Bosco, Ph.D., Thesis Advisor

_____
Melissa J. Moore, Ph.D., Member of Committee

_____
Robert H. Brown Jr., DPhil, MD, Member of Committee

_____
Jill Zitzewitz, Ph.D., Member of Committee

_____
Miguel Sena-Esteves, Ph.D., Member of Committee

_____
Jeffrey Agar, Ph.D., Member of Committee

The signature of the Chair of the Committee signifies that the written dissertation meets the requirements of the Dissertation Committee

_____
Lawrence J. Hayward, MD, Ph.D., Chair of Committee

The signature of the Dean of the Graduate School of Biomedical Sciences signifies that the student has met all graduation requirements of the School

_____
Anthony Carruthers, Ph.D.
Dean of the Graduate School of Biomedical Sciences

Cell and Developmental Biology
March 28, 2014

I WISH TO DEDICATE THIS THESIS TO MY PARENTS FOR ALL THEIR LOVE, SUPPORT AND INSPIRATION

ACKNOWLEDGMENTS

I would like to express my deepest gratitude to my thesis advisor Dr. Daryl Bosco. I would like to thank her for being my mentor and giving me an opportunity to work in her lab and learn to become an independent scientist. She has been a wonderful mentor throughout my time in her lab. She was extremely supportive and always encouraged me to try out my own ideas and yet ensured that I stayed on track and focused on my thesis research. She was available always and helped me out whenever needed. She is an extremely hard worker and had a great passion for science, which had always been a great motivation to me. As excellent a science mentor she was, she also always had some great advice regarding my career plans. Thank you, Daryl.

I would like to thank all the great scientists in my Thesis Research Committee – Dr. Lawrence Hayward, Dr. Melissa Moore, Dr. Jill Zitzewitz and Dr. Miguel Sena-Esteves. I was very fortunate to have you all on my committee providing me with valuable suggestions throughout my graduate studies. I greatly appreciate your time. I am extremely thankful to Dr. Robert H. Brown Jr. and Dr. Jeffrey Agar for being part of my Dissertation Exam Committee.

I would also like to acknowledge the help and guidance from Dr. Anthony Imbalzano who has been extremely helpful throughout my graduate school. I would like to thank Dr. Syed Noorwez, who was my initial mentor in research and continued to be my mentor and friend.

I am extremely fortunate to have worked with all the wonderful lab-mates, Catherine Ward, Melissa Rotunno, Laura Kaushansky, Sivakumar Boopathy, Dr. Desiree Barron, Dr. Kristin Boggio, Maeve Tischbein and Nathan Lemay. You have all been there for me when I needed you, helped with my experiments, provided valuable suggestions and input into my research. I am glad to have worked with such a wonderful group.

Finally, I would like to thank my family members who have been extremely supportive at all times. I am blessed to have such wonderful people in my life. Without their constant support and motivation, I would not have been able to achieve what I did.

ABSTRACT

Amyotrophic lateral sclerosis (ALS), also known as Lou Gehrig's disease is a fatal neurodegenerative disease. ALS is typically adult onset and is characterized by rapidly progressive loss of both upper and lower motor neurons that leads to death usually within 3-5 years. About 90% of all the cases are sporadic with no family history while the remaining 10% are familial cases with mutations in several genes including *SOD1, FUS/TLS, TDP43 and C9ORF72.*

FUS/TLS (Fused in Sarcoma/Translocated in Liposarcoma or FUS) is an RNA/DNA binding protein that is involved in multiple cellular functions including DNA damage repair, transcription, mRNA splicing, RNA transport and stress response. More than 40 mutations have now been identified in FUS that account for about 5% of all the familial cases of ALS. However, the exact mechanism by which FUS causes ALS is unknown. While significant progress has been made in understanding the disease mechanism and identifying therapeutic strategies, several questions still remain largely unknown. The work presented here aims at understanding the normal functions of FUS as well as the pathogenic mechanisms by which it leads to disease.

Several studies showed the association of mutant-FUS with structures made up of RNA and proteins, called stress granules that form under various stress conditions. However, little is known about the role of endogenous FUS under stress conditions. I have shown that under hyperosmolar conditions, the predominantly nuclear FUS translocates into the cytoplasm and incorporates into

stress granules. The response is specific to hyperosmolar stress because FUS remains nuclear under other stress conditions tested, such as oxidative stress, ER stress and heat shock. The response of FUS is rapid, and cells with reduced FUS levels are susceptible to the hyperosmolar stress, indicating a pro-survival role for FUS. In addition to investigating the functions of endogenous wild-type (WT) FUS, the work presented also focuses on identifying the pathogenic mechanism(s) of FUS variants. Using various biochemical techniques, I have shown that ALS-causing FUS variants are misfolded compared to the WT protein. Furthermore, in a squid axoplasm based vesicle motility assay, the FUS variants inhibit fast axonal transport (FAT) in a p38 MAPK dependent manner, indicating a role for the kinase in mutant-FUS mediated disease pathogenesis. Analysis of human ALS patient samples indicates higher levels of total and phospho p38, supporting the notion that aberrant regulation of p38 MAPK is involved in ALS.

The results presented in this dissertation 1) support a novel prosurvival role for FUS under hyperosmolar stress conditions and, 2) demonstrate that protein misfolding and aberrant kinase activation contribute to ALS pathogenesis by FUS variants.

TABLE OF CONTENTS

LIST OF TABLES

Chapter I

Chapter III

LIST OF FIGURES

Chapter III

Chapter IV

LIST OF THIRD PARTY COPYRIGHTED MATERIAL

The following chapter was reproduced from Journals

	Publisher	License number
Chapter II	John Wiley and Sons	3335921094006

The following appendices were reproduced from journals: No permission required

	Publisher
Appendix I	American Society for Biochemistry and Molecular Biology
Appendix II	BioMed Central

LIST OF ABBREVIATIONS

AdOx – Adenosine-2', 3'-dialdehyde

ALS – Amyotrophic lateral sclerosis

APC – Adenomatous polyposis coli

BMAA – β- methylamino-L-alanine

CLIP-seq – Crosslinking immunoprecipitation-high-throughput sequencing

EMSA – Electrophoretic mobility shift assays

ER – Endoplasmic reticulum

EWS – Ewing sarcoma

fALS – Familial amyotrophic lateral sclerosis

FAT – Fast axonal transport

FET – FUS, EWS, TAF15

FTD or FTLD – Frontotemporal lobar degeneration

FUS or FUS/TLS – Fused in sarcoma/Translocated in liposarcoma

G-rich – Glycine-rich

G3BP – GTPase activating protein (SH3 domain) binding protein 1

HITS-CLIP – High-throughput sequencing of RNA isolated by crosslinking immunoprecipitation

hnRNP – Heterogeneous ribonuclear protein

iCLIP – individual-nucleotide resolution crosslinking and immunoprecipitation

LMN – Lower motor neuron

MAPK – Mitogen-activated protein kinase

MLS – Myxoid liposarcomas

ND1 – NADH dehydrogenase 1

NLS – Nuclear localization signal

NSC – Neuroblastoma x spinal cord hybrid

ORE – Osmotic response element

PAR-CLIP – Photoactivatable ribonucleoside-enhanced crosslinking and immunoprecipitation

PFN1 – Profilin 1

PRMT – Protein methyl arginine transferase

QGSY-rich – Glutamine-glycine-serine-tyrosine-rich

RIP-Chip – RNA-binding protein immunopurification-microarray

RRM – RNA recognition motif

RGG – Arginine-glycine-glycine

sALS – Sporadic amyotrophic lateral sclerosis

SARFH – Sarcoma-associated RNA-binding fly homolog

SDS-PAGE – Sodium dodecyl sulfate – Polyacrylamide gel electrophoresis

SEC – Size exclusion chromatography

SELEX – Systematic evolution of ligands by exponential enrichment

SOD1 – Cu/Zn superoxide dismutase 1

SYGQ – Serine-tyrosine-glycine-glutamine

TAF15 or TAFII68 – TATA box binding protein associated factor 68 kDa

TARDP or TDP43 – Transactive response DNA binding protein 43

TET – TLS, EWS, TAF15

TFA – Tryptophan fluorescence anisotropy

TIAR – TIA1-related protein

TonE – Tonicity enhancer

Trp – Tryptophan

TRP – Transient receptor potential

UMN – Upper motor neuron

ZFD – Zinc-finger domain

PREFACE

Parts of this dissertation will appear in:

Functions of FUS/TLS from DNA repair to stress response: implications for ALS.

Sama RRK*, Ward CL*, Bosco DA (*Co-first authors)

Parts of this dissertation appeared in:

FUS/TLS assembles into stress granules and is a prosurvival factor during hyperosmolar stress. 2013. *J Cell Physiol* 228:2222-2231. Sama RRK, Ward CL, Kaushansky LJ, Lemay N, Ishigaki S, Urano F, Bosco DA

CHAPTER I

INTRODUCTION

AMYOTROPHIC LATERAL SCLEROSIS

Amyotrophic lateral sclerosis (ALS), also known as Lou Gehrig's disease, is a fatal neurodegenerative disease that primarily affects the upper and lower motor neurons of the brain and spinal cord. Typically an adult onset disease, ALS progresses very rapidly and leads to the death usually within 3-5 years after onset. Even though the disease has been known for over 100 years, there is not a complete understanding of this complex disease nor is there an effective treatment or cure.

SIGNS AND SYMPTOMS

Diseases affecting the motor neurons are often referred to as motor neuron diseases (MNDs) and include diseases such as ALS, progressive bulbar palsy, pseudobulbar palsy, primary lateral sclerosis, spinal muscular atrophy and post-polio syndrome (NINDS, 2013). ALS affects both upper and lower motor neurons while most other MNDs are restricted to either upper or lower motor neurons (NINDS, 2013). Even though descriptions of ALS-like symptoms were reported early in the 19th century (Rowland, 2001), Jean-Martin Charcot, also known as the father of modern neurology, is often credited for first identifying and using the term "amyotrophic lateral sclerosis" to describe the disease in 1874 (Goetz, 2000; Rowland, 2001). Correlating autopsy pathology with clinical

symptoms, Charcot provided evidence for the degeneration of both upper motor neurons (UMN) and lower motor neurons (LMN) (Goetz, 2000; Rowland, 2001). The clinical symptoms of UMN degeneration include spasticity (muscle stiffness) and hyperreflexia (exaggerated reflexes) while that of LMN degeneration includes fasciculation (muscle twitching), cramps, muscle atrophy and weakness (Gordon, 2013; NINDS, 2013). Symptoms are first presented in only one particular group of muscles. For limb-onset ALS this would be either the arms or legs and for bulbar-onset ALS, muscles that control speech and swallowing. About two-thirds of the patients present limb-onset ALS, that often starts in one of the limbs, and then progresses very rapidly to other limbs and the rest of the body (Gordon, 2013). Some of the early symptoms include loss of dexterity, weakness and difficulty using the arms or legs. As the disease progresses, the patients lose the ability to move arms or walk (Gordon, 2013). On the other hand, in bulbar-onset ALS, which is observed in 20-30% of the patients, dysphagia (difficulty with swallowing) and dysarthria (difficulty with speech) are the most common symptoms (Gordon, 2013). Bulbar-onset ALS appears to have a worse prognosis, including shorter survival period, compared to limb-onset form of the disease (Chio *et al.*, 2002; Magnus *et al.*, 2002; del Aguila *et al.*, 2003). Irrespective of the site of onset of the disease, during late stages of the disease, a combination of both UMN and LMN degeneration symptoms appear that ultimately culminates in death of the patient mostly likely due to respiratory and other cardio-pulmonary complications (Silani *et al.*, 2011).

DIAGNOSIS AND TREATMENT

The absence of a single confirmatory clinical test or reliable biomarker makes it challenging to diagnose ALS. The current diagnosis procedure relies on confirming LMN and UMN manifestations as well as excluding ALS-like diseases. Thus the current diagnosis involves not only a careful examination of the patient for motor neuron symptoms, but also includes a long list of tests to eliminate the ALS-mimicking diseases (Silani *et al.*, 2011). The "El Escorial criteria" (Brooks, 1994; Brooks *et al.*, 2000), developed by the World Federation of Neurology, have been formulated to assist in the diagnosis process and for research study/trial classification of ALS patients. The criterion depends on the number of regions (bulbar, cervical, thoracic, lumbosacral) affected and classifies patients into categories that include "clinically probable" to "clinically definite". Despite the criteria and clinical advancements, the diagnosis often takes a long time, in some cases up to a year (Silani *et al.*, 2011). Unfortunately, even after a definitive diagnosis there is no cure for this disease. Much of the attention is thus placed on managing the disease and prolonging life while trying to mitigate the symptoms as much as possible. Patients are often treated with Riluzole, the only treatment approved by US Food and Drug Administration (FDA) for ALS despite only being able to increase lifespan marginally – on the order of a few months (Zoccolella *et al.*, 2007; Miller *et al.*, 2012).

EPIDEMIOLOGY

About 5,000 people are diagnosed with ALS each year in the US and there are about 20,000-30,000 people currently living with ALS in the US (NINDS, 2013). ALS is the most common neuromuscular disease and affects people throughout the world. Several studies have aimed at identifying the risk factors for ALS; however, most of these had weak findings and were often inconclusive and contradictory. Some of the major risk factors that have been investigated over the years are highlighted below:

Gender – Several earlier studies reported nearly two-fold higher incidence rates in males compared to females although recent studies point toward indifference in gender based incidence rates (Logroscino *et al.*, 2008).

Ethnicity/race – Caucasian populations have been associated with higher incidence rates than Asian populations (Cronin *et al.*, 2007). In the US, the incidence rates are lower in African-American and Hispanic populations than non-Hispanic Caucasians (Cronin *et al.*, 2007).

Geographical location and diet – ALS-like symptoms have been reported at a higher incidence rate among the Chamorro people of Guam and other Mariana islands (Papapetropoulos, 2007; Karamyan and Speth, 2008). The high incidence was later attributed, albeit without conclusive evidence, to β-methylamino-L-alanine (BMAA) which was present in cycad seeds that are part of the dietary intake in those regions (Papapetropoulos, 2007; Karamyan and Speth, 2008). Dietary products in general have not been found as strong risk

factors for developing ALS. Other than BMAA, one study showed an inverse relation with chicken consumption; higher chicken consumption is associated with lower risk of ALS (Morozova *et al.*, 2008).

Alcohol consumption and smoking – While alcohol consumption is associated with lower risk of ALS (de Jong *et al.*, 2012), cigarette smoking is often associated with higher risk of developing ALS (Wang *et al.*, 2011; de Jong *et al.*, 2012).

Physical activity and sports – It has been suspected that people involved in high intensity physical activities, such as sports, are at higher risk for developing ALS; however, the findings from several studies have been inconsistent and need further validation (Veldink *et al.*, 2005; Chio *et al.*, 2009; Beghi *et al.*, 2010). One study found a significant increase in risk of ALS in Italian professional football players, although the increased risk has been attributed to not only football related activities, such as heading the ball (Piazza *et al.*, 2004), but also to the use of performance enhancing drugs (Belli and Vanacore, 2005) and exposure to pesticides on the field (Chio *et al.*, 2005).

Exposure to toxins – Exposure to toxic chemicals during activities that might be related to agriculture, sports and/or war, has been suspected to increase the risk of ALS (Trojsi *et al.*, 2013).

Gulf war veterans – US veterans who served during Gulf war of 1991 had nearly twofold higher risk of ALS (Horner *et al.*, 2003; Coffman *et al.*, 2005). The exact reason for this increased risk is unclear, but exposure to cyanobacteria, BMAA or

other toxins has been suggested as a possible reason (Spencer *et al.*, 1998; Cox *et al.*, 2009). However, even non-deployed soldiers had similar rates of ALS incidence (Kasarskis *et al.*, 2009)and the higher risk remained only during the decade following the war (Horner *et al.*, 2008).

FAMILIAL ALS

About 10% of all the ALS cases have a family history of the disease and are categorized as familial ALS (fALS). The first ALS-causing mutations were identified in the gene *Cu/Zn superoxide dismutase 1 (SOD1)* (Rosen *et al.*, 1993) and over 150 ALS-causing mutations have now been identified in *SOD1*. These mutations account for ~20% of the fALS cases. Mutations in several other genes including *FUS/TLS* (Kwiatkowski *et al.*, 2009; Vance *et al.*, 2009), *TARDP or TDP43* (Gitcho *et al.*, 2008; Kabashi *et al.*, 2008; Rutherford *et al.*, 2008; Sreedharan *et al.*, 2008; Van Deerlin *et al.*, 2008; Yokoseki *et al.*, 2008) and *PFN1* (Wu *et al.*, 2012), have also been linked to fALS and are all typically inherited in an autosomal dominant fashion (Gordon, 2013). More recently hexanucleotide repeat expansions of GGGGCC in *C9ORF72* have also been linked to fALS (DeJesus-Hernandez *et al.*, 2011; Renton *et al.*, 2011). All of these mutations combined, account for about 40-60% of all fALS cases. Thus, there is a huge interest in identifying the remaining ALS-causing genes. Much of the understanding about ALS has come from the studies of the genes involved in fALS. Histopathology studies show that the protein products of these genes are found in inclusions within the motor neurons and other cell types such as glia

(Gordon, 2013). In the case of *C9ORF72*, RNA foci containing the hexanucleotide repeat mRNA as well as inclusions that are positive for several proteins including TDP43 have been identified (Gendron *et al.*, 2014). Studies on these genes showed that several cellular pathways are perturbed. Protein misfolding/aggregation, oxidative stress, altered calcium metabolism, mitochondrial dysfunction, defective axonal transport, excitotoxicity, altered RNA processing and inflammation have all been implicated in various stages of disease etiology (Pasinelli and Brown, 2006; Gordon, 2013).

SPORADIC ALS

About 90% of all ALS cases have no evidence of family history and are thus categorized as sporadic ALS (sALS). Despite the majority of all ALS cases being sporadic, much less is known about this form of the disease. The clinical symptoms of both sporadic and familial forms of ALS are largely indistinguishable, indicative of converging pathways between these two forms of the disease. Supporting this notion, mutations in many fALS-associated genes, such as *SOD1, FUS* and *TDP43,* have been found in sALS patients (Renton *et al.*, 2014). The most common genetic cause of sALS is hexanucleotide repeat expansions in *C9ORF72* gene, with about 7% of all sporadic cases involving repeat expansions (Renton *et al.*, 2014). Despite all of these findings, only ~11% of all the sALS cases are accounted for by means of genetic mutations. Interestingly, pathological inclusions in several of the sALS patients contain the fALS-linked protein TDP43 and in few cases SOD1 and FUS, despite the

absence of any genetic mutations in them (Neumann *et al.*, 2006; Deng *et al.*, 2010; Rotunno and Bosco, 2013). While protein misfolding has been implicated as the major reason for such association in inclusions, the precise mechanism or causal events are unclear.

SIMILARITY TO FTLD

Frontotemporal lobar degeneration (FTLD or FTD) is a group of pathologically and genetically heterogeneous neurodegenerative disorders that result in progressive damage to frontal and temporal lobes of the brain. Progressive loss of speech and behavior represent the hallmark characteristics of FTLD. About 50% of all cases are familial with mutations in genes such as *MAPT* (Hutton *et al.*, 1998) and *PGRN* (Baker *et al.*, 2006; Cruts *et al.*, 2006). Although distinct from ALS, there is a strong overlap in diagnosis, pathology, and genetics of these two diseases that can affect the same family or even the same individual (Zago *et al.*, 2011). In fact, histological subtype classification of FTLD includes FTLD-TDP43 and FTLD-FUS, which are characterized by the inclusions positive for the respective proteins. While recent studies point toward a genetic link between ALS and FTLD by means of proteinaceous inclusions and mutations in genes such as *TDP43* (Lagier-Tourenne *et al.*, 2010; Mackenzie *et al.*, 2010), the repeat expansions of C9ORF72 represent the strongest genetic link between these two diseases (Hardy and Rogaeva, 2013). Thus, despite the same proteins being involved with both diseases, it is still unclear as to what exact factors dictate the occurrence of one disease versus the other.

FUS/TLS and the FET FAMILY

Mutations in FUS account for ~5% of the fALS cases. FUS belongs to the FET (previously TET) family of proteins that also includes EWS (Ewing Sarcoma), TAF15 (TATA box binding protein associated factor 68 kDa or TAFII68) and the Drosophila homolog SARFH (Law *et al.*, 2006; Tan and Manley, 2009). The proteins of this family contain several conserved domains including the N-terminal QGSY-rich region, a Glycine-rich region, an RNA-recognition motif (RRM), a zinc-binding domain and C-terminal RGG-rich domains (domain structure of FUS is shown in Fig. 1.1). The N-terminal transcriptional activation domain of FUS, EWS and TAF15 is found to be fused with the C-terminal DNA binding domains of many transcription factors in several sarcomas. The FET family proteins are ubiquitously expressed. They are predominantly localized in the nucleus; however, they shuttle between the nucleus and cytoplasm. They can bind DNA and RNA, and they are implicated in numerous cellular processes including transcription, RNA transport, splicing and translation. While these proteins all have similar functions, they also have several non-redundant functions that make each of them an interesting candidate to study. The general functions of FET family proteins and their role in cancer have been discussed in detail by several groups (Law *et al.*, 2006; Riggi *et al.*, 2007; Kovar, 2011)

Figure 1.1 Domain structure of FUS

Depiction of FUS protein showing the various domains with residue numbers indicated below. QGSY-rich, glutamine-glycine-serine-tyrosine-rich; G-rich, glycine-rich; RRM, RNA recognition motif; RGG, arginine-glycine-glycine-rich; ZFD, zinc-finger domain; NLS, nuclear localization signal.

FUS IN CANCER

A member of the FET family and an RNA/DNA binding protein, FUS was initially identified as part of a chimeric oncogene, resulting from a chromosomal translocation in myxoid liposarcomas (MLS). Multiple fusion-oncogenes like FUS-CHOP (Crozat *et al.*, 1993; Rabbitts *et al.*, 1993), FUS-DDIT3, FUS-ERG (Ichikawa *et al.*, 1994; Panagopoulos *et al.*, 1994; Shing *et al.*, 2003), FUS-ATF-1 (Panagopoulos *et al.*, 1994) and FUS-BBF2H7 (Storlazzi *et al.*, 2003) have been identified in MLS and other cancers. The N-terminal transcriptional activation domain of FUS is fused with the DNA binding domain of the transcription factor and results in an abnormal transcription factor. A majority of the myxoid liposarcomas contain these fusions (Law *et al.*, 2006) and transgenic mouse models of FUS-CHOP have shown that the presence of this fusion is sufficient to initiate cancer (Perez-Losada *et al.*, 2000b; Perez-Losada *et al.*, 2000a). Interestingly a recent study showed that FUS is a putative tumor suppressor and the levels of FUS regulate the tumor properties in prostate cancer models (Brooke *et al.*, 2010). Much of the earlier research on FUS was thus focused on understanding its role in these cancers. Nevertheless, the research helped identify several key cellular functions of FUS.

NORMAL FUS FUNCTIONS

FUS normally functions across several tiers of the central dogma of biology, which represents the transfer of genetic information from DNA, to RNA, to proteins. Proteins in turn regulate the flow of this genetic information at various levels. A few of those proteins act at multiple levels of regulation. FUS is one such multifunctional protein and has been associated with several key cellular functions such as DNA damage repair, RNA processing and stress response.

FUS interacts with both single- and double-stranded DNA (Baechtold *et al.*, 1999). FUS is also known as hPOMp75 and is involved in homologous DNA-pairing. It also associates with higher order DNA structures such as D-loops (Akhmedov *et al.*, 1995; Baechtold *et al.*, 1999; Bertrand *et al.*, 1999) and G-quadruplexes (Takahama and Oyoshi, 2013; Takahama *et al.*, 2013). FUS is located at the telomeres (Dejardin and Kingston, 2009; Takahama *et al.*, 2009) and the association of FUS with telomeres has been proposed to regulate telomere length (Takahama *et al.*, 2013). FUS also rapidly localizes to sites of laser induced DNA damage indicating a role in DNA damage repair (Mastrocola *et al.*, 2013; Rulten *et al.*, 2013; Wang *et al.*, 2013). FUS is known to act as transcriptional factor and regulate the expression of several genes including PGC-1α (Sanchez-Ramos *et al.*, 2011) and CCND1 (Wang *et al.*, 2008).

FUS is also known as hnRNP (heterogeneous ribonuclear protein) P2, implying its role as an RNA binding protein (Calvio *et al.*, 1995). Early SELEX (systematic evolution of ligands by exponential enrichment) and EMSA

(electrophoretic mobility shift assays) analyses demonstrated that recombinant FUS selectively binds RNAs containing a GGUG motif with nanomolar affinity *in vitro* (Lerga *et al.*, 2001). However, recent RNA cross-linking and deep-sequencing studies aimed at identifying mRNAs bound by FUS *in vivo* have generated mixed results ((Hoell *et al.*, 2011; Colombrita *et al.*, 2012; Ishigaki *et al.*, 2012; Lagier-Tourenne *et al.*, 2012; Rogelj *et al.*, 2012; Nakaya *et al.*, 2013) and table 1.1). Thus, even though FUS is able to bind GU-rich sequences *in vitro* and *in vivo*, it appears that such sequences are neither sufficient nor required for interactions between FUS and RNA. A consistent finding across most RNA cross-linking and deep-sequencing studies is the binding of FUS to long introns.

One functional outcome of the binding of FUS to RNA transcripts is the regulation of mRNA splicing. A role for FUS in splicing was suggested from earlier observations that FUS associated with components of the spliceosome (Yang *et al.* 1998; Meissner *et al.* 2003; Kameoka *et al.* 2004) and regulated 5'-splice site selection in E1A pre-mRNA (Lerga, JBC, 2001; Hallier, JBC 1998). The global effect of FUS on alternative splicing has been recently revealed through several genome-wide exon array analyses (reviewed in (Ling *et al.*, 2013) and table 1.1). These studies demonstrated that FUS binds several hundreds of mRNAs including its own mRNA, suggesting an autoregulatory mechanism for FUS expression (Lagier-Tourenne *et al.*, 2012; Nakaya *et al.*, 2013). Zhou et al recently demonstrated that FUS regulates splicing of exon 7, but that this splicing activity is impaired for FUS variants that mislocalize to the

cytoplasm (Zhou *et al.*, 2013). A misregulation of FUS expression may in turn contribute to the pathogenic accumulation of FUS that is observed in disease.

		Investigations of FUS in RNA processes				
Publication: General description		**mRNA Expression (method)**	**mRNA Splicing (method)**	**Binding targets (method)**	**RNA binding specificity**	**Key categories identified by Gene Ontology (GO) Term analysis**
Hoell *et al.*, 2011	Comparison of FET family and mutant FUS RNA targets	FUS knockdown in HEK-293 cells (microarray)	N/A	HA-tagged WT, R521H or R521G in HEK-293 cells (PAR-CLIP[i])	Introns; AU-rich stem loops (15-fold higher affinity than GGU repeat)	RNAs uniquely bound by mutant-FUS: endoplasmic reticulum and ubiquitin-proteasome related
Colombrita *et al.*, 2012	Comparison of FUS and TDP-43 RNA targets	N/A	N/A	Cytoplasmic fraction of NSC-34 (RIP-CHIP[ii])	3'UTR; limited sequence specificity	RNAs bound by FUS: transcriptional regulation, cell cycle, ribonucleoprotein biogenesis, RNA splicing, stress response/ DNA repair, purine ribonucleotide binding and ubiquitin-mediated proteolysis
Ishigaki *et al.*, 2012	RNA binding specificity of FUS; expression and splicing regulation by FUS	FUS knockdown in primary cortical neurons (exon array)	FUS knockdown in primary cortical neurons (exon array)	mouse cerebellum (HITS-CLIP[iii])	Introns and 3'UTR; regions with secondary structure	Changes in mRNA abundance: signaling cascades and metabolic processes Alternatively spliced mRNA: vesicle transport, neuronal impulse and neuronal projection
Rogelj *et al.*, 2012	Comparison of FUS and TDP-43 RNA targets; expression and splicing regulation by FUS	*FUS -/-* embryonic mouse brain (splice-junction microarray)	*FUS -/-* embryonic mouse brain (splice-junction microarray)	embryonic mouse brain (iCLIP[iv])	Long introns; no preference for stem-loops; limited sequence specificity	Alternatively spliced mRNA: cell adhesion, apoptosis, neuronal development and axonogenesis
Lagier-Tourenne *et al.*, 2012	Species comparison of FUS RNA targets; comparison of targets, expression and splicing regulation between FUS and TDP-43	FUS knockdown in adult mouse brain and spinal cord (RNA-seq)	*FUS -/-* embryonic mouse brain; FUS knockdown in adult mouse brain (splicing-sensitive microarrays)	Naïve mouse brain; non-disease human brain (CLIP-seq[v])	Long introns and 3'UTR; GUGGU is an enriched RNA sequence motif	RNAs bound by FUS: components of the synapse and molecules residing in neuronal projections
Nakaya *et al.*, 2013	Species comparison of FUS RNA targets; expression and splicing regulation by FUS	FUS knockdown in embryonic stem cell (ESC) derived mouse neurons (RNA-seq)	FUS knockdown in ESC derived mouse neurons (RNA-seq)	human temporal lobe cortices; ESC derived mouse neurons (HITS-CLIP[iii])	Introns; limited sequence specificity	RNAs bound by FUS: synapse, cell adhesion, neuronal projection and neuronal recogni ion processes
van Blitterswijk *et al.*, 2013	Comparison of FUS overexpression, FUS knockdown and expression of mutant-FUS on mRNA expression and splicing	FUS knockdown; overexpression of WT, R521G or R522G in HEK-293 cells (RNA-seq)	FUS knockdown; overexpression of WT, R521G or R522G in HEK-293 cells (RNA-seq)	N/A	N/A	Changes in mRNA abundance: ribosome, spliceosome, mismatch repair and DNA replication

Table 1.1 Summary of investigations of FUS involvement in RNA processes.

[i]PAR-CLIP – photoactivatable ribonucleoside-enhanced crosslinking and immunoprecipitation

[ii]RIP-Chip - RNA-binding protein immunopurification, microarray

[iii]HITS-CLIP - High-throughput sequencing of RNA isolated by crosslinking immunoprecipitation

[iv]iCLIP – individual-nucleotide resolution crosslinking and immunoprecipitation

[v]CLIP-seq – crosslinking immunoprecipitation, high-throughput sequencing

Another functional outcome of FUS binding to RNA is the transport of RNA from the nucleus to the cytoplasm and throughout the cell. While FUS is predominantly expressed in the nucleus of most cells, it shuttles between the nucleus and cytoplasm (Zinszner *et al.*, 1997). Using heterocells formed by fusion of human and mouse or Xenopus cells, Zinszner *et al.* demonstrated nucleo-cytoplasmic shuttling of FUS was functionally linked to the transport of mRNA from the nucleus to the cytoplasm (Zinszner *et al.*, 1997). The nuclear localization of FUS is mediated by the nuclear import receptor transportin (or karyopherinβ2) (Dormann *et al.*, 2010), an interaction that is modulated by methylation of arginine residues within FUS (Dormann *et al.*, 2012). Arginine-methylation, catalyzed by protein arginine methyltransferases (PRMT), represents a post-translational modification that regulates the subcellular localization and function of proteins (Bedford and Clarke, 2009).

FUS has been identified to associate with several motor proteins, including the ATP-dependent actin binding motors Myo5A (Yoshimura *et al.* 2006) and Myo6 (Takarada *et al.* 2009), and it has also been isolated as part of the large granule that associates with the microtubule-dependent kinesin motor protein KIF5B (Kanai *et al.*, 2004). The association of FUS with such transport machinery and the transport of FUS to different regions of the cell may be important for FUS mediated local translation (Fujii *et al.*, 2005; Fujii and Takumi, 2005; Yasuda *et al.*, 2013). In response to the glutamate receptor mGluR5 mediated synaptic activation, FUS translocates from dendrites of hippocampal

neurons into the spines where it is believed to facilitate local translation of actin-associated proteins, such as Nd1-L, that are necessary to develop spine morphology (Fujii and Takumi, 2005). This hypothesis is supported by the abnormal spine morphology and attenuated spine density in hippocampal pyramidal neurons derived from *FUS -/-* mice (Fujii *et al.*, 2005). Thus by regulating aspects of mRNA transport, FUS could affect local translation and have significant implications on cell fate. Recently, adenomatous polyposis coli (APC)-containing RNA granules, which are located at cell protrusions and may mediate cell migration, were shown to contain FUS. Moreover, translation of kank-2 (KN motif and ankyrin repeat domains 2), a component of APC granules, was dependent upon FUS expression (Yasuda *et al.*, 2013), further underscoring the role of FUS in local translation.

FUS IN STRESS RESPONSE AND ALS

More than 40 mutations in FUS have now been identified to cause ALS (Da Cruz and Cleveland, 2011). A majority of these mutations are localized to the C-terminal NLS of the protein and result in varying degrees of cytoplasmic mislocalization (Bosco *et al.*, 2010a; Dormann *et al.*, 2010; Ito *et al.*, 2010; Gal *et al.*, 2011; Kino *et al.*, 2011). While it is still unclear whether these mutations result in loss of function(s) or gain-of-toxic function(s), it is somewhat clear that the degree of cytoplasmic localization corresponds to the severity of the disease (Dormann and Haass, 2013). FUS plays a role in multiple cellular functions such as DNA damage repair, transcriptional regulation, mRNA splicing, RNA transport and stress response. Thus many pathways could be affected by FUS variants that can ultimately lead to disease. Indeed much research is focused on investigating how mutations in FUS can affect these pathways.

The assembly of ALS-linked FUS variants into cytoplasmic puncta called stress granules under various conditions of applied stress has also drawn considerable attention within the field over the past few years (reviewed in (Wolozin, 2012; Bentmann *et al.*, 2013; Li *et al.*, 2013)). Stress granules are stalled translational complexes that form in response to environmental or metabolic stress. The proposed function of stress granules is in the triage of mRNAs, dictating their fate for expression, degradation or suppression in order to express the appropriate repertoire of proteins to re-establish homeostasis (Kedersha and Anderson, 2002). ALS-linked FUS has consistently been

detected within stress granules under conditions of protein over-expression, oxidative stress, heat-shock and endoplasmic reticulum (ER)-stress (Bosco *et al.*, 2010a; Dormann *et al.*, 2010; Gal *et al.*, 2011; Kino *et al.*, 2011; Bentmann *et al.*, 2012). Endogenous or ectopically expressed WT-FUS is rarely found in stress granules in response to these commonly employed stressors and when reported is most often found in a small percentage of cells and/or is a result of over-expression (Goodier *et al.*, 2007; Andersson *et al.*, 2008; Ito *et al.*, 2010; Kino *et al.*, 2011; Kato *et al.*, 2012). Rather, the association of FUS with stress granules correlates with cytoplasmic expression, with ALS-causing variants, such as FUS P525L and R495X, exhibiting robust levels of both cytoplasmic mislocalization and stress granule incorporation. Conversely, FUS variants with nuclear expression remain nuclear and excluded from stress granules (Bosco *et al.*, 2010a; Dormann *et al.*, 2010). The notion that FUS must be in the cytoplasm and already "poised" to enter stress granules at the time stress is applied was supported by Dormann *et al.*, who demonstrated that WT FUS assembled into stress granules only when its expression was restricted to the cytoplasm by blocking the nuclear importer transportin (Dormann *et al.*, 2010).

That only FUS variants robustly incorporate into stress granules under conditions of applied stress raises the possibility that FUS variants impair cellular stress response in ALS. While there is no functional assay per se for stress granules, Baron et al demonstrated that the presence of FUS variants in stress granules altered several properties that may be important for stress granule

function (Baron *et al.*, 2013). Under conditions of sodium arsenite (an inducer of oxidative stress), the expression of FUS variants delayed the assembly and expedited the disassembly of stress granules. Moreover, FUS variants increased the dynamics of stress granules as measured by FRAP (fluorescence recovery after photobleaching). These observations are consistent with a destabilizing effect of FUS variants on stress granules. Interestingly, the size and abundance of stress granules were enhanced by FUS variants, which may be an outcome of the increased protein- and/or mRNA-load that is sequestered into these structures by FUS variants (Baron *et al.*, 2013). Intriguingly, stress granule marker proteins have been detected in pathological aggregates of post-mortem tissues from individuals with ALS and FTLD (Dormann *et al.*, 2010; Liu-Yesucevitz *et al.*, 2010; Bentmann *et al.*, 2013), suggesting that these granules may accumulate during chronic stress and thus serve as precursors to the end-stage pathological aggregates seen in these disorders (Wolozin, 2012).

Stress granules are composed of many (>50) RNA-binding proteins that contain aggregation-prone domains, including “low complexity”, “prion-like” domains (Anderson and Kedersha, 2008; Kato *et al.*, 2012; Li *et al.*, 2013). This domain in FUS (residues 1- ~165) was shown to facilitate aggregation in yeast (Sun *et al.*, 2011) and to drive the association of FUS with hydrogels, a biomaterial that is composed of amyloid-like fibrils and that has been proposed to mimic the physicochemical properties of stress granules (Han *et al.*, 2012; Kato *et al.*, 2012). Kato *et al.*, and Han *et al.*, demonstrated that modifications to the

prion-like domain of FUS prevented the association of FUS with hydrogels and stress granules in cell culture (Han *et al.*, 2012; Kato *et al.*, 2012), which is at odds with other reports demonstrating a minimal contribution of this domain for the assembly of ALS-FUS variants into stress granules (Bentmann *et al.*, 2012; Baron *et al.*, 2013). Bentmann *et al.*, and Baron *et al.*, show that the C-terminal RGG-rich regions of FUS are the most important for association with stress granules. The methylation of arginine residues is another factor that may modulate the assembly of FUS into stress granules. Arginine residues within the RGG domains of FUS are hypermethylated (Rappsilber *et al.*, 2003), and methylated FUS was detected in post-mortem aggregates of ALS patient tissues (Dormann *et al.*, 2012). However, Baron *et al.*, demonstrated that methylation of FUS was not a prerequisite for stress granule incorporation under sodium arsenite stress (Baron *et al.*, 2013). A key question that awaits further exploration is whether FUS is being recruited to stress granules through interactions with proteins, RNA or both types of molecules.

While the dogma in the stress granule field indicates that translation is silenced in stress granules (Kedersha and Anderson, 2002), a recent report demonstrating that FUS is present in translationally active RNA granules (Yasuda *et al.*, 2013) raises the intriguing possibility that FUS variants may inappropriately turn on translation in stress granules under conditions of stress. To date, however, there is no evidence that FUS variants actually influence protein translation in either direction (i.e., repression vs upregulation) under

conditions of stress.

The various and diverse functions of FUS may ultimately all be involved in the role of FUS in response to stress. Cells experience many endogenous and exogenous stimuli and stressors on a regular basis. Therefore, there exist specific pathways and processes within a cell that elicit quick and effective responses to help maintain cellular homeostasis. The role of FUS in stress response is a new area of research and is the main topic of this thesis, to be discussed in greater detail in Chapters II and III.

The role of FUS and its ALS-linked variants has been extensively examined under stress conditions; however, these conditions have been limited to oxidative, ER stress and heat shock. In Chapter II, I have explored the response of FUS to hyperosmolar stress and have demonstrated that even WT endogenous FUS, which does not respond to any of the aforementioned stressors, translocates into the cytoplasm and incorporates into stress granules. This is a very specific response to hyperosmolar stress, since FUS remains nuclear under other stress conditions tested (oxidative stress, ER stress and heat shock). Furthermore, I have demonstrated that FUS plays a prosurvival role under hyperosmolar conditions because reduction of FUS decreased the cell viability under such conditions.

While it is clear that mutations in FUS result in mislocalization of the protein to the cytoplasm, it is still not clear what other fundamental properties of FUS are affected by mutations that may contribute to disease. I demonstrate that

mutations alter the structure of FUS and result in protein misfolding. The misfolded FUS proteins, in turn, inhibit fast axonal transport in anterograde and retrograde directions. I have shown that the inhibition is mediated by stress-activated p38 MAP kinase. Finally, I have shown the evidence for aberrant p38 MAP kinase regulation in ALS patients. Take all together, my work demonstrates that FUS has a role in cellular stress response and perturbations to its structure caused by genetic mutations results in pathogenic effects.

Preface to Chapter II

A large part of the work presented in this chapter was performed by Reddy Ranjith K Sama (RRKS) with the exceptions below:

Immunofluorescence experiments were performed by RRKS and Nathan Lemay. Confocal imaging and analysis was performed by Laura Kaushansky. Stable NSC34 cells were prepared by Shinsuke Ishigaki and Fumihiko Urano. MTT assays and analysis were performed by RRKS and Catherine Ward.

CHAPTER II

FUS/TLS assembles into stress granules and is a prosurvival factor during hyperosmolar stress

Reddy Ranjith K Sama[1,2], Catherine L. Ward[1,3], Laura J. Kaushansky[1,3], Nathan Lemay[1], Shinsuke Ishigaki[4], Fumihiko Urano[5], Daryl A. Bosco [1,2,3]

[1]Department of Neurology,

[2]Department of Cell and Developmental Biology,

[3]Department of Biochemistry and Molecular Pharmacology,

University of Massachusetts Medical School, Worcester, MA, USA.

[4]Department of Neurology, Center for Neurological Diseases and Cancer,

Nagoya University Graduate School of Medicine, Nagoya, Japan.

[5]Division of Endocrinology, Metabolism and Lipid Research,

Department of Medicine and Department of Pathology and Immunology,

Washington University School of Medicine, St. Louis, MO, USA.

ABSTRACT

FUsed in Sarcoma/Translocated in LipoSarcoma (FUS/TLS or FUS) has been linked to several biological processes involving DNA and RNA processing, and has been associated with multiple diseases, including myxoid liposarcoma and amyotrophic lateral sclerosis (ALS). ALS-associated mutations cause FUS to associate with stalled translational complexes called stress granules under conditions of stress. However, little is known regarding the normal role of endogenous (non-disease linked) FUS in cellular stress response. Here, we demonstrate that endogenous FUS exerts a robust response to hyperosmolar stress induced by sorbitol. Hyperosmolar stress causes an immediate re-distribution of nuclear FUS to the cytoplasm, where it incorporates into stress granules. The redistribution of FUS to the cytoplasm is modulated by methyltransferase activity, whereas the inhibition of methyltransferase activity does not affect the incorporation of FUS into stress granules. The response to hyperosmolar stress is specific, since endogenous FUS does not redistribute to the cytoplasm in response to sodium arsenite, hydrogen peroxide, thapsigargin, or heat shock, all of which induce stress granule assembly. Intriguingly, cells with reduced expression of FUS exhibit a loss of cell viability in response to sorbitol, indicating a prosurvival role for endogenous FUS in the cellular response to hyperosmolar stress.

INTRODUCTION

Fused in sarcoma/translocated in liposarcoma (FUS/TLS or FUS) is an RNA/DNA-binding protein that is implicated in a diverse array of cellular processes. FUS, also known as heterogeneous ribonuclear protein hnRNP P2 (Calvio *et al.*, 1995), is a member of the FET (previously TET) family of proteins that also includes EWS (Ewing's sarcoma) and TAF15 (TATA-binding protein-associated factor 15) (Tan and Manley, 2009). FUS was originally discovered in the context of a fusion oncoprotein in myxoid liposarcoma cells (Crozat *et al.*, 1993). Since then, this multifunctional protein has been linked to various aspects of RNA and DNA-processing, including mRNA splicing (Ishigaki *et al.*, 2012), transcription (Wang *et al.*, 2008), and DNA repair (Kuroda *et al.*, 2000). Recently, mutations in FUS have been linked to the fatal neurodegenerative disease amyotrophic lateral sclerosis (ALS) (Kwiatkowski *et al.*, 2009; Vance *et al.*, 2009).

FUS is predominately expressed in the nucleus of most cells (Andersson *et al.*, 2008), although it shuttles between the nucleus and cytoplasm during mRNA transport (Zinszner *et al.*, 1997; Fujii and Takumi, 2005). Several reports have shown that ALS-linked FUS variants associate with cytoplasmic stress granules under conditions of oxidative stress and heat shock (Bosco *et al.*, 2010a; Dormann *et al.*, 2010; Gal *et al.*, 2011). Stress granules are stalled translational complexes comprised of mRNA, ribosomes, and RNA-binding proteins that form in response to induced stress, such as hyperosmolar stress,

oxidative stress, heat shock, ultraviolet irradiation and viral infection (Anderson and Kedersha, 2009). These dynamic complexes are thought to play a role in sorting mRNAs for expression, storage or degradation (Kedersha and Anderson, 2002). More recently, stress granules have also been shown to directly regulate protein activity in the context of cellular signaling (Wippich *et al.*, 2013). In contrast to the aforementioned FUS variants, much less is known about the association of endogenous FUS with stress granules and the role of endogenous FUS in stress response.

Herein, we sought to examine the response of endogenous FUS to various cellular stressors. We found that inducers of stress granule assembly shown to direct FUS variants into stress granules, such as sodium arsenite, thapsigargin, hydrogen peroxide, and heat shock, had no effect on the subcellular distribution of endogenous FUS. In striking contrast, endogenous FUS exhibited a robust redistribution from the nucleus to the cytoplasm and assembled into stress granules under conditions of hyperosmolar stress induced by sorbitol, mannitol, sucrose, sodium chloride, and polyethylene glycol (PEG). Not only was the response of FUS stress-specific, it was also regulated by methyltransferase activity. Cells with reduced FUS expression were more susceptible to sorbitol-induced toxicity, suggesting that FUS plays protective role with regard to cellular homeostasis. These data establish a novel role for the multifunctional FUS protein in cellular stress response.

RESULTS

Endogenous FUS redistributes to the cytoplasm and assembles into stress granules in response to hyperosmolar stress.

In order to investigate the role of FUS in stress response, we examined the nucleo-cytoplasmic distribution of FUS in response to various cellular stressors. Hyperosmolar stress induced by the administration of 0.4 M sorbitol to HeLa cells for 1 h resulted in a striking redistribution of FUS from the nucleus to the cytoplasm, where FUS assembled into numerous puncta. A majority of FUS-positive puncta co-localized with the stress granule marker proteins, G3BP (Fig. 2.1A) and TIAR (Fig. 2.1B) (Kedersha and Anderson, 2007). Since stress granules are functionally related to processing bodies (P-bodies), which are cellular sites of mRNA degradation (Moore, 2005), we also probed for the co-localization of endogenous FUS with GE-1/hedls, a constituent of P-bodies but not stress granules (Kedersha and Anderson, 2007). The majority of P-bodies did not co-localize with FUS-positive granules. However, some P-bodies appeared to associate with and/or dock onto FUS-positive granules (Fig. 2.1C), consistent with the physical association between P-bodies and stress granules that has been previously described (Kedersha *et al.*, 2005; Bosco *et al.*, 2010a).

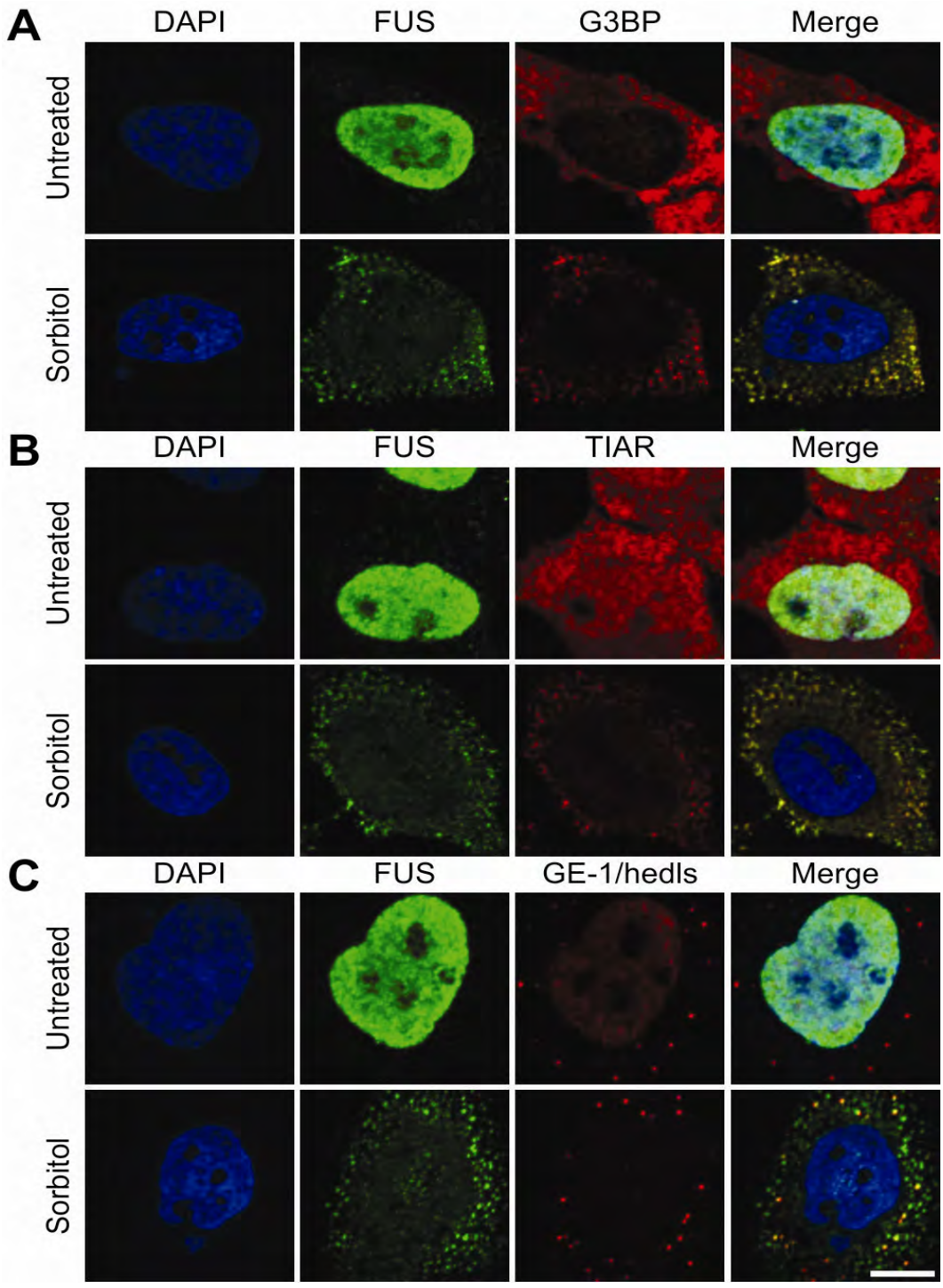
A
DAPI
FUS
G3BP
Merge
Untreated
Sorbitol
B
DAPI
FUS
TIAR
Merge
Untreated
Sorbitol
C
DAPI
FUS
GE-1/hedls
Merge
Untreated
Sorbitol

Figure 2.1

Figure 2.1 Endogenous FUS redistributes to the cytoplasm and localizes to cytoplasmic stress granules in response to sorbitol.

Confocal images of untreated HeLa cells (top row in each panel) as compared to cells treated with 0.4 M sorbitol for 1 h (bottom row in each panel; A–C) are shown. Cells probed with an anti-FUS antibody (green) and either the stress granule marker anti-G3BP (A) or anti-TIAR (B) revealed that FUS co-localizes with stress granules in response to sorbitol. C) P-bodies were detected by anti-GE-1/hedls antibody in both untreated and treated conditions; however, the majority of P-bodies did not exhibit co-localization with FUS. Cells were counter stained with the nuclear marker DAPI (blue; A–C). Images are representative of at least n = 3 experiments. Scale bar represents 10 μm.

The redistribution and incorporation of FUS into stress granules in response to sorbitol is reminiscent of other nuclear hnRNPs, such as hnRNP A1 (Guil *et al.*, 2006) and TDP-43 (Dewey *et al.*, 2010). However, not all hnRNP proteins redistribute to stress granules in response to sorbitol (van der Houven van Oordt *et al.*, 2000), suggesting a functional role in stress response for those hnRNPs that do localize to these structures. In addition to sorbitol, hyperosmolar stress induced by mannitol, sucrose, sodium chloride, PEG3350 and PEG8000 also caused FUS to redistribute to the cytoplasm and incorporate into stress granules (Fig. 2.2). Thus the response of FUS is a more generalized response to hyperosmolar conditions and not specific to sorbitol treatment.

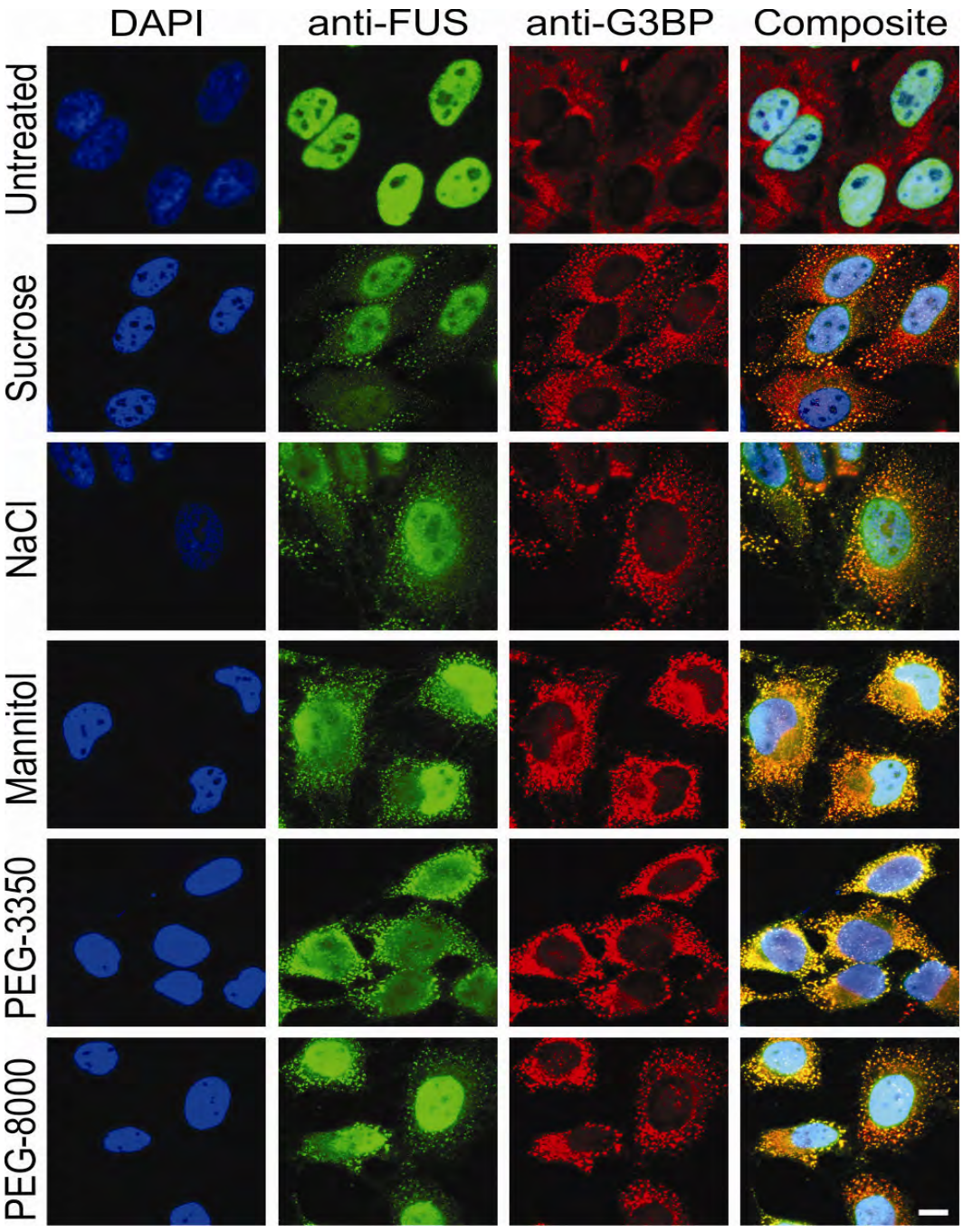
DAPI
anti-FUS
anti-G3BP
Composite
Untreated
Sucrose
NaCl
Mannitol
PEG-3350
PEG-8000

Figure 2.2

Figure 2.2 Endogenous FUS responds to hyperosmolar stress

HeLa cells untreated (top row) or treated with 300 mM sucrose, 0.2 M sodium chloride (NaCl), 0.4 M mannitol, 20% polyethylene glycol (PEG)–3350 or 20% PEG–8000 for 1 h were fixed and imaged. Cells probed with anti-FUS (green) and anti-G3BP antibodies revealed that FUS co-localized with stress granules in response to all the hyperosmolar stress inducing agents. Cells were counter stained with the nuclear marker DAPI (blue). Images are representative of at least n=3 experiments. Scale bar represents 10 μm.

Next, we investigated the effect of sorbitol in additional cell lines. Administration of sorbitol to HEK (human embryonic kidney)-293T, MEFs (mouse embryonic fibroblasts) and NSC-34 (neuroblastoma x spinal cord hybrid) (Cashman *et al.*, 1992) cell lines recapitulated the results from HeLa cells; FUS redistributed from the nucleus to the cytoplasm, where it assembled into G3BP- and TIAR-positive stress granules (Fig. 2.3). Therefore, the response of FUS to hyperosmolar stress is not a cell type- or species-specific phenomenon, but rather is detected in several different mammalian cell lines.

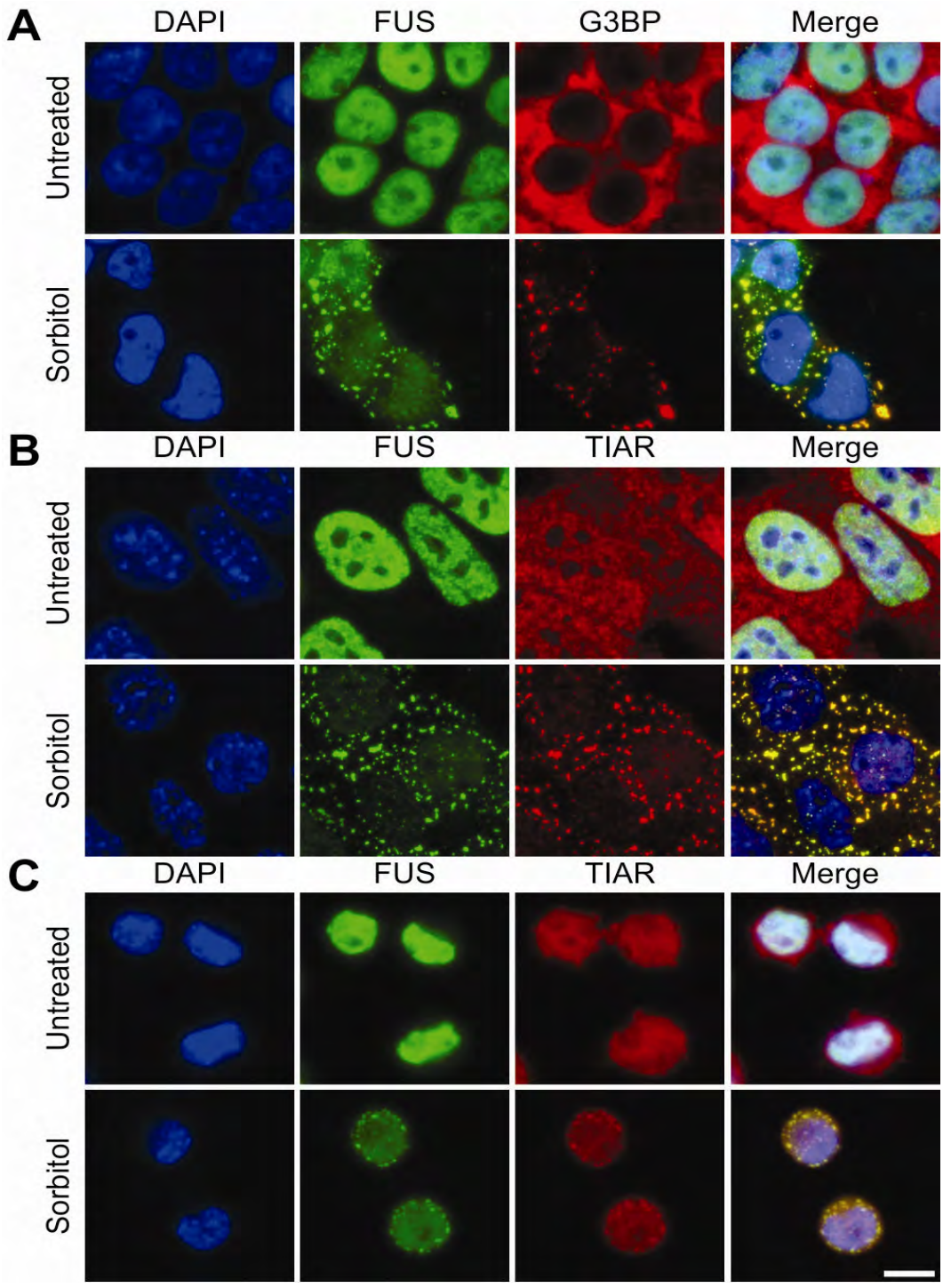
A
DAPI
FUS
G3BP
Merge
Untreated
Sorbitol
B
DAPI
FUS
TIAR
Merge
Untreated
Sorbitol
C
DAPI
FUS
TIAR
Merge
Untreated
Sorbitol

Figure 2.3

Figure 2.3 The response of FUS to sorbitol is recapitulated in several mammalian cell lines.

HEK-293 (A), MEF (B) and NSC-34 (C) cells were either untreated (top row in each panel) or treated (bottom row in each panel) with 0.4 M sorbitol for 1 h. Immunofluorescence with anti-FUS (green) and anti-G3BP (A) or anti-TIAR (B and C) antibodies showed that FUS localized to stress granules in response to sorbitol in all three cell lines. Cells were counter-stained with the nuclear marker DAPI (blue; A-C). All images are representative of n=3 independent experiments. Scale bar represents 10 μm.

In contrast to sorbitol and other hyperosmolar stress conditions, FUS did not redistribute to the cytoplasm when HeLa cells were exposed to inducers of oxidative stress (e.g., sodium arsenite and hydrogen peroxide), endoplasmic reticulum (ER) stress (e.g., thapsigargin) or heat shock, all of which induce the formation of stress granules in a majority of cells (Fig. 2.4) (Kedersha and Anderson, 2007; Emara *et al.*, 2012). Endogenous FUS was not detected in any of the G3BP-positive stress granules that formed under these conditions; we did not detect any cells with elevated cytoplasmic FUS or FUS-positive stress granules under these conditions. Similarly, exogenously expressed wild-type FUS did not redistribute nor assemble into stress granules under the aforementioned conditions (Bosco *et al.*, 2010a; Dormann *et al.*, 2010; Bentmann *et al.*, 2012; Daigle *et al.*, 2013), although the effect of sorbitol on endogenous or exogenous FUS has not been reported. Thus our results demonstrate that the formation of stress granules by general stressors is not sufficient to cause a redistribution of FUS to the cytoplasm, indicating that there are specific factors associated with hyperosmolar stress that elicit this response for endogenous FUS.

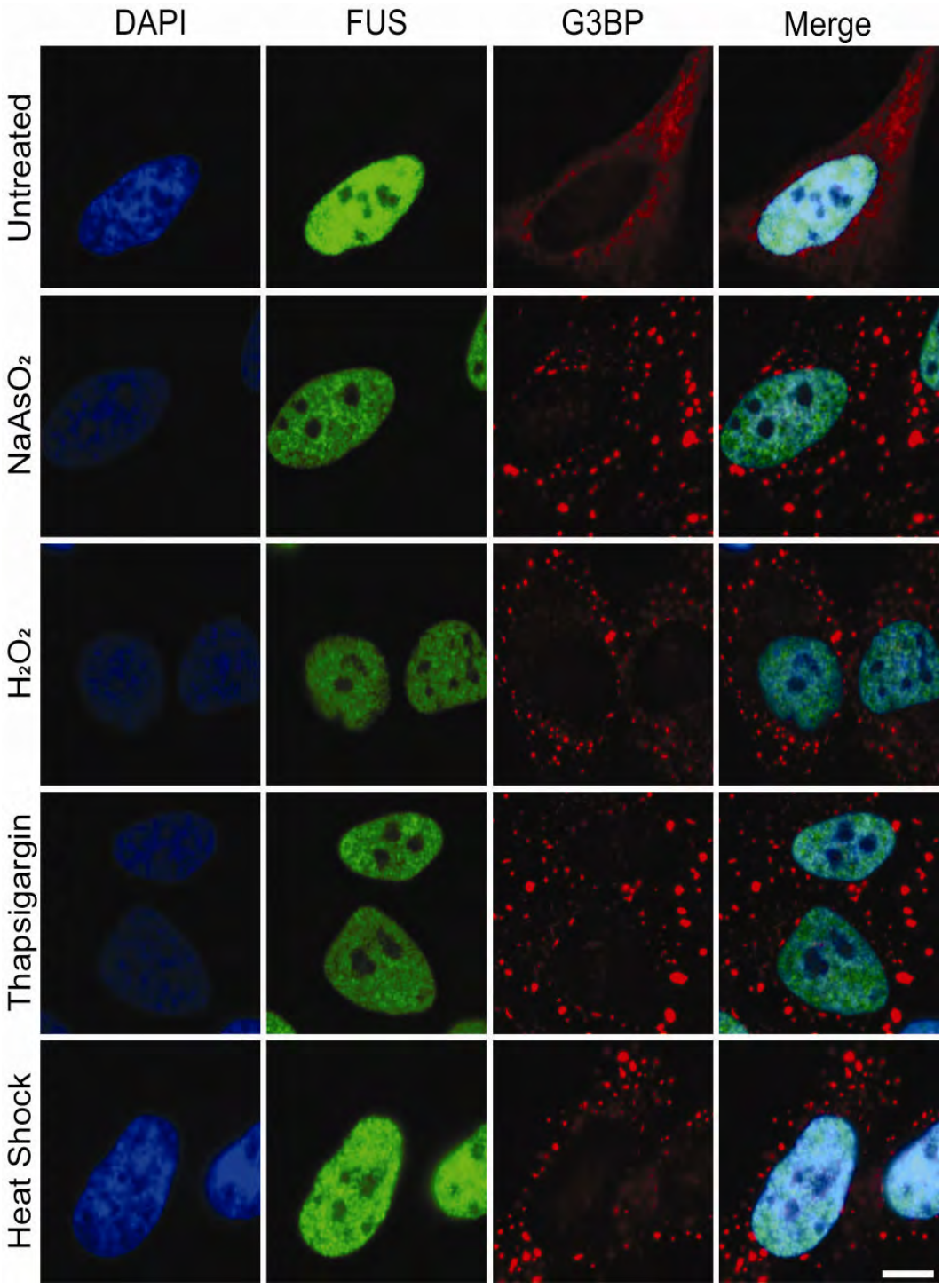
DAPI
FUS
G3BP
Merge
Untreated
NaAsO2
H2O2
Thapsigargin
Heat Shock

Figure 2.4

Figure 2.4 The recruitment of FUS to cytoplasmic stress granules is stress-specific.

HeLa cells were treated with either 0.5 mM sodium arsenite ($NaAsO_2$) for 1 h, 1.5 mM hydrogen peroxide (H_2O_2) for 2 h, 50 µM thapsigargin for 30 min, or heat shock at 43° C for 30 min. Immunofluorescence revealed that G3BP-positive stress granules (red) formed under all stress conditions. FUS (green) remained nuclear and absent from stress granules under these stress conditions, similar to the unstressed condition (top part). Nuclei were stained with DAPI (blue). All images are representative of n = 3 independent experiments. Scale bar represents 10 µm.

The assembly of FUS into stress granules is rapid and reversible.

The formation of stress granules represents a fast, almost immediate, response of cells to induced stress. To determine the time frame in which FUS responds to sorbitol, we monitored the cellular redistribution of FUS by immunofluorescence microscopy over a one-hour time course of sorbitol exposure. G3BP is an effector of stress granule assembly (Tourriere *et al.*, 2003; Aulas *et al.*, 2012) and was therefore used as a marker to monitor the assembly process. The cytoplasmic redistribution of FUS was detected within 10 min of sorbitol treatment, a time point that preceded the appearance of discreet G3BP-positive cytoplasmic foci, demonstrating that FUS starts to accumulate in the cytoplasm before stress granules are fully formed (Fig. 2.5A). Within 20 min of sorbitol treatment, discreet G3BP-positive stress granules containing FUS were detected. Therefore FUS appears to incorporate into stress granules on the same time scale that these foci are being formed. G3BP- and FUS-positive stress granules appear fully formed by 60 min, at which time a substantial fraction of FUS was redistributed to the cytoplasm.

The formation of stress granules is a reversible process (Anderson and Kedersha, 2008). After the induced stress is removed, stress granules disassemble as the cell re-establishes homeostasis. We monitored the disassembly of stress granules in HeLa cells pre-treated with sorbitol to determine the subcellular fate of FUS as cells re-established homeostasis. The disassembly of stress granules was initiated by replacing media containing

sorbitol with fresh media lacking sorbitol, and cells were monitored for 60 min by immunofluorescence microscopy as described above. Within 10 min of removing sorbitol from the media, FUS dissociated from stress granules and re-distributed to the nucleus in virtually all (~90%) cells. However, G3BP-positive, FUS-negative foci persisted in approximately one third of cells at this time point (Fig. 2.5B). For the remainder of the time course, FUS was localized to the nucleus while G3BP-positive stress granules gradually continued to disassemble until the 60 min time point, when ~20% of cells contained G3BP-positive stress granules. These data show that FUS exhibits a rapid response not only to the administration of sorbitol (Fig. 2.5A), but also to the removal of this stressor (Fig. 2.5B).

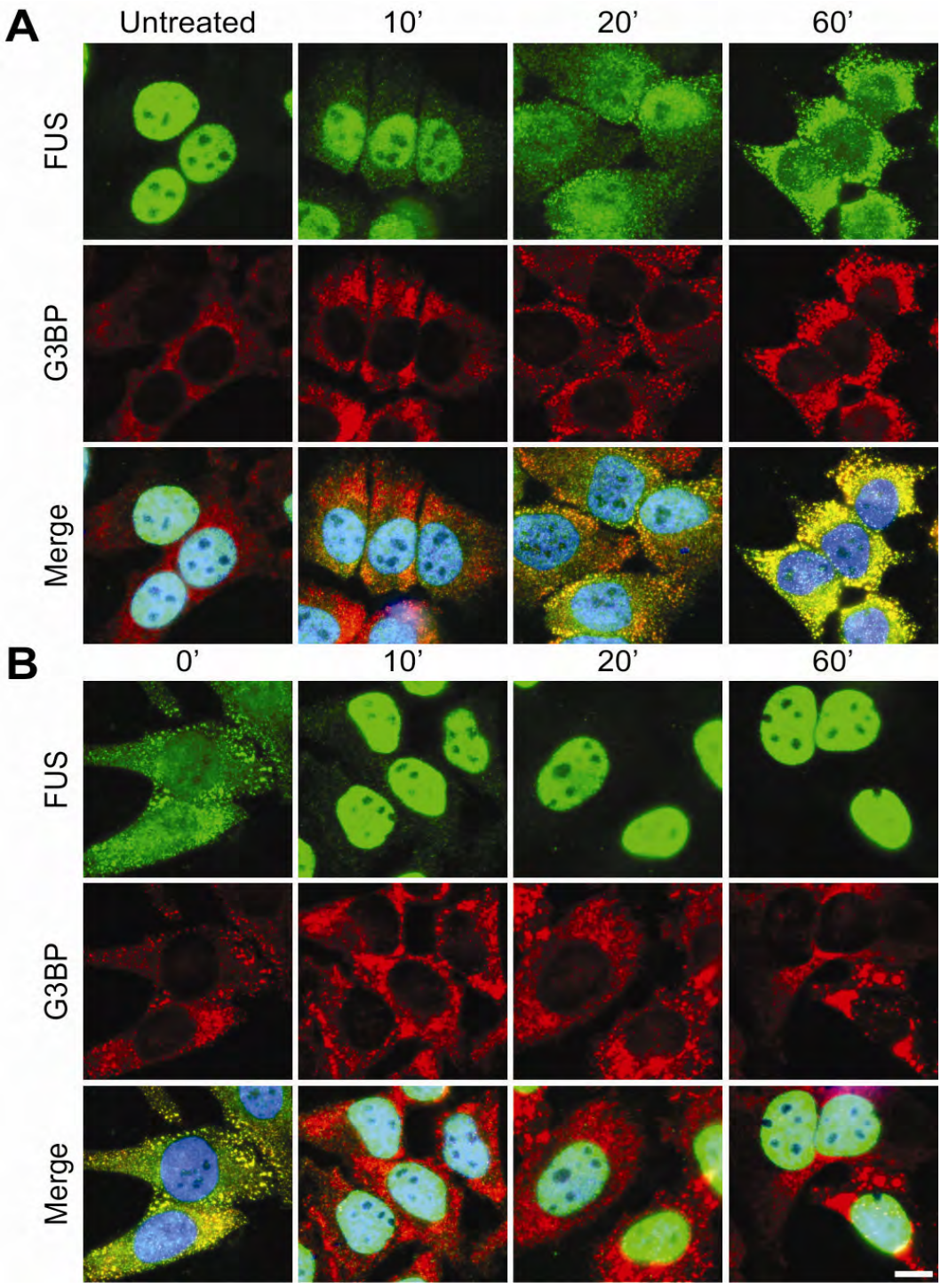

Figure 2.5

Figure 2.5 The response of FUS to sorbitol is rapid and reversible.

A) A representative time-course for the cytoplasmic redistribution of FUS into stress granules upon exposure to hyperosmolar stress. HeLa cells were treated with 0.4 M sorbitol for the indicated time points, fixed, and assessed by immunofluorescence with anti-FUS (green) and anti-G3BP (red) antibodies, and the nuclear marker DAPI (blue). Elevated levels of cytoplasmic FUS were detected as early as 10 min. FUS accumulated into discreet stress granules by 20 min. The nucleo-cytoplasmic distribution of FUS continued to shift towards the cytoplasm over the remaining time course. B) A representative time-course for the return of FUS to the nucleus and the concomitant disassembly of stress granules upon withdrawal of sorbitol. HeLa cells were treated with 0.4 M sorbitol for 1 h, after which the sorbitol was replaced with fresh media and the cells were processed as described in (A). A majority of FUS re-localized to the nucleus within 10 min. Some G3BP positive stress granules persisted for up to 1 h. Images are representative of at least n = 3 experiments. Scale bar represents 10 μm.

Stress granule assembly is required for robust cytoplasmic redistribution of FUS.

FUS is a nucleo-cytoplasmic shuttling protein. Therefore, the accumulation of FUS in the cytoplasm can result from increased export of the protein from the nucleus and/or decreased import to the nucleus from the cytoplasm. The nucleo-cytoplasmic equilibrium of FUS may be shifted towards the cytoplasm through FUS binding interactions. For example, injection of anti-FUS antibodies into cells trapped the majority of FUS in the cytoplasm within 2 h (Zinszner *et al.*, 1997). Since the timescale of FUS redistribution from the nucleus to the cytoplasm under conditions of hyperosmolar stress (1 hour, Fig. 2.5) is similar to that in aforementioned antibody study (2 hours, (Zinszner *et al.*, 1997)), we asked whether or not stress granules serve as a "cytoplasmic sink" that effectively traps FUS in the cytoplasm through mass action. Stress granule assembly was inhibited by the addition of 50 μg/mL emetine, which stabilizes polysomes and blocks translation elongation (Kedersha *et al.*, 2000), for 1 h prior to the administration of hyperosmolar stress. As expected, only diffuse G3BP signal (*i.e.*, no G3BP-positive stress granules) was observed under these conditions (Fig 2.6). Interestingly, emetine treatment also markedly reduced the cytoplasmic redistribution of FUS (Fig. 2.6) in the presence of sorbitol. These data implicate stress granule formation as a requisite for the cytoplasmic redistribution of FUS, and suggest that the full response of FUS to hyperosmolar stress includes its assembly into stress granules.

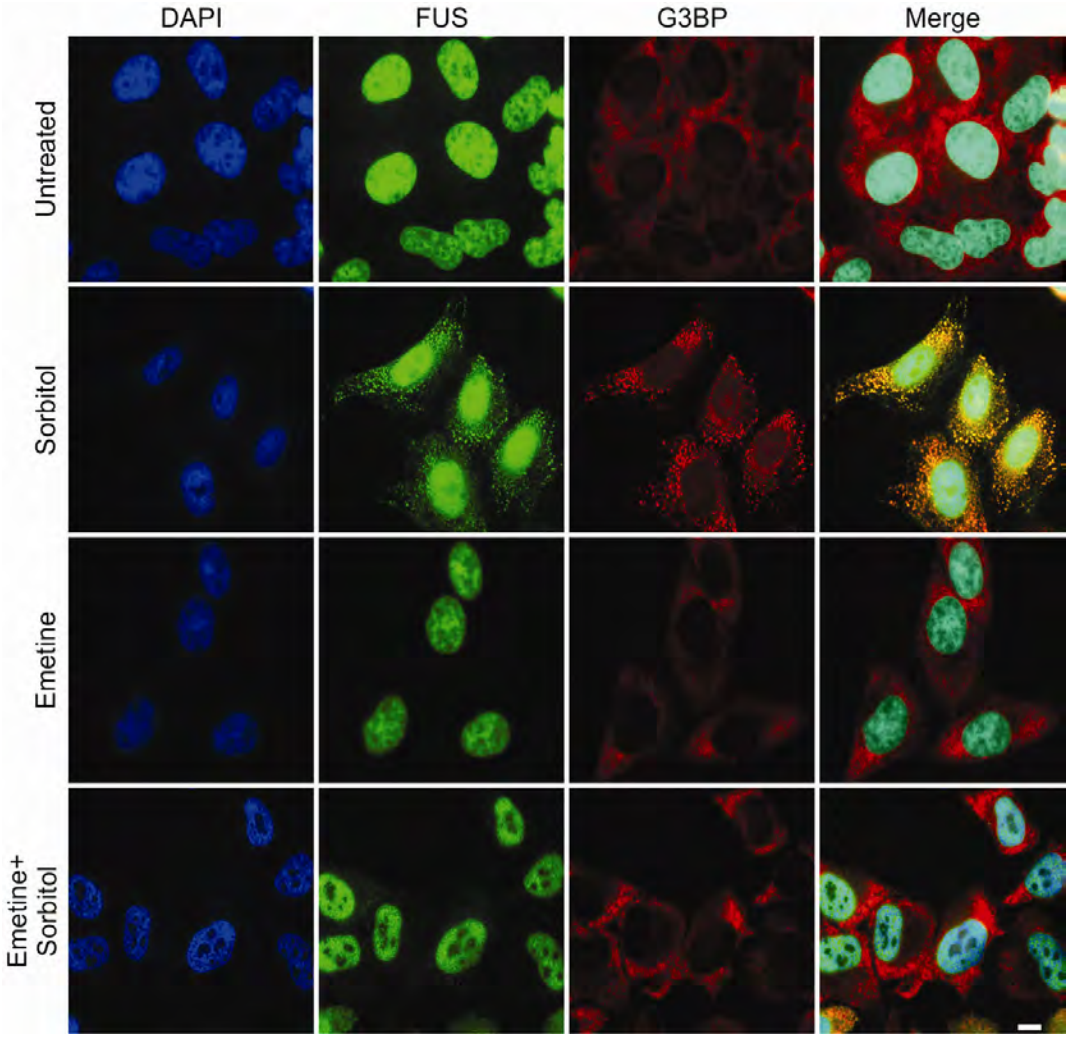
DAPI
FUS
G3BP
Merge
Untreated
Sorbitol
Emetine
Emetine+
Sorbitol

Figure 2.6

Figure 2.6 An inhibitor of stress granule assembly prevents the cytoplasmic redistribution of FUS.

HeLa cells were treated with 0.4 M sorbitol for 1 h, 50 µg/mL emetine for 1 h or pre-treated with emetine followed by sorbitol treatment. Cells were then fixed and probed by immunofluorescence for DAPI (blue), FUS (green), and G3BP (red). Emetine pre-treatment inhibited both stress granule assembly, as evidenced by the diffuse G3BP signal, and the cytoplasmic redistribution of FUS in the presence of sorbitol. All images are representative of at least n = 3 independent experiments. Scale bar represents 10 µm.

Next we investigated the role of FUS in stress granule assembly under conditions of hyperosmolar stress. HeLa cells were first treated with either siRNA specific for FUS or non-targeting siRNA as a control for 48 hrs, and were then exposed to 0.4 M sorbitol for 30 min to induce the formation of stress granules (Fig. 2.7A). Although cells treated with FUS siRNA exhibited a ~90% reduction in FUS protein levels (Fig. 2.7B), these cells produced G3BP-positive stress granules in response to sorbitol that were indistinguishable from control cells (Fig. 2.7A). While the physical response of FUS to hyperosmolar stress depends on the formation of stress granules (Fig. 2.6), FUS does not appear to dictate the ability of stress granules to form as they are formed even when FUS knocked down.

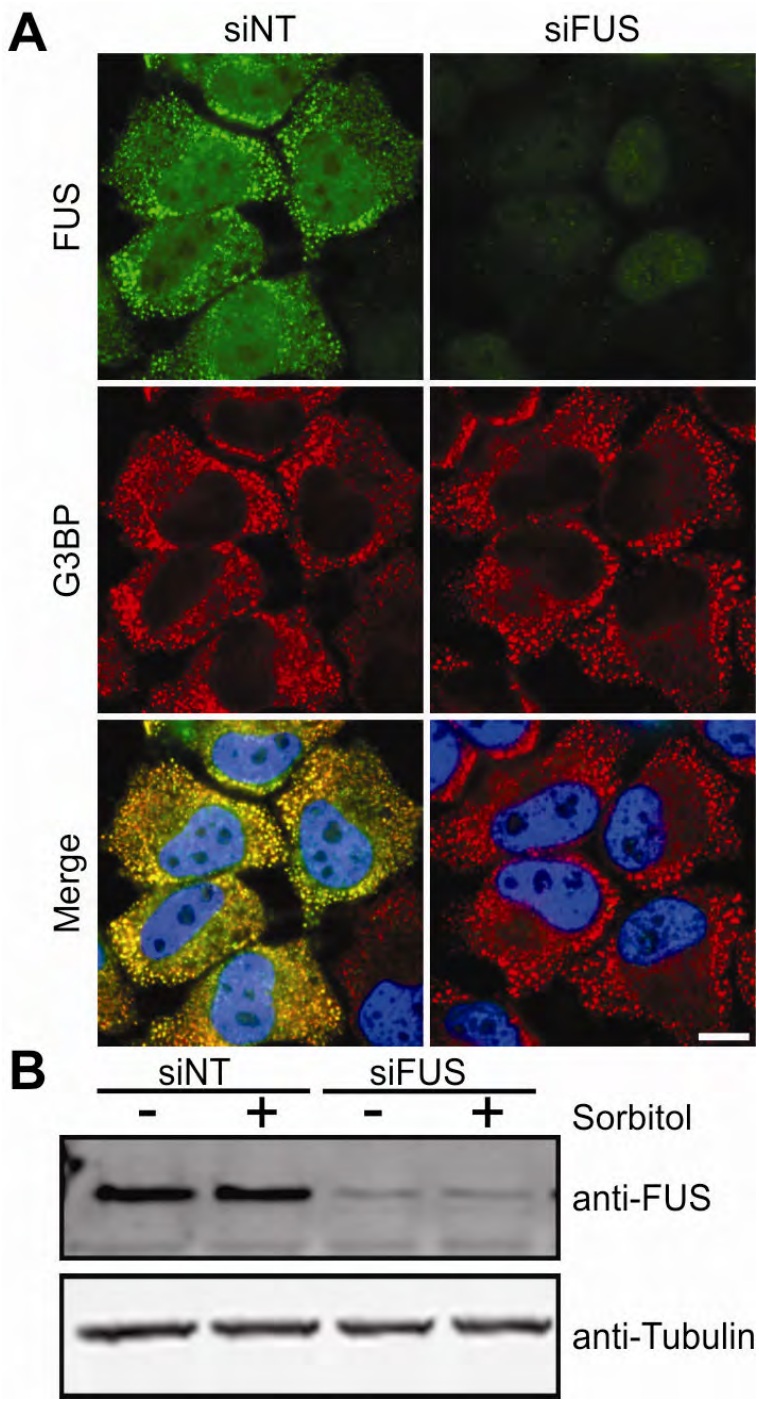
A
siNT
siFUS
FUS
G3BP
Merge
B
siNT
siFUS
-
+
-
+
Sorbitol
anti-FUS
anti-Tubulin

Figure 2.7

Figure 2.7 FUS is not required for stress granule assembly.

A) HeLa cells were transfected with non-targeting siRNA (siNT) or siRNA against FUS (siFUS) for 48 h and subsequently treated with 0.4 M sorbitol for 1 h. Cells were then fixed and probed by immunofluorescence for DAPI (blue), FUS (green), and G3BP (red). Cells treated with either siFUS or siNT exhibited normal stress granule formation (red) in response to sorbitol, despite a significant reduction in FUS protein levels in siFUS treated cells as evidenced by immunofluorescence (green) and Western blot (B). All images are representative of at least n = 3 independent experiments. Scale bar represents 10 μm.

Methylation regulates the nucleo-cytoplasmic distribution of FUS under hyperosmolar stress.

Next we investigated the mechanisms by which FUS relocalizes to the cytoplasm and incorporates into stress granules in response to hyperosmolar stress. Methylation of arginine residues is a post-translational modification that modulates the nucleo-cytoplasmic distribution of hnRNP proteins, such as the cold-inducible RNA-binding protein (CIRP) (De Leeuw *et al.*, 2007). Some reports implicate a link between the arginine methylation status of ALS-linked FUS and its subcellular localization (Tradewell *et al.*, 2012; Yamaguchi and Kitajo, 2012). In fact, mass spectrometry analyses demonstrate that up to 20 arginine residues are asymmetrically dimethylated in FUS (Rappsilber *et al.*, 2003). That protein arginine N-methyltransferase-1 (PRMT1), which accounts for ~85% of arginine methylation in the cell (Bedford and Clarke, 2009), and FUS interact suggests that the methylation of FUS is catalyzed by PRMT1 (Du *et al.*, 2011; Tradewell *et al.*, 2012; Yamaguchi and Kitajo, 2012). Interestingly, stress granules contain arginine methylated hnRNP proteins, raising the possibility that this post-translational modification influences stress granule dynamics (Xie and Denman, 2011). This notion is supported by an attenuation of fragile X mental retardation protein (FMRP) in stress granules upon exposure to adenosine-2', 3'-dialdehyde (AdOx) (Dolzhanskaya *et al.*, 2006), a general inhibitor of methyltransferases (O'Dea *et al.*, 1987).

To determine whether or not the methylation status of FUS regulates its subcellular localization under conditions of hyperosmolar stress, we examined the nuclear-cytoplasmic distribution of FUS after treatment of HeLa cells with AdOx. FUS remained predominantly nuclear in the presence of AdOx alone, similar to untreated cells (data not shown). However, when cells were pre-treated with AdOx prior to sorbitol exposure, there was a significant effect on the nuclear-cytoplasmic partitioning of FUS compared to cells treated with sorbitol alone (Fig. 2.8A and B). While sorbitol treatment resulted in a ~50% reduction of nuclear FUS compared to control cells, pre-treatment with AdOx restored ~30% of FUS to the nucleus (Fig. 2.8B). To quantify the methylation status of the FUS protein itself, FUS was immunoprecipitated from untreated cells or from cells treated with AdOx in combination with sorbitol and probed for asymmetrically dimethylated arginine residues with the ASYM24 antibody, which recognizes proteins that are asymmetrically methylated on arginine residues (Tradewell *et al.*, 2012). Arginine methylation of FUS in untreated cells was detected by ASYM24 (Fig. 2.8C), which is expected since FUS is reportedly arginine methylated under homeostatic conditions (Rappsilber *et al.*, 2003). The level of methylated FUS was not significantly altered by the addition of sorbitol (data not shown). However, the arginine methylation status of FUS decreased by more than 50% in cells pre-treated with AdOx (data not shown) or AdOx in combination with sorbitol (Figs. 2.8C and D). Since AdOx is a general methyltransferase inhibitor, we cannot exclude the possibility that other methylation events

influence the subcellular distribution of FUS in these experiments. Nonetheless, these data suggest that the methylation status of FUS must be maintained in order for it to redistribute to the cytoplasm under conditions of hyperosmolar stress, and are consistent with the notion that hypomethylated forms of FUS fail to shuttle out of the nucleus (Tradewell *et al.*, 2012; Yamaguchi and Kitajo, 2012).

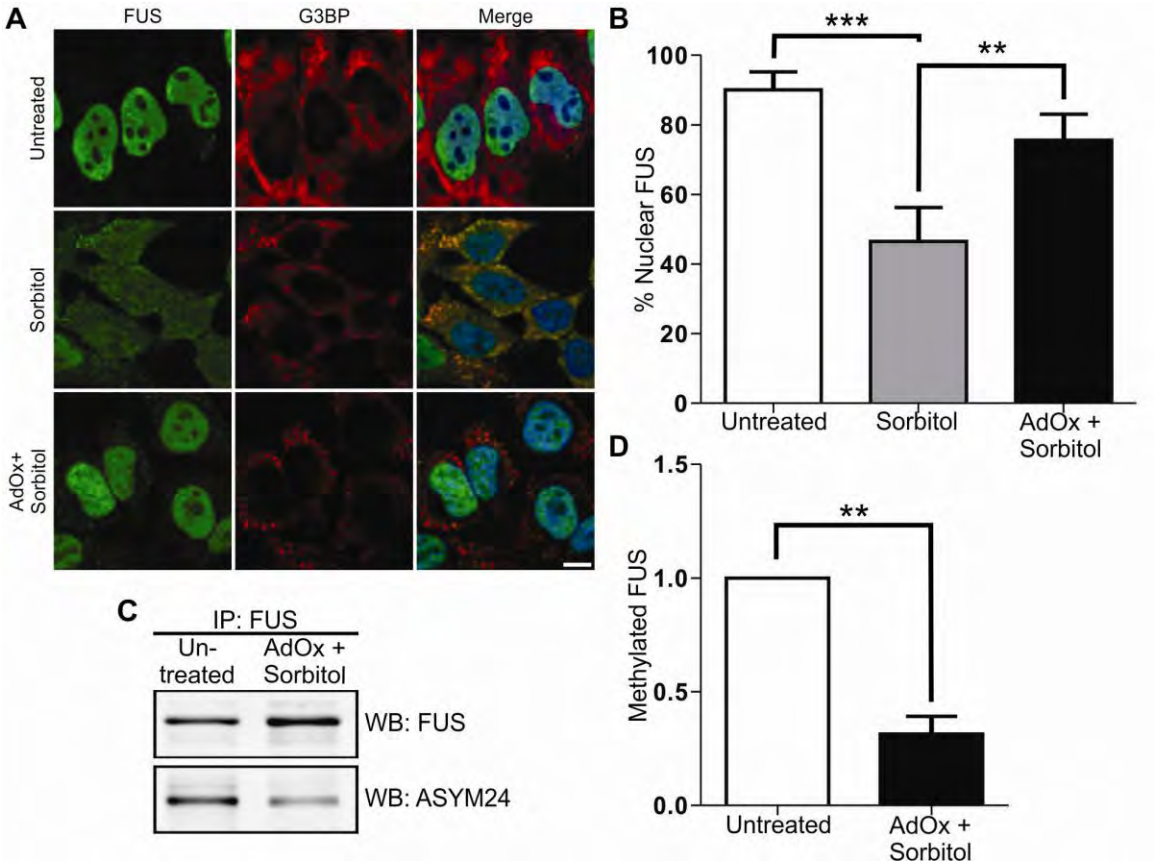
A
FUS
G3BP
Merge
Untreated
Sorbitol
AdOx+ Sorbitol
B
***
**
% Nuclear FUS
100
80
60
40
20
0
Untreated
Sorbitol
AdOx + Sorbitol
C
IP: FUS
Un-treated
AdOx + Sorbitol
WB: FUS
WB: ASYM24
D
**
Methylated FUS
1.5
1.0
0.5
0.0
Untreated
AdOx + Sorbitol

Figure 2.8

Figure 2.8 Methylation regulates the nucleo-cytoplasmic distribution of FUS.

A,B) HeLa cells were treated with 0.4 M sorbitol for 1 h, or pre-treated with 50 µM AdOx for 24 h prior to sorbitol treatment (AdOx + sorbitol) and subjected to confocal immunofluorescence imaging with anti-FUS (green) and anti-G3BP (red) antibodies. Sorbitol decreased the percentage of cellular FUS in the nucleus from 90 ± 5.1% in untreated cells to 46.5 ± 9.8%. Pre-treatment of cells with AdOx prior to sorbitol increased the percentage of cellular FUS in the nucleus to 75.6 ± 7.4%. Data shown are the average of three independent experiments ± standard deviation. Statistical significance was determined by ANOVA and Tukey's post hoc pairwise test (**$P < 0.005$, ***$P < 0.0005$). No other comparisons were statistically significant. Scale bar represents 10 µm. C) FUS was immunoprecipitated from untreated HeLa cells or from AdOx + sorbitol cells and probed with the ASYM24 antibody by Western blot. FUS was used as a loading control. D) Densitometry analysis of (C) revealed a 68.6 ± 7.8% decrease in the amount of FUS that is arginine dimethylated when cells were pre-treated with AdOx compared to untreated cells. Data shown are the average of three independent experiments ± standard deviation. Statistical significance was determined by Student's *t*-test (**$P < 0.005$).

Next we sought to determine if hypomethylated FUS could still assemble into stress granules. Since the assembly of FUS into stress granules occurs concomitantly with cytoplasmic accumulation (Fig. 2.5), it was necessary to first dissect these two processes. To this end, we transiently transfected HeLa cells with the GFP-tagged FUS 515X truncation construct, which lacks the nuclear localization signal and is therefore retained in the cytoplasm under homeostatic conditions (Bosco *et al.*, 2010a). GFP-FUS 515X assembled into stress granules in response to 0.4 M sorbitol, and the extent of this association was the same whether cells were pre-treated with AdOx or not (Figs. 2.9A and B). The same outcome was observed in HEK-293 cells stably expressing GFP-FUS 515X (data not shown). In contrast to the GFP-FUS signal, there was a dramatic decrease in the ASYM24 signal in cells pre-treated with AdOx (Figs. 2.9A and B), indicating that pre-treatment with AdOx effectively inhibited methyltransferase activity within these cells. Immunoprecipitation with anti-GFP followed by western blot analysis with the ASYM24 antibody confirmed that GFP-FUS 515X was indeed hypomethylated due to AdOx pre-treatment (Fig. 2.9C). Thus, despite a large reduction in the methylation status of FUS in AdOx pre-treated cells (Figs. 5 and 6), FUS still robustly associated with stress granules. We note that a small fraction of FUS remained dimethylated in the AdOx condition (Fig. 2.9C), presumably FUS protein that was methylated prior to AdOx exposure but had not turned over during the course of the experiment (Xie and Denman,

2011). In the absence of commercially available antibodies that are specific for dimethylated FUS, we cannot exclude the possibility that stress granules contain some dimethylated FUS in these experiments. However, the dramatic decrease in ASYM24 signal is consistent with a reduced load of methylated proteins within stress granules, and therefore it is unlikely that all of the residual methylated FUS is sequestered into these structures. Together, these studies argue against a role for arginine methylation in regulating the incorporation of FUS in stress granules.

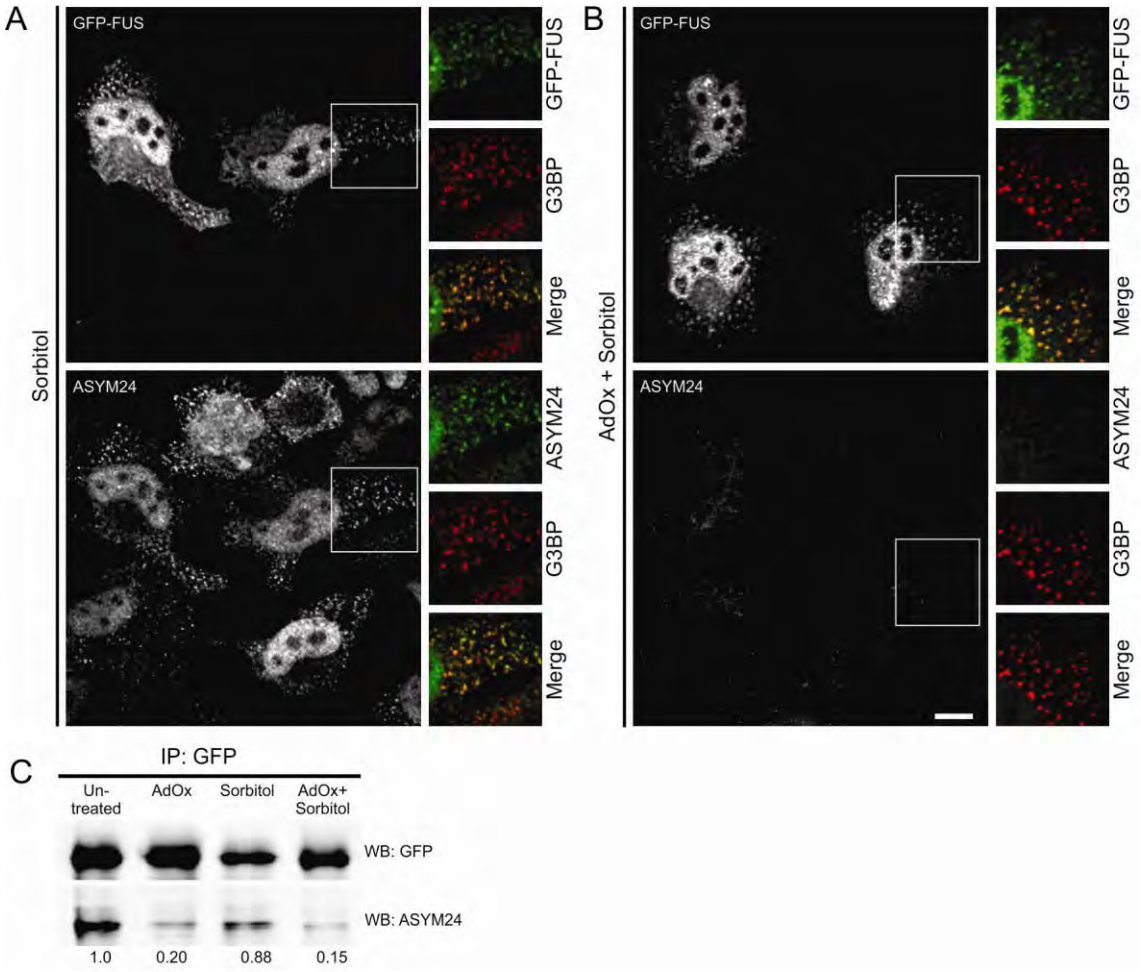
A
GFP-FUS
ASYM24
Sorbitol
GFP-FUS
G3BP
Merge
ASYM24
G3BP
Merge
B
GFP-FUS
ASYM24
AdOx + Sorbitol
GFP-FUS
G3BP
Merge
ASYM24
G3BP
Merge
C
IP: GFP
Un-treated
AdOx
Sorbitol
AdOx+ Sorbitol
WB: GFP
WB: ASYM24
1.0
0.20
0.88
0.15

Figure 2.9

Figure 2.9 Methylation does not regulate the incorporation of FUS into stress granules.

HeLa cells were transiently transfected to express GFP-FUS G515X. Cells were exposed to 0.4 M sorbitol for 1 h either (A) in the absence of AdOx or (B) after cells had been pre-treated with 25 μM AdOx for 8 h. A) Confocal imaging showed that GFP-FUS G515X (green) assembles into G3BP-positive stress granules (red) upon sorbitol treatment (top panel). Co-staining with the ASYM24 antibody (a far-red fluorescence probe was employed; green is used in the images for clarity) revealed that these same stress granules contained asymmetrically dimethylated proteins (bottom panel). B) While the ASYM24 signal is dramatically decreased within stress granules and cells pre-treated with AdOx (bottom panel), there is still a robust association of GFP-FUS with stress granules under the same conditions (top panel). Scale bar represents 10 μm. C) Immunoprecipitation of GFP-FUS G515X with an anti-GFP antibody and a subsequent Western blot analysis with ASYM24 revealed that FUS is hypomethylated due to AdOx pretreatment. The ratio of the ASYM24 signal intensity to that of GFP was determined by densitometry and normalized to the untreated condition. Ratios are shown below the blot for each condition. All data are representative of n = 3 independent experiments.

Cells are susceptible to sorbitol toxicity and death when FUS expression is reduced.

Given that the full response of FUS to hyperosmolar stress includes its assembly into stress granules, and that the role of stress granules is to overcome stress and re-establish cellular homeostasis, we investigated whether the expression of FUS is important for cellular viability under conditions of hyperosmolar stress. The normal cellular response to hyperosmolar stress includes cell cycle arrest, during which time cells may adapt to stress and resume proliferation (Burg *et al.*, 2007). However, severe hyperosmolar stress induces apoptosis and cell death (Burg *et al.*, 2007; Bevilacqua *et al.*, 2010). To address the susceptibility of cells to hyperosmolar toxicity in the absence of FUS, we employed inducible NSC-34 cell lines that stably express either shRNA specific for FUS (shFUS) or a scrambled control shRNA (shSC) sequence. These cell lines are advantageous for cell viability measurements since cell death resulting from chemical transfection protocols is eliminated. NSC-34 cells were induced with doxycycline for 48 hrs, resulting in ~70% knock down of FUS in the shFUS line (Fig. 7A) but not a loss of cell viability in either shFUS or shSC cells (data not shown). Cells were then treated for 8 hrs with either 0.4 M sorbitol or 0.25 mM sodium arsenite as a negative control. Sodium arsenite induces stress granule assembly, however endogenous FUS does not associate with stress granules under this condition (Fig. 2.4). Moreover, others have reported that mammalian cells with knocked-down FUS expression are not susceptible to

sodium arsenite (Aulas *et al.*, 2012). In agreement with this report, we did not detect a difference in percentage cell viability (Fig. 2.10B) or cell death (Fig. 2.10C) between shFUS and shSC cells in response to sodium arsenite using the MTT and LDH assays, respectively. In contrast, the percentage of viable cells was approximately two-fold lower in the shFUS cells compared to shSC cells after sorbitol treatment (Fig. 2.10B). That shFUS cells are more susceptible to sorbitol-induced toxicity was confirmed by the LDH cell death assay, which revealed 3-fold greater cell death in shFUS cells treated with sorbitol compared to shSC cells under the same conditions. Therefore, while the expression of FUS is not required for the assembly of stress granules (Fig. 2.7), cellular homeostasis and survival during hyperosmolar stress is mediated by the expression of FUS.

.

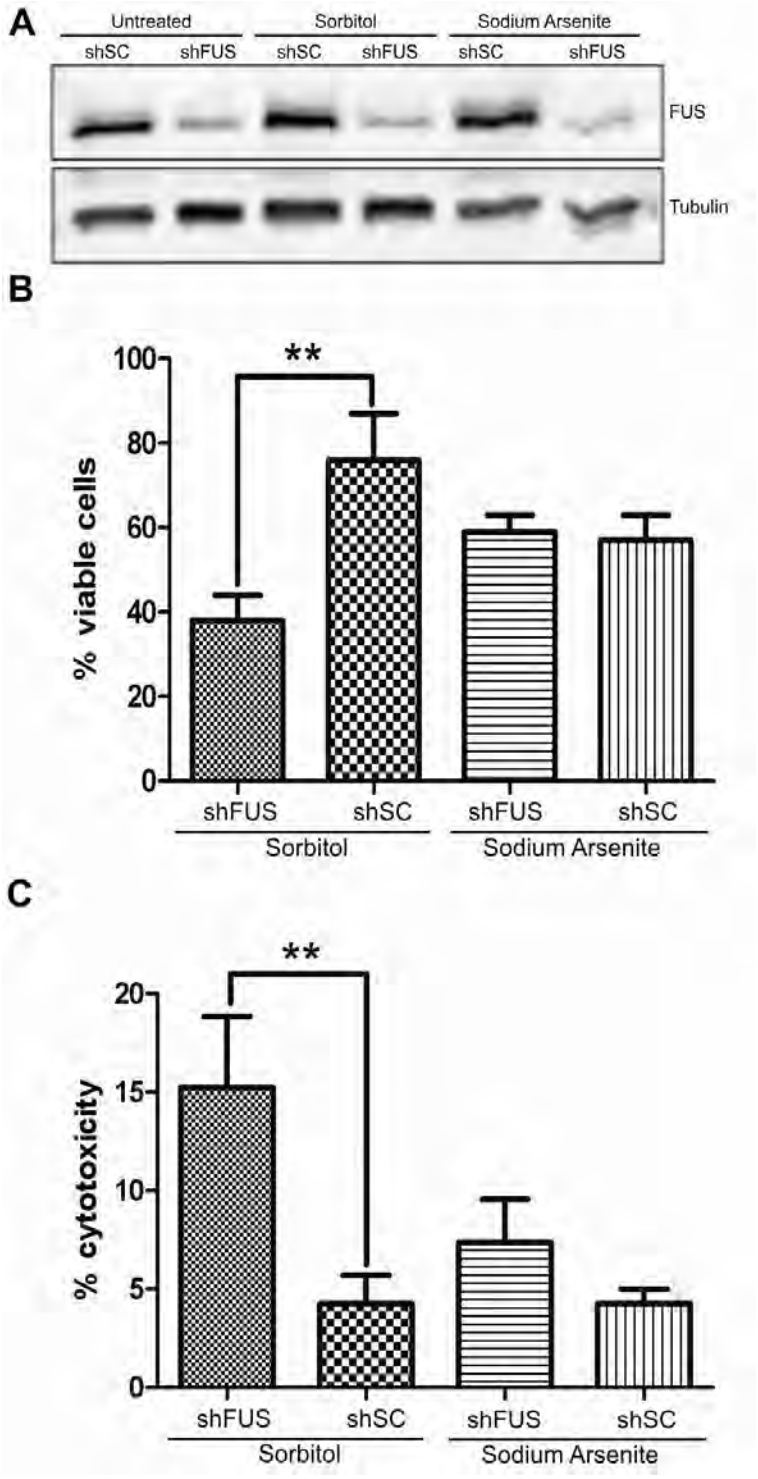
A
Untreated
Sorbitol
Sodium Arsenite
shSC
shFUS
shSC
shFUS
shSC
shFUS
FUS
Tubulin
B
% viable cells
100
80
60
40
20
0
**
shFUS
shSC
shFUS
shSC
Sorbitol
Sodium Arsenite
C
% cytotoxicity
20
15
10
5
0
**
shFUS
shSC
shFUS
shSC
Sorbitol
Sodium Arsenite

Figure 2.10

Figure 2.10 Reduced FUS expression causes cells to become susceptible to sorbitol induced toxicity. A) Expression of either a non-targeting scrambled shRNA (shSC) or shRNA against FUS (shFUS) was induced by doxycycline for 48 h in NSC-34 cell lines, resulting in ~70% knock-down of the FUS protein as determined by Western blot. Tubulin was used as a loading control. Cells were then treated with 0.4 M sorbitol or 0.25 mM sodium arsenite for 8 h and subjected to the (B) MTT cell viability assay or (C) LDH cell toxicity assay. B) A significant decrease in cell viability was detected in shFUS cells (38 ± 6%) compared to shSC cells (76 ± 11%) when treated with sorbitol, whereas shFUS cells did not exhibit an analogous susceptibility to sodium arsenite (59 ± 4% for shFUS vs. 57 ± 6% for shSC). C) A higher percentage of cell death was detected in shFUS cells (15.2 ± 3.6%) compared to shSC cells (4.2 ± 1.4%) in response to sorbitol, whereas no difference in cell death was detected when these lines were stressed with sodium arsenite (7.4 ± 2.2% for shFUS vs. 4.3 ± 0.7% for shSC). B,C) Data shown are an average from n = 3 independent experiments ± standard deviation. Statistical significance was determined by Student's *t*-test (**$P < 0.005$).

DISCUSSION

Although FUS is predominately expressed in the nucleus of most cell types (Andersson *et al.*, 2008), it can shuttle between the nucleus and the cytoplasm during mRNA transport (Zinszner *et al.*, 1997; Fujii and Takumi, 2005). The equilibrium of FUS expression can be shifted towards the cytoplasm using inhibitors against RNA polymerase II (Pol II) (Zinszner *et al.*, 1994) or against the nuclear import receptor Transportin-1 (Trp), also known as Karyopherin β2 (Dormann *et al.*, 2010). Genetic perturbations of its nuclear localization signal (NLS) also increase the cytoplasmic expression of FUS in the neurodegenerative disease ALS (Kwiatkowski *et al.*, 2009; Vance *et al.*, 2009). Herein we demonstrate a novel and robust response of endogenous FUS to hyperosmolar stress, whereby FUS redistributes from the nucleus to the cytoplasm within minutes of exposure to sorbitol (Fig. 2.1), mannitol, sodium chloride, sucrose or polyethylene glycol (Fig. 2.2).

A role for FUS in hyperosmolar stress response is further supported by its association with stress granules under this condition. Stress granules are stalled translational complexes; as such, they are thought to regulate mRNAs processing during stress (Anderson and Kedersha, 2008). Recently, the activity of mTORC1 was shown to correlate with its sequestration inside stress granules, suggesting that these complexes can also regulate cell signaling at the protein level (Wippich *et al.*, 2013). Importantly, no other chemical or environmental stressor has been shown to cause endogenous FUS to redistribute from the

nucleus into the cytoplasm and enter into stress granules. While different stressors, such as oxidative stress and heat shock, have been shown to influence the association of ALS-linked FUS variants with stress granules, the nature of the NLS mutations causes FUS to accumulate in the cytoplasm irrespective of stress (Bosco *et al.*, 2010a; Dormann *et al.*, 2010). In contrast, hyperosmolar stress triggers both the cytoplasmic redistribution of FUS and its assembly into stress granules. Therefore, the response of endogenous FUS to hyperosmolar stress represents an altogether different mechanism compared to the previously described FUS variants. Furthermore, our data support a normal and important role for endogenous FUS in stress response (discussed further below), whereas the association of ALS-linked FUS with stress granules is thought represent a pathogenic mechanism in disease (Wolozin, 2012).

In order to dissect the processes governing the cytoplasmic redistribution of FUS from its incorporation into stress granules, we employed the GFP-FUS G515X construct, which lacks the nuclear localization domain. This allowed us to investigate the role of methylation as a post-translational modification in both events. Inhibition of methyltransferases with AdOx significantly reduced the cytoplasmic redistribution of FUS during hyperosmolar stress (Fig. 2.8). Moreover, analysis with the ASYM24 antibody revealed that FUS is asymmetrically dimethylated at arginine residues under homeostatic conditions but is hypomethylated in the presence of AdOx (Figs. 2.8 and 2.9). These observations, together with a mass spectrometry study demonstrating that ~20

arginine residues within FUS are asymmetrically dimethylated (Rappsilber *et al.*, 2003), supports the possibility that methylation of the FUS protein itself dictates its subcellular localization during hyperosmolar stress. Conversely, the methylation status of FUS, or other cellular factors for that matter, does not appear to regulate the association of FUS with stress granules (Fig. 2.9). A remaining possibility is that other post-translational modifications of FUS influence its association with stress granules.

What are the biological implications of FUS in hyperosmolar stress response? Hyperosmolar stress is implicated in a myriad of disease conditions in humans, including renal failure, diabetes, neurodegeneration and inflammation, as well as disorders of the eye, heart and liver (Brocker *et al.*, 2012). Moreover, the cell shrinkage caused by hyperosmolar stress triggers many adverse subcellular events, such as mitochondrial depolarization, inhibition of DNA replication and transcription, damage to DNA and proteins, and cell cycle arrest, all of which can ultimately lead to cell death (Alfieri and Petronini, 2007; Burg *et al.*, 2007; Brocker *et al.*, 2012).

Our results are consistent with a prosurvival mechanism for endogenous FUS in human conditions that involve hyperosmolar stress. First, the response to hyperosmolar stress is specific, since alternative stressors that induce stress granule assembly such as oxidative stress and heat shock fail to elicit a similar response from endogenous FUS (Figs. 2.4). This data suggests a potentially distinct cellular response to hyperosmolar conditions compared to other

stressors. Second, cells are more susceptible to hyperosmolar toxicity when FUS expression is reduced (Fig. 2.10), supporting a prosurvival role for FUS in this type of stress response.

Other nuclear hnRNPs, such as hnRNP A1, also respond to hyperosmolar stress by redistributing to the cytoplasm and assembling into stress granules. When localized to stress granules, hnRNP A1 is thought to specifically suppress the translation of anti-apoptotic factors and in turn initiates apoptosis under conditions of severe hyperosmolar stress (Bevilacqua *et al.*, 2010). An intriguing possibility is that FUS sequesters specific mRNAs and proteins into stress granules, thereby altering their expression and/or function in response to the hyperosmolar stress. Indeed, recent PAR-CLIP (Hoell *et al.*, 2011) and RIP-Chip (Colombrita *et al.*, 2012) analyses have identified thousands and hundreds, respectively, of mRNA transcripts that are bound by FUS in the cell under homeostatic conditions. Interestingly, FUS binds mRNA that encodes genes involved in DNA damage repair and cell cycle regulation (Colombrita *et al.*, 2012), two pathways that are altered during hyperosmolar stress (Burg *et al.*, 2007).

In summary, our results support a prosurvival function for endogenous FUS during hyperosmolar stress. These findings have implications for human disorders with an etiology that involves hyperosmolar stress. Identifying the factors that regulate the response of FUS to hyperosmolar stress, as well as the

pathways affected by FUS under this stress condition, will be critical to further our understanding of this prosurvival role of FUS.

MATERIALS AND METHODS

Cell culture and induced stress

HeLa cells and HEK293 cells were cultured in minimal essential medium (MEM, Gibco, Grand Island, NY, USA) supplemented with 10% fetal bovine serum (FBS, Sigma, St. Louis, MO, USA) and 1% penicillin and streptomycin (P/S, Gibco, Grand Island, NY, USA) under standard culture conditions (37°C, 5% CO_2/95% air). NSC-34 cells and mouse embryonic fibroblasts (MEFs) were cultured in Dulbecco's MEM (DMEM, Gibco, Grand Island, NY, USA) supplemented with 10% FBS and 1% P/S under standard culture conditions. FlpIn HEK293 cells with stably integrated GFP-FUS G515X were cultured as described previously (Bosco *et al.*, 2010a). Sorbitol, mannitol (Sigma, St. Louis, MO, USA), PEG-3350 and PEG-8000 (Fisher Scientific, Pittsburgh, PA, USA) were dissolved directly into the media to obtain the indicated final concentrations and added to the cells (Kedersha and Anderson, 2007). Sucrose (Electron Microscopy Sciences, Fort Washington, PA, USA) was dissolved into media to obtain a final concentration of 600 osmol/L and added to the cells (Bevilacqua *et al.*, 2010). Stock solutions of 100 mM sodium arsenite (Sigma, St. Louis, MO, USA) in DMSO (Sigma, St. Louis, MO, USA), 10 mM thapsigargin (Sigma, St. Louis, MO, USA) in DMSO, 1 M hydrogen peroxide (Sigma, St. Louis, MO, USA) in media, 30 mM emetine (Sigma, St. Louis, MO, USA) in water, 20 mM Adenosine-2′,3′-dialdehyde (AdOx, Sigma, St. Louis, MO, USA) in water and 5 M sodium chloride (Fisher Scientific, Pittsburgh, PA, USA) in water were prepared

and added to the media to obtain the final concentrations of 0.5 mM, 50 μM, 1.5 mM, 50 μg/mL, 50 μM and 0.2 M respectively. Doxycycline (Sigma, St. Louis, MO, USA) was used at a final concentration of 1 μg/mL from a stock of 50 mg/mL prepared in water. Cells were exposed to heat shock by adding media, pre-warmed to 43°C, followed by immediate transfer to an incubator set to 43°C. ON-TARGETplus SMARTpool (Dharmacon, Waltham, MA, USA) consisting of a pool of siRNAs against FUS (Cat # L-009497-00-0005,) and ON-TARGETplus Non-targeting pool siRNA (Cat # D-001810-10-05) as control were transfected using Lipofectamine-2000 (Invitrogen, Grand Island, NY, USA) according to the manufacturer's instructions.

NSC-34 cell lines were a kind gift from Dr. Neil Cashman (University of British Columbia). Stable NSC-34 cell lines expressing short hairpin (sh) RNA against mouse FUS (shFUS) or non-targeting scrambled RNA (shSC) were prepared by first transducing with the Tet repressor. A single clone that demonstrated good induction without any leaky expression was then selected. NSC34-TetR cells were then transduced with inducible lentivirus-Tet-on/shFUS or Tet-on/shSC (Ishigaki *et al.*, 2012). Cells were treated with 1 μg/mL doxycycline to induce the expression of the shRNAs.

Immunofluorescence

Immunofluorescence was performed as described in (Bosco *et al.*, 2010a). Primary antibody incubation conditions were as follows: 1:500-1000 rabbit anti-FUS (A300-293A, Bethyl Labs, Montgomery, TX, USA); 1:2500 mouse anti-TIAR

(610352, BD Transduction Labs, San Jose, CA, USA); 1:1500 rabbit ant-ASYM24 (07-414, Millipore, Billerica, MA, USA); 1:2500 mouse anti-G3BP (611126, BDTransduction Labs, San Jose, CA, USA) for 1 hr at room temperature; and 1:250 mouse anti-GE-1/hedls/p70 S6 kinase (sc-8418, Santa Cruz Biotechnology, Santa Cruz, CA, USA) for 12 hrs at 4°C. Secondary anti-mouse IgG antibody conjugated to Dylight 549 (715-505-151, Jackson ImmunoResearch Labs, West Grove, PA, USA) was used at 1:1500–1:3000. Secondary anti-rabbit IgG antibody conjugated to Dylight 488 (711-485-152, Jackson ImmunoResearch Labs, West Grove, PA, USA) and secondary anti-rabbit IgG antibody conjugated to Cy5 (711-175-152, Jackson ImmunoResearch Labs, West Grove, PA, USA) were used at 1:1500–1:3000. GFP signal was enhanced using 1:2000 Alexa Fluor 488-conjugated rabbit anti-GFP (A21311, Invitrogen, Grand Island, NY, USA). Nuclei were stained with 50 nM 4',6'-diamidine-2-phenylindole dihydrochloride (DAPI; D1306, Invitrogen, Grand Island, NY, USA) for 5 min at room temperature. Coverslips were mounted with ProLong Gold Antifade Reagent (P36930, Invitrogen, Grand Island, NY, USA).

Image acquisition and quantification

Fixed cell images were acquired using a Solamere Technology Group CSU10B (Salt Lake City, UT, USA) spinning disk confocal system as described (Bosco *et al.*, 2010a) or using a Leica DMI6000B microscope (Leica Microsystems, Buffalo grove, IL, USA). For images acquired with the Leica microscope, a 100x objective was used with LAS AF One Software (Leica

Microsystems, Buffalo Grove, IL, USA) and the Leica DFC365FX camera. Maximum projection images were created from acquired image stacks (z=0.2-0.25µm, n=6-44 planes) and analyzed using NIH Image J software.

For quantifying the percentage (%) of nuclear FUS, image stacks (z=0.2µm, n=13 planes) of 60 cells were collected from n=3 experiments with the spinning disk confocal system above. Images were analyzed using MetaMorph software (Molecular Devices, Sunnyvale, CA, USA). Sum projections of each image stack were created after subtracting the background signal as described (Bosco *et al.*, 2010a). The integrated morphometry analysis tool was used to calculate the percent (%) nuclear FUS. Statistical significance between conditions was determined by an ANOVA and Tukey's post-hoc pairwise test.

Western blots

Western blots were performed essentially as described previously (Bosco *et al.*, 2010a). Briefly, blots were incubated at 4°C with shaking overnight in the presence of primary antibodies as per the following dilutions: 1:500 anti-tubulin (Sigma, St. Louis, MO, USA), 1:500 anti-FUS (in house antibody created against 264-284 peptide sequence of FUS, Genscript, Piscataway, NJ, USA), 1:500 anti-FUS (47711, Santacruz, Santa Cruz, CA, USA) and 1:1000 anti-ASYM24 (07-414, Millipore, Billerica, MA, USA). Densitometry was performed using the Odyssey infrared imaging systems software (Licor Biosciences, Lincoln, NE, USA).

Immunoprecipitation

Cells resuspended in 50 mM Tris HCl (pH 7.5) supplemented with 1% NP-40, 150 mM NaCl, 5 mM EDTA, 10% glycerol and complete protease inhibitor (lysis buffer) were briefly sonicated and incubated at 4°C with shaking for 30 min. The lysates were centrifuged for 15 min at 13000 rpm and 4°C. Pre-clearing of the supernatants was achieved by incubation with 100 µL of Biomag Protein G beads (Invitrogen, Grand Island, NY, USA) at 4°C with shaking for 2 hrs. The beads were removed with a magnet and the protein concentration of the supernatant was determined using a bicinchoninic assay (ThermoScientific, Billerica, MA, USA). Anti-FUS (Genscript, Piscataway, NJ, USA) or anti-GFP antibody (ab290, Abcam, Cambridge, MA, USA) was bound to fresh beads with shaking for 2 hrs at 4°C. A total of 1 mg of the pre-cleared supernatant was then added to 100 µL of antibody-bound beads and incubated overnight with shaking at 4°C. The lysate was removed and beads were washed three times with lysis buffer. Proteins bound to the beads were eluted with 1X SDS sample buffer at 95°C for 5 min, and probed by western as described above.

Cell toxicity assays

NSC-34 cell lines shSC and shFUS were plated in 24 well dishes. 48 hrs after induction with doxycyline, cells were treated with 0.4 M sorbitol or 0.25 mM sodium arsenite for 8 hrs. For the MTT (3-[4,5-dimethylthiazol-2-yl]-2,5-diphenyl tetrazolium bromide) assay 100 µL of 5 mg/mL MTT (Invitrogen, Grand Island, NY, USA) was added to the wells for 35 min followed by cell lysis overnight with

300 µl lysis buffer (10% SDS in 1:1 *N*,*N*_-dimethylformamide:water/2% acetic acid/2.5% HCl 1 M) and absorbance measurement at 550 nm using the VICTOR V plate reader (Perkin Elmer, Waltham, MA, USA). Cell viability for each sample was calculated using the formula: % viability = 100 × (OD_{Sample} – OD_{Blank})/($OD_{Untreated}$ – OD_{Blank}). LDH (Lactate dehyrodenase) assay was performed as per manufacturer's protocol (CytoTox 96® Non-radioactive Cytotoxicity Assay, Promega, Madison, WI, USA). After the 8 hr treatment, 50 µL of media from each well was transferred to wells of 96 well plate. 50 µL of substrate mix was then added to each well and the plates were covered and incubated at ambient temperature, protected from light for 30 min. After the incubation, 50 µL stop solution was added to each well and absorbance was recorded at 490 nm using the above plate reader. Percentage (%) cytotoxicity was determined for each experimental condition (Expt) using the formula: % cytotoxicity = 100 × (OD_{Expt} – $OD_{Untreated}$)/(OD_{Max} – $OD_{Untreated}$), where OD_{Max} represents the absorbance of the media from a well with complete lysis of cells releasing maximum LDH. All assays were performed at least three independent times. Statistical significance was determined by a two-tailed Student's t-test.

Acknowledgements

We acknowledge the assistance from Dr. Paul Furcinitti of the UMass Medical School Core Digital Imaging Facility. We would like thank Maeve Tischbein for her assistance with the immunofluorescence experiments, and Dr. Neil Cashman from University of British Columbia for naïve NSC-34 cell lines. We acknowledge financial support from the Worcester Foundation (DAB) and the US National Institutes of Health/ National Institute on Neurological Disorders and Stroke (R01NS078145-01 to DAB) for this work.

Preface to Chapter III

A large part of the work presented in this chapter was performed by Reddy Ranjith K Sama (RRKS) with the exceptions below:
Vesicle motility assays were performed by RRKS, Yuyu Song, Gerardo Morfini and Scott T Brady. Limited proteolysis experiments were performed by RRKS and Melissa Rotunno. Fluorescence anisotropy was performed and analyzed by Osman Bilsel. Size exclusion chromatography and mass spectrometry analyses were performed by Melissa Rotunno.

Chapter III

Protein misfolding and aberrant kinase activation contribute to the pathogenicity of ALS-causing FUS variants.

Reddy Ranjith K Sama[1,2], Melissa Rotunno[1,2], Yuyu Song[3], Osman Bilsel[4], Robert H Brown Jr.[1], Gerardo Morfini[5], Scott T Brady[5] , Daryl A Bosco[1,2,4]

[1]Department of Neurology,

[2]Department of Cell and Developmental Biology,

[4]Department of Biochemistry and Molecular Pharmacology,

University of Massachusetts Medical School, Worcester, MA, USA.

[3]Department of Genetics, HHMI, School of Medicine,

Yale University, New Haven, CT, USA

[5]Department of Anatomy and Cell Biology,

University of Illinois at Chicago, Chicago, IL, USA.

ABSTRACT

More than 40 mutations in the gene encoding Fused in Sarcoma/Translocated in Liposarcoma (FUS/TLS or FUS) have been identified as a causal link to familial amyotrophic lateral sclerosis (fALS) – a progressive neurodegenerative disease characterized by loss of motor neurons. However, the pathogenic mechanisms by which FUS variants cause this disease remain largely unknown. Using recombinant GST-tagged FUS proteins we show that ALS mutations (R521G, R495X and G230C) induce protein misfolding compared to the WT protein. Interestingly, these FUS variants inhibit fast axonal transport (FAT) in a squid axoplasm based vesicle motility assay. The inhibitory effect was specific to the FUS variants as WT protein had no effect on FAT. Inhibitors of p38 MAPK completely rescued mutant-FUS mediated FAT inhibition. Importantly, tissue samples from several ALS patients with FUS mutations demonstrated higher p38 expression and phosphorylation compared to non-ALS controls. These results indicate that the pathogenic mechanism of FUS variants in causing ALS involves the p38 MAP kinase pathway, possibly a result of structural perturbations induced by the disease causing mutations in FUS.

INTRODUCTION

Mutations in several genes including *SOD1* (Rosen *et al.*, 1993), *FUS* (Kwiatkowski *et al.*, 2009; Vance *et al.*, 2009), *TARDP* (Gitcho *et al.*, 2008; Kabashi *et al.*, 2008; Rutherford *et al.*, 2008; Sreedharan *et al.*, 2008; Van Deerlin *et al.*, 2008; Yokoseki *et al.*, 2008), *PFN1* (Wu *et al.*, 2012) and *C9ORF72* (DeJesus-Hernandez *et al.*, 2011; Gijselinck *et al.*, 2011; Renton *et al.*, 2011) have been associated with familial amyotrophic lateral sclerosis (fALS), a progressive neurodegenerative disease that primarily affects both lower and upper motor neurons of brain and spinal cord. About 10% of all ALS cases are fALS and have a disease history within the families of patients, while the remaining 90% of the cases are sporadic (sALS) with no family history. Multiple pathogenic events affect various cellular pathways throughout the rapid course of the disease. Impaired axonal transport, mitochondrial dysfunction, excitotoxicity, oxidative stress, protein misfolding, inflammation, abnormal activation of proteases and kinases, have all been thought to contribute to the disease pathology (Pasinelli and Brown, 2006).

Mutations in FUS account for about 5% of all fALS cases. FUS, also known as TLS or FUS/TLS, is an RNA/DNA binding protein that has been implicated in numerous cellular functions including DNA damage repair, transcription, RNA processing and stress response. The domain structure of FUS includes an N-terminal SYGQ-rich domain, a Glycine-rich region, an RNA-binding domain (RRM), a zinc-binding domain and the C-terminal RGG-rich domains and

a putative nuclear localization sequence (NLS). The C-terminal NLS harbors the majority of fALS causing mutations in FUS. Even though FUS, a nucleo-cytoplasmic shuttling protein, is found predominantly in the nucleus under normal conditions, most of these mutations result in cytoplasmic mislocalization of the protein. Such a mislocalization seems to result in both loss of normal function and gain of toxic function for FUS. While several studies have focused on understanding the implications of mutant-FUS mislocalization, how these FUS variants exert their toxic effects is not completely understood. In particular, whether the mutations produce structural changes that result in protein misfolding is still unknown.

Accumulation of misfolded proteins and/or their aggregates in various neuronal tissues has been observed in several neurodegenerative diseases. In fact, such an accumulation serves as the characteristic feature of several of these diseases. Protein misfolding can occur due to both genetic (mutations) and non-genetic perturbations (eg. post-translational modifications). The toxic confirmation resulting from protein misfolding can impair several cellular functions/pathways that can ultimately cause neuronal dysfunction and/or apoptosis (Soto and Estrada, 2008). Thus, protein misfolding has been a key area of investigation in ALS pathogenesis. In particular, the consequences of SOD1 misfolding and its role in ALS have been extensively investigated (reviewed in (Rotunno and Bosco, 2013)).

However, as mentioned earlier, whether ALS-causing mutations result in FUS misfolding is unclear and whether such misfolding contributes to the pathogenic effects of FUS is unknown. In the present study, we show that ALS-linked FUS variants are misfolded using fluorescence anisotropy and limited proteolysis of recombinant proteins. We also show that misfolding has a functional consequence in that the FUS variants specifically inhibit fast axonal transport (FAT) as determined by a squid based vesicle motility assay while the WT FUS had no effect. The inhibition was rescued when p38 MAP kinase activity was blocked, indicating a role for the p38 pathway in mediating the effects of FUS variants. Furthermore, we show that p38 expression and phosphorylation is upregulated in patients with ALS. These results provide a novel insight into the mechanism by which FUS variants can lead to pathogenic effects in ALS.

RESULTS

ALS-linked mutations induce structural perturbations in FUS

Mutations in FUS that cause ALS result in subcellular mislocalization of the FUS protein, impaired transcriptional regulation and altered stress granule dynamics (Baron *et al.*, 2013; Dormann and Haass, 2013). However, whether these changes are a consequence of FUS misfolding is not known. In order to examine conformational differences between WT and FUS variants, purified GST-tagged FUS proteins (WT, R521G, R495X and G230C; Fig 3.1) were subjected to time-resolved anisotropy by measuring the excited-state decay of tryptophan (Trp) residues in the GST-FUS proteins. The variants used here were chosen so as to represent the numerous mutations within FUS in terms of their location and severity of disease - G230C in the Gly-rich region, R521G in the C-terminal NLS region and the truncation mutant R495X which truncates the entire NLS and has a relatively severe disease phenotype (Bosco *et al.*, 2010a; Waibel *et al.*, 2012). All GST-FUS proteins have 4 Trp residues in the GST region and 3 Trp residues in the FUS regions (Fig 3.1). The difference in mobility (tumbling) of these Trp residues, serves as an indicator of the structural differences between those proteins. The raw intensity-decay data obtained were fit to an associative decay model (Fig 3.2A). The anisotropy was then determined from both the raw and fitted intensity-decay data for each FUS protein (Fig 3.2B). Both the intensity-decay data and anisotropy data correlated exactly with the fitted model. Overlay of the fitted anisotropy data revealed that the WT FUS had an anisotropy

that is different from all the three FUS variants, which had a very similar anisotropy to one another (Fig 3.2C). Correlation times of the FUS variants were determined to be very long (59.4 ns for R521G, 50.7 ns for R495X and 44.7 ns for G230C) indicating limited mobility of the FUS variants. However, the correlation time of WT was much longer (> 60ns) than that of the FUS variants, indicating severely limited mobility of the Trp side chain. Thus these results indicate that WT FUS is structurally different than the three FUS variants.

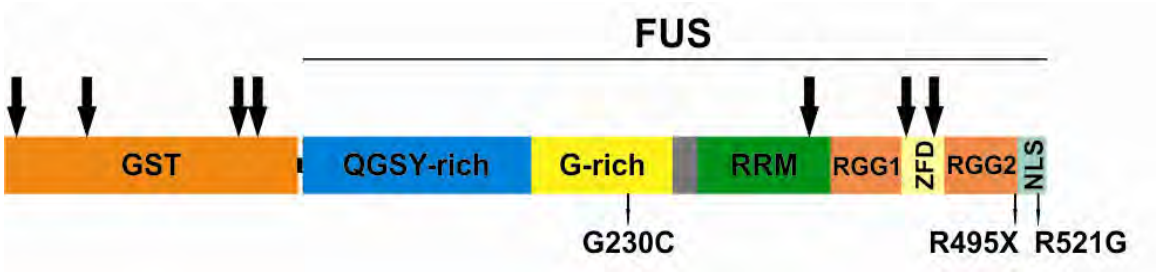

Figure 3.1

Figure 3.1 Domain structure of GST-FUS protein and ALS mutations.

Secondary structure of FUS with N-terminal GST-tag and the ALS-linked mutations, R521G, G230C and R495X are shown. Arrows indicate the amino acid position of tryptophan residues. QGSY-rich, glutamine-glycine-serine-tyrosine-rich; G-rich, glycine-rich; RRM, RNA recognition motif; RGG, arginine-glycine-glycine-rich; ZFD, zinc-finger domain; NLS, nuclear localization signal. Arrows indicate the position of tryptophan residues.

A)

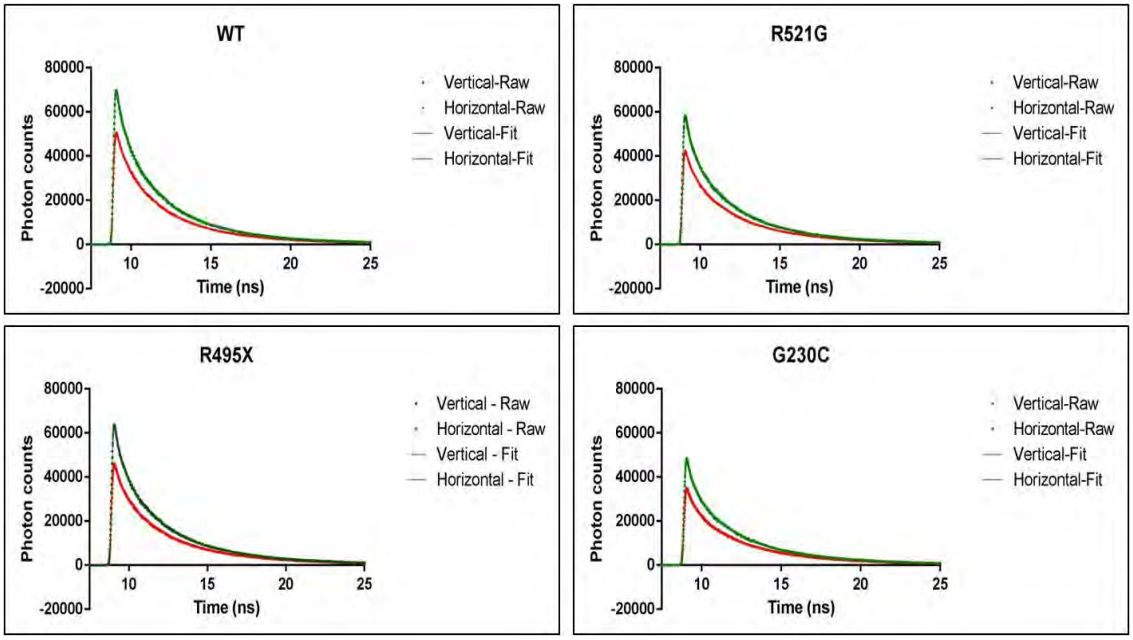
WT
R521G
R495X
G230C
Photon counts
Time (ns)
Vertical-Raw
Horizontal-Raw
Vertical-Fit
Horizontal-Fit
Vertical - Raw
Horizontal - Raw
Vertical - Fit
Horizontal - Fit

B)

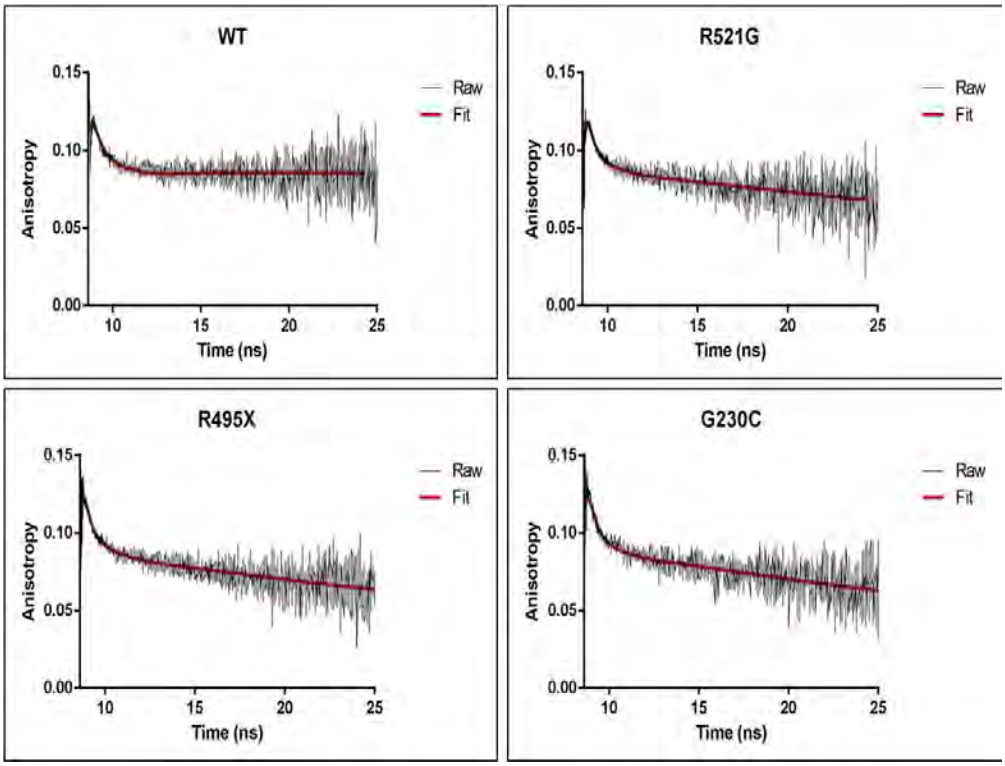
WT
R521G
R495X
G230C
Anisotropy
Time (ns)
Raw
Fit

C)

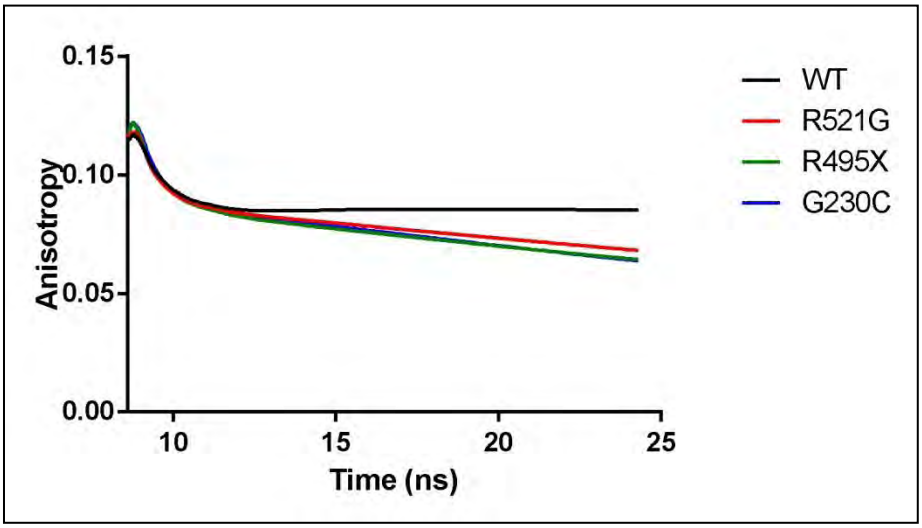
0.15
0.10
0.05
0.00
Anisotropy
10
15
20
25
Time (ns)
WT
R521G
R495X
G230C

Figure 3.2

Figure 3.2

Figure 3.2 Tryptophan fluorescence anisotropy of FUS proteins

A) The intensity decay plots showing the overlay of raw data of vertical and horizontal components of the emitted light with their corresponding fitted data shows the reliability of the model. B) Similarly the raw and fitted anisotropy calculated from the corresponding intensity decay values shows that modeled data corresponds with the raw data. C) Overlay of the modeled anisotropy plots of WT and the three FUS variants (R521G, R495X, G230C) show that the anisotropy of WT is different from that of the three variants which themselves are similar to one another.

A limited proteolysis experiment was performed next to identify structural differences between WT and ALS-linked FUS variants. FUS proteins (WT, R521G, R495X and G230C) were subjected to varying concentrations of chymotrypsin for 20 min at 25 °C. Enzymatically cleaved proteins were separated using SDS-PAGE and stained with coomassie blue to visualize the protein fragments. Limited proteolysis of WT exhibited a distinct cleavage pattern compared to the three FUS variants, all of which were identical to one another (Fig 3.3), indicating that WT is structurally distinct from FUS variants. In particular, three fragments of molecular weight (MW) between 25 and 37 kD appeared equally prominent among the FUS variants (Figure 3.3) while only one fragment appeared in the WT in that MW range. Furthermore, peptides between 37 and 50 kD that were present for the FUS variants (Figure 3.3) were absent in the WT. Although a loss of arginine in R521G and R495X could affect the way peptides get separated on SDS-PAGE, due to the charge differences, a similar peptide pattern was observed with G230C, indicating that the loss of arginine does not have an effect on the SDS-PAGE of the peptides. Overall, these results are consistent with a misfolded conformation for ALS-linked FUS proteins.

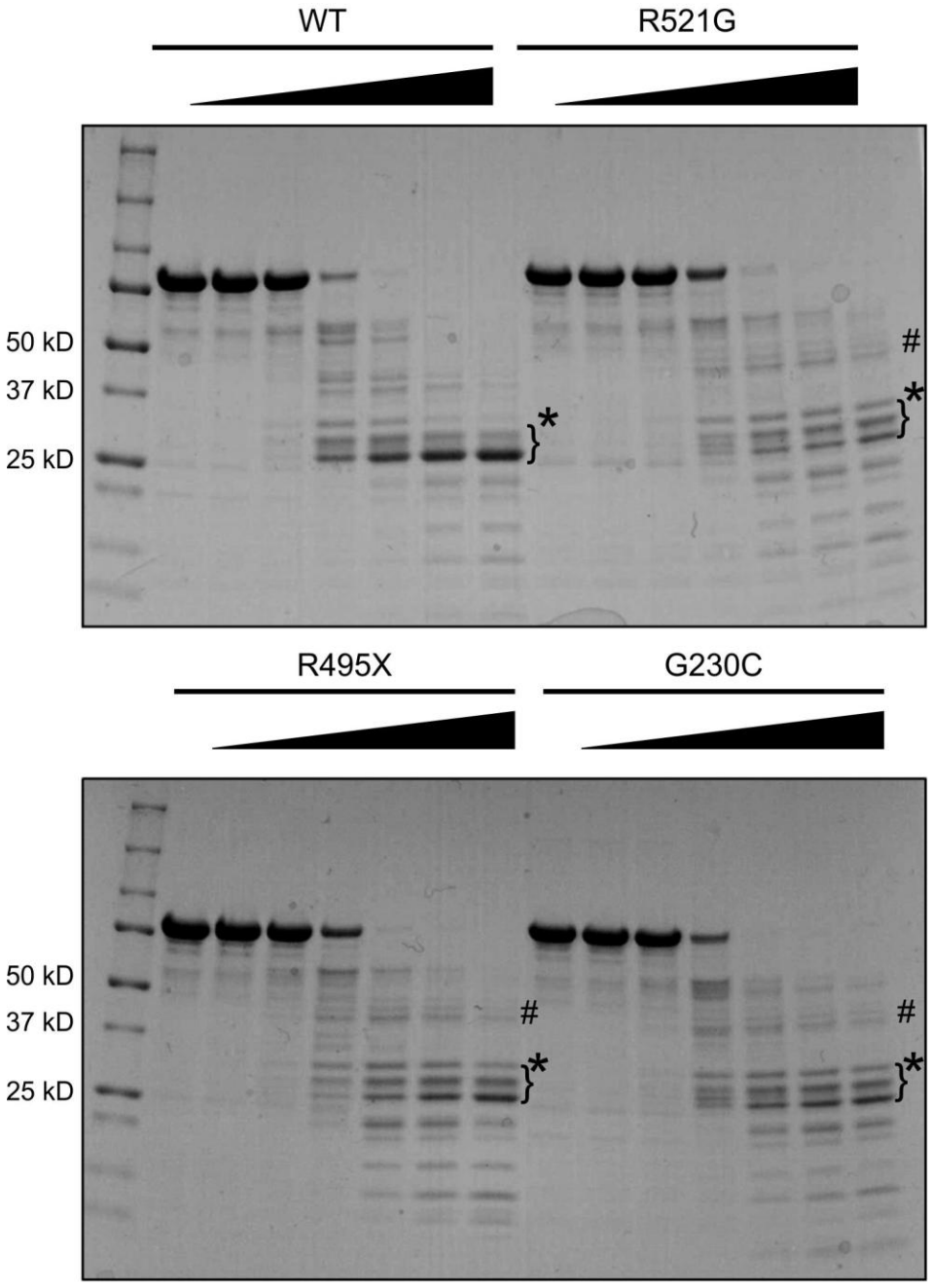

Figure 3.3

Figure 3.3 Structural differences between WT and ALS-linked FUS proteins

FUS proteins (WT, R521G, R495X and G230C) were digested with increasing concentrations of chymotrypsin (0, 1:250000, 1:25000, 1:1250, 1:833, 1:500 (w/w) enzyme to protein) for 20 min at 25 °C and the peptides were separated by SDS-PAGE. Representative gels (n=3) stained with coomassie blue revealed that the cleavage pattern of WT was distinct from the three FUS variants, all of which exhibited the same pattern. Peptides denoted by # are present in the FUS variants but not in the WT protein while peptides within the region denoted by * has three prominent bands for FUS variants and only one prominent band for the WT.

The limited proteolysis experiments show that fragments between 25 and 37 kD, preferentially accumulate in the FUS variants as chymotrypsin concentration is increased. When FUS proteins (WT and R521G) were digested with a fixed concentration of chymotrypsin (1:500 (w/w) enzyme to protein) over a time course (0, 10, 20 min, 2 or 24 h), the cleavage pattern looked similar between WT and mutant-FUS by 24 h (Fig 3.4). However mutant-FUS required longer incubation time to obtain cleavage similar to WT, as the pattern was different between these proteins for at least the first 2 h of the experiment. These results indicate that mutant FUS structure is better protected from enzymatic digestion compared to WT FUS and requires longer incubation with chymotrypsin to be digested to a similar extent as WT FUS.

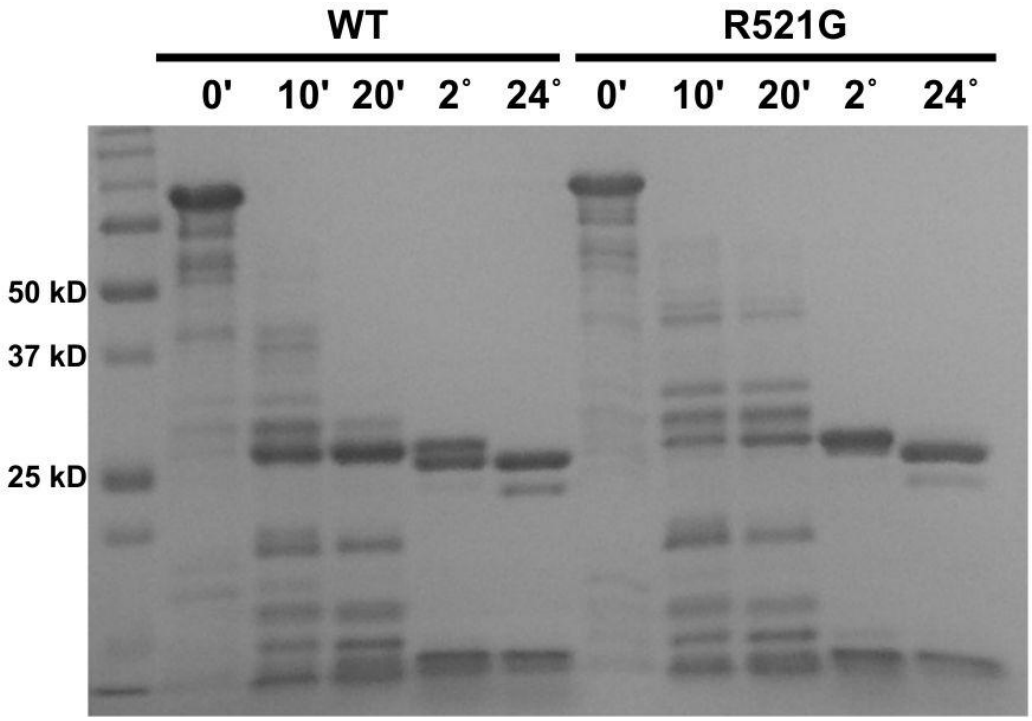

Figure 3.4

Figure 3.4 Mutant-FUS proteins require longer chymotrypsin incubation for complete digestion

FUS proteins (WT and R521G) were digested with chymotrypsin (1:500 (w/w) enzyme to protein) for 0, 10, 20 min, 2 or 24 h and the peptides were separated by SDS PAGE. Representative gels (n=2) stained with coomassie blue revealed that the cleavage pattern of WT FUS was distinct than that of the mutant-FUS protein at least until 2 h. By 24 h, both the patterns were indistinguishable. These results indicate that mutant-FUS requires longer incubation with chymotrypsin to be digested to a similar degree as WT FUS.

Limited proteolysis experiments show that despite differences in the sequence location of FUS mutations (G230C in the glycine-rich region, R521G in the C-terminal NLS region, and the truncation mutation R495X which completely eliminates the NLS) they all result in misfolding of FUS. The resistance of FUS mutants to chymotrypsin cleavage, indicated by the presence of higher number of peptides, suggests that the mutants are protected better from chymotrypsin digestion than WT. In order to identify the regions that are variably protected between WT and FUS variants, the fragments obtained after digestion with chymotrypsin were probed with an antibody against GST (Ab1) and several antibodies against different regions of FUS (Ab2-7; Fig 3.5A) by western blot. All the antibodies recognized the four undigested FUS proteins. Interestingly, the GST antibody (Ab1) and Ab2 (against residues 1-50 at N-terminal of FUS) identified several peptides in the FUS variants but only one major peptide in WT (Fig 3.5B). That these antibodies recognize GST and the N-terminal region of FUS suggests that the N-terminal region of FUS variants is protected from proteolysis by chymotrypsin. On the other hand, none of the other antibodies showed any major differences in the digestion pattern between the FUS proteins (Fig 3.5C). These results indicate that there are minimal to no structural differences in other regions of the proteins or that the conditions used here (enzyme, concentration, time of digestion) only captures differences in the N-terminal region.

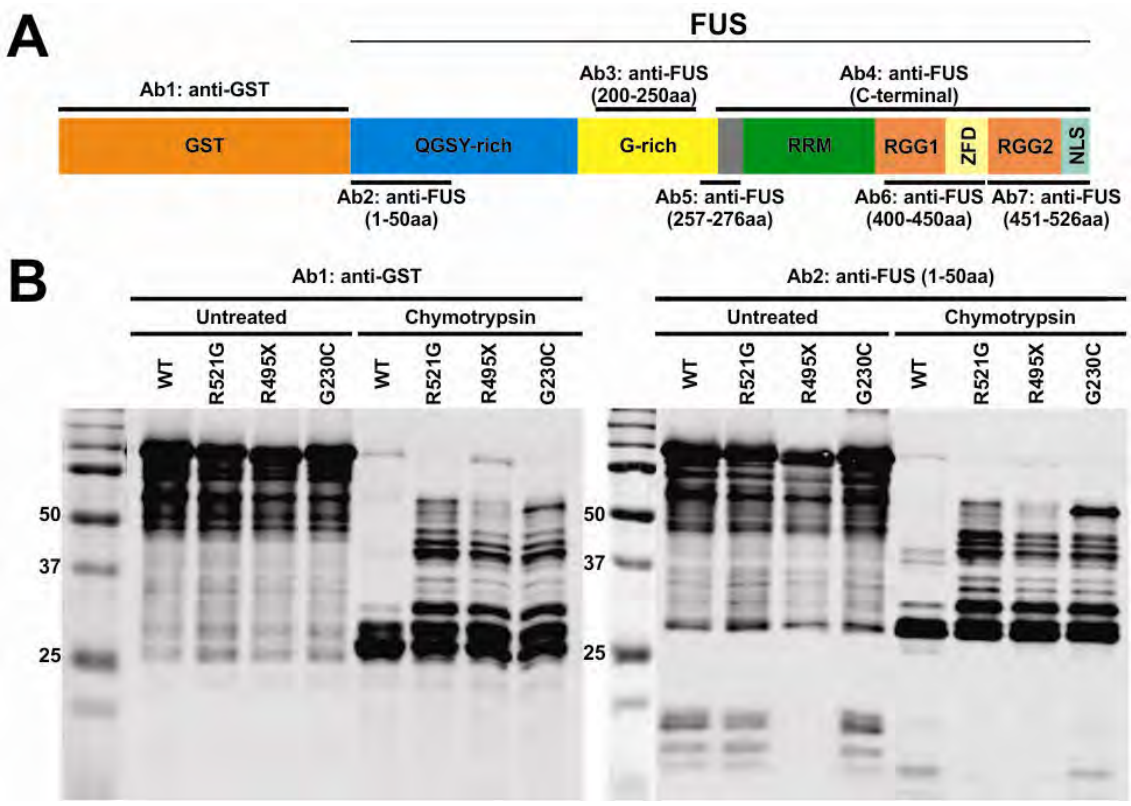
A
FUS
Ab1: anti-GST
Ab3: anti-FUS
(200-250aa)
Ab4: anti-FUS
(C-terminal)
GST
QGSY-rich
G-rich
RRM
RGG1
ZFD
RGG2
NLS
Ab2: anti-FUS
(1-50aa)
Ab5: anti-FUS
(257-276aa)
Ab6: anti-FUS
(400-450aa)
Ab7: anti-FUS
(451-526aa)
B
Ab1: anti-GST
Ab2: anti-FUS (1-50aa)
Untreated
Chymotrypsin
WT
R521G
R495X
G230C
50
37
25

Figure 3.5

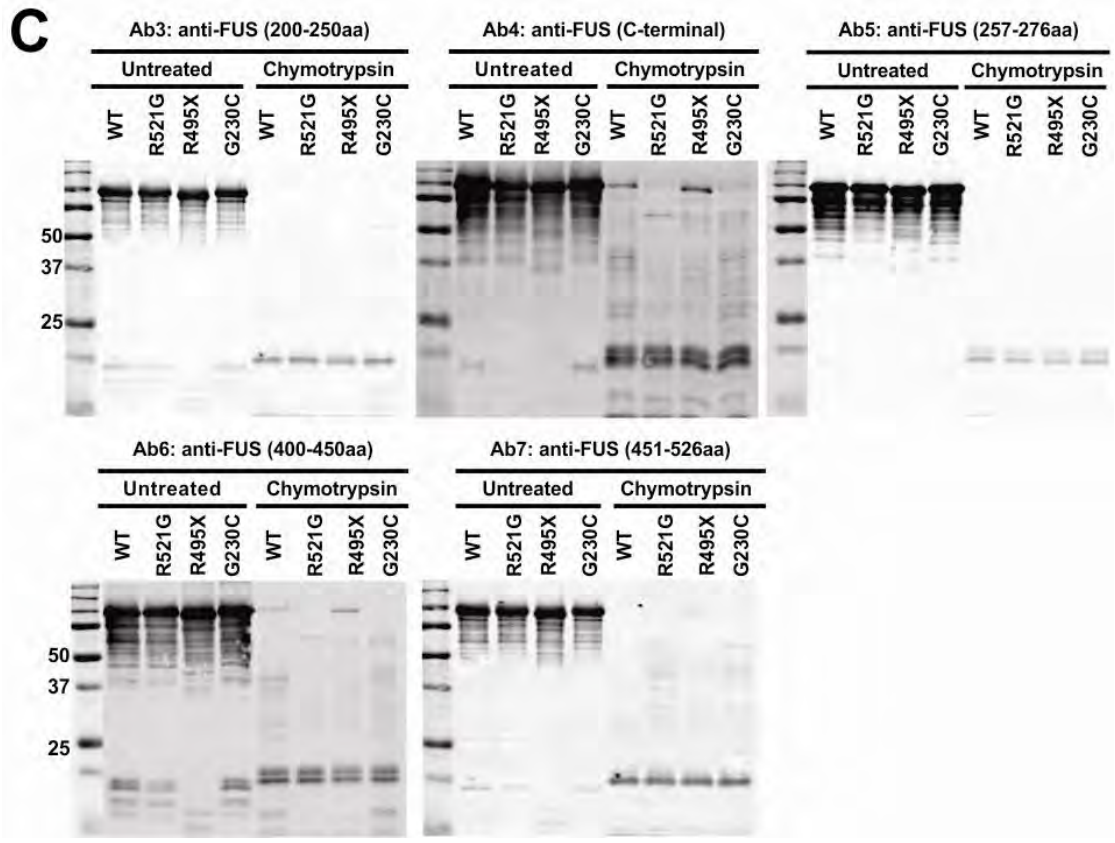
C
Ab3: anti-FUS (200-250aa)
Ab4: anti-FUS (C-terminal)
Ab5: anti-FUS (257-276aa)
Ab6: anti-FUS (400-450aa)
Ab7: anti-FUS (451-526aa)
Untreated
Chymotrypsin
WT
R521G
R495X
G230C
50
37
25

Figure 3.5

Figure 3.5 Antibody mapping of enzymatically digested FUS peptides

A) The epitopes for the indicated anti-GST and FUS antibodies used in this study are mapped onto the domain structure of GST-FUS. B) FUS proteins were either undigested or digested with chymotrypsin for 20 min at 25 °C and western blot analyses were performed using the antibodies indicated in (A). Intact FUS proteins were detected by all antibodies tested. B) Both GST (Ab1) and FUS (Ab2) antibodies revealed differences in digestion pattern between WT and FUS variants. C) None of the other antibodies (Ab3-7) showed any major differences between WT and FUS variants.

In order to identify the specific N-terminal region that is better protected in FUS variants, the bands between 25 and 37 kD (three for R521G and 1 for WT, see Fig 3.3) were excised from the gel and subjected to mass spectrometry analysis (Fig. 3.6A). To determine the abundance of each peptide, extraction ion chromatogram (EIC) was generated first for each peptide identified in both WT and R521G samples from two independent experiments (Fig. 3.6B). The peak area for the peptides was determined from the EICs and the ratio of WT/R521G was calculated as an average for the two independent experiments (Table 3.1). An increase or decrease by 50% or more (WT/R521G<=0.5 or >=1.5) indicated a change in peptide abundance while the rest of the peptides were considered as unchanged. The WT/R521G ratio revealed several peptides within the QGSY-rich region of FUS that are more abundant in the mutant (WT/R521G <= 0.5; Table 3.1 and Fig. 3.6C, shown in blue). Furthermore, the peptides identified in this region were all higher in R521G strengthening the confidence of the result suggesting that this region is better protected in mutant-FUS. While a majority of peptides remained unchanged (0.5<WT/R521G<1.5; Table 3.1 and Fig. 3.6C, shown in gray) a few peptides were higher in WT (WT/R521G ratio>1.5; Table 3.1 and Fig. 3.6C, shown in red) in the GST region and RRM/RGG1 region of FUS. The lesser protection of N-terminal region of WT FUS explains the higher abundance of peptides in GST region for WT FUS. The RRM/RGG1 region peptides abundant in the WT-FUS indicate that this region could be better protected, although the relatively small number of peptides indentified does not

provide the confidence to support such protection. Analysis of all the peptides obtained after chymotrypsin digestion, could provide better insight on those regions of FUS. Combining the peptides that were significantly higher in the mutant-FUS revealed a 41-amino acid region (residues G15 to Y55 in FUS) that is better protected in R521G than in WT from chymotrypsin digestion (Fig 3.6D). These results indicate that the mutations in FUS cause the N-terminal region of FUS to be better protected from chymotrypsin digestion.

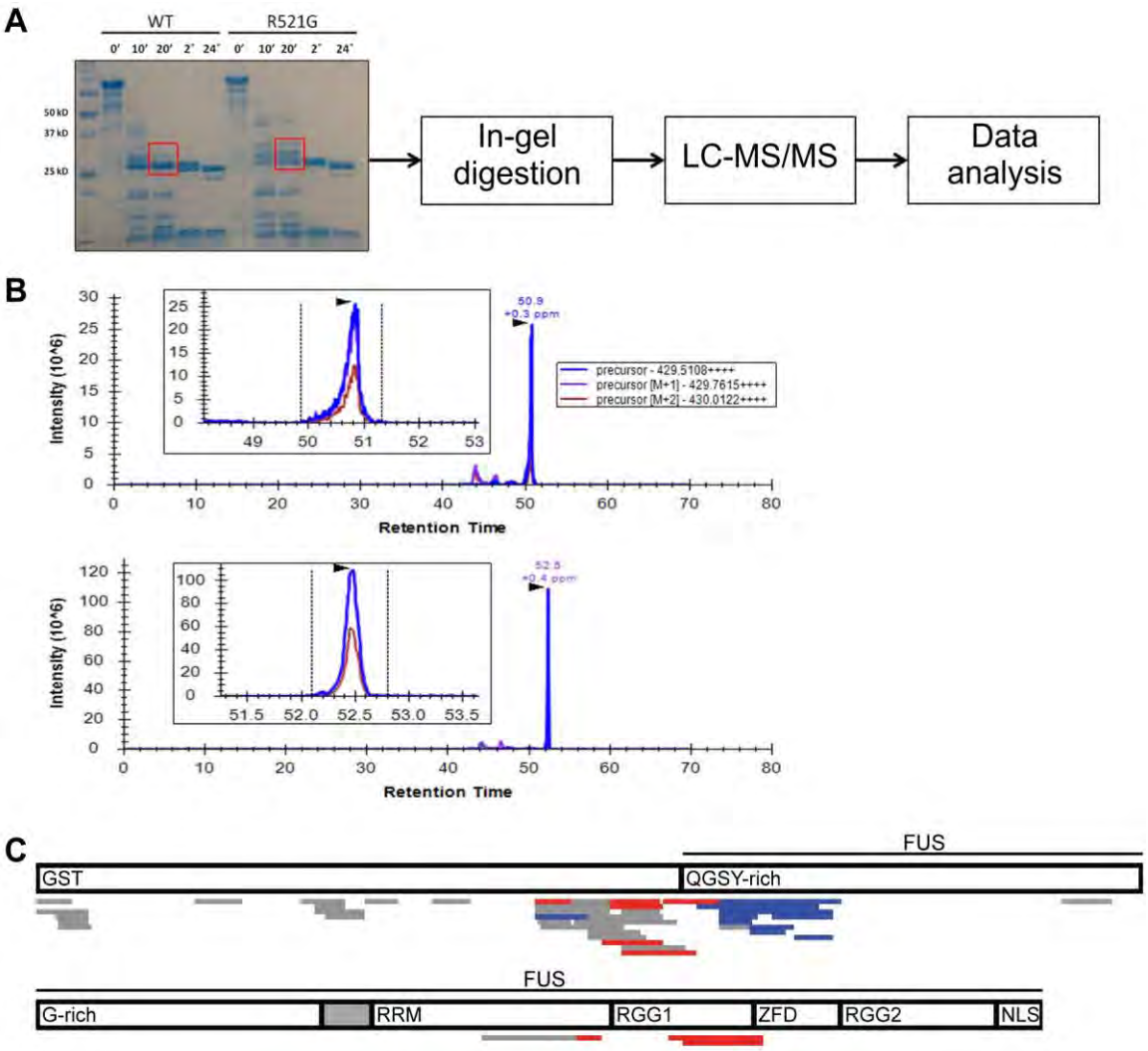
A
WT
R521G
0' 10' 20' 2° 24°
50 kD
37 kD
25 kD
In-gel digestion
LC-MS/MS
Data analysis
B
Intensity (10^6)
Retention Time
precursor - 429.5108++++
precursor [M+1] - 429.7615++++
precursor [M+2] - 430.0122++++
C
FUS
GST
QGSY-rich
FUS
G-rich
RRM
RGG1
ZFD
RGG2
NLS
D
MASNDYTQQATQSYGAYPTQPGQGYSQQSSQPYGQQSYSGYSQSTDTSGYGQSSYSSYGQSQNTGYGTQSTPQG
YGSTGGYGSSQSSQSSYGQQSSYPGYGQQPAPSSTSGSYGSSSQSSSYGQPQSGSYSQQPSYGGQQQSYGQQQ
SYNPPQGYGQQNQYNSSSGGGGGGGGGGNYGQDQSSMSSGGGSGGGYGNQDQSGGGGSGGYGQQDRGGRG
RGGSGGGGGGGGGGYNRSSGGYEPRGRGGGRGGRGGMGGSDRGGFNKFGGPRDQGSRHDSEQDNSDNNTIFV
QGLGENVTIESVADYFKQIGIIKTNKKTGQPMINLYTDRETGKLKGEATVSFDDPPSAKAAIDWFDGKEFSGNPIKVSFAT
RRADFNRGGGNGRGGRGRGGPMGRGGYGGGGSGGGGRGGFPSGGGGGGGQQRAGDWKCPNPTCENMNFSW
RNECNQCKAPKPDGPGGGPGGSHMGGNYGDDRRGGRGGYDRGGYRGRGGDRGGFRGGRGGGDRGGFGPGKM
DSRGEHRQDRRERPY

Figure 3.6

Figure 3.6 N-terminal region of FUS variants is better protected from limited proteolysis

FUS proteins (WT and R521G) were subjected to limited proteolysis by chymotrypsin. The digested peptides were separated using SDS-PAGE and stained with coomassie blue to visualize the peptides. A) Boxed regions were in-gel digested with chymotrypsin, extracted from the gel and subjected to mass spectrometry analysis. B) Extraction ion chromatograms (EIC) of peptides in WT (first panel) and R521G (second panel) used were generated as shown. Peptide abundance was determined by calculating the peak area from the EIC and normalizing to the total intensity of the sample. Subsequently the ratio of each peptide in the WT and R521G sample (WT/R521G) was determined. C) The average of the ratios from n=2 experiments were calculated and peptides with ratio <0.5 (more abundant in R521G) are shown in blue, peptides with ratio >1.5 (more abundant in WT) are shown in red and peptides with ratios 0.5-1.5 (unchanged between WT and R521G) are shown in gray. D) The analysis revealed that a 41 amino acid region (G15 to Y55, highlighted in green) in QGSY-rich domain of FUS is better protected in R521G than in WT.

Peptide	WT/R521G	Std Dev	SEM
MSPILGYWKIKGLVQPT	0.98	0.44	0.31
MSPILGYWKIKGLVQPTRL	1.28	0.25	0.17
MSPILGYWKIKGL	0.86	0.13	0.09
WKIKGLVQPTRL	0.63	0.03	0.02
KIKGLVQPTRL	0.80	0.05	0.03
KIKGLVQPTRLL	0.97	0.24	0.17
YIDGDVKLTQSMAIIRY	0.86	0.15	0.11
EGAVLDIRYGVSRIAY	0.87	0.21	0.15
DIRYGVSRIAY	0.86	0.07	0.05
DIRYGVSRIAYSKDFETL	0.78	0.44	0.31
GVSRIAYSKDFETL	0.71	0.08	0.06
KVDFLSKLPEML	0.76	0.20	0.14
LNGDHVTHPDFMLY	1.17	0.23	0.16
KKRIEAIPQIDKY	1.53	0.41	0.29
KKRIEAIPQIDKYL	1.04	0.29	0.21
KKRIEAIPQIDKYLK	1.26	0.06	0.04
KKRIEAIPQIDKYLKSSKY	0.50	0.67	0.47
KRIEAIPQIDKY	1.03	0.28	0.20
RIEAIPQIDKYLKSSKY	1.22	0.27	0.19
LKSSKYIAWPLQGW	1.24	0.18	0.13
KSSKYIAWPLQGW	1.10	0.30	0.21
KSSKYIAWPLQGWQATF	1.12	0.31	0.22
SSKYIAWPLQGW	1.18	0.10	0.07
IAWPLQGWQATF	1.22	0.16	0.11
IAWPLQGWQATFG	0.66	0.14	0.10
IAWPLQGWQATFGGGDHPP	0.66	0.14	0.10
IAWPLQGWQATFGGGDHPPKSD	1.03	0.18	0.13
QGWQATFGGGDHPPKSDLEVLF	2.11	0.74	0.52
QATFGGGDHPPKSDLEVL	1.56	0.37	0.26
QATFGGGDHPPKSDLEVLF	1.97	0.06	0.04
GGGDHPPKSDLEVL	1.24	0.21	0.15
GGGDHPPKSDLEVLF	1.27	0.26	0.18
GGGDHPPKSDLEVLFQGPLG	0.83	0.08	0.06
GGGDHPPKSDLEVLFQGPLGSMA	0.63	0.18	0.13
GGGDHPPKSDLEVLFQGPLGSMASNDY	2.43	1.12	0.79
QGPLGSMASNDYTQQATQSY	1.61	0.50	0.35
TQQATQSYGAYPTQPGQGY	0.44	0.02	0.02
GAYPTQPGQGY	0.62	0.05	0.04
GAYPTQPGQGYS	0.18	0.03	0.02
GAYPTQPGQGYSQQ	0.23	0.05	0.03
GAYPTQPGQGYSQQSSQPYGQQSY	0.37	0.01	0.01
GAYPTQPGQGYSQQSSQPYGQQSYSGY	0.16	0.03	0.02
SQQSSQPYGQQSY	0.26	0.08	0.05
SQQSSQPYGQQSYSGY	0.16	0.09	0.06
SQQSSQPYGQQSYSGYSQSTDTSGY	0.36	0.13	0.09
SGYSQSTDTSGYGQSSY	0.03	0.01	0.00
SQSTDTSGYGQSSY	0.02	0.01	0.00
SQSTDTSGYGQSSYSSY	0.07	0.01	0.00
GQQSYSGYSQSTDTSGYGQSSY	0.01	0.00	0.00
GQQQSYNPPQGY	1.13	0.27	0.19
TDRETGKLKGEATVSFDDPPSAKAAIDWFDGKEF	0.94	0.24	0.17
SGNPIKVSF	1.57	0.30	0.21
GRGGYGGGGSGGGGRGGFPSGGGGGGGGQQRAGDW	2.10	0.90	0.63
GGGGSGGGGRGGFPSGGGGGGGGQQRAGDW	1.53	0.34	0.24

WT/R521G
<0.5
0.5 to 1.5
>1.5

Table 3.1

Table 3.1 Quantification of peptides in WT and R521G FUS samples

Relative abundance of identified peptides were calculated from the peak area of the EIC (n=2). The peak area was used to determine the ratio of peptide levels in WT FUS compared to R521G (standard deviation, Std Dev; standard error, SEM) Peptides increased in WT by more than 50% (WT/R521G ratio >1.5) are indicated in red, while peptides decreased in WT by more than 50% (WT/R521G ratio <0.5) are shown in blue. Unchanged peptides (WT/R521G ratio 0.5<1.5) are shown in gray.

FUS variants inhibit anterograde and retrograde fast axonal transport

Limited proteolysis studies demonstrate that ALS-linked FUS variants G230C, R521G and R495X are all misfolded. In order to investigate the functional consequence of protein misfolding, we used a squid axoplasm based assay to monitor the effect of FUS proteins on vesicular motility (Brady *et al.*, 1993). The squid assay has been used successfully to demonstrate the toxicity of several other proteins involved in neurodegenerative diseases, such as misfolded WT and mutant-SOD1 (Bosco *et al.*, 2010b; Morfini *et al.*, 2013; Song *et al.*, 2013), both of which demonstrated an inhibitory effect on fast axonal transport. FUS proteins were perfused into a membrane free axoplasm preparation. Video-enhanced microscopy was used to monitor the velocities of membrane bound organelles, allowing us to quantify fast axonal transport (FAT) in both anterograde and retrograde directions. Perfusion of 2.5 μM WT FUS protein had no effect on FAT in either direction for the duration of the assay (50 min; Fig 3.7A). Strikingly, perfusion of 2.5 μM of R521G, R495X or G230C FUS resulted in inhibition of FAT in both directions (Figs 3.7B, C and D), demonstrating a mutant-specific phenotype for FUS proteins.

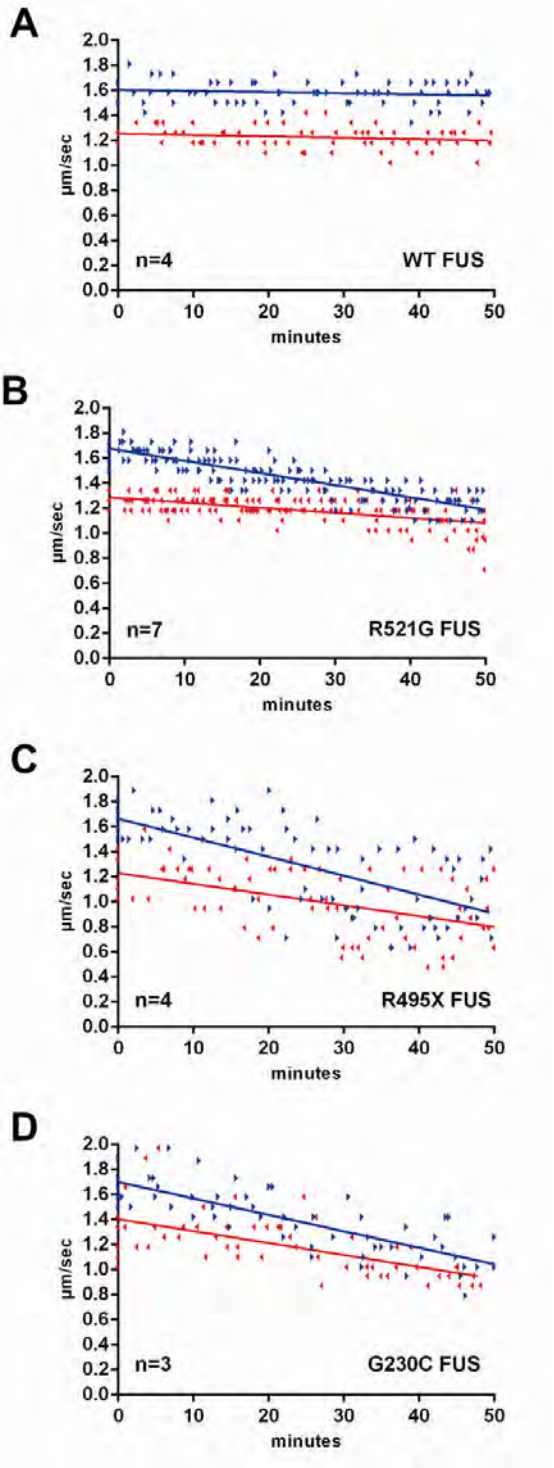
A
B
C
D
µm/sec
minutes
n=4
WT FUS
n=7
R521G FUS
n=4
R495X FUS
n=3
G230C FUS

Figure 3.7

Figure 3.7 ALS-linked FUS proteins inhibit axonal transport

FUS proteins were perfused onto extruded squid axoplasm and vesicular transport (velocity μm/s), representing fast axonal transport (FAT), was plotted against time (minutes). Blue arrows and line represent anterograde velocities while red arrows and line represent retrograde velocities. Perfusion of WT FUS (A) had no effect on transport in either direction while perfusion of FUS mutants R521G (B), R495X (C) or G230C (D) inhibited FAT in both anterograde and retrograde directions.

FAT inhibition by mutant-FUS is mediated by p38 MAPK

Specific protein kinases have usually been found to mediate axonal transport inhibition by several misfolded and toxic proteins (Morfini *et al.*, 2009). In the case of ALS causing SOD1 proteins, which inhibit axonal transport only in the anterograde direction, p38 MAP kinase mediates FAT inhibition (Morfini *et al.*, 2013). In order to determine if p38 MAP kinase played a similar role in FUS mediated FAT inhibition, FUS R521G was co-perfused with inhibitors of p38 MAPK, SB203580 or MW-069 (Munoz *et al.*, 2007). p38 inhibition rescued the FAT inhibition completely (Fig 3.8A and B). In contrast, co-perfusion of JNK kinase inhibitor SP600125 did not rescue the FAT inhibition by FUS R521G (Fig 3.8C). These results indicate that mutant-FUS mediated FAT inhibition is regulated by p38 MAP kinase specifically. Furthermore, even though mutant-SOD1 and mutant-FUS have distinct effects on FAT, i.e., ALS causing SOD1 only inhibits anterograde transport whereas ALS FUS inhibits both anterograde and retrograde axonal transport, they are at least in part regulated by the same MAPK pathway. Interestingly the different isoforms of p38 MAPK have different effects on FAT as the alpha isoform has been shown to inhibit anterograde transport while the beta isoform inhibits anterograde and retrograde transport (Morfini *et al.*, 2013). Thus in the case of mutant-FUS, where both directions are affected, the inhibition is presumably mediated by p38β alone or through a combination of both p38α and β isoforms.

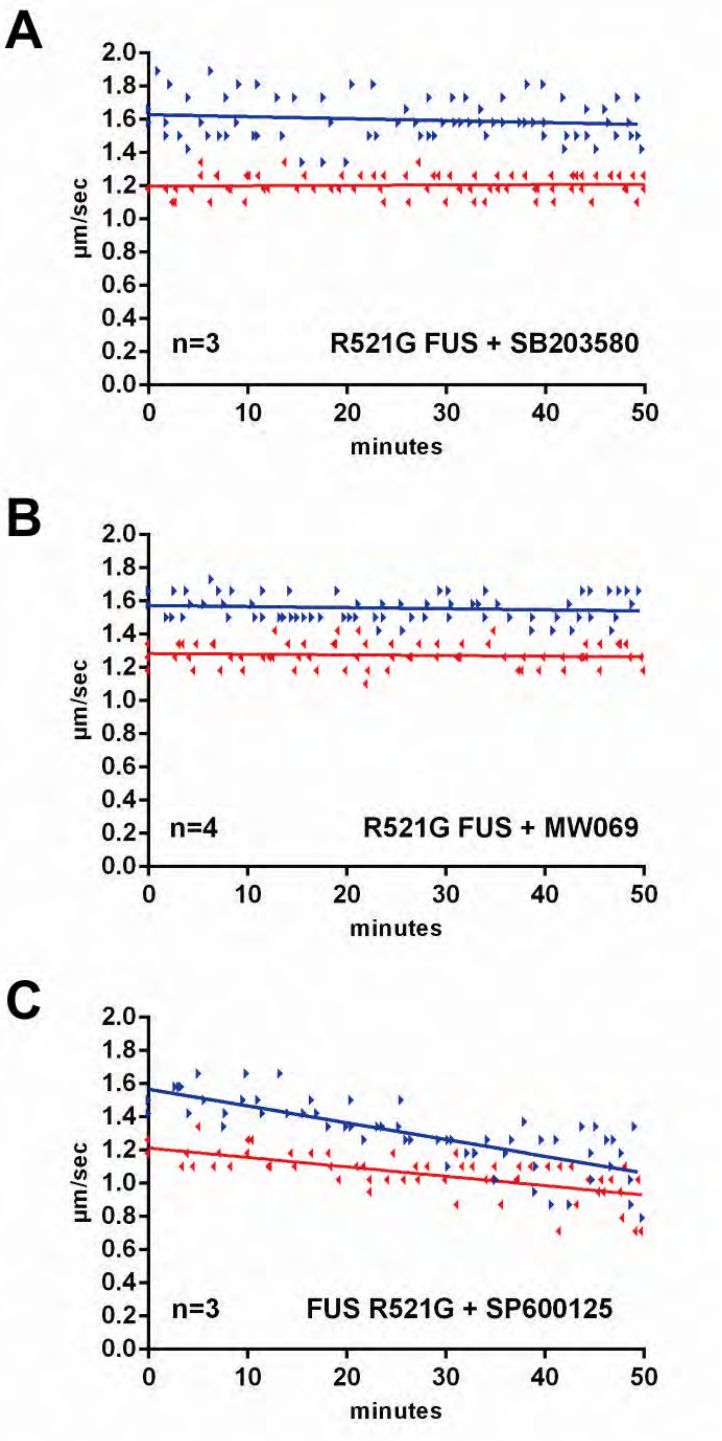
A
2.0
1.8
1.6
1.4
1.2
1.0
0.8
0.6
0.4
0.2
0.0
µm/sec
n=3
R521G FUS + SB203580
0
10
20
30
40
50
minutes
B
2.0
1.8
1.6
1.4
1.2
1.0
0.8
0.6
0.4
0.2
0.0
µm/sec
n=4
R521G FUS + MW069
0
10
20
30
40
50
minutes
C
2.0
1.8
1.6
1.4
1.2
1.0
0.8
0.6
0.4
0.2
0.0
µm/sec
n=3
FUS R521G + SP600125
0
10
20
30
40
50
minutes

Figure 3.8

Figure 3.8 p38 MAPK mediates FAT inhibition by mutant-FUS

Co-perfusion of either of the p38 MAPK inhibitors, SB203850 (A) or MW069 (B), rescued FUS R521G-induced inhibition of FAT (Fig. 3.8) indicating a role for p38 activation in mediating the inhibitory effect on FAT. Co-perfusion of the JNK inhibitor SP600125 (C) did not rescue the FAT inhibition by mutant-FUS, indicating a specific role for p38 MAPK.

In order to determine if FUS variants exert their inhibitory effect on FAT by p38 MAPK alone or if upstream kinases are involved, FUS R521G was co-perfused with an inhibitor (NQDI-1) against ASK1, an upstream MAP kinase of p38 MAPK. Monitoring the axonal transport revealed that retrograde transport was rescued completely and anterograde transport was partially rescued indicating a role for the upstream factors in the MAPK cascade in mediating the inhibitory effect on FAT (Fig 3.9A, C). These results are in agreement with a recent study showing that MST1 mediates the activation of p38 MAPK by ALS linked mutant-SOD1 (G93A), supporting the notion that the MAP kinase cascade itself might be involved (Lee *et al.*, 2013). Furthermore, one study showed that HSP110, a nucleotide exchange factor for HSP70, rescued the inhibitory effect of ALS-linked mutant-SOD1 protein G85R, presumably by mitigating the toxic effects of protein misfolding (Song *et al.*, 2013). Since the ALS linked FUS proteins used in this study are misfolded (Figs. 3.2-3.6), we tested if protein misfolding is involved in exerting toxic effects on axonal transport. To that end, FUS R521G was co-perfused with recombinant HSP110 and axonal transport was monitored as above (Fig 3.9B). HSP110 was able to rescue axonal transport in both directions to levels comparable to that of WT FUS (Fig. 3.7A), indicating a role for protein misfolding in exerting toxic effects on axonal transport.

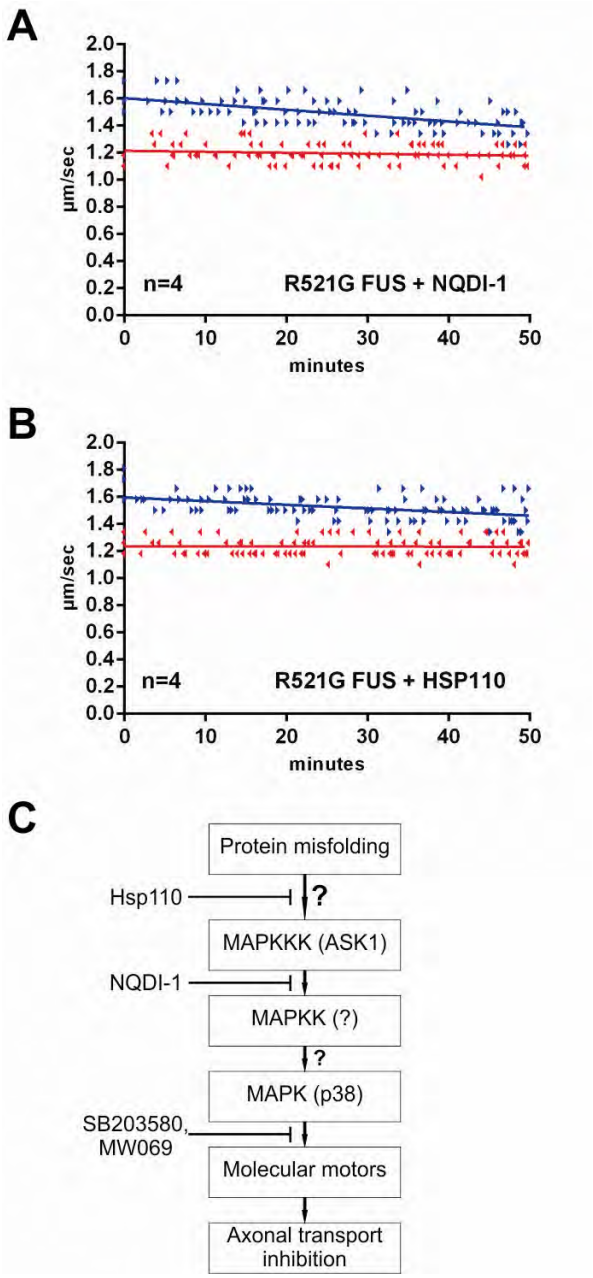
A
2.0
1.8
1.6
1.4
1.2
1.0
0.8
0.6
0.4
0.2
0.0
µm/sec
n=4
R521G FUS + NQDI-1
0
10
20
30
40
50
minutes
B
2.0
1.8
1.6
1.4
1.2
1.0
0.8
0.6
0.4
0.2
0.0
µm/sec
n=4
R521G FUS + HSP110
0
10
20
30
40
50
minutes
C
Protein misfolding
Hsp110
?
MAPKKK (ASK1)
NQDI-1
MAPKK (?)
?
MAPK (p38)
SB203580,
MW069
Molecular motors
Axonal transport
inhibition

Figure 3.9

Figure 3.9 Aberrant kinase activation caused by protein misfolding inhibits axonal transport

A) Co-perfusion of NQD1, an inhibitor of ASK1 which is upstream of p38 MAPK, with FUS R521G partially rescued FAT inhibition, indicating a role for the MAPK cascade in mediating inhibitory effect on axonal transport. B) Co-perfusion of HSP110 also rescued the inhibitory effect of mutant-FUS supporting that protein misfolding results in aberrant activation of the MAPK cascade thereby affecting axonal transport. C) Model of aberrant kinase activation caused by protein misfolding. Misfolded FUS proteins result in the activation of the p38 MAPK cascade that involves ASK1 as the upstream MAPKKK. Activated p38 MAPK inhibits axonal transport by targeting and impairing molecular inhibitors such as kinesin and dynein. Correction of protein misfolding by molecular chaperones such as Hsp110 or inhibition of kinase activity by small molecule inhibitors (NQDI-1 for ASK1 and SB203580 or MWO69 for p38) rescues the axonal transport inhibition mediated by misfolded FUS.

P38 MAPK expression and phosphorylation is increased in fALS patients with FUS mutations

Activation of p38 MAPK has been implicated in several neurodegenerative diseases including ALS (Bendotti *et al.*, 2005; Correa and Eales, 2012). Increased p38 MAPK immunoreactivity has been reported in sporadic ALS cases and a familial ALS patient with SOD1 mutation H48Q (Ackerley *et al.*, 2004; Bendotti *et al.*, 2004). However, there is no evidence of p38 MAPK activation in fALS patients with FUS mutations. In order to investigate the changes in expression and activation of p38 MAPK, tissue samples obtained from control and fALS-FUS patients were analyzed by western blot for total p38 as well as phosphorylated p38 indicative of activated kinase. Interestingly both the total and phosphorylated forms of p38 were increased in several fALS patients compared to the mean of the control population in both brain and spinal cord tissues (Fig 3.10). However statistical significance was not achieved between the control and ALS groups, which could be due to small sample size owing to the rareness of the disease and inconsistencies in tissue collection and storage procedures. Nonetheless, these results not only further support that aberrant activation of p38 MAPK could be a component of ALS disease pathology, but also lays precedence for the involvement of aberrant processing of p38 MAPK that results in altered expression. Whether this aberrant processing is a consequence of mutations in FUS is being currently explored in our lab. In particular the role of mircoRNAs in mediating the pathogenic effects of FUS variants is being

investigated. One microRNA of interest is miR-124, which is downregulated in injured motor neurons (Nagata *et al.*, 2014) as well as in cells when FUS levels are reduced (Morlando *et al.*, 2012). Interestingly miR-124, along with miR-128, suppresses the expression of p38α in neurons (Lawson *et al.*, 2013). Thus, we are investigating whether or not misregulation of miR-124 by mutant-FUS could alter the expression of p38 MAPK.

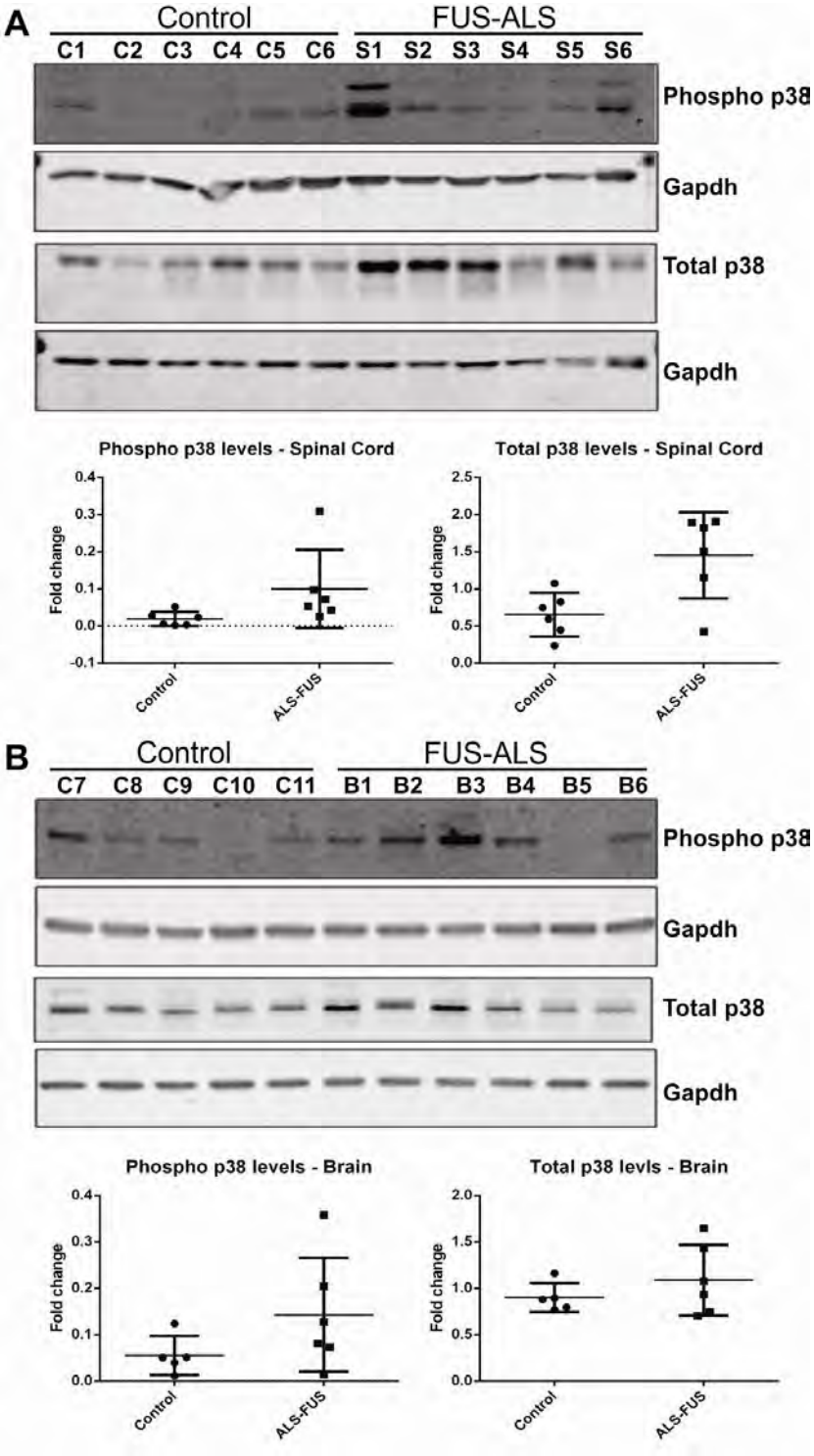
A
Control
FUS-ALS
C1 C2 C3 C4 C5 C6 S1 S2 S3 S4 S5 S6
Phospho p38
Gapdh
Total p38
Gapdh
Phospho p38 levels - Spinal Cord
Total p38 levels - Spinal Cord
Fold change
Control
ALS-FUS
B
Control
FUS-ALS
C7 C8 C9 C10 C11 B1 B2 B3 B4 B5 B6
Phospho p38
Gapdh
Total p38
Gapdh
Phospho p38 levels - Brain
Total p38 levls - Brain
Fold change
Control
ALS-FUS

Figure 3.10

Figure 3.10 Activation of p38 MAPK in ALS patients

Post-mortem tissue samples of control (C1-11) and FUS-fALS patients (S1-6 & B1-6) were prepared for western blot analysis and probed for total and phospho-p38 (indicative of activated p38) levels. Western analysis revealed that in both brain (A, B) and spinal cord (C, D) tissue samples of FUS-fALS patients, total and phospho-p38 levels, indicative of activated p38 MAPK, were higher in several of the ALS cases relative to the mean of the control group.

DISCUSSION

FUS is a multifunctional protein that is associated with several types of cancers and the neurodegenerative diseases, ALS and FTLD (Frontotemporal lobar degeneration). Ever since the association with ALS was discovered, there has been an increased attention for both understanding the disease mechanisms and normal functions of FUS. While significant progress has been made in understanding the normal functions of FUS, resulting in the emergence of novel functional roles in DNA damage repair and stress response, the knowledge on how mutations in FUS can lead to ALS is still very limited. FUS is a DNA/RNA binding protein that shuttles between the nucleus and cytoplasm but is found mostly in the nucleus under normal conditions (Zinszner *et al.*, 1997). A majority of ALS-linked mutations have been found in the C-terminal nuclear localization signal (NLS) and thereby result in mislocalization of the FUS variants. While a few mutations also span the central Glycine rich regions, these mutations have been rarely examined. One recent study however showed that even these mutations are pathogenic in the context of DNA damage repair (Wang *et al.*, 2013).

Thus in order to understand not only the pathogenic effects of FUS mutations in general but also to understand the differences across various FUS mutations, we have used three FUS variants for our studies – G230C in the Gly-rich region, R521G in the C-terminal NLS region and the truncation mutant R495X, which truncates the entire NLS. Despite the differences in domain

location of these three variants, they showed a similar digestion pattern with chymotrypsin indicating that these pathogenic mutations affect the protein structure in a similar way (Fig 3.3). Interestingly, mass spectrometry and antibody mapping experiments revealed that regardless of where the mutation is located within the protein, structural perturbations occurred in the N-terminal QGSY-rich region of FUS (Figs 3.5 and 3.6). This is very interesting in that previous studies reported mutations in the NLS significantly perturbed transportin binding, which affected the nuclear import of these proteins and results in cytoplasmic mislocalization (Dormann *et al.*, 2012; Niu *et al.*, 2012; Zhang and Chook, 2012). Our results however, indicate that structural differences also persist in the N-terminal region of FUS, which potentially mediates the pathogenic effects of the proteins. Interestingly a prion-like domain has been identified in the N-terminal region of FUS that is thought to promote aggregation of FUS (Gitler and Shorter, 2011; Sun *et al.*, 2011). Thus despite being unclear as to how mutations in different regions result in perturbing the prion-like domain of FUS, these structural perturbations appear to inflict pathogenic properties to the FUS variants as demonstrated by axonal transport assays (Fig 3.7 and 3.8).

A recent study using recombinant FUS proteins showed that WT FUS protein was extremely aggregation prone and mutations did not enhance aggregation propensity of the FUS protein (Sun *et al.*, 2011). Thus the proteins could exert their pathogenic effects by other means. In our current study we investigated the pathogenic effect of FUS variants on axonal transport. For this

purpose we used a squid axoplasm based vesicle motility assay. The assay has been previously used to demonstrate the toxic effects of several neurodegenerative disease-causing proteins as well as identifying the pathogenic mechanisms (Morfini *et al.*, 2009). We have shown here that FUS variants all inhibit fast axonal transport (Fig 3.7). This is one of the few instances where a mutant-specific phenotype has been observed in contrast to most cases where WT FUS also exerted pathogenic effects.

Interestingly, a recent study demonstrated that the ALS-linked TDP43 impaired axonal transport of mRNP particles (Alami *et al.*, 2014). Thus it is possible that axonal transport impairment, which appears to be central to axonal degeneration and can ultimately lead to the death of the neuron (Fischer-Hayes *et al.*, 2013), plays a major role in ALS pathogenesis as suggested previously (Pasinelli and Brown, 2006).

For several years, SOD1 has been the only known cause of fALS and hence most of our understanding about the pathways affected in ALS has been deduced from studies of SOD1. However, with the discovery of proteins such as FUS and TDP43, there has been an interest in determining the common/converging pathways that are part of the disease pathogenesis. For instance, functions related to RNA processing are thought play a role in disease pathogenesis given the role of both FUS and TDP43 in various aspects of RNA processing. We show here that ALS-linked FUS variants inhibit axonal transport, supporting impaired axonal transport as a common pathway in ALS as suggested

by the similar effects produced by ALS-linked SOD1 (Bosco *et al.*, 2010b; Morfini *et al.*, 2013) and TDP43 (Alami *et al.*, 2014). Furthermore, we also show here that ALS-causing FUS proteins inhibit axonal transport in both anterograde and retrograde directions (Fig 3.7). As mentioned earlier such inhibition is potentially mediated by either p38β isoform alone or both p38 α and β isoforms, unlike for SOD1 whose pathogenic effects are mediated by p38α isoform in inhibiting anterograde axonal transport. Thus despite the pathogenic effects of ALS causing proteins are affecting the same pathways, the mechanism might be different.

Finally we investigated the brain and spinal cord tissue samples of ALS patients for both p38 levels and activation (Fig 3.10). As expected, an increase in phosphorylated p38 levels was observed in several patient samples. Surprisingly, even the total p38 levels were higher in many patient samples. Given the role of FUS in transcriptional regulation, it is possible that FUS can also regulate the expression of several genes, such as p38 in this case. These results indicate the involvement of aberrant kinase regulation in ALS disease pathology.

MATERIALS AND METHODS

Recombinant FUS expression and purification

FUS WT, R521G, R495X or G230C constructs cloned into pGEX-6P1 vector (GE Life Sciences) were transformed into Rosetta DE3 cells (Novagen). The cells were streaked onto LB (Luria broth)-agar plates containing 50 µg/mL ampicillin and incubated overnight at 37 °C. Single colonies were inoculated into 5 mL LB medium containing 100 µg/mL ampicillin (amp) and 34 µg/mL chloramphenicol (cam) and incubated on a shaker at 37 °C for 8 hours. The starter cultures were then inoculated into 150 mL (intermediate culture) LB media (containing amp and cam) and incubated at 30 °C for ~24 hours. The intermediate cultures were then inoculated into 2 liter LB medium (containing amp and cam) such that the OD_{600} of the culture is between 0.1-0.2. The large cultures were then incubated on a shaker at 20 °C until the OD_{600} reaches ~0.8. FUS expression was induced by addition of IPTG (Isopropyl β-D-1-thiogalactopyranoside) to a final concentration of 150 µM. $Zncl_2$ was also added to a final concentration of 50 µM, and the cultures were incubated on the shaker for 22 hours at 20 °C. The cultures were centrifuged and the cell pellets were resuspended in lysis buffer – 50 mM Tris pH 8.0 with 1 mM DTT (Dithiothreitol), 0.1 mM EDTA (Ethylenediaminetetraacetic acid) and protease inhibitor cocktail (Roche). 10 µg/mL of RNase A was added to the resuspended cells, and the cells were lysed by sonicating on ice at the following amplitudes and for the indicated durations making sure the lysate does not become warm by incubating

it on ice between each sonication step – 10% for 15 s; twice at 20% for 15 s; twice at 30% for 15 s; 35% for 15 s and thrice at 40% for 12 s. The lysate was spun down twice at 13000 rpm for 20 min at 4 °C in a refrigerated centrifuge and the supernatant was incubated with Glutathione-Agarose (Sigma, #G4510) resin that was pre-washed several times with 50 mM Tris buffer pH 8.0 on an end-over-end rocker at 4 °C for 2 hours. The unbound lysate was removed by centrifuging the lysate/resin at 4000 rpm for 5 min at 4 °C. The resin was then transferred into a 5 mL polypropylene column (Pierce, #29922) and the GST-FUS protein bound to the resin was eluted with elution buffer – 50 mM Tris pH 9.5 with 10 mM L-Glutathione reduced (Sigma, #G4251) and 1 mM DTT. The collected protein was concentrated and buffer-exchanged into 25 mM Hepes buffer containing 1 mM DTT. The protein was aliquoted and stored at -80 °C until further use.

Time-resolved anisotropy

Time-resolved anisotropy was obtained from the excited-state decay of Trp residues recorded using time-correlated single photon counting (TCSPC) (Wu *et al.*, 2008; Arai *et al.*, 2011). The TCSPC system utilized an SPC-150 (Becker and Hickl, Berlin, Germany) and fast photomultiplier tube. The excitation was provided by the 292 nm tripled output of a Ti:sapphire laser at 3.8 MHz repetition rate (Coherent, Palo Alto, CA). Excitation power was kept at several hundred μWatts. A single L-format arrangement was used with a motorized Glan-Taylor polarizer. The polarization alternated between vertical and

horizontal polarization and ~20x30 s acquisitions were collected and summed for each polarization per sample. Counting rates were limited to ~5x10^5 counts per second. A 357 nm 40 nm wide bandpass filter (Semrock, Rochester, NY) was used to select the Trp emission. Excitation was vertically polarized. The G-factor was obtained from the integrated intensity of N-acetyl-tryptophanamide (NATA) with the data prior to 1 ns after the pulse arrival excluded to insure complete depolarization of NATA. The instrument response was obtained by detecting scattered light with a 292 nm filter.

A home-built autosampler running custom LabVIEW software (available at www.osmanbilsel.net) was used for all time-resolved anisotropy measurements. Approximately 500 µL of each sample in a 96-well microplate was brought into a flow cell (1mm x 1mm) using a computer controlled syringe pump and flowed in an oscillating pattern at a flow rate of10 µL/s during data collection. This reduced continuous exposure of the sample to the beam to <1 s and minimized photobleaching. All samples were run in triplicate.

The TCSPC anisotropy data were fit to an associative decay model as described previously (Bilsel *et al.*, 1999). Briefly, the horizontal and vertical excited state decays are described by the following expressions:

$$I_{vv}(t) = \sum_{i=1}^{n} S_i(t)(1 + 2r_i(t))/3 \quad (1)$$

$$I_{vh}(t) = \sum_{i=1}^{n} S_i(t)(1 - r_i(t))/3 \quad (2)$$

where n is the number of molecular species,

$$S_i(t) = \sum_{j-1}^{m} \alpha_j e^{-t/\tau_j} \quad (3)$$

$$r_i(t) = \sum_{k=1}^{p} \beta_k e^{-t/\varphi_k} \quad (4)$$

The total intensity is obtained in the usual manner, $S(t)=I_{vv}(t)+2GI_{vh}(t)$, where $G=I_{hv}/I_{hh}$ (Lakowicz, 2006). In the above expressions Si(t) and ri(t) are the fluorescence intensity and anisotropy, respectively, for species i. The fluorescence lifetime and rotational correlation time are represented by τ and ϕ, respectively. Thus, the total fluorescence for species *i* is represented by *m* exponential terms and the anisotropy decay is represented by *p* rotational correlation times. In this manner one obtains α_j, τ_j, β_k and ϕ_k. All non-linear least-squares analysis utilized the Marquardt-Levenberg algorithm using the package Savuka (Bilsel *et al.*, 1999).

Limited Proteolysis

FUS proteins were incubated with the indicated amounts of chymotrypsin (Promega, #V1062) for 20 min at 25 ºC. The enzymes were inactivated by adding 6X SDS sample buffer (Boston Bioproducts, BP-111R) and boiling the samples for 10 min. The samples were cooled down to room temperature and were used for western blot, gel staining or mass spectrometry analysis.

Western Blot

Western blots were performed as described (Bosco *et al.*, 2010a). Briefly, samples were separated using SDS-PAGE and transferred onto a nitrocellulose membrane. The blots were incubated in blocking buffer (Li-cor, #927-40000) for 1

h followed by overnight incubation with shaking at 4 °C in the presence of the following primary antibodies at a dilution of 1:1000-1:2000: anti-GST (GE Healthcare, #27-4577-01), anti-FUS (Bethyl Laboratories, #A300-302A, #A300-292A, #A300-293A), anti-FUS (in house antibody created against 264-284 peptide sequence of human FUS, Genscript), anti-FUS (Santacruz Biotechnology, #47711, #373888), anti-phospho-p38 (Cell Signaling, #9215), anti-total-p38 (Sigma, #M0800) and anti-gapdh (Sigma, #G8795). Densitometry was performed using the Odyssey infrared imaging systems software (Li-cor).

Gel staining

Samples were separated using SDS-PAGE and the gels were stained with coomassie brilliant blue G250 (Sigma, #27815) or silver stain (Bio-rad, #161-0449) to visualize the protein samples. In the case of coomassie, the gels were incubated in the presence of coomassie solution (0.25% (w/v) coomassie brilliant blue, 40% (v/v) methanol and 10% (v/v) acetic acid) for 30 min on a shaker and then transferred to the destaining solution until the protein/peptide bands become visible while replacing the destaining solution with fresh solution occasionally.

Identification of FUS sequence by mass spectrometry

Following limited proteolysis, SDS-PAGE, and Coomassie stain (described above), the indicated bands were excised from the gel and subjected to in-gel digestion with chymotrypsin (10 ng/μl) for 18 h at 25°C, as previously described (Shevchenko *et al.*, 2006). The extracted peptides (50 μL volume) were dried down in a speedvac, resuspended in 12 μl of 5% acetonitrile

containing 0.1% (v/v) trifluoroacetic acid and separated on a NanoAcquity (Waters) UPLC. The run conditions follow the "sensitive" conditions recommended by (Kelstrup *et al.*, 2012) for optimizing the operations of the Q Exactive for low abundance proteins. Briefly, a 4.5 µL injection was loaded in 5% acetonitrile containing 0.1% formic acid at 4.0 µL/min for 4.0 min onto a 100 µm I.D. fused-silica pre-column packed with 2 cm of 5 µm (200Å) Magic C18AQ and eluted using a gradient at 300 nL/min onto a 75 µm I.D. analytical column packed with 25 cm of 3 µm (100Å) Magic C18AQ particles to a gravity-pulled tip. The solvents were A, water (0.1% formic acid); and B, acetonitrile (0.1% formic acid). A linear gradient was developed from 5% solvent A to 35% solvent B in 60 minutes. Ions were introduced by positive electrospray ionization via liquid junction into a Q Exactive hybrid mass spectrometer (Thermo). Mass spectra were acquired over *m/z* 300-1750 at 70,000 resolution (*m/z* 200) and data-dependent acquisition selected the top 12 most abundant precursor ions for tandem mass spectrometry by HCD fragmentation using an isolation width of 1.2 Da, and collision energy of 25, and a resolution of 35,000. The raw data was searched against a database containing the GST-FUS sequence in Proteome Discoverer 1.3 with parent tolerance of 10 ppm and fragment ion tolerance of 0.05 Da. Peak areas from extracted ion chromatograms (Skyline) were used to quantify the abundance of the peptides in each sample. The individual peak areas were normalized to the sum of all peak areas identified as FUS peptides.

Peptides in GST-FUS WT were further normalized to the corresponding peptide in GST-FUS R521G. Only changes of >50% were included in the analyses.

Squid axoplasm vesicle motility assays

Vesicular motility assays were performed as described previously (Morfini *et al.*, 2013). FUS proteins alone or in combination with pharmacological inhibitors or HSP110 protein were diluted into X/2 buffer (175 mM potassium aspartate, 65 mM taurine, 35 mM betaine, 25 mM glycine, 10 mM Hepes, 6.5 mM $MgCl_2$, 5 mM EGTA, 1.5 mM $CaCl_2$, 0.5 mM glucose, pH 7.2) supplemented with 2–5 mM ATP, and 25 µL were perfused into the membrane-free axoplasms. The final concentrations are as follows: 2.5 µM of FUS proteins, 5 µM of SB203580, 0.5 µM of SP600125, 10 µM of MW-069, 20 µM NQDI1 and 0.6 µM HSP110. Vesicular transport rates in both anterograde and retrograde directions were obtained and plotted using Prism (GraphPad software).

Human Tissue analysis

Human post-mortem tissues were obtained from ALS patients and control individuals after obtaining informed consent. The tissues were frozen until further analysis. All protocols were approved by Institutional Review Board by all the institutions involved. For western analysis, tissue samples were transferred to 2 mL borosilicate glass tube (Wheaton, #358028) and lysis buffer was added. The samples were homogenized using a tissue grinder (Wheaton, #358029)

connected to an overhead stirrer (Wheaton, #903475) homogenizer by stirring for 3 min at setting 2 and 4˚C. The lysate was transferred to centrifuge tubes and was centrifuged using a table top refrigerated centrifuge for 15 min at 13000 rpm and 4˚C. The supernatant was transferred to fresh tubes and centrifuged again for 15 min at 13000rpm and 4˚C. The supernatants were collected and protein concentration was determined using a colorimetric assay based on bicinchonic acid (BCA) (ThermoScientific, #23227) for western analysis.

Acknowledgements

We would like to thank Dr. Arthur L. Horwich for providing recombinant HSP110 protein. We would like to thank Diane McKenna-Yasek for her assistance with the human tissue samples.

CHAPTER IV

DISCUSSION AND CONCLUSIONS

Amyotrophic lateral sclerosis is a deadly neurodegenerative disease that affects nearly 5,000 individuals every year in the USA. The debilitating nature of this disease severely affects the individuals and their families. Despite being known for over one hundred years now, only one FDA approved treatment exists, Riluzole, which only extends life by a few months. The encouraging news, however, is that there has been a significant development in our understanding of ALS owing to research findings over the last few years, bringing us closer than ever to finding a treatment and/or cure. Particularly, genetics have helped us identify several genes linked to the disease. This in turn has helped us understand the molecular mechanisms behind the pathogenesis of ALS. *FUS/TLS or FUS* is a key gene in which mutations causing ALS have been discovered. Mutations in FUS account for nearly 5% of all familial ALS cases. Understanding the normal functions of FUS and its pathogenic role in causing ALS has recently gained considerable attention in the ALS field. Chapter II of this dissertation deals with a novel prosurvival function for FUS under hyperosmolar stress conditions. Additionally, in chapter III we explored how ALS causing mutations can induce structural perturbations in FUS and lead to protein misfolding and aberrant kinase activation. Thus the work presented in this dissertation is aimed at advancing our understanding of potential pathogenic

mechanisms of this deadly disease and to hopefully obtain some clues as to how to find a treatment and/or even a cure.

FUS is a multifunctional protein that is involved in several key cellular functions such as DNA damage repair, transcriptional regulation, RNA processing and stress response (Dormann and Haass, 2013; Ling *et al.*, 2013). It is still unclear if a loss of one or more of these functions or if gain-of-toxic function(s) by FUS variants leads to ALS. Interestingly the cellular functions investigated usually seem to dictate the type of mechanism. For instance, despite some conflicting results, ALS-linked FUS variants appear to be defective in DNA damage repair supporting a loss of function mechanism (Mastrocola *et al.*, 2013; Rulten *et al.*, 2013; Wang *et al.*, 2013). On the other hand, one study investigating the mRNA targets bound by WT and mutant-FUS, show that mislocalization of FUS resulted in the mutant-FUS binding several hundreds of novel mRNAs, supporting a gain of toxic function hypothesis (Hoell *et al.*, 2011). The key focus of the work presented in this dissertation is the role of FUS in stress response. Previous studies showed that FUS variants that are mislocalized to the cytoplasm incorporate into stress granules (Bosco *et al.*, 2010a; Dormann *et al.*, 2010; Gal *et al.*, 2011; Kino *et al.*, 2011; Bentmann *et al.*, 2012) and alter several properties of stress granules, supporting a gain of function hypothesis (Baron *et al.*, 2013). However, a majority of studies that looked at the role of FUS in stress granules were limited by the type of stress conditions used and thus did not reveal a role for endogenous FUS under such

conditions. The work presented in Chapter II of this dissertation demonstrates that WT endogenous FUS not only responds to hyperosmolar stress, but also plays a pro-survival role under such conditions. The response of FUS involves immediate translocation to the cytoplasm and incorporation into stress granules. But how does mutant-FUS respond to hyperosmolar stress? Our work using an artificial truncation mutation, G515X that eliminates the NLS showed that the mutant protein still incorporates into stress granules (Fig 2.9). Whether ALS-causing FUS variants also incorporate into stress granules has not been investigated. Evaluating whether the FUS variants still play a pro-survival role under hyperosmolar conditions and disassociate from stress granules in the same manner as WT FUS would be key in determining whether this function of FUS is linked to the pathogenesis of ALS. Also interesting would be to investigate if the cytoplasmic translocation of FUS proteins also causes a loss of nuclear functions, which could be exacerbated with variants that are already mislocalized to cytoplasm.

Stress granules are formed in response to transient stress and disassemble upon removal of the applied stress. However, under chronic stress conditions, stress granules have been suggested to act as precursors to end-stage aggregates that are usually detected in neurons of ALS patients (Wolozin, 2012). Supporting this notion, several stress granule marker proteins were detected in inclusions of ALS and FTD patients (Dormann *et al.*, 2010; Liu-Yesucevitz *et al.*, 2010; Bentmann *et al.*, 2013). Interestingly, expression of ALS-

causing FUS variants in cultured cells resulted in varying degrees of FUS mislocalization alone without any toxicity. However, upon stressing the cells with oxidative stress, ER stress, or heat shock, cytoplasmically mislocalized FUS variants incorporated into stress granules (Bosco *et al.*, 2010a; Dormann *et al.*, 2010; Gal *et al.*, 2011; Kino *et al.*, 2011). This led to a two-hit hypothesis wherein the genetic mutations that result in cytoplasmic mislocalization of FUS represent the first-hit while the stress conditions represent the second-hit (Dormann and Haass, 2011). The work presented in chapter II demonstrating the pro-survival role of FUS under hyperosmolar stress conditions provides a basis for examining not only the role of hyperosmolar stress as that second-hit stressor but also the role of osmotic imbalance in ALS and neurodegeneration in general.

ALS and Hyperosmolar Stress

Interestingly, several studies and observations point towards a role of hyperosmolar stress in ALS. First, other ALS proteins are implicated in hyperosmolar stress response. Similar to FUS, the ALS-associated proteins TDP43 and hnRNP A1 respond to hyperosmolar stress by translocating into the cytoplasm and incorporating into stress granules (van der Houven van Oordt *et al.*, 2000; Guil *et al.*, 2006; Dewey *et al.*, 2010; Sama *et al.*, 2013). Indeed, these proteins are required for recovery and/or survival of cells under hyperosmolar stress conditions. Expression of mutant-*tdp-1*, an orthologue of *TDP43*, in *C elegans* increased the sensitivity of the worms to osmotic stress (Vaccaro *et al.*, 2012). Similarly, the neurodegenerative phenotype observed in mutants of *alpha-*

1, an orthologue of ALS causing gene *C9ORF72*, was worsened by osmotic stress in *C elegans* (Therrien *et al.*, 2013). SOD1, another ALS associated protein, is required for survival of *S. cerevisiae* under hyperosmolar stress conditions (Garay-Arroyo *et al.*, 2003). Furthermore, since cytoskeletal rearrangement is a pronounced feature during hyperosmolar conditions (Brocker *et al.*, 2012), it wouldn't be surprising if the recently discovered ALS protein Profilin 1, a key regulator of actin dynamics (Wu *et al.*, 2012), also responds and has a role under such stress conditions.

Second, several key cellular adaptive and pathogenic events in response to hyperosmolar stress overlap with the pathogenic events reported in ALS. Cell shrinkage caused by hyperosmolar stress triggers many adverse subcellular events, such as oxidative stress, mitochondrial depolarization, inhibition of DNA replication and transcription, damage to DNA and proteins, and cell cycle arrest, all of which can ultimately lead to apoptosis (Alfieri and Petronini, 2007; Burg *et al.*, 2007; Brocker *et al.*, 2012). Interestingly, protein misfolding and aggregation, oxidative stress, mitochondrial dysfunction, and impaired DNA/RNA metabolism have all been suggested to contribute to ALS pathogenesis and ultimately lead to apoptosis of motor neurons (Pasinelli and Brown, 2006). Furthermore, inflammation, a key contributor to ALS pathogenesis (Barbeito *et al.*, 2010; Calvo *et al.*, 2010; Papadimitriou *et al.*, 2010), is tightly linked with hyperosmolar stress (Brocker *et al.*, 2012). Despite being controversial, strenuous exercise, sports and intense physical activity have been linked to ALS (Scarmeas *et al.*, 2002;

Chio *et al.*, 2005; Beghi *et al.*, 2010; Huisman *et al.*, 2013). It is possible that the dehydration/osmotic imbalance resulting from these intense activities is causal for ALS through a hyperosmolar stress response. Moreover, hyperosmolar stress is implicated in a myriad of disease conditions in humans, including renal failure, diabetes, inflammation as well as disorders of the eye, heart and liver (Brocker *et al.*, 2012) underscoring its importance in disease. Despite these studies and observations, further research must be done to conclusively determine the role of hyperosmolar stress in ALS.

Osmotic stress – sensing mechanisms

In order to understand the potential role of FUS in response to hyperosmolar stress, several mechanisms involved in sensing the stress and signaling are discussed below (summarized in Fig 4.1). The mechanisms by which mammalian cells detect changes in extracellular osmotic concentrations, however, are poorly understood. Exposure of cells to hypotonic or hypertonic medium induces rapid cellular swelling or shrinkage, respectively, and thus cell volume appears to be the key parameter that is monitored to induce a cellular response. Changes in cell volume trigger adaptive responses to either mitigate the toxic effects or initiate apoptosis. Interestingly, numerous other processes and pathways including metabolism, cell division, migration, motility, membrane trafficking and apoptosis are regulated by cell volume changes (Lang *et al.*, 1998). But exactly how is the volume of a cell registered/monitored under osmotic stress conditions? While there are no clear answers, recent studies point

toward characteristics such as macromolecular crowding, plasma membrane properties, cytoskeletal organization, ionic strength and structural changes of intracellular organelles as potential indicators of cell volume changes (Schliess *et al.*, 2007). Each is discussed below.

Macromolecular crowding: Increased macromolecular crowding can alter molecular interactions as well as the stability and structure of DNA, RNA and proteins. Such changes can have a profound effect on key cellular processes such transcription and translation (Morelli *et al.*, 2011). In fact, changes in cytoplasmic protein concentration have been shown to act as an indicator of cell volume changes (Colclasure and Parker, 1992; Parker and Colclasure, 1992; Garner and Burg, 1994). Thus macromolecular crowding can contribute to the osmosenisng mechanism of the cell.

Plasma membrane properties: Plasma membrane properties such as tension, composition and membrane curvature are potential indicators of cell volume alterations (Schliess *et al.*, 2007). Stretch-activated ion channels, which are mechanosensitive channels localized to plasma membranes, play a role in both hypo- and hyperosmolar stress conditions. For instance, the TRP (Transient Receptor Potential) family channels respond to changes in osmotic conditions and are well studied in the context of cell volume regulation (Pedersen and Nilius, 2007). Additionally, cell adhesion molecules such as integrins and cadherins, which are involved in binding with other cells or the extra cellular matrix, are also potential cell volume sensors (Haussinger and Lang, 1992; Ko *et*

al., 2001; Juliano, 2002; Moeckel *et al.*, 2006). Finally, although there is no evidence that they respond to osmotic stress, BAR *(Bin–Amphiphysin–Rvs)* domain containing family of proteins are implicated as candidates with the potential to sense osmotic stress (Zulys, 2008). These proteins, which are curved (banana-shaped) themselves, bind to curved membranes and have different curvature preferences (Peter *et al.*, 2004; Zimmerberg and McLaughlin, 2004; Gallop and McMahon, 2005). Furthermore, BAR domain family proteins are implicated in numerous cellular functions that could be relevant to osmotic stress, such as actin cytoskeletal regulation, secretory vesicle fusion, ion flux across membranes, signal transduction and apoptosis (Ren *et al.*, 2006).

Cytoskeletal organization: Although the role of the cytoskeleton as an osmosensor is controversial, cytoskeletal rearrangement is known to occur during cellular swelling or shrinkage and therefore cytoskeletal dynamics may contribute to the osmosensing mechanisms of the cell. Furthermore, the structural reorganization of actin filaments could regulate membrane channels that impact cell volume homeostasis (Henson, 1999; Pedersen *et al.*, 2001).

Ionic strength: The concentration of intracellular ions may also contribute to the cellular sensing of osmotic imbalance (Gamba, 2005). Altered ionic strength can stimulate ion transporters (Nilius *et al.*, 1998) and activate signaling cascades involved in cell volume regulation (discussed further below) (Di Ciano-Oliveira *et al.*, 2003; Nielsen *et al.*, 2007).

Structural changes of intracellular organelles: Osmotic stress induced defects in endoplasmic reticulum (ER) to golgi transport, result in loss of structural integrity of those organelles (Lee and Linstedt, 1999). Furthermore, mitochondrial fragmentation has been reported as a response to hyperosmolar stress (Zulys, 2008). Such a loss of structural integrity of major organelles is associated with cellular stress response (Welch and Suhan, 1985; Hicks and Machamer, 2005) and thus could be a potential indicator of cell volume changes.

Thus, it appears that the cells employ several sensing mechanisms, which alone or in combination, may trigger adaptive responses.

Hyperosmolar stress – signaling and effects

Despite specific signaling events and effects associated with hypoosmolar stress, due to the response of FUS to hyperosmolar stress, the discussion below is focused on the signaling events and their effects in response to hyperosmolar stress. Hyperosmolar stress triggers several pathways including receptor and non-receptor tyrosine kinases, MAP kinases, lipid kinases, serine/threonine kinases and the Rho family small GTPases (Fig 4.1). The specific roles of each of these pathways have been discussed in detail elsewhere (Zulys, 2008). Of interest to my current research is the p38 MAP kinase, which mediates the pathogenic effects of mutant FUS proteins in the squid axoplasm (Chapter 3).

The upstream events of p38 MAPK activation include the binding of OSM (Osmosensing Scaffold for MEKK3) to the GTPase Rac and the kinases MEKK3 (MAPK/extracellular-regulated kinase (ERK) kinase kinases) and MKK3

(Mitogen-activated protein kinase kinase kinase 3) (Uhlik *et al.*, 2003). The activated p38 translocates to nucleus and enhances the transcriptional activity of NFAT5 (Nuclear factor of activated T-cells 5), also known as TonEBP/OREBP, a transcription factor that, among other things, drives the expression of genes involved in osmolyte synthesis and channel proteins (Ko *et al.*, 2002). The transcriptional activity of NFAT5 is regulated by the presence of a DNA sequence element known as the osmotic response element (ORE) or tonicity enhancer (TonE) sequence upstream of the various osmoprotective genes (Ferraris *et al.*, 1996; Ko *et al.*, 1997; Miyakawa *et al.*, 1998; Ko *et al.*, 2000). Hyperosmolar stress induces translocation of NFAT5 from cytoplasm to nucleus (Cai *et al.*, 2005), where it binds the ORE as a homodimer (Stroud *et al.*, 2002). The translocation of NFAT5 appears to be regulated by phosphorylation of its serine and tyrosine residues and/or its dimerization ability (Dahl *et al.*, 2001). The best studied genes regulated by NFAT5 include transporters, which restore ionic homeostasis by transporting organic osmolytes such as glycine, betaine, ionositol and taurine into the cell, as well as enzymes such as aldose reducatse involved in sorbitol synthesis (Smardo *et al.*, 1992). NFAT5 also regulates the transcription of the molecular chaperone HSP70 (Woo *et al.*, 2002), which aids in restoring protein folding, and aquaporins (Hasler *et al.*, 2006), which regulate water permeability of membranes. Although NFAT5 is the most studied regulator of gene expression in response to hyperosmolar stress, changes in levels of several proteins that are not known to be regulated by NFAT5 have been

reported (Mao *et al.*, 2008; Soufi *et al.*, 2009), suggesting the influence of other transcription factors and/or signaling processes in regulating gene expression. In fact, regulation of mRNA turnover in yeast cells contributes to altered gene expression (Romero-Santacreu *et al.*, 2009). Furthermore, several studies provide evidence for translational inhibition in response to hyperosmolar stress supporting that gene expression under such conditions is regulated at multiple levels (Burg *et al.*, 2007).

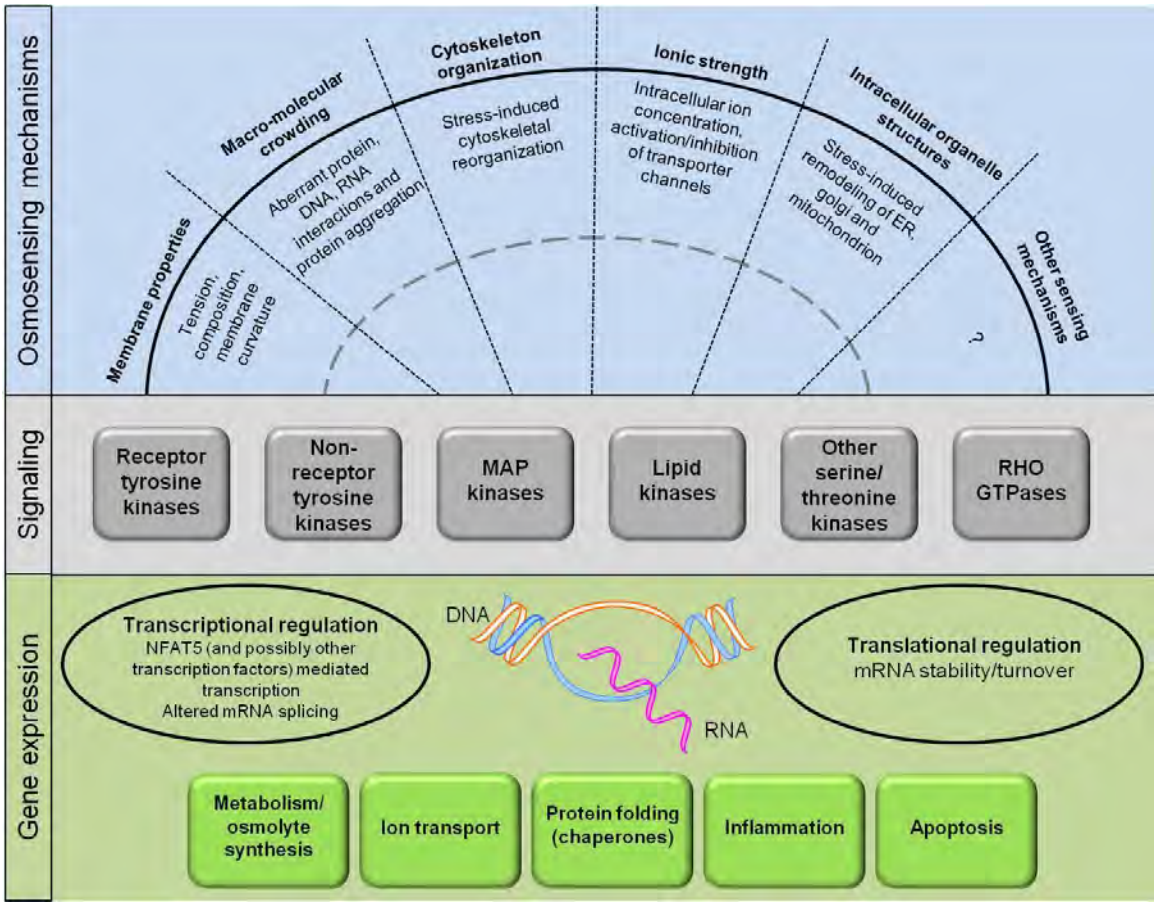
Osmosensing mechanisms
Membrane properties
Tension, composition, membrane curvature
Macro-molecular crowding
Aberrant protein, DNA, RNA interactions and protein aggregation
Cytoskeleton organization
Stress-induced cytoskeletal reorganization
Ionic strength
Intracellular ion concentration, activation/inhibition of transporter channels
Intracellular organelle structures
Stress-induced remodeling of ER, golgi and mitochondrion
Other sensing mechanisms
?
Signaling
Receptor tyrosine kinases
Non-receptor tyrosine kinases
MAP kinases
Lipid kinases
Other serine/ threonine kinases
RHO GTPases
Gene expression
Transcriptional regulation
NFAT5 (and possibly other transcription factors) mediated transcription
Altered mRNA splicing
DNA
RNA
Translational regulation
mRNA stability/turnover
Metabolism/ osmolyte synthesis
Ion transport
Protein folding (chaperones)
Inflammation
Apoptosis

Figure 4.1

Figure 4.1 Potential sensing mechanisms, signaling and gene expression regulation in response to hyperosmolar stress

Hyperosmolar stress induced cell shrinkage is detected by a single or combination of parameters including membrane properties, macromolecular crowding, cytoskeleton organization, ionic strength and intracellular organelle structures. Upon detection of hyperosmolar stress, several key signaling cascades such as receptor- and non-receptor tyrosine kinases, MAP kinases, lipid kinases, other serine/threonine kinases and RHO GTPases mediate the subsequent gene expression changes (discussed in detail in (Zulys, 2008)).Gene expression is regulated at transcriptional level (transcription factors such as NFAT5 and splicing regulation) and translational level (mRNA stability/turnover) modulating the expression of proteins involved in key cellular functions including osmolyte synthesis, ion transport, protein folding, inflammation and apoptosis.

FUS and Hyperosmolar stress

Hyperosmolar stress induces cytoplasmic translocation of FUS, which plays a pro-survival role under such conditions (Sama *et al.*, 2013). What is the mechanism by which FUS plays this role? FUS is an RNA binding protein and binds to transcripts of several hundred genes involved in key cellular functions (Table 1.1). Knock-down of FUS alters the binding of FUS to those transcripts and also results in altered expression and splicing of transcripts (Table 1.1). Albeit in a study using ALS causing mutant FUS, cytoplasmic mislocalization of FUS has been implicated in altered expression and splicing of several hundred mRNAs (van Blitterswijk *et al.*, 2013). These studies suggest that factors affecting the expression and or localization of FUS could have profound effects on gene expression. Hyperosmolar stress-induced cytoplasmic accumulation of FUS is also accompanied by a nuclear depletion of FUS, possibly effecting the expression of several genes. Of interest would be to determine if those genes are involved in apoptosis, since reduced FUS levels rendered cells susceptible to hyperosmolar stress induced toxicity (Sama *et al.*, 2013). Furthermore, the translation and expression of pro-survival proteins XIAP (X-linked inhibitor of apoptosis protein) and Bcl-xL (B-cell lymphoma-extra large) (Lewis *et al.*, 2007; Bevilacqua *et al.*, 2010) during hyperosmolar stress is regulated by hnRNP A1, another RNA binding protein that also translocates to the cytoplasm and incorporates into stress granules in response to hyperosmolar stress (van der Houven van Oordt *et al.*, 2000). It is possible that FUS exerts a similar effect on

specific genes involved in apoptosis by regulating their expression and/or splicing. It is also possible that FUS might exert such an effect indirectly by modulating the functions of other proteins. For instance, FUS is known to interact with both hnRNP A1 (Perrotti *et al.*, 2000; Iervolino *et al.*, 2002) and TDP-43 (Kim *et al.*, 2010), proteins that also translocate to the cytoplasm and incorporate into stress granules in response to hyperosmolar stress (van der Houven van Oordt *et al.*, 2000; Dewey *et al.*, 2010). Nevertheless, given that not all RNA binding proteins respond to hyperosmolar stress (van der Houven van Oordt *et al.*, 2000) and that WT FUS responds selectively to hyperosmolar stress (Sama *et al.*, 2013) is suggestive of a specific functional role for FUS during hyperosmolar stress.

Methylation of FUS and ALS

Post translational modifications (PTMs) regulate key cellular events and are a major factor in the pathogenesis of several diseases (Karve and Cheema, 2011). In particular, protein arginine methylation regulates several cellular processes and has been implicated in many human diseases (Aletta and Hu, 2008). Interestingly protein arginine methylation, regulated largely by PRMT1 (protein argnine methyl transferase), has been shown to dictate the subcellular distribution of endogenous as well as ALS-linked FUS (Du *et al.*, 2011; Dormann *et al.*, 2012; Tradewell *et al.*, 2012; Yamaguchi and Kitajo, 2012). Furthermore, inclusions in ALS-FUS patients contained methylated FUS while inclusions in FTD-FUS were devoid of methylated FUS, indicating a role for protein arginine

methylation in disease pathogenesis (Dormann *et al.*, 2012). In chapter II we show that the subcellular distribution of FUS in response to hyperosmolar stress is also regulated by methylation (Fig 2.8). Further investigation is needed to determine if PRMT1 specifically regulates FUS localization under hyperosmolar stress conditions as well. Our data shows, however, that methylation did not have any role in regulating the incorporation of FUS into stress granules (Fig 2.9), indicating that the arginine methylation status affects only certain aspects of FUS.

A model for FUS in cellular stress response and ALS

What is the role of FUS in cellular stress response and what are the implications of its role in ALS? While much more research has to be done to precisely answer these questions, the current knowledge from our work here and published work from others lead to a model as described below. Under normal conditions WT FUS is predominantly localized to the nucleus. However, FUS is involved in RNA transport and shuttles between the nucleus and cytoplasm and hence a minor fraction of FUS is present in the cytoplasm (Fig 4.2A). On the other hand, a majority of ALS-linked FUS variants undergo varying degrees of mislocalization to the cytoplasm causing a corresponding nuclear depletion of FUS (Fig 4.2A). Under stress conditions such as oxidative stress, heat shock and ER stress, the WT FUS remains nuclear and only the small fraction in the cytoplasm incorporates into stress granules (Fig 4.2B), perhaps making it difficult to detect by routine immunofluorescence techniques. However, under those

stress conditions, ALS-variants that are already in the cytoplasm due to mutations incorporate into stress granules (Fig 4.2B). Such an incorporation of FUS variants into stress granules suggest a gain-of-toxic function by the FUS variants. However, a similar gain-of-toxic function mechanism cannot be applied to mutations that do not induce cytoplasmic mislocalization, such as those in the Gly-rich region, as these proteins remain nuclear with or without the aforementioned stress conditions. Hyperosmolar stress on the other hand causes endogenous WT FUS to undergo cytoplasmic translocation and incorporation into stress granules (Fig 4.2C). The question that remains is how do FUS variants respond to hyperosmolar stress? Assuming a loss of nuclear function by ALS-causing FUS variants, hyperosmolar stress could worsen this condition as the nucleus is further deprived of functional FUS protein under such conditions (Fig 4.2C). Assuming a cytoplasmic gain-of-toxic function mechanism by FUS variants, once again this condition could be worsened by hyperosmolar stress as more protein accumulates in the cytoplasm as a result of translocation of WT FUS (Fig 4.2C). Thus hyperosmolar stress is a suitable model of disease for not only the cytoplasmically mislocalized FUS, but also for the variants that retain nuclear localization. However, further investigation is needed to determine the relevance of hyperosmolar stress in ALS.

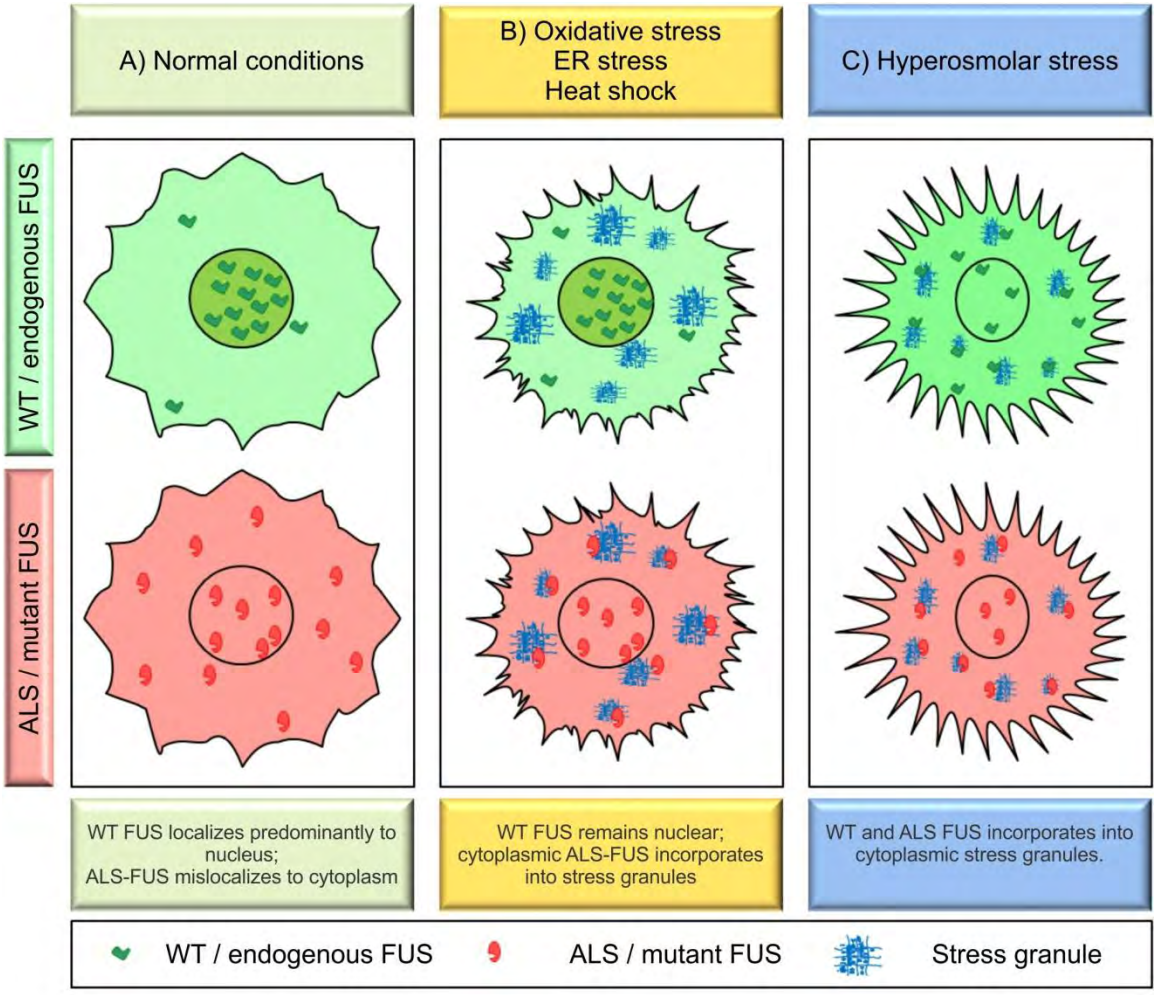
A) Normal conditions
B) Oxidative stress
ER stress
Heat shock
C) Hyperosmolar stress
WT / endogenous FUS
ALS / mutant FUS
WT FUS localizes predominantly to nucleus;
ALS-FUS mislocalizes to cytoplasm
WT FUS remains nuclear;
cytoplasmic ALS-FUS incorporates into stress granules
WT and ALS FUS incorporates into cytoplasmic stress granules.
WT / endogenous FUS
ALS / mutant FUS
Stress granule

Figure 4.2

Figure 4.2 The different responses of FUS variants to cellular stress.

Cells expressing exogenous WT- or endogenous FUS (top panels) and ALS-linked FUS varaints (bottom panels) are shown under different cellular conditions. A) Under normal conditions WT/endogenous FUS is localized predominantly to the nucleus while ALS-linked FUS variants (i.e., with mutations in the nuclear localization domain) undergo varying degrees of cytoplasmic mislocalization. B) Under conditions of oxidative stress, heat shock or ER stress, WT/endogenous FUS remains nuclear while FUS variants that are already mislocalized to cytoplasm incorporate into stress granules. C) Under conditions of hyperosmolar stress, WT/endogenous FUS translocates to cytoplasm and incorporates into stress granules. Under these conditions, endogenous FUS is thought to play a pro-survival role. FUS variants that are already mislocalized to cytoplasm also associate with stress granules (unpublished data), although the implications of this interaction for ALS are unknown.

Misfolding of FUS – Insights and Implications

Cytoplasmic mislocalization has been largely attributed to the pathogenic effects of FUS variants. For instance, ALS-causing mutations in FUS do not disrupt its ability to bind RNA. However, a subset of mRNAs are bound by cytoplasmic mutant-FUS and not by WT FUS, which has been attributed to the mislocalization of mutant-FUS (Hoell *et al.*, 2011). Furthermore, as mentioned earlier, the role of FUS in stress granules under certain stress conditions is only applicable to variants that are already mislocalized to the cytoplasm. Cytoplasmic mislocalization however, is not the only feature of FUS variants that contributes to ALS pathogenesis. In chapter III of this dissertation we show that ALS-linked FUS variants inhibit axonal transport, whereas WT do not, despite being located outside of the nucleus. In this case, localization of the protein was not a factor, and instead, the inhibition of axonal transport was attributed to the misfolding of the mutant-FUS. Protein misfolding has indeed been suggested as part of ALS pathogenesis owing to an impairment of protein homeostasis during aging as well as the increased aggregation propensity of mutant proteins, as in the case for SOD1 (Pasinelli and Brown, 2006). However, even though WT FUS was shown to be extremely aggregation prone by itself, ALS mutations did not enhance its aggregation propensity (Sun *et al.*, 2011). How then do FUS mutations exert their pathogenic effects? In order to address this question we made use of N-terminally GST-tagged recombinant WT and ALS-linked FUS variants expressed in *E. coli*. In contrast to other types of recombinant FUS

proteins, including untagged FUS or N- and C-terminally His-tagged FUS, N-terminal GST tagged FUS remains soluble (Sun *et al.*, 2011). Furthermore, despite the GST-tag, the recombinant FUS proteins retain several key functions and appear to be very similar to cellular FUS (Kim *et al.*, 2010; Wang *et al.*, 2013; Qiu *et al.*, 2014).

A limited proteolysis experiment showed that the ALS-linked FUS variants are structurally different from WT FUS (Fig 3.3). Mass spectrometry analysis of differentially cleaved peptides identified a region in the N-terminal prion like domain of mutant-FUS that is protected despite being digested in the WT FUS. Interestingly, the N-terminal prion like domain is essential for the aggregation of FUS (Sun *et al.*, 2011). This could imply that the FUS variants used in our analysis were aggregated and thus the N-terminal region was protected from proteolytic digestion. Thus, it would be very informative to determine if there is any aggregation/oligomerization of the FUS proteins. Despite that, tryptophan fluorescence anisotropy also clearly showed that the FUS variants are structurally different than that of WT in solution. These insights into the structural differences between WT and FUS variants raise a few important questions. Why is this N-terminal aggregation-prone region protected in FUS variants, but exposed in the WT protein? Furthermore, how do mutations in the C-terminal region (R521G and R495X) and Gly-rich region (G230C) result in structural differences at the N-terminus of the protein? One possibility is that the mutations in various regions of FUS can induce allosteric perturbations in the protein that

somehow propagate to the N-terminal region. Further structural analysis of FUS will provide a much needed insight into the pathogenic effects of its variants.

Why is untagged FUS extremely aggregation prone and insoluble? FUS is a DNA/RNA binding protein and most of the functions of FUS have to do with its ability to bind DNA and/or RNA. Furthermore, FUS is found in complexes with several other cellular proteins and some of those interactions are even mediated by RNA. Thus the environment of the cell provides factors that can stabilize FUS, which is difficult to replicate in *in vitro* experiments. This also underscores that such an environment can have a profound effect on the structure of the FUS. While it is difficult to exactly replicate such conditions, we are currently investigating the binding effect of known sequences of DNA and RNA, which have high affinity for FUS, on the structure of the protein. In particular the effect of DNA/RNA binding on limited proteolysis with chymotrypsin is being examined. Furthermore, assays that can at least partially replicate the cellular environment would be of even more relevance in understanding the pathogenic nature of FUS variants. We have therefore employed the squid axoplasm based vesicle motility assays to study the effect of FUS proteins on axonal transport.

Axonal transport and ALS

Axons are a unique feature of neurons, with some types of neurons having axons up to thousand times larger than their cell bodies. With only limited protein synthesis occurring in the axonal compartment, cells rely heavily on axonal transport to traffic proteins and cargo between the cell body and synapse. Thus

impaired axonal transport has been implicated in numerous diseases related to neurons (Morfini *et al.*, 2009). Both upper and lower motor neurons are selectively vulnerable in ALS. Despite an in depth investigation of the mechanisms of ALS-associated genes, little is known about the reason behind selective vulnerability of the motor neurons. Defects in axonal transport have been documented early on in ALS patients (Sasaki and Iwata, 1996) and similar defects have also been found in animal models of ALS (Sasaki *et al.*, 2005) providing a basis for selectivity of motor neuron degeneration in ALS. Thus we have examined the effect of the FUS proteins on axonal transport in squid axoplasm and demonstrated that the FUS variants specifically inhibited axonal transport in both anterograde and retrograde directions (Fig 3.7). These results further highlight the role of impaired axonal transport as a pathogenic event in ALS. Interestingly, transgenic rats expressing mutant-FUS display degeneration of the motor axons, however, the role of axonal transport in such degeneration has not been investigated (Huang *et al.*, 2011). Further investigation into aspects of axonal transport with assistance from reliable ALS-FUS animal models could address whether transport defects occur early on and are part of the disease pathogenesis or not.

The recent discovery of ALS causing mutations in genes such as *FUS*, *TDP43*, *PFN1* and *C9ORF72*, implicate several pathways in the disease pathogenesis. However, a majority of these pathways have been specific to only a subset of these proteins and cannot explain a common pathogenic property of

ALS proteins. In chapter III, we show that ALS-linked FUS variants inhibit fast axonal transport (FAT) in a squid-based vesicle motility assay (Fig 3.7). Interestingly ALS-causing mutant-SOD1, as well as misfolded WT SOD1 implicated in sporadic ALS, also inhibits FAT in similar assays (Bosco *et al.*, 2010b; Morfini *et al.*, 2013). Furthermore, for both proteins, the inhibition is mediated by p38 MAPK. In the case of FUS, the inhibition is potentially mediated by either the p38β isoform alone or both p38 α and β isoforms, as inhibition is observed in both anterograde and retrograde directions (Fig 3.8 and (Morfini *et al.*, 2013)). In the case of SOD1 mediated inhibition on the other hand, the inhibition is potentially mediated by p38α isoform, as this isoform specifically inhibits the anterograde FAT. Despite these differences, in both cases the upstream kinase ASK1 is involved demonstrating the involvement of the kinase cascade (Fig 3.9). In fact, the p38 MAP kinase cascade has been implicated in several neurodegenerative diseases (Correa and Eales, 2012). Phosphorylated p38 MAPK, representing the active form of the protein, regulates key signaling events and is often indicative of the involvement of the kinase cascade in several cellular events. Increased immunoreactivity for activated p38 MAPK has been reported in spinal cord tissue of ALS patients (Bendotti *et al.*, 2004). Furthermore, activated p38 has been detected in spinal cord motor neurons of early and late stage SOD1-ALS transgenic mice (Tortarolo *et al.*, 2003; Morfini *et al.*, 2013). Thus we investigated the activation of p38 MAPK as well as its expression in ALS-FUS patients and demonstrated that several patients had

higher p38 levels and activation (Fig 3.10). That some ALS-FUS tissue samples lacked a large p38 signal could be explained by differences in tissue collection and storage conditions, which could affect protein integrity. Furthermore, due to the limited availability of the tissue, the samples were not matched for age, gender or any demographic attributes raising the need for caution in interpreting these results. Nevertheless, investigating if other ALS associated proteins have similar effects on axonal transport and if such an effect is mediated by p38 MAPK would unravel its role in ALS.

CONCLUSION

ALS is a fatal neurodegenerative disease and there is still no cure to this disease. Research has advanced greatly over years and several new genes that cause ALS have now been identified. Investigation of these genes provided great insights into the disease causing mechanisms. The current dissertation aimed at investigating one such gene, *FUS/TLS* or *FUS*, and identified a novel functional role for the protein under hyperosmolar stress. The work presented also lays precedence for investigating the role of hyperosmolar stress in ALS. Furthermore, the investigation of the role of FUS variants in ALS identified that protein misfolding and aberrant kinase activation contribute to pathogenic effects of the FUS mutations. The findings of this dissertation will not only extend our current understanding of the disease but also could provide directions to develop treatment and/or cure for ALS.

APPENDIX I

A large part of this work was done by Syed Noorwez (SN) with the following exceptions: Western blots analyses and immunoprecipitation were performed by Reddy Ranjith K Sama (RRKS) and SN. Plasmid transfections were performed by RRKS.

Protein Structure and Folding:

Calnexin Improves the Folding Efficiency of Mutant Rhodopsin in the Presence of Pharmacological Chaperone 11-*cis*-Retinal

Syed M. Noorwez, Reddy Ranjith K. Sama
and Shalesh Kaushal

J. Biol. Chem. 2009, 284:33333-33342.
doi: 10.1074/jbc.M109.043364 originally published online October 2, 2009

THE JOURNAL OF BIOLOGICAL CHEMISTRY VOL. 284, NO. 48, pp. 33333–33342, November 27, 2009

Calnexin Improves the Folding Efficiency of Mutant Rhodopsin in the Presence of Pharmacological Chaperone 11-*cis*-Retinal*

Received for publication, July 10, 2009 and in revised form, September 4, 2009 Published, JBC Papers in Press, October 2, 2009, DOI 10.1074/jbc.M109.043364

Syed M. Noorwez, Reddy Ranjith K. Sama, and Shalesh Kaushal[1]

From the Department of Ophthalmology, University of Massachusetts Medical School, Worcester, Massachusetts 01605

The lectin chaperone calnexin (Cnx) is important for quality control of glycoproteins, and the chances of correct folding of a protein increase the longer the protein interacts with Cnx. Mutations in glycoproteins increase their association with Cnx, and these mutant proteins are retained in the endoplasmic reticulum. However, until now, the increased interaction with Cnx was not known to increase the folding of mutant glycoproteins. Because many human diseases result from glycoprotein misfolding, a Cnx-assisted folding of mutant glycoproteins could be beneficial. Mutations of rhodopsin, the glycoprotein pigment of rod photoreceptors, cause misfolding resulting in retinitis pigmentosa. Despite the critical role of Cnx in glycoprotein folding, surprisingly little is known about its interaction with rhodopsin or whether this interaction could be modulated to increase the folding of mutant rhodopsin. Here, we demonstrate that Cnx preferentially associates with misfolded mutant opsins associated with retinitis pigmentosa. Furthermore, the overexpression of Cnx leads to an increased accumulation of misfolded P23H opsin but not the correctly folded protein. Finally, we demonstrate that increased levels of Cnx in the presence of the pharmacological chaperone 11-*cis*-retinal increase the folding efficiency and result in an increase in correct folding of mutant rhodopsin. These results demonstrate that misfolded rather than correctly folded rhodopsin is a substrate for Cnx and that the interaction between Cnx and mutant, misfolded rhodopsin, can be targeted to increase the yield of folded mutant protein.

Calnexin is a membrane-bound molecular chaperone of the endoplasmic reticulum (ER)[2] that is an important component of ER protein homeostasis (proteostasis) and participates in QC of glycoproteins (1–3). Cnx assists folding of nascent glycoproteins through repeated interactions until they fold properly or are targeted for degradation (4). Cnx clients include secreted proteins, membrane channels, receptors, and G protein-coupled receptors (5–7). The critical role of Cnx in QC of glycoproteins is underscored by embryonic lethality and severe developmental defects that result due to Cnx mutations or knock down (8). Cnx displays dual behavior with regard to its chaperoning activity with wild type (WT) and mutant glycoproteins. Cnx binds transiently to immature folding intermediates of WT glycoproteins, helping them to fold and exit the ER QC system. Misfolded mutant glycoproteins, on the other hand, are bound stably by Cnx and are retained in the ER (6, 7, 9–12). However, enhanced ER retention and prolonged association with Cnx are not known to increase the yields of folded mutant glycoproteins.

ER proteostasis could be manipulated through regulation of molecular chaperone levels alone or in conjunction with pharmacological chaperones (PCs) (3, 13). Such proteostasis modulation has resulted in ameliorating diseases of protein misfolding. For example, small molecule proteostasis regulators increased cellular heat shock protein levels and increased the amount of trafficking-competent Gaucher disease-related mutant proteins. This increase was further enhanced by presence of a PC (13). Also, overexpression of heat shock proteins resulted in suppression of some neurodegenerative diseases (14, 15). However, there is no reported instance of increased folding of a mutant glycoprotein by manipulation of ER proteostasis by increasing cellular levels of Cnx.

Rhodopsin, the prototypical G protein-coupled receptor, is a membrane glycoprotein that is responsible for dim light vision (16) and like most other glycoproteins is folded in the ER (17). Proper folding of rhodopsin is critically important for visual transduction because light-absorbing pigment is generated by binding of the natural ligand 11-*cis*-retinal to fully folded opsin. Misfolded opsin is incapable of generating pigment (18, 19). Mutations throughout rhodopsin cause its misfolding and intracellular aggregation (19–23). Mutations within the N-terminal region, for example P23H and T17M, result in improper folding of opsin and poor binding of the ligand (24) (Fig. 1*A*). P23H is clinically the most common autosomal dominant RP mutation found in North America. It is located in the N-terminal region of rhodopsin, an integral part of the N-terminal plug that keeps the ligand in its proper position. P23H opsin is a misfolded protein most of which is retained within the ER (19, 22) and is degraded via the ubiquitin-proteasome pathway (20, 21). Similarly, mutations affecting the sole disulfide bond in rhodopsin (*e.g.* C110Y) (Fig. 1*A*) result in a significantly misfolded molecule. These misfolding mutations negatively affect cellular proteostasis and result in blinding disorders known as retinitis pigmentosa. However, considering the central role of Cnx in glycoprotein folding, surprisingly little is known about the direct interaction of calnexin with WT or mutant rhodopsin.

The few reports that describe Cnx-rhodopsin interaction come from different organisms and have yielded conflicting

* This work was supported by Research to Prevent Blindness (unrestricted grant) and Charlie Mack Overstreet Retinal Diseases Fund.

[1] To whom correspondence should be addressed: 381 Plantation St., Biotech 5, Ste. 250. Tel.: 508-334-0687; E-mail: shalesh.kaushal@umassmemorial.org.

[2] The abbreviations used are: ER, endoplasmic reticulum; Cnx, calnexin; QC, quality control; RP, retinitis pigmentosa; PC, pharmacological chaperone; WT, wild type.

results (2, 25, 26). Moreover, none of these reports directly address the role of Cnx in folding of misfolded mutant rhodopsin. An association between misfolded rhodopsin and Cnx was indirectly demonstrated in a mouse model of RP using immunocolocalization. However, no direct biochemical interaction or characterization of this interaction was reported (25). An important role of Cnx was demonstrated in *Drosophila*, indicating that Cnx is required for maturation of Rh1 rhodopsin, which is a homolog of mammalian rhodopsin (26). However, Cnx is not required for maturation of mammalian rhodopsin (2). This difference in observations is not surprising because *Drosophila* rhodopsin differs significantly from vertebrate rhodopsin (27). These results demonstrate that rhodopsin, across phylogenetic lines, is a Cnx substrate and also indicate that the role of Cnx in the QC of rhodopsin may differ among different organisms. Thus, given that mutant, misfolded rhodopsins cause RP, it is important to delineate and clarify the physical interaction of Cnx with mammalian rhodopsin.

Here, we characterize this interaction using cell culture and mouse models of RP. We show that only misfolded rhodopsin is the substrate for Cnx and that the extent of this association directly corresponds with the severity of the mutation. Finally, through modulation of ER proteostasis in the presence of the pharmacological chaperone 11-*cis*-retinal, we demonstrate that Cnx can increase the efficiency of mutant P23H rhodopsin folding.

EXPERIMENTAL PROCEDURES

Reagents—The antibody against calnexin was obtained from StressGen; tubulin and ubiquitin antibodies were procured from Abcam. 1D4 was obtained from the University of British Columbia. IRdye700- and IRdye800-conjugated secondary antibodies were purchased from LI-COR Biosciences. Dodecyl maltoside was procured from Anatrace. 11-*cis*-Retinal was a gift from Dr. Rosalie Crouch, Medical University of South Carolina.

Stable Cell Lines and Culture—Tetracycline-inducible stable cell lines used in this study were constructed and cultured as described previously (28). In addition to P23H and WT opsin genes, C110Y and T17M mutant synthetic bovine opsin genes were also introduced in HEK293 cells using the described method. Opsin production was induced from the stable cell lines by addition of 1 μg/ml tetracycline into the culture medium and incubating the cells for 48 h at 5% CO_2 and 37 °C. All experiments were carried out at least three times. Representative spectra and Western blots are shown in the figures.

Immunoaffinity Purification of Rhodopsin—After 48 h of incubation, rhodopsin was purified under dim red light from the stable cell lines; SDS-PAGE was conducted, and Western blots were performed essentially as described previously (28). Briefly, the cells were harvested and washed with ice-cold PBS (10 mM sodium phosphate and 130 mM NaCl, pH 7.2) by centrifuging at 7000 rpm for 10 min. Cell pellets were resuspended in ice-cold PBS and incubated with 50 μM 11-*cis*-retinal for 1 h to regenerate photopigment from opsin produced from the cell lines. The cells were then lysed in PBSD (PBS containing 1.0% dodecyl maltoside and protease inhibitor mixture) for 1 h. The lysate was spun at 13,000 rpm to remove cell debris. The supernatant was collected, and total protein was estimated using the DC protein assay kit (Bio-Rad). Equal amounts of total protein were then added to 1D4-Sepharose immunoaffinity beads and incubated for 1 h at 4 °C. The beads were washed three times with cold PBSD (without protease inhibitor) and then two times with 10 mM sodium phosphate buffer, pH 6. Rhodopsin was then eluted from the beads with elution buffer (a competing peptide corresponding to the last 18 amino acids of rhodopsin in the same buffer).

In pharmacological chaperoning experiments, the cells were grown in the presence of the PC for 48 h in the dark after addition of tetracycline. The cells were then harvested and washed with ice-cold PBS and then lysed with PBSD, and rhodopsin was purified exactly as mentioned above. The purified rhodopsin was then scanned in a Cary50 spectrophotometer (Varian) between 250 and 650 nm. The characteristic rhodopsin absorbance at 498 nm (for WT and T17M rhodopsin) and 492 nm (for P23H rhodopsin) was used to quantify pigment yields.

For separation of folded rhodopsin from misfolded opsin, the samples were treated as described above, and then the 1D4-Sepharose immunoaffinity beads were extensively eluted with elution buffer until no rhodopsin was spectrophotometrically detected in the eluate. The misfolded forms of rhodopsin were then eluted with the competing peptide mixed with PBSD.

Rhodopsin Purification from Mice Eyes—All procedures were conducted according to approved IACUC protocols. The procedure was conducted under dim red light. One-month-old C57 and P23H hemizygous mice (29) were sacrificed by cervical dislocation, and entire eyes were removed. Both eyes from one mouse were pooled, and 1 ml of PBSD was added. The eyes were sonicated three times for 5 s each. The suspension was rotated end to end for 1 h at 4 °C. Further steps in rhodopsin purification were the same as those described for cell culture.

Calnexin Overexpression—For overexpression of calnexin, whole-length calnexin in pCMV-SPORT6 (p-SPORT6-Cnx) mammalian expression vector (Invitrogen) was transiently transfected in WT and P23H opsin-producing stable cell lines using Lipofectamine transfection reagent (Invitrogen). Plates were incubated for 48 h after which opsin production was induced for another 48 h. The cells were then harvested, and rhodopsin was purified as described earlier.

Immunoprecipitation—In experiments where rhodopsin was not purified for spectrophotometric analysis, whole cell lysates were quantified for total protein, and equal protein was loaded onto 1D4-Sepharose beads. After 1 h of binding, the beads were washed three times for 5 min each, and the bound proteins were directly eluted with 100 μM C-18 peptide. The eluted proteins were then subjected to SDS-PAGE and Western blot analysis.

RESULTS

Cnx Preferentially Associates with Mutant Opsin—To assess the effect of P23H mutation on the levels of total opsin production and on the levels of properly folded rhodopsin, we stably expressed WT and P23H opsin in HEK293 cells. As a control, we used the HEK293 stable cell line expressing only the empty vector. Total opsin levels were 10-fold lower in P23H cells than in WT cells (Fig. 1*B*, *left panel*). Next, we determined the levels of correctly folded rhodopsin from WT and P23H cells using

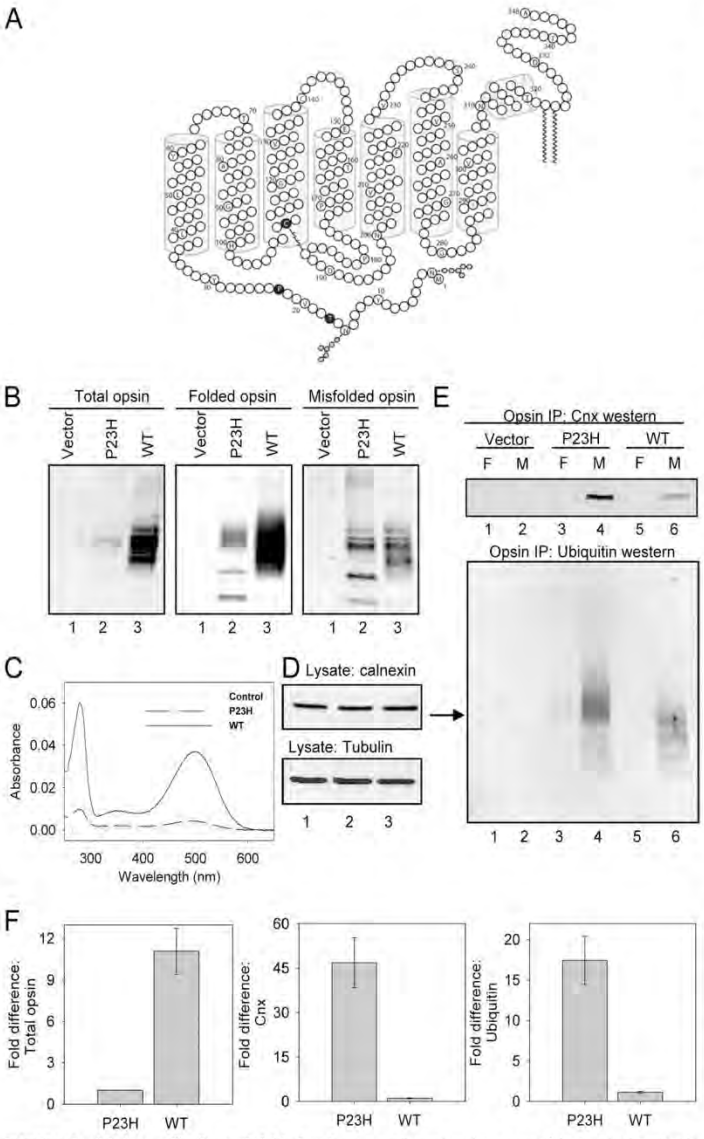

FIGURE 1. **Cnx binds specifically to misfolded opsin.** *A*, two-dimensional structure of rhodopsin showing the two glycosylation sites (*gray*) and positions of P23H, T17M, and C110Y mutations that cause RP (*black circles*). *B*, Western blots of total cellular levels of opsin from stable cell lines (*left panel*) show a 10-fold lower recovery of P23H than WT opsin. Vector control does not show any trace of opsin. *Middle panel* shows the Western blot of immunoaffinity-purified folded rhodopsins from the cells. *Right panel* shows the misfolded forms of P23H and WT opsin. *C*, spectra of immunoaffinity-purified folded rhodopsin produced from P23H (*dashed line*) and WT (*boldface trace*) cells show a 10-fold lower yield of P23H rhodopsin from the cells. No trace of any rhodopsin seen in vector cells (*dotted line*). *D*, total cellular Cnx levels do not change on induction of P23H (*lane 2*) and WT (*lane 3*) opsins. Sample from vector cells is in *lane 1*. Tubulin was used as a loading control. *E*, folded and misfolded fractions were immunoblotted with antibodies to Cnx (*upper panel*) and ubiquitin (*lower panel*). Cnx associated only with misfolded (*M*) forms of P23H and WT opsins. The folded fractions (*F*) do not show any trace of Cnx. Ubiquitination is also seen mostly in the misfolded fractions except for P23H, where a trace of ubiquitination is also seen in folded fraction (*arrow, lane 3*). *IP*, immunoprecipitation. *F*, quantification of cellular opsin levels generated from the cells (*left panel*). The *middle* and the *right panels* show quantification of the fold increase in Cnx and ubiquitin, bound to misfolded opsins, respectively.

selective immunoaffinity methods described previously (22, 23). Immunoblots of folded rhodopsin from the two cell lines showed the same relationship between P23H and WT rhodopsin levels as was seen for total opsin (Fig. 1*B*, *middle panel*). After exhaustive elution of folded rhodopsin, we collected the remaining misfolded opsin. Western blots of these misfolded opsins showed more misfolded P23H opsin than misfolded WT opsin in terms of their ratio to total opsins (Fig. 1*B*, *right panel*). The control cells containing the empty vector did not produce any detectable opsin (Fig. 1*B*, *all panels*). Because folded rhodopsin has a distinct absorption at 498 nm, folded rhodopsin from these cells was spectrophotometrically analyzed and compared (Fig. 1*C*). No detectable absorbance was seen for vector control cells (Fig. 1*C*, *dotted spectrum*). A very small amount of 498-nm absorbing pigment was recovered from P23H cells (Fig. 1*C*, *dashed spectrum*), and the yield of WT rhodopsin was 10-fold more than P23H rhodopsin (*boldface spectrum*). We also analyzed the levels of Cnx in cell lysates to determine whether expression of opsin affected Cnx expression. Cellular Cnx levels did not show any appreciable difference related to opsin expression in these cells (Fig. 1*D*).

To identify molecular chaperones associated with rhodopsin, eluates of either the correctly folded or misfolded fractions were probed on immunoblots for different chaperones. Cnx immunoblots revealed specific association of Cnx with misfolded fractions of both P23H (Fig. 1*E*, *upper panel*) and WT opsins (Fig. 1*E*, *upper panel*). No Cnx was detected in control lanes or correctly folded P23H and WT lanes (Fig. 1*E*, *upper panel*). (For the rest of this article, "folded" means correctly folded, in contrast to misfolded.) We also probed the folded and misfolded rhodopsin for ubiquitination. The misfolded fractions of both P23H and WT rhodopsin were highly ubiquitinated (Fig. 1*E*,

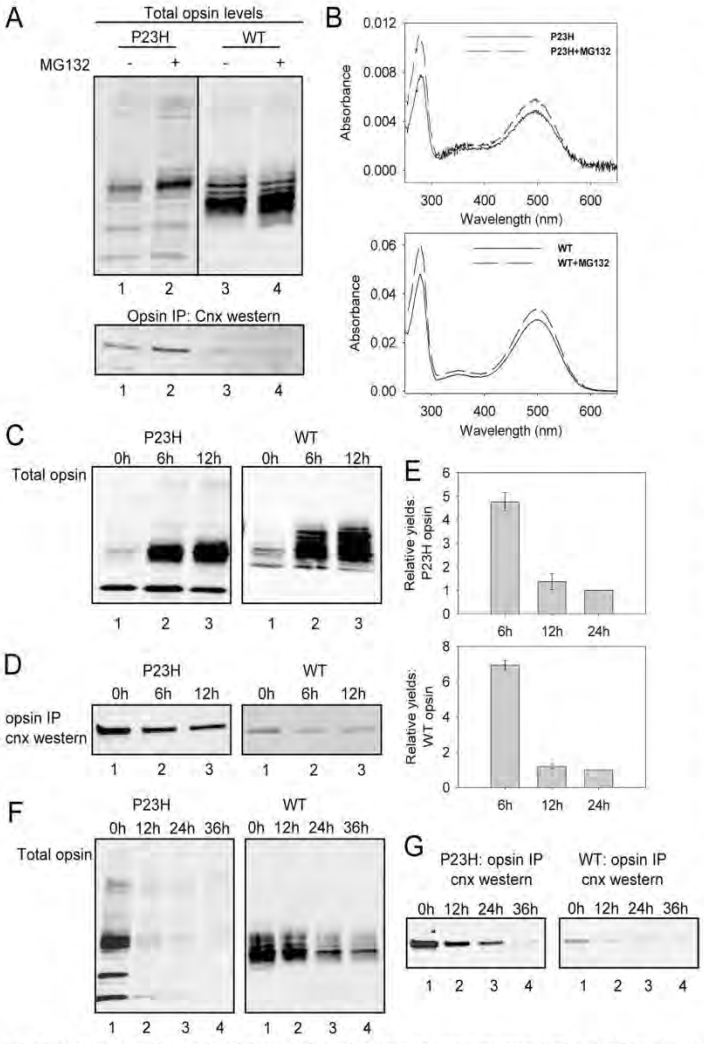

FIGURE 2. **Opsin is an ER-associated degradation substrate and associates transiently with Cnx.** *A*, Western blot (*upper panel*) of total P23H and WT opsin levels in absence (*lanes 1* and *3*) and presence (*lanes 2* and *4*) of MG132. The immunoprecipitated (*IP*) Cnx for the corresponding samples is shown in the Cnx Western blot in the *lower panel*. Lanes are as in *upper panel*. *B*, spectra of purified folded P23H (*upper panel*) and WT (*lower panel*) rhodopsin generated in the presence of MG132. Spectra generated from MG132-treated samples are shown as *dashed traces*. *C*, opsin levels steadily increase with time after induction. Immunoblots of P23H (*left panel*) and WT opsin (*right panel*) were collected at given time points. *D*, maximum Cnx is associated with opsins at early time points. Cnx immunoblots show a decrease in immunoprecipitated Cnx at the indicated time points after induction. *E*, ratio of immunoprecipitated Cnx to the total opsin in *C* is quantified for each time point after opsin induction for P23H (*upper panel*) and WT (*lower panel*). *F*, immunoblots of total P23H opsin (*left panel*) and WT opsin (*right panel*) collected at different time points after cycloheximide addition (0 h). *G*, Cnx Western blots of proteins immunoprecipitated with P23H (*left panel*) and WT opsin (*right panel*) after cycloheximide treatment show a prolonged association of Cnx with P23H opsin.

lower panel). Folded WT rhodopsin did not show any detectable ubiquitination. However, folded P23H rhodopsin showed traces of ubiquitination, reflecting a difference between the folded forms of the two proteins (Fig. 1*E*, *lower panel*, *arrow* points to the position of ubiquitin signal in *lane 3*). The folded and misfolded fractions were also probed for the presence of calreticulin, because many glycoproteins that interact with Cnx also interact with calreticulin. No trace of associated calreticulin was detected in the Western blots. Hsp70 also was not detected in the blots (data not shown).

To better quantify the relative amounts of Cnx and ubiquitin associated with rhodopsin, their ratio to total opsin was determined. We found that 45-fold more Cnx and 15-fold more ubiquitin were associated with P23H than with WT (Fig. 1*F*, *middle* and *right panels*).

Prolonged Cnx Association with Mutant Opsin—Because misfolded P23H and WT rhodopsin were highly ubiquitinated, we investigated their fates as ER-associated degradation substrates. To study this, we expressed P23H and WT opsin in the presence of the proteasome inhibitor MG132, which resulted in a 2-fold increase in P23H opsin levels, indicating preservation from degradation (Fig. 2*A*, *upper panel*). The WT opsin levels increased only by 10% (Fig. 2*A*, *upper panel*). A marginal increase in the amount of WT opsin reflected that only a small fraction of it was misfolded and targeted for degradation through the proteasome. We next determined the levels of Cnx bound to MG132-treated WT and P23H opsins. Cnx immunoblots of MG132-treated P23H cells showed 2-fold more Cnx bound with the misfolded fractions (Fig. 2*A*, *lower panel*). No increase in bound Cnx was seen for WT opsin (Fig. 2*A*, *lower panel*), possibly because a 10% increase may not be sufficient for detection of differences in Cnx levels.

We further investigated whether the folded forms of the two opsins were also targeted for proteasomal degradation. On treatment with MG132, the amount of pigment increased by 20% for P23H (Fig. 2*B*, *upper panel*) and 10% for WT rhodopsin (Fig. 2*B*, *lower panel*). A 20% increase in folded protein suggests that folded P23H rhodopsin is also targeted for proteasomal degradation but to a lesser extent than its misfolded counterpart.

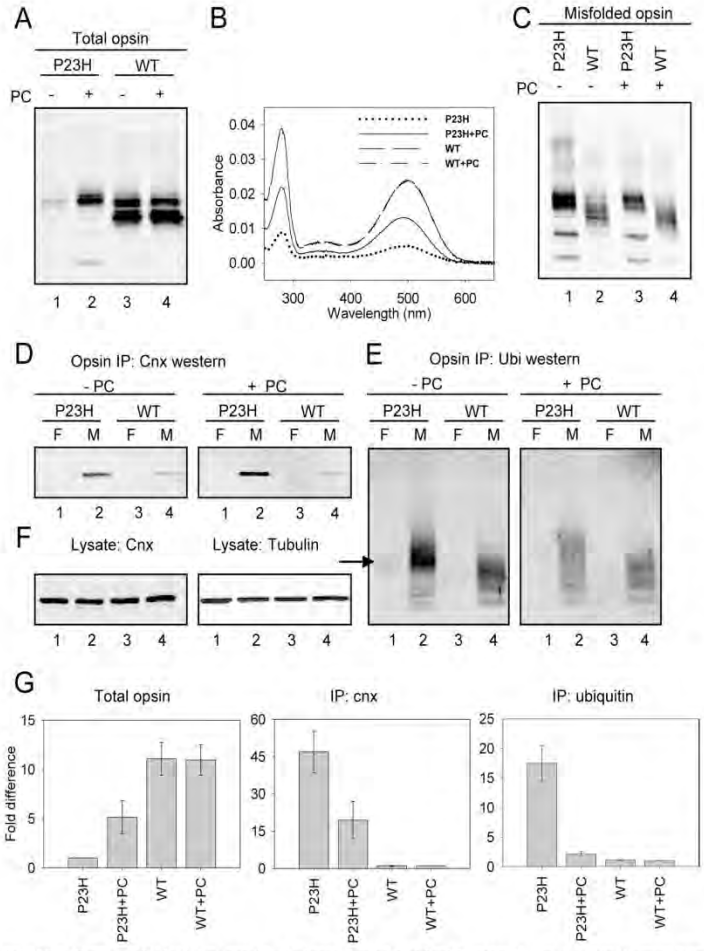

FIGURE 3. **Pharmacological chaperoning reduces Cnx and ubiquitin association.** *A*, opsin Western blot shows 5-fold increase in P23H opsin levels on addition of PC (*lane 2*). WT levels remain unaffected. *B*, spectra of immunopurified folded rhodopsins from PC-treated P23H show a 5-fold increase (*boldface*) in comparison with untreated sample (*dotted*). WT rhodopsin levels were not affected in either case (spectra are superimposed). *C*, immunoblot of misfolded opsins show that misfolded P23H opsin reduces on addition of the PC (*lane 3*) in comparison with untreated P23H (*lane 1*). Misfolded forms of WT opsin are not significantly altered (*lanes 2* and *4*). *D*, Cnx Western blots showing Cnx levels associated with misfolded (*M*) forms of P23H and WT opsins in the PC untreated (*left panel*) and treated (*right panel*) conditions. Folded (*F*) forms do not show any trace of Cnx. *IP*, immunoprecipitation. *E*, ubiquitin Western blots of the folded (*F*) and misfolded (*M*) opsin from the PC treated (*right panel*) or untreated (*left panel*) cells. Pharmacological chaperoning (*right panel*) reduces ubiquitination of misfolded forms. Ubiquitination of folded P23H is also reduced (*right panel, lane 1*). *F*, total cellular levels of Cnx (*left panel*) and tubulin (*right panel*) remain unaltered in absence or presence of the PC. *G*, *left panel* quantifies relative yields of cellular opsin levels in presence or absence of the PC. *Middle* and *right panels* show quantification of Cnx and ubiquitin ratios to total opsin, respectively, as fold difference.

Different molecular chaperones interact with newly folded proteins at different times during biogenesis. To determine whether Cnx interacted early with rhodopsin, we induced WT and P23H cells for 6, 12, and 24 h, after which we immunoprecipitated rhodopsin and compared opsin and Cnx levels. Total opsin levels increased steadily with time for both WT and P23H opsins (Fig. 2*C*). The maximum amount of Cnx (4-fold) was recovered at 6 h, which was the earliest time point tested after opsin induction (Fig. 2*D*). At later time points the rhodopsin/Cnx ratio decreased (Fig. 2, *D* and *E*). These data demonstrate that recognition by Cnx is an early event during opsin biosynthesis (when the bulk of Cnx is bound to the nascent opsin molecules), presumably helping them to fold.

We further characterized the stability of the Cnx-rhodopsin interaction to determine whether this relationship was transient or long lasting. We induced P23H and WT cells for 12 h (0 h in Fig. 2*F*) and then added cycloheximide to stop further protein synthesis. Cells were harvested at 12, 24, and 36 h after cycloheximide treatment, and opsin was immunoprecipitated. Opsin levels fell sharply for P23H after cycloheximide addition, indicating rapid cellular clearance (Fig. 2*F*, *left panel*). WT opsin, on the other hand, was more stable and cleared more slowly from the cells (Fig. 2*F*, *right panel*). For P23H, immunoblots showed increased Cnx levels until 24 h after inhibition of protein synthesis (Fig. 2*G*, *left panel*), which is in sharp contrast with WT, for which associated Cnx levels reached steady-state levels in half the time (*i.e.* 12 h) (Fig. 2*G*, *right panel*). These observations demonstrate the transient nature of Cnx association with WT but a prolonged Cnx association with P23H opsin.

Pharmacological Chaperone Reduces Cnx Association with Mutant Rhodopsin—We next investigated the effect of opsin conformation on Cnx association by inducing P23H opsin to fold in the presence of a PC (11-*cis*-retinal). P23H and WT cells were expressed in the presence of the PC. Immunoblot of cell lysates showed a 5-fold increase in opsin levels in PC-treated P23H cells compared with untreated controls (Fig. 3*A*). WT opsin levels were not affected appreciably in either case (Fig. 3*A*, *lanes 3* and *4*), indicating the absence of any significant amounts of misfolded forms in the total rhodopsin pool. The effect of PC on the folded forms was determined spectrophotometrically; 5-fold more pigment was detected from PC-treated P23H cells (Fig. 3*B*) than untreated P23H cells. Pigment levels were not affected by the presence of PC in WT cells (Fig. 3*B*, *superimposed dashed spectra*). The yield of mis-

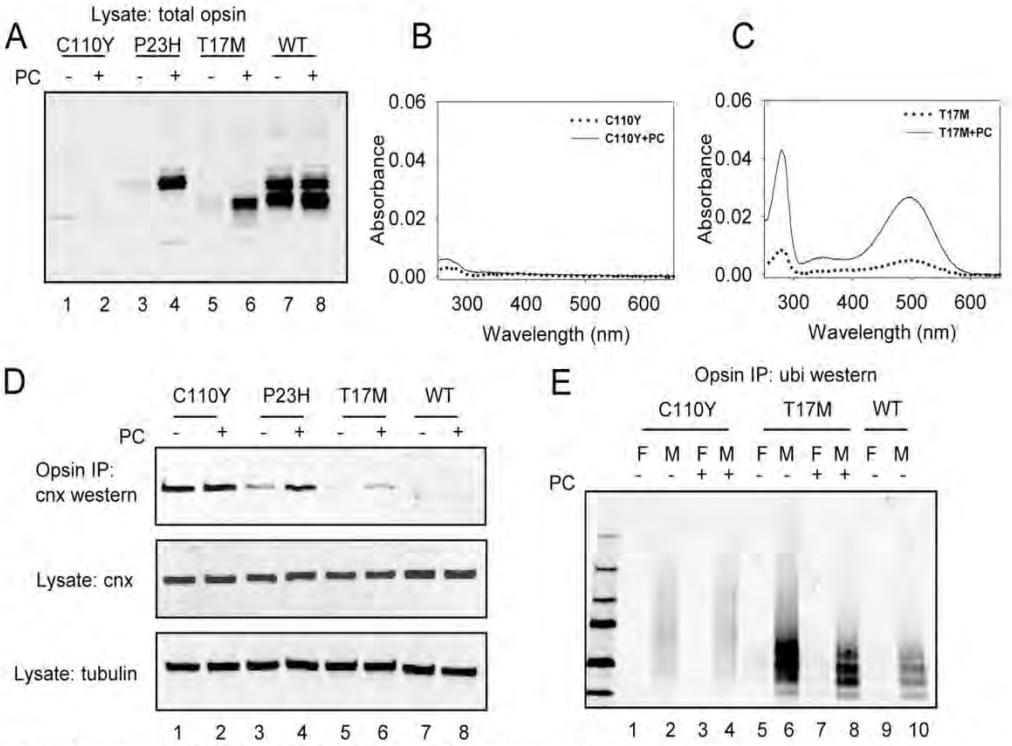

FIGURE 4. **Cnx associates with other misfolded rhodopsin mutants.** *A*, Western blot of total opsin levels shows no difference in total opsin levels for the PC-treated (*lane 2*) and untreated (*lane 1*) C110Y. T17M (*lane 6*) rhodopsin levels increase on PC addition. P23H and WT opsins show same behavior as before. *B*, spectra of folded rhodopsin from the PC treated (*dotted trace*) and untreated (*boldface trace*) C110Y cells show that this mutant could not be rescued. *C*, rhodopsin spectra from the PC-treated (*dashed trace*) and untreated (*boldface trace*) T17M cells show a 5-fold increase in folded rhodopsin on PC addition. *D*, *upper panel* shows the levels of immunoprecipitated Cnx. These levels do not change for C110Y on addition of the PC (*lane 2*). The apparent levels of associated Cnx increase for T17M on PC addition, but normalization to total opsin (*A*, *lane 6*) shows that these levels are lower than in the absence of the PC. Western blots of total Cnx (*middle panel*) and tubulin (*lower panel*) show no effect of opsin expression or PC addition on the levels of these proteins. *E*, Western blot shows ubiquitination of misfolded forms of all the opsins. Folded fractions (*F*) of the PC untreated T17M (*lane 5*) is ubiquitinated, which reduces on addition of the PC (*lane 7*).

folded opsin was reduced 2-fold in PC-treated P23H cells (Fig. 3*C*). Misfolded WT opsin levels did not change appreciably with PC addition (Fig. 3*C*).

Furthermore, we investigated the effect of PC on Cnx binding to misfolded rhodopsin. Cnx preferentially associated with misfolded opsins (Fig. 3*D*). Normalization of associated Cnx levels with total opsin levels revealed a 3-fold reduction of Cnx when PC was added (Fig. 3*D*). For WT rhodopsin, the bound Cnx levels did not change with PC treatment (Fig. 3*D*). Cellular Cnx levels did not change appreciably when rhodopsin production was induced in the presence of PC (Fig. 3*F*).

Because non-native forms of proteins are ubiquitinated and marked for degradation during QC, we also studied the effect of PC on the amount of ubiquitinated P23H opsin. Ubiquitination of misfolded opsins from the PC-treated cells was reduced compared with untreated cells (Fig. 3*E*). Correctly folded P23H rhodopsin showed ubiquitination (Fig. 1*E*; Fig. 3*E*, *arrow*), which was significantly reduced on addition of PC. The difference in the levels of opsin generated, bound Cnx, and ubiquitination in the absence or presence of the PC are quantified in Fig. 3*G*.

Cnx Associates with Other RP-causing Mutants of Rhodopsin—Having observed enhanced Cnx association with misfolded P23H rhodopsin, we investigated this association in two other RP-associated mutants (*i.e.* T17M and C110Y). To determine whether greater Cnx association was specific for P23H or was a more general feature of misfolded opsins, we expressed mutant T17M and C110Y stably in HEK293 cells. The mutation T17M also abolishes one of the glycosylation sites (Asn-15) on rhodopsin. First, we studied the effect of the PC on these mutants. Opsin immunoblots showed only minute traces of the C110Y protein in either the absence or presence of the PC (Fig. 4*A*). T17M, on the other hand, produced 5-fold more total opsin in the presence of the PC (Fig. 4*A*). We then studied the effect of PC on protein folding in these mutants. No pigment formation was observed for C110Y, in either the absence or presence of the PC (Fig. 4*B*), demonstrating that the conformation of the mutant could not be induced to fold by pharmacological meth-

ods. In contrast, T17M, when expressed in a stable cell line without the aid of the PC, produced only a small amount of pigment (Fig. 4*C*, *dotted spectrum*); the presence of the PC led to a 5-fold increase in folded rhodopsin (Fig. 4*C*, *boldface spectrum*). These observations showed that although T17M could be rescued pharmacologically, C110Y was structurally too distorted to accommodate the PC.

We then studied the nature of Cnx association with these mutants. The amount of bound Cnx showed an inverse correlation with the ability of a mutant to be pharmacologically rescued (Fig. 4*D*, *upper panel*). The greatest amounts of Cnx were associated with C110Y, the most severe mutation, which could not be pharmacologically corrected. The Cnx levels were similar in the presence or absence of the PC, which confirms previous observation that folded rhodopsin levels in C110Y did not differ under similar conditions (Fig. 4*B*). In sharp contrast, T17M showed reduction in the levels of associated Cnx in the presence of the PC. In comparison with P23H, C110Y opsin was bound by 2-fold more Cnx, although T17M had 3-fold less Cnx associated with it (Fig. 4*D*). We also investigated whether induction of these mutants increased cellular levels of Cnx. As with P23H, Cnx levels were not significantly altered in these cell lines on expression of C110Y and T17M mutant rhodopsin (Fig. 4*D*, *middle panel*).

Having observed that even the folded fractions of P23H opsin were ubiquitinated, we determined whether folded fractions of C110Y and T17M proteins were also ubiquitinated. No trace of ubiquitination was seen in immunoblots of C110Y probably because little opsin could be isolated from these cells. In T17M, on the other hand, ubiquitination was observed in the folded fraction (Fig. 4*E*, *lane 5*). Confirming our previous observation of P23H, ubiquitination of the pharmacologically rescued T17M was reduced with PC treatment (Fig. 4*E*).

Cnx and Misfolded Opsin Are Associated in a Mouse Model of RP—To extend our observations further, we investigated whether our results from cell culture corresponded with a mouse model of RP. Total rhodopsin from the eyes of 1-month-old P23H and C57/B6 (WT) mice was solubilized, and cell lysate was probed for opsin and Cnx. The opsin immunoblots of the lysates revealed 10-fold more rhodopsin in WT mice than in the age-matched P23H mice (Fig. 5*A*). This difference in opsin level was also reflected in the levels of folded rhodopsin from the two mice (Fig. 5*B*). Total Cnx levels in the lysates of eyes did not differ significantly between WT and P23H mice (Fig. 5*A*, *middle panel*). We then determined the levels of Cnx associated with the folded and misfolded forms of the two opsins. The folded fractions of both WT and P23H rhodopsin showed no trace of Cnx, which exclusively associated with misfolded forms (Fig. 5*C*, *upper panel*). As observed previously in cell culture, despite the low amounts of total opsin in P23H mice, the misfolded fraction was more ubiquitinated than misfolded WT opsin (Fig. 5*C*, *lower panel*). But unlike cell culture, in which no trace of ubiquitination was seen in folded WT rhodopsin (Fig. 1*E* and Fig. 3*E*), the immunoblots of folded rhodopsin from WT mice showed the presence of ubiquitination (Fig. 5*C*, *lower panel, lane 1*). The folded rhodopsin fraction from P23H mice showed 2-fold more ubiquitination than WT mice. On normalizing to total opsin, 3-fold more Cnx was associated with rhodopsin isolated from P23H mice than the WT mice (Fig. 5*D*, *lower panel*). The *upper panel* in Fig. 5*A* quantifies the results. Hsp70 and calreticulin were not detected in folded or misfolded fractions of the mouse rhodopsins (data not shown). Collectively, these observations correlate well with our data from the cell culture experiments.

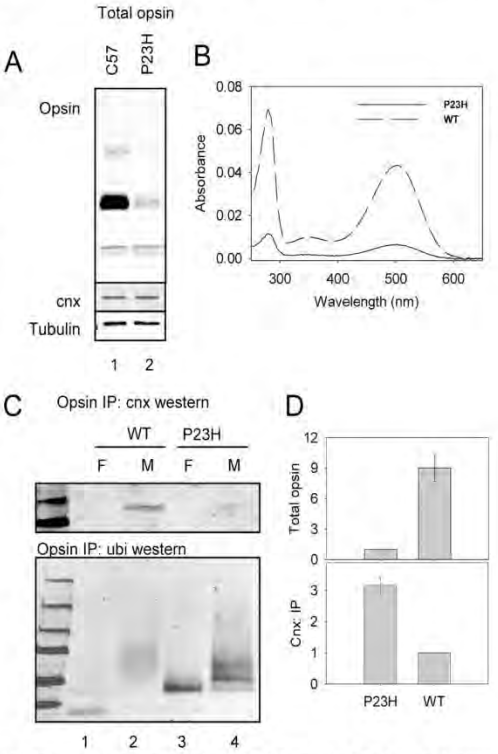

FIGURE 5. **Cnx associates with misfolded opsin in P23H mice.** *A*, opsin Western blot shows 10-fold less opsin in P23H mice as compared with WT C57 mice (*upper panel*). Total cellular levels of Cnx (*middle panel*) and tubulin (*lower panel*) are not significantly different in the eyes of both mice. *B*, spectra of immunopurified folded rhodopsin from P23H (*boldface trace*) and WT (*dashed trace*) mice show 10-fold more rhodopsin in WT mice. *C*, Cnx immunoblots show Cnx association with misfolded (*M*) WT (*upper panel, lane 2*) and P23H (*upper panel, lane 4*) opsin from mice. Folded fractions (*F*) show no Cnx. Ubiquitination is seen for both folded (*F*) and misfolded (*M*) fractions of mice rhodopsin. *D*, *upper panel* quantifies the relative yields of total opsin from the two mice. Immunoprecipitated (*IP*) Cnx is quantified in *lower panel*. The yields of Cnx were normalized to total opsin in both the mice.

Cnx Overexpression Causes Greater Accumulation of Misfolded P23H Opsin—To further elucidate the importance of the Cnx-rhodopsin association, we overexpressed Cnx in the opsin-producing cell lines. We investigated whether increased cellular Cnx levels led to either the accelerated degradation of misfolded opsin or to its appropriate folding. Cnx constructs were transiently transfected in opsin-producing cell lines. At 48 h post-transfection, Cnx levels increased 2.5–3-fold and remained at that level for the next 24 h (Fig. 6*A*). The cell lines were induced to express opsin 48 h after Cnx transfection so that opsin production occurred during increased cellular levels

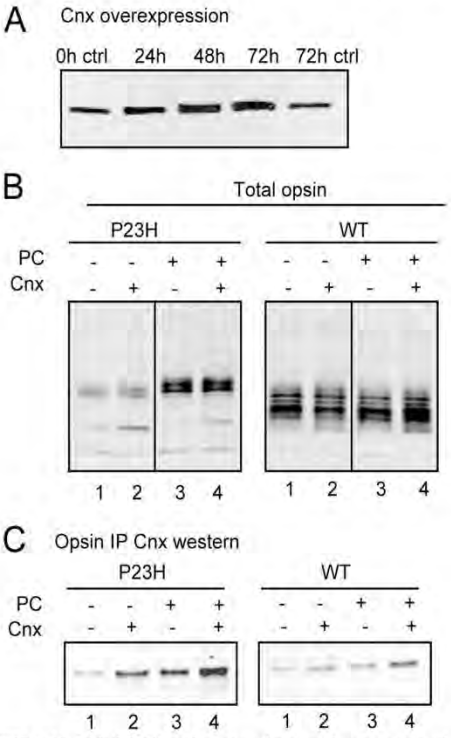

FIGURE 6. **Misfolded P23H opsin accumulates on Cnx overexpression.** *A*, Cnx Western blot shows a 2.5-fold increase in total cellular levels of Cnx after 48 h of transient transfection of pCMV-SPORT6-Cnx. *Ctrl*, control. *B*, opsin immunoblots of P23H (*left panel*) and WT opsin level (*right panel*) in the presence or absence of PC and Cnx overexpression. P23H opsin levels increase on Cnx overexpression. Such increase is not seen on overexpressing Cnx in the presence of the PC (*lanes 3* and *4*). *C*, immunoblots of Cnx precipitated with P23H (*left panel*) and WT (*right panel*) opsins in the absence and presence of overexpressed Cnx or the PC. Cnx overexpression increases Cnx associated 3-fold (*lanes 2*). Addition of the PC increases the apparent Cnx levels only in P23H (*lane 3*), whereas the presence of both overexpressed Cnx and the PC increases Cnx levels 5-fold higher (*lane 4*, *left panel*). *IP*, immunoprecipitated.

of Cnx. Under these conditions, P23H opsin levels increased by 35% (Fig. 6*B*, *left panel*). However, the WT levels did not increase, suggesting there was no effect of Cnx overexpression on WT levels (Fig. 6*B*, *right panel*). Thus, a preferential accumulation of mutant protein with Cnx overexpression appeared to be present.

We then investigated the effect of PCs on total opsin levels in the presence of overexpressed Cnx. As demonstrated previously, the presence of PC resulted in a 5-fold increase in P23H opsin levels, but no further increase or decrease was observed in this level when Cnx was overexpressed (Fig. 6*B*, *left panel*). Similarly, no increase was seen for WT opsin. A 3-fold higher Cnx association was observed in P23H cells transfected with Cnx in comparison with untransfected cells (Fig. 6*C*, *left panel*). A 3-fold higher Cnx association was also seen in PC-treated cells when Cnx was overexpressed (Fig. 6*C*, *left panel*, *lanes 3* and *4*). Despite this 3-fold excess of Cnx, P23H opsin levels did not increase in the presence of PC. These observations demonstrate that association with Cnx slows the degradation of the mutant protein. In the presence of the PC, total levels of both opsins do not increase with Cnx overexpression.

Cnx Overexpression Increases the Yield of Folded P23H Opsin Only in the Presence of a PC—Because we observed increased cellular levels of P23H opsin when Cnx was overexpressed, we explored whether this pool of protein included more folded rhodopsin. We compared spectrophotometrically the yields of immunopurified folded rhodopsin generated in the absence or presence of Cnx overexpression alone. No significant increase in the P23H pigment was observed in the presence of only overexpressed Cnx (Fig. 7*A*, *left panel*); similar to the effect on yield of total WT opsin, no difference in folded WT rhodopsin level was observed in the presence of overexpressed Cnx (Fig. 7*A*, *middle panel*). These data demonstrate that direct association of increased amounts of Cnx with P23H or WT opsin was not sufficient to increase the yield of folded P23H or WT rhodopsins.

We next investigated the effect of increased Cnx levels on rhodopsin folding in a milieu where opsin molecules were actively assisted to fold (*i.e.* in the presence of a PC). The amount of folded P23H rhodopsin increased 25% with Cnx overexpression in the presence of the PC (Fig. 7*B*, *left panel*). This effect was specific for the mutant protein, as no such increase was observed in the case of WT (Fig. 7*B*, *right panel*). Because the previous experiments showed that the total P23H opsin levels did not increase in the presence of both the overexpressed Cnx and the PC, the selective increase in folded P23H rhodopsin indicated an increased, intracellular efficiency of mutant rhodopsin folding.

DISCUSSION

In this study, we examined the interaction of Cnx with WT and mutant opsins associated with RP. Cnx preferentially associates with the misfolded fraction of WT and mutant opsins. These fractions were also highly ubiquitinated. The folded WT rhodopsin was not bound to Cnx and was not ubiquitinated. However, the folded forms of the P23H and T17M rhodopsin, even though not bound to Cnx, were mildly ubiquitinated. Because rhodopsin is a substrate for proteasomal degradation (20, 21), ubiquitination of these folded molecules may be the reason for their lower recovery in comparison with WT rhodopsin. The degradation of WT and P23H opsins was inhibited by MG132, demonstrating that they are substrates for the proteasome. Although to a lesser extent, even folded WT and P23H rhodopsin accumulated with proteasome blockage, indicating that similar to the misfolded opsin, the folded rhodopsin pool in the cell is susceptible to the proteasome. The fact that folded P23H was ubiquitinated was reflected in the higher accumulation of P23H-folded than WT-folded rhodopsin.

Association with Cnx serves different functions for WT and mutant glycoproteins, based on studies of different model proteins. Cnx functions as a folding chaperone for WT glycoproteins (10, 30), but it only increases the cellular retention of mutant glycoproteins. In addition, the association of WT glycoproteins with Cnx is transient, whereas for mutants Cnx association can be prolonged and stable (5, 7, 11, 12, 31, 32). Our study results showed a similar dual role of Cnx for WT and

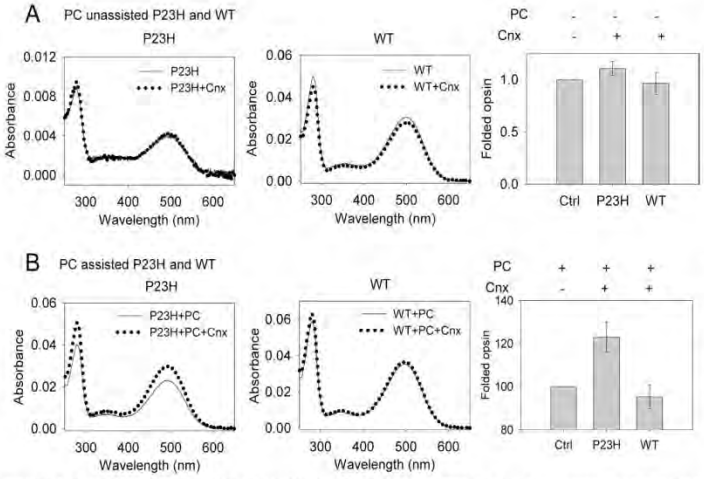

FIGURE 7. **Cnx increases yield of folded P23H rhodopsin in the presence of PC.** *A*, spectra of folded P23H (*left panel*) and WT (*middle panel*) generated by overexpressing of Cnx in the absence of PC. Folded rhodopsin yields do not significantly alter on overexpression of Cnx. The respective yields are quantified in the *graph* in the *right panel*. The yield of rhodopsin in the absence of Cnx overexpression was taken as 1. *Ctrl*, control. *B*, spectra of folded P23H (*left panel*) and WT (*middle panel*) rhodopsin generated by overexpressing Cnx in the presence of PC. Folded P23H rhodopsin yields significant increases on overexpressing Cnx in the presence of PC. Relative increases of both rhodopsins are plotted in the *graph* in the *right panel*. The yield of rhodopsin in the presence of the PC was taken as 1.

mutant rhodopsin. Its association with WT rhodopsin was transient, although it could be detected with P23H opsin for extended periods despite very low levels of the P23H protein.

Immunoprecipitation of C110Y and T17M revealed that Cnx association was not limited to P23H opsin but was a more general feature of misfolded mutants. The extent of Cnx association with the three mutant opsins varied with the nature of the mutation. The largest amount of Cnx precipitated with C110Y, the most severe mutation of the three studied and clinically the most severe phenotype among them. More Cnx was associated with P23H than with T17M; P23H is clinically more severe than T17M. Significantly less association of Cnx with T17M, in our experiments, may be the consequence of both the loss of one of the two glycosylation sites of rhodopsin by this mutation and also the inherent misfolded state of this protein. Because P23H and T17M produce similar levels of folded rhodopsin, the association of significantly more Cnx with P23H may be responsible for the greater severity of P23H than T17M. A similar distinction was seen between two types of mutants of fukutin-related protein that cause congenital muscular dystrophy. The mutant proteins that bound more Cnx (S221R, A455D, and P448L) caused more severe diseases than L276I, which did not bind with Cnx to the same extent and caused less severe disease (11).

Our observations of the rhodopsin isolated from WT and P23H mice showed a direct correlation with our cell culture observations. In WT as well as P23H mice, only the misfolded fractions of opsin associated with Cnx. Additionally, on a unit opsin basis, significantly greater amounts of Cnx were bound to rhodopsin from P23H mice than from WT mice. Misfolded forms of opsin from both mice were also highly ubiquitinated. However, unlike the cell culture experiments (where no trace of ubiquitination was seen for folded forms of WT rhodopsin), in our observations the folded rhodopsin from WT mice was ubiquitinated; this may reflect a potentially more stringent QC monitoring system in the rod photoreceptor cell or possibly a higher proportion of molecules in non-native conformations.

Incubation of P23H and T17M cells with PC showed significant reduction in the amounts of Cnx bound with mutant rhodopsins. However, Cnx levels did not fall for C110Y with the addition of a PC because of the severe alteration of the structure of the protein, which is too severe to be corrected by the presence of a PC. Therefore, the mutants that responded to the PC showed reduction of bound Cnx, whereas the mutant that was insensitive to the presence of the PC did not show any reduction in bound Cnx levels. This clearly demonstrates that Cnx association with rhodopsin is conformation-dependent. Taken together, our observations with misfolded rhodopsin agree strongly with reports from other mutant glycoproteins that demonstrate a reciprocal relationship between the effect of a PC and the amounts of Cnx bound to misfolded proteins (31, 33, 34).

It is generally accepted that the longer a glycoprotein associates with Cnx, the more likely that correct folding of the protein will be achieved (35). This is, however, applicable only to WT glycoproteins, because longer association of Cnx with mutant glycoproteins is not known to increase their folding. Previous studies on modulation of ER proteostasis showed that Cnx overexpression may not have any effect on some proteins, although it may increase the expression of other WT glycoproteins, suggesting that the effect of this intervention is substrate-specific (30, 36–39). We utilized a similar approach to determine what role Cnx has in controlling either the folding or degradation of opsin. WT rhodopsin levels did not change with Cnx overexpression, whereas P23H levels increased indicating that increased Cnx levels led to greater ER QC stringency but did not enhance opsin degradation. However, under these conditions, we did not observe an increase of P23H pigment, which provides direct biochemical evidence that Cnx by itself did not assist in the folding of mutant rhodopsin and corroborates a recent report indicating that Cnx does not affect maturation of rhodopsin (2).

Proteostasis modulation in the presence of a PC was tested previously for human gonadotropin-releasing hormone receptor (GnRHR). Cnx overexpression in the presence of a PC increased the amount of folded WT receptor. However, in the case of the mutant, such an effect could not be ascertained. An increased amount of Cnx was found to be associated with the

mutant, but it could not be determined whether this treatment resulted in plasma membrane localization of the mutant, which is indicative of more efficient folding and trafficking (40). Because we have previously demonstrated that PCs assist folding of misfolded P23H (22, 23, 28), we reasoned that addition of a PC might provide the right folding milieu to test whether a folding component of Cnx could be deciphered in such a folding-prone environment. The presence of the PC alone increased the levels of P23H opsin/rhodopsin 5-fold, but with Cnx overexpression in the presence of the PC, no further increase in total P23H opsin level was seen. However, analysis of the folded P23H rhodopsin generated under these conditions, as measured by pigment levels, showed a 25% increase over folded P23H rhodopsin generated in the presence of PC alone. Our results suggest that Cnx holds P23H opsin in a degradation-protected but functionally misfolded state until the PC can assist the actual folding. Because the total opsin level did not increase, the increase in folded rhodopsin may reflect an equilibrium shift toward the folded state, in which more of the misfolded proteins tend to fold. Our results also indicate that Cnx can participate in increasing the efficiency of the folding process in the ER when cellular conditions are favorable to folding. Furthermore, the effect was selective for P23H, because no difference in WT rhodopsin yield was observed.

In summary, we have characterized the physical interaction of Cnx with rhodopsin and provide evidence that this interaction can be targeted to increase the yields of correctly folded mutant rhodopsin. In the future, it may be possible to increase cellular calnexin levels via small molecule or gene therapy approaches. Such a targeted approach may provide a general method for treating protein conformational disorders.

Acknowledgments—We thank Dr. Mark Krebs for comments and discussions and Linda Stein for technical help.

REFERENCES

1. Ellgaard, L., and Helenius, A. (2003) *Nat. Rev. Mol. Cell Biol.* **4,** 181–191
2. Kosmaoglou, M., and Cheetham, M. E. (2008) *Mol. Vis.* **14,** 2466–2474
3. Balch, W. E., Morimoto, R. I., Dillin, A., and Kelly, J. W. (2008) *Science* **319,** 916–919
4. Ellgaard, L., and Frickel, E. M. (2003) *Cell Biochem. Biophys.* **39,** 223–247
5. Le, A., Steiner, J. L., Ferrell, G. A., Shaker, J. C., and Sifers, R. N. (1994) *J. Biol. Chem.* **269,** 7514–7519
6. Markkanen, P. M., and Petäjä-Repo, U. E. (2008) *J. Biol. Chem.* **283,** 29086–29098
7. Morello, J. P., Salahpour, A., Petäjä-Repo, U. E., Laperrière, A., Lonergan, M., Arthus, M. F., Nabi, I. R., Bichet, D. G., and Bouvier, M. (2001) *Biochemistry* **40,** 6766–6775
8. Ni, M., and Lee, A. S. (2007) *FEBS Lett.* **581,** 3641–3651
9. Dickson, K. M., Bergeron, J. J., Shames, I., Colby, J., Nguyen, D. T., Chevet, E., Thomas, D. Y., and Snipes, G. J. (2002) *Proc. Natl. Acad. Sci. U.S.A.* **99,** 9852–9857
10. Farinha, C. M., and Amaral, M. D. (2005) *Mol. Cell. Biol.* **25,** 5242–5252
11. Esapa, C. T., McIlhinney, R. A., and Blake, D. J. (2005) *Hum. Mol. Genet.* **14,** 295–305
12. Kim, P. S., Lee, J., Jongsamak, P., Menon, S., Li, B., Hossain, S. A., Bae, J. H., Panijpan, B., and Arvan, P. (2008) *Mol. Endocrinol.* **22,** 477–484
13. Mu, T. W., Ong, D. S., Wang, Y. J., Balch, W. E., Yates, J. R., 3rd, Segatori, L., and Kelly, J. W. (2008) *Cell* **134,** 769–781
14. Barral, J. M., Broadley, S. A., Schaffar, G., and Hartl, F. U. (2004) *Semin. Cell Dev. Biol.* **15,** 17–29
15. Warrick, J. M., Chan, H. Y., Gray-Board, G. L., Chai, Y., Paulson, H. L., and Bonini, N. M. (1999) *Nat. Genet.* **23,** 425–428
16. Okada, T., and Palczewski, K. (2001) *Curr. Opin. Struct. Biol.* **11,** 420–426
17. Deretic, D. (2006) *Vision Res.* **46,** 4427–4433
18. Sung, C. H., Schneider, B. G., Agarwal, N., Papermaster, D. S., and Nathans, J. (1991) *Proc. Natl. Acad. Sci. U.S.A.* **88,** 8840–8844
19. Kaushal, S., and Khorana, H. G. (1994) *Biochemistry* **33,** 6121–6128
20. Saliba, R. S., Munro, P. M., Luthert, P. J., and Cheetham, M. E. (2002) *J. Cell Sci.* **115,** 2907–2918
21. Illing, M. E., Rajan, R. S., Bence, N. F., and Kopito, R. R. (2002) *J. Biol. Chem.* **277,** 34150–34160
22. Noorwez, S. M., Kuksa, V., Imanishi, Y., Zhu, L., Filipek, S., Palczewski, K., and Kaushal, S. (2003) *J. Biol. Chem.* **278,** 14442–14450
23. Noorwez, S. M., Malhotra, R., McDowell, J. H., Smith, K. A., Krebs, M. P., and Kaushal, S. (2004) *J. Biol. Chem.* **279,** 16278–16284
24. Rattner, A., Sun, H., and Nathans, J. (1999) *Annu. Rev. Genet.* **33,** 89–131
25. Frederick, J. M., Krasnoperova, N. V., Hoffmann, K., Church-Kopish, J., Rüther, K., Howes, K., Lem, J., and Baehr, W. (2001) *Invest. Ophthalmol. Vis. Sci.* **42,** 826–833
26. Rosenbaum, E. E., Hardie, R. C., and Colley, N. J. (2006) *Neuron* **49,** 229–241
27. Katanosaka, K., Tokunaga, F., Kawamura, S., and Ozaki, K. (1998) *FEBS Lett.* **424,** 149–154
28. Noorwez, S. M., Ostrov, D. A., McDowell, J. H., Krebs, M. P., and Kaushal, S. (2008) *Invest. Ophthalmol. Vis. Sci.* **49,** 3224–3230
29. Krebs, M. P., White, D. A., and Kaushal, S. (2009) *Invest. Ophthalmol. Vis. Sci.* **50,** 2956–2965
30. Okiyoneda, T., Niibori, A., Harada, K., Kohno, T., Michalak, M., Duszyk, M., Wada, I., Ikawa, M., Shuto, T., Suico, M. A., and Kai, H. (2008) *Biochim. Biophys. Acta* **1783,** 1585–1594
31. Gong, Q., Jones, M. A., and Zhou, Z. (2006) *J. Biol. Chem.* **281,** 4069–4074
32. Bradley, C. A., Taghibiglou, C., Collingridge, G. L., and Wang, Y. T. (2008) *J. Biol. Chem.* **283,** 22043–22050
33. Robert, J., Auzan, C., Ventura, M. A., and Clauser, E. (2005) *J. Biol. Chem.* **280,** 42198–42206
34. Leskelä, T. T., Markkanen, P. M., Pietilä, E. M., Tuusa, J. T., and Petäjä-Repo, U. E. (2007) *J. Biol. Chem.* **282,** 23171–23183
35. Paulsson, K., and Wang, P. (2003) *Biochim. Biophys. Acta* **1641,** 1–12
36. Butz, J. A., Niebauer, R. T., and Robinson, A. S. (2003) *Biotechnol. Bioeng.* **84,** 292–304
37. Higgins, M. K., Demir, M., and Tate, C. G. (2003) *Biochim. Biophys. Acta* **1610,** 124–132
38. Klabunde, J., Kleebank, S., Piontek, M., Hollenberg, C. P., Hellwig, S., and Degelmann, A. (2007) *FEMS Yeast Res.* **7,** 1168–1180
39. Prasad, S. A., Yewdell, J. W., Porgador, A., Sadasivan, B., Cresswell, P., and Bennink, J. R. (1998) *Eur. J. Immunol.* **28,** 907–913
40. Brothers, S. P., Janovick, J. A., and Conn, P. M. (2006) *J. Mol. Endocrinol.* **37,** 479–488

APPENDIX II

Desiree Baron (DB), Laura Kaushansky (LK), and Catherine Ward planned and performed the majority of experiments; DB, Alex J. Quaresma and Jeffrey A. Nickerson planned, performed and analyzed data for FRAP; Ru-Ju Chian cloned deletion constructs for structure-function analyses; Reddy Ranjith K Sama and Kristin Boggio contributed to the design and data interpretation for experiments.

Baron et al. Molecular Neurodegeneration 2013, 8:30
http://www.molecularneurodegeneration.com/content/8/1/30

MOLECULAR NEURODEGENERATION

RESEARCH ARTICLE Open Access

Amyotrophic lateral sclerosis-linked FUS/TLS alters stress granule assembly and dynamics

Desiree M Baron[1], Laura J Kaushansky[1], Catherine L Ward[1], Reddy Ranjith K Sama[1], Ru-Ju Chian[1], Kristin J Boggio[1], Alexandre J C Quaresma[2], Jeffrey A Nickerson[2] and Daryl A Bosco[1,3*]

Abstract

Background: Amyotrophic lateral sclerosis (ALS)-linked fused in sarcoma/translocated in liposarcoma (FUS/TLS or FUS) is concentrated within cytoplasmic stress granules under conditions of induced stress. Since only the mutants, but not the endogenous wild-type FUS, are associated with stress granules under most of the stress conditions reported to date, the relationship between FUS and stress granules represents a mutant-specific phenotype and thus may be of significance in mutant-induced pathogenesis. While the association of mutant-FUS with stress granules is well established, the effect of the mutant protein on stress granules has not been examined. Here we investigated the effect of mutant-FUS on stress granule formation and dynamics under conditions of oxidative stress.

Results: We found that expression of mutant-FUS delays the assembly of stress granules. However, once stress granules containing mutant-FUS are formed, they are more dynamic, larger and more abundant compared to stress granules lacking FUS. Once stress is removed, stress granules disassemble more rapidly in cells expressing mutant-FUS. These effects directly correlate with the degree of mutant-FUS cytoplasmic localization, which is induced by mutations in the nuclear localization signal of the protein. We also determine that the RGG domains within FUS play a key role in its association to stress granules. While there has been speculation that arginine methylation within these RGG domains modulates the incorporation of FUS into stress granules, our results demonstrate that this post-translational modification is not involved.

Conclusions: Our results indicate that mutant-FUS alters the dynamic properties of stress granules, which is consistent with a gain-of-toxic mechanism for mutant-FUS in stress granule assembly and cellular stress response.

Keywords: Stress granule, Amyotrophic lateral sclerosis, Frontotemporal lobar degeneration, FUS/TLS, Oxidative stress

Background

Mutations in the gene encoding fused in sarcoma/translocated in liposarcoma (FUS/TLS or FUS), also known as the heterogeneous nuclear ribonucleoprotein (hnRNP) P2 [1], are linked to inherited cases of amyotrophic lateral sclerosis (ALS) [2,3]. ALS is a fatal neurodegenerative disease characterized by motor neuron loss, progressive muscle weakening and paralysis [4]. Most ALS-linked FUS mutations are located within the C-terminal nuclear localization signal (NLS) that binds transportin, the nuclear importer that translocates FUS from the cytoplasm into the nucleus [5,6]. Although FUS is predominately localized to the nucleus in most cell types [7], it has nucleo-cytoplasmic shuttling capabilities that may be important for mRNA transport [8]. In fact, FUS is thought to play a role in local translation at the dendrites of neuronal cells [9-11]. Disruption of the FUS/transportin interaction leads to nuclear depletion with concomitant cytoplasmic accumulation of FUS in cultured mammalian cells [6]. The potential relevance of this interaction is underscored by the cytoplasmic accumulation of FUS in both ALS [2,3] and frontotemporal lobar degeneration (FTLD) [12] post-mortem central nervous system (CNS) tissues.

The extent to which FUS mutants redistribute to the cytoplasm correlates with ALS disease severity [6,13].

* Correspondence: Daryl.Bosco@umassmed.edu
[1]Department of Neurology, University of Massachusetts Medical School, Worcester, MA, USA
[3]Department of Biochemistry and Molecular Pharmacology, University of Massachusetts Medical School, Worcester, MA, USA
Full list of author information is available at the end of the article

For example, individuals with the FUS R495X mutation, which leads to truncation of the NLS and significant cytoplasmic retention of FUS, exhibit early disease onset and a relatively severe disease course [13]. Nuclear depletion of FUS may impair putative nuclear functions involving mRNA [14,15] and DNA [16,17] processing. An alternative, though not mutually exclusive, possibility is that mutant-FUS exerts a gain-of-toxic function in the cytoplasm [18].

Recently, a two-hit model has been proposed to account for cytoplasmic FUS toxicity in ALS and FTLD [19]. Cytoplasmic mislocalization of FUS, either through genetic mutations or other unidentified factors, represents the first hit. The first hit alone may not be sufficient to cause disease. However, a second hit stemming from cellular stress directs cytoplasmic FUS into stress granules. Stress granules are stalled translational complexes that form as a normal response to induced stressors such as oxidation, heat-shock, viral infection or hypoxia [20]. The function of stress granules is thought to be in the triage of mRNAs that are destined for expression, storage or degradation, which in turn restores cellular homeostasis [21]. Stress granule function may not be limited to mRNA processing, as the activity of certain proteins can also be controlled by their sequestration into stress granules [22]. It follows that the association of mutant-FUS with stress granules may impair stress response and ultimately cause disease [23]. This notion is supported by evidence of stress granule marker proteins within the pathological aggregates of neurodegenerative disease tissues [6,24,25].

While we and others have firmly established a mutant-specific phenotype with respect to FUS in stress granules [5,6,13,26-30], there is little evidence that mutant-FUS actually alters the properties of stress granules. Although there is no functional assay per se for stress granules, the properties of stress granules that are thought to be relevant to their function include assembly kinetics, dynamics, morphology and abundance [21,31]. Under conditions of oxidative stress, we show that mutant-FUS delays stress granule formation in mammalian cell culture. Once sodium arsenite-induced stress granules are formed, however, those containing mutant-FUS are more dynamic, larger and more abundant compared to stress granules lacking FUS. Upon removal of stress, stress granules disassemble more rapidly in cells expressing cytoplasmic mutant-FUS. Further, we identified the RGG domains within FUS as playing a key role in the assembly of mutant-FUS into stress granules, although the methylation of arginine residues within these RGG domains does not play a significant role. The evidence presented here supports the hypothesis that the association of mutant-FUS with stress granules represents a gain-of-toxic interaction in ALS pathogenesis.

Results

The expression of cytoplasmic mutant FUS influences stress granule assembly and disassembly

We and others previously demonstrated that ALS-linked FUS mutants assemble into stress granules to an extent that directly correlates with their cytoplasmic mislocalization [6,13]. These experiments were performed under conditions of acute stress such that stress granules assembled rapidly and did not address whether mutant-FUS affects the processes of stress granule assembly and disassembly. First, we employed our previously characterized, doxycycline-inducible HEK-293 cell lines expressing GFP-tagged wild-type FUS and ALS-linked FUS mutants (R495X and H517Q) [13] to examine the effect of mutant-FUS on stress granule assembly under conditions of oxidative stress. The R495X mutation truncates the nuclear localization signal (NLS), causing FUS to significantly redistribute from the nucleus to the cytoplasm (Figure 1A and [13]). On the opposite end of the mislocalization spectrum is H517Q, an autosomal recessive mutation in the NLS that induces a mild mislocalization phenotype (Figure 1A and [2,13]).

Stress granule assembly was initiated in GFP-FUS (WT, R495X, and H517Q) cell lines with 0.25 mM sodium arsenite, an inducer of oxidative stress [32] and an environmental toxicant that can cause neural defects [33,34]. Sodium arsenite has been shown to induce the incorporation of cytoplasmic FUS-mutants into stress granules, but does not influence endogenous FUS or exogenously expressed GFP-FUS WT proteins [13,35]. In fact there is no difference in cellular response to sodium arsenite with respect to stress granule formation or cell viability when FUS expression is reduced [31,35]. Therefore, sodium arsenite induces a mutant-specific phenotype with respect to FUS localization to stress granules. The concentration of sodium arsenite employed here was reduced from the 0.5 mM concentration that is typically used [13,36] in order to lengthen the timescale of stress granule assembly and resolve differences in this process between cell lines. Ras GTPase-activating protein-binding protein 1 (G3BP), a stress granule specific marker [36], was used to probe for stress granules by immunofluorescence (IF) over a 90 min time course of sodium arsenite exposure. At 0 min, there were no stress granules; G3BP remained diffusely cytoplasmic and no cytoplasmic GFP-FUS puncta were detected in any cell line (Figure 1A). By 90 min, all cell lines contained stress granules in virtually every cell. As expected, GFP-FUS R495X co-localized with G3BP in stress granules, as did GFP-FUS H517Q albeit to a far lesser degree. In contrast, GFP-FUS WT remained entirely nuclear and was not detected within these structures (Figure 1A and Additional file 1). Strikingly, fewer GFP-FUS R495X expressing cells contained G3BP-positive stress granules compared to GFP-FUS (WT

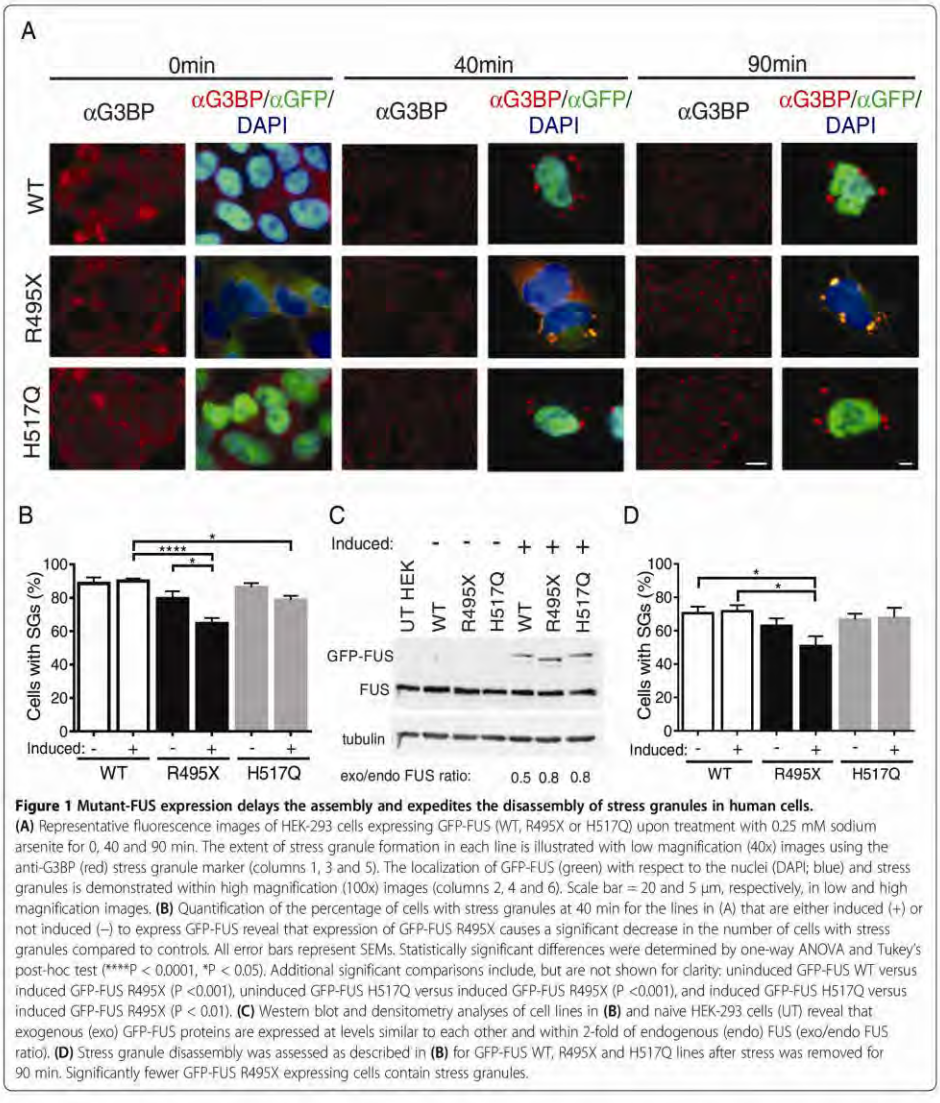

Figure 1 Mutant-FUS expression delays the assembly and expedites the disassembly of stress granules in human cells. **(A)** Representative fluorescence images of HEK-293 cells expressing GFP-FUS (WT, R495X or H517Q) upon treatment with 0.25 mM sodium arsenite for 0, 40 and 90 min. The extent of stress granule formation in each line is illustrated with low magnification (40x) images using the anti-G3BP (red) stress granule marker (columns 1, 3 and 5). The localization of GFP-FUS (green) with respect to the nuclei (DAPI; blue) and stress granules is demonstrated within high magnification (100x) images (columns 2, 4 and 6). Scale bar = 20 and 5 μm, respectively, in low and high magnification images. **(B)** Quantification of the percentage of cells with stress granules at 40 min for the lines in (A) that are either induced (+) or not induced (–) to express GFP-FUS reveal that expression of GFP-FUS R495X causes a significant decrease in the number of cells with stress granules compared to controls. All error bars represent SEMs. Statistically significant differences were determined by one-way ANOVA and Tukey's post-hoc test (****$P < 0.0001$, *$P < 0.05$). Additional significant comparisons include, but are not shown for clarity: uninduced GFP-FUS WT versus induced GFP-FUS R495X ($P < 0.001$), uninduced GFP-FUS H517Q versus induced GFP-FUS R495X ($P < 0.001$), and induced GFP-FUS H517Q versus induced GFP-FUS R495X ($P < 0.01$). **(C)** Western blot and densitometry analyses of cell lines in **(B)** and naïve HEK-293 cells (UT) reveal that exogenous (exo) GFP-FUS proteins are expressed at levels similar to each other and within 2-fold of endogenous (endo) FUS (exo/endo FUS ratio). **(D)** Stress granule disassembly was assessed as described in **(B)** for GFP-FUS WT, R495X and H517Q lines after stress was removed for 90 min. Significantly fewer GFP-FUS R495X expressing cells contain stress granules.

and H517Q) lines after approximately 40 min of sodium arsenite exposure (Figure 1A).

Quantification of these results revealed that the greatest difference in cells containing stress granules occurred between the GFP-FUS R495X (65 ± 3.3%) and GFP-FUS WT (90 ± 1.5%) lines after 40 min of sodium arsenite exposure (Figure 1B). Stress granules were also assembled in GFP-FUS H517Q cells (79 ± 2.5%), though to a lesser extent than WT cells. Therefore, the expression of mutant-FUS is not sufficient to cause a delay in stress granule assembly, but rather, the delay in assembly depends on the extent that FUS is redistributed to the cytoplasm (WT<H517Q<R495X). Artifacts from FUS over-expression are not expected to influence these results since the expression levels of all exogenous GFP-FUS proteins were similar to each other and within two-

fold of endogenous FUS (Figure 1C). To rule out an inherent difference between cell lines irrespective of GFP-FUS expression, identical experiments were performed in uninduced cells (i.e., without doxycycline). Uninduced GFP-FUS (WT and H517Q) lines did not express detectable GFP-FUS and behaved similarly to induced GFP-FUS WT cells, confirming that GFP-FUS WT expression has no effect on stress granule assembly. There was a small yet insignificant difference between uninduced GFP-FUS (WT and R495X) lines (Figure 1B). We suspect this may be due to low levels, below the limit of detection via western analysis (Figure 1C), of GFP-FUS R495X expression in the absence of doxycycline. Nonetheless, induced expression of GFP-FUS R495X in these cells significantly attenuated the assembly of stress granules compared to the uninduced condition in the same line (Figure 1B).

The reversible nature of stress granules is an important functional feature of these structures; upon removal of stress, stress granules disassemble as the cell re-establishes homeostasis. Since mutant-FUS delays the assembly of stress granules, we sought to determine whether mutant FUS also influences the reverse process of disassembly. Cells were treated with 0.25 mM sodium arsenite for 1 h, at which point ~100% of cells in all cell lines contained stress granules. The disassembly process was initiated by replacing sodium arsenite with fresh media, and the percentage of cells with stress granules was quantified after 90 min. At this time point, fewer GFP-FUS R495X expressing cells (51 ± 6.0%) contained stress granules compared to GFP-FUS WT (72 ± 3.7%) and GFP-FUS H517Q (68 ± 6.0%). Therefore, expression of GFP-FUS (WT and H517Q) had virtually no effect, while expression of the cytoplasmic GFP-FUS R495X exerted the most pronounced effect on the kinetics of stress granule disassembly (Figure 1D). Interestingly, a similar effect on stress granule assembly and disassembly was observed upon depletion of endogenous TAR DNA-binding protein 43 (TDP-43) [37], which, unlike FUS, is thought to play a normal role in arsenite-induced stress response [31]. Thus, both a loss of TDP-43 function and a potential toxic gain of mutant-FUS function manifests in delayed stress granule assembly and more rapid stress granule disassembly under conditions of oxidative stress.

While HEK-293 GFP-FUS lines are ideal for microscopic measurements of stress granule properties, owing to the GFP tag on FUS and the relatively flat nature of these cells, we wanted to both confirm these stress granule assembly trends in neuronal cells and rule out a potential "tag effect" from GFP. To this end, motor neuron-like NSC-34 [38] cell lines were engineered to constitutively express untagged human FUS WT or FUS R495X using a lentiviral transduction expression system. FUS protein expression in these cells was accomplished with an IRES-containing bicistronic vector (CSCW2-IRES-GFP), which allowed for the simultaneous expression of both FUS and GFP separately (i.e., not as a fusion protein) but from the same RNA transcript. Therefore, GFP served as a reporter for cells transduced to express either untagged FUS WT or R495X. The expression levels of FUS (WT and R495X) proteins were similar to each other and within two-fold of endogenous FUS (Figure 2A and Additional file 2). In the absence of stress, elevated levels of cytoplasmic FUS were observed in NSC-34 cells expressing FUS R495X, and diffuse cytoplasmic G3BP signal was observed in both FUS R495X and WT cells. Upon exposure to 0.25 mM sodium arsenite for 1 hr, FUS was detected within G3BP-positive stress granules only in cells expressing FUS R495X. Although sodium arsenite exposure lead to fewer NSC-34 cells with stress granules overall compared to HEK-293 cells, the same phenotype was observed in that fewer cells formed stress granules in FUS R495X expressing cells compared to those expressing FUS WT (Figure 2B). Quantification of this phenotype revealed a 2.4-fold lower percentage of stress granule-containing NSC-34 cells for FUS R495X (23 ± 1.6%) compared to FUS WT (55 ± 2.8%) lines (Figure 2C). To assess whether the expression of exogenous human FUS proteins had any effect on stress response in these cells, the percentage of cells with stress granules was also quantified in the parent, or non-transduced, NSC-34 cell line after 1 h of sodium arsenite exposure. While FUS WT and R495X lines exhibited the most significant difference, there were also more FUS WT cells with stress granules relative to the parent (37 ± 3.6%) line (Figure 2C). Possible explanations for why an effect of exogenous FUS WT is observed in NSC-34 but not HEK-293 (Figure 1B) cells is that the expression of exogenous human FUS WT exerts an additional stress due to i) higher relative protein levels (compare exogenous to endogenous FUS in Figures 1C and 2A), and/or ii) different species of cells (expression of human FUS in mouse versus human cells), either of which could heighten the stress response of these cells to sodium arsenite. In fact, expression of FUS WT is sufficient to induce stress and toxicity in different model organisms [39-41]. Nonetheless, the efficiency of stress granule assembly in the parent NSC-34 line is more similar to that of FUS WT than FUS R495X (Figure 2C). Moreover, one would expect FUS R495X to also impose an additional stress, and yet stress granule assembly is attenuated in these cells, providing further evidence that expression of mutant-FUS interferes with the assembly of stress granules under conditions of stress.

Unlike HEK-293 cells (Figure 1), the percentage of NSC-34 cells containing stress granules never reached 100% in any line, and the FUS WT line always contained double the percentage of cells with stress granules compared to FUS R495X. This behavior precluded our ability to perform a similar disassembly analysis as described

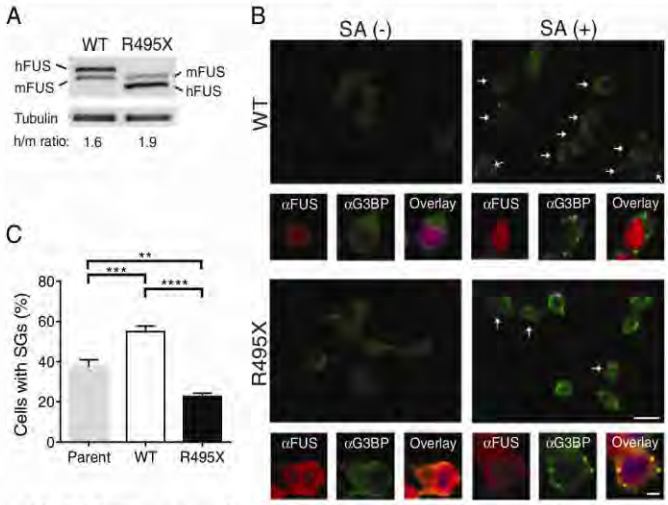

Figure 2 Expression of the FUS R495X mutant interferes with stress granule assembly in neuronal cells. (A) Exogenous human (h) FUS proteins are similar to each other and within 2-fold of endogenous mouse (m) FUS as determined by western blot and densitometry analyses. The ratio of hFUS/mFUS proteins is indicated for each cell line. **(B)** Immunofluorescence images of NSC-34 cells expressing untagged FUS (WT and R495X) either in the absence (–) or presence (+) of 0.25 mM sodium arsenite (SA) for 1 hr. Low magnification (40x) images of SA (+) treated cells using the anti-G3BP stress granule marker (green) show a greater number of stress granule-positive cells (denoted by arrows) in the FUS WT line compared to the FUS R495X line. High magnification (100X) images showing a single cell reveal the localization of FUS (red) and G3BP (note: the far red channel was used for detection of G3BP and the images are shown in green for clarity) under all conditions. DAPI (nuclei) is included in the overlay images. Note that in cells with stress granules, cytoplasmic R495X co-localizes to these structures as expected (see overlay image in bottom right). Scale bar = 20 and 5 μm, respectively, in low and high magnification images. **(C)** Quantitative analysis (as described in Figure 1B) of the percentage of NSC-34 cells with stress granules after 1 hr of sodium arsenite treatment revealed that expression of FUS R495X inhibited stress granule assembly compared to cells expressing FUS WT and the parent line. All error bars represent SEMs. Statistically significant differences were determined by one-way ANOVA and Tukey's post-hoc test (****$P < 0.0001$, ***$P < 0.001$, **$P < 0.01$).

above for HEK-293 cells (Figure 1D), which compared the absolute percentage of cells with stress granules at different time points.

The expression of cytoplasmic mutant-FUS alters the dynamic binding properties of stress granule-associated proteins

Stress granules are highly dynamic structures [32,42,43]. Proteins and mRNA continuously shuttle in and out of stress granules, reversibly binding to other stress granule components in a manner that is thought to regulate both protein signaling activity [22] and mRNA fates towards translational arrest, expression or decay [20]. To study the effect of stress granule-associated mutant-FUS on the dynamic properties of stress granules, we employed fluorescence recovery after photobleaching (FRAP). FRAP measures the relative kinetics and affinities of protein binding within complexes, such as stress granules, over the time course of the experiment [44,45]. Because FRAP reports on binding events in live cells, fluorescently tagged-proteins were employed for these experiments [32,42,43,46]. We transiently expressed monomeric RFP (mRFP)-tagged proteins T-cell-restricted intracellular antigen-1 (TIA-1) or G3BP, two established stress granule-associated proteins, to mark stress granules for FRAP within HEK-293 GFP-FUS (WT and R495X) cells. Overexpression of G3BP is sufficient to form inclusions that resemble stress granules in the absence of stress [31,47]. Since it is not clear whether these G3BP overexpression-induced stress granules have different properties than sodium arsenite-induced stress granules, conditions were optimized for transfection of mRFP-G3BP that minimized the formation of G3BP-positive inclusions *a priori* of sodium arsenite treatment (Figure 3A; see Materials and methods).

During a FRAP experiment on stress granules, the fluorescence from a tagged species (GFP-FUS R495X, mRFP-TIA-1 or mRFP-G3BP in our case) is bleached. The fluorescence signal recovers as bleached molecules unbind from sites in the stress granules, un-bleached fluorescent molecules exchange back into the photobleached area and then bind. The fluorescence recovery time is limited by

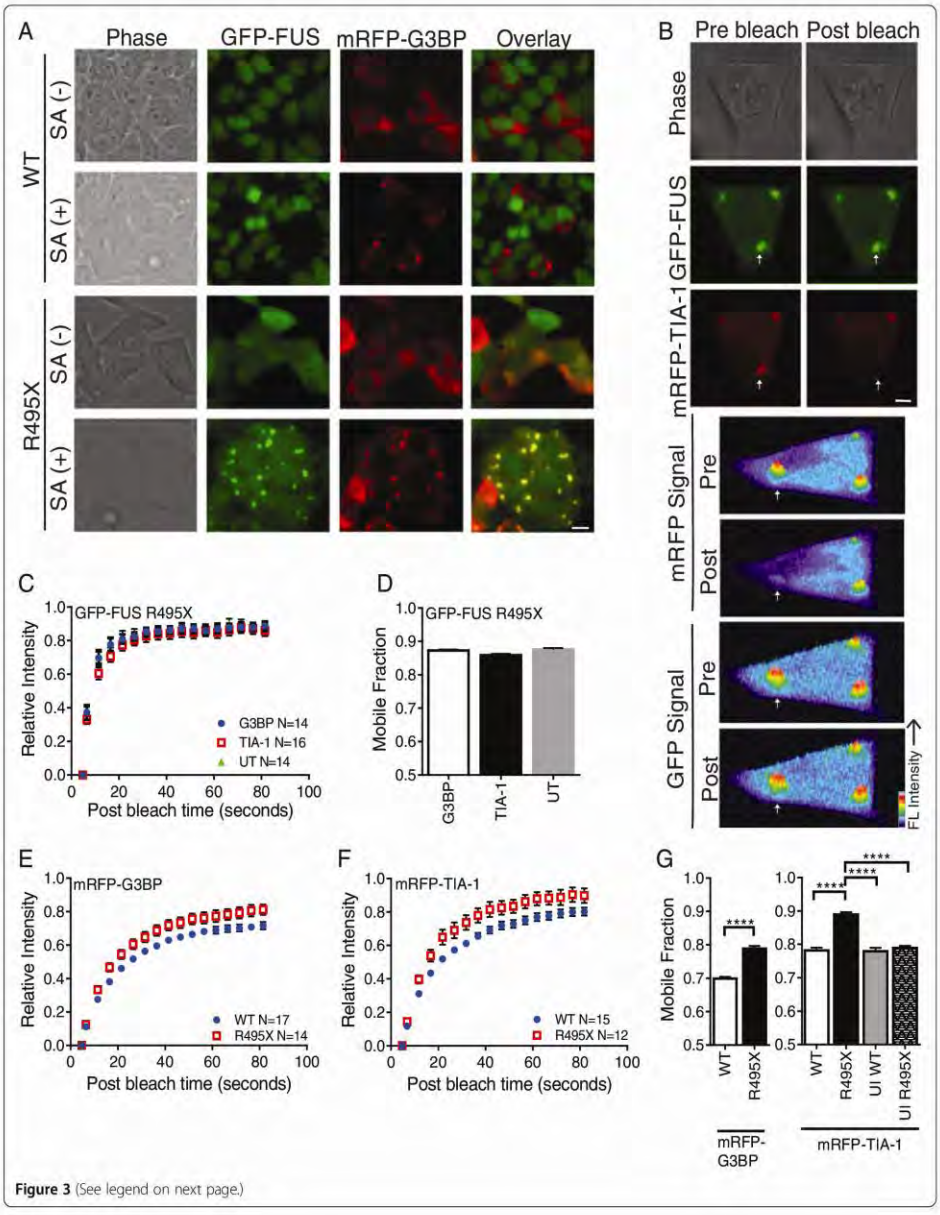

Figure 3 (See legend on next page.)

(See figure on previous page.)
Figure 3 GFP-FUS R495X is weakly bound to stress granules and alters binding of stress granule-associated proteins. (A) Live cell images of GFP-FUS (WT and R495X) expressing HEK-293 cells transfected with mRFP-G3BP. Images are shown before (–) and after (+) treatment with 0.2 mM sodium arsenite (SA) for 1 hr. Scale bar = 10 μm. **(B)** Top three panels: exemplar GFP and mRFP images of a SA treated cell for a mRFP-TIA-1 FRAP experiment before and after photobleaching. The mRFP signal, but not GFP signal, is lost from the stress granule (indicated by arrow). Scale bar = 5 μm. Bottom four panels: fluorescence intensity profiles corresponding to the above panels (rotated 90° clockwise). **(C)** The recovery curve for GFP-FUS R495X in untransfected (UT; green triangle) cells are indicative of fast fluorescence recovery. The GFP-FUS R495X profile does not change upon transfection with either mRFP-G3BP (blue circle) or mRFP-TIA-1 (red square). **(D)** Nearly identical mobile fractions support the conclusions in **(C)**. **(E & F)** Recovery curves for mRFP-G3BP **(E)** and mRFP-TIA-1 **(F)** differ for GFP-FUS WT (blue circle) and R495X (red square) expressing cells. **(G)** Mobile fractions for the curves in **(E & F)** are significantly higher for GFP-FUS R495X (black bars) relative to GFP-FUS WT (white bars) cells. Mobile fractions for mRFP-TIA-1 are the same for the following control experiments: GFP-FUS WT expressing cells (white bars), uninduced (UI) GFP-FUS WT cells (grey bar) and uninduced GFP-FUS R495X cells (hatched bar). Asterisks indicate statistically significant differences between cell lines as determined by two-way ANOVA and Tukey's post-hoc test (****$P < 0.0001$) on data from at least n=2 independent experiments. All error bars represent SEMs. The total number (N) of stress granule analyzed is indicated on the recovery panels.

either diffusion, which is faster than the rates we report here, or by binding kinetics; thus, proteins that are tightly bound to other proteins or cellular structures exhibit relatively long half times of fluorescence recovery ($t_{1/2}$) [44]. The population of fluorescent molecules that exchange with their bleached counterparts over the time course of the experiment comprise the "mobile fraction" [44]. The "immobile fraction" is the population that is tightly bound and does not exchange over the time course of the experiment. Here, each experiment was carried out such that the photobleaching occurred in only a single channel and fluorescence was diminished evenly over the entire stress granule (Figure 3B). Initially, the dynamics of GFP-FUS R495X within stress granules were investigated since the dynamic binding properties of this protein under stress conditions have not been reported. GFP-FUS R495X cells alone or transfected with either mRFP-G3BP (Figure 3A) or mRFP-TIA-1 (Figure 3B) were exposed to 0.20 mM sodium arsenite for 1 hr, at which point the majority of cells contained fully formed stress granules. The fast recovery ($t_{1/2}$ of 3.6 ± 2.1s; Figure 3C) of GFP-FUS R495X by FRAP shows that this protein re-binds within stress granules relatively quickly compared to other stress granule-associated proteins (see below). Moreover, ~87% of GFP-FUS R495X molecules constituted the mobile fraction, indicating that GFP-FUS R495X is weakly bound within stress granules (Figure 3D). Neither the $t_{1/2}$ nor the mobile fraction of GFP-FUS R495X changed significantly upon transient transfection of either mRFP-G3BP or mRFP-TIA-1 (Figure 3C and D). Therefore, neither the process of transient transfection itself, nor the over-expression of stress-granule associated proteins, influenced the dynamic properties of mutant-FUS.

Next we performed FRAP on mRFP-G3BP or mRFP-TIA-1 to determine the effect of mutant-FUS on the dynamic properties of proteins within stress granules. Fluorescence recovery for mRFP-G3BP ($t_{1/2}$ 12 ± 4.4s; 70 ± 2% mobile) and mRFP-TIA-1 ($t_{1/2}$ 12 ± 3.9s; 78 ± 2% mobile) within GFP-FUS WT expressing cells was observed (Figure 3E and F). Our measurements of mRFP-TIA-1 in control HEK-293 cells were similar to those reported for GFP-TIA-1 COS7 cells [32]. In cells expressing GFP-FUS R495X, the fluorescence recovery half times were nearly the same for mRFP-G3BP ($t_{1/2}$ 11 ± 2.8s) and mRFP-TIA-1 ($t_{1/2}$ 10 ± 2.8s). However, the mobile fraction for both mRFP-G3BP and mRFP-TIA-1 increased significantly in GFP-FUS R495X cells to 79 ± 3% and 89 ± 4%, respectively, compared to GFP-FUS WT cells (Figure 3E-G). Control experiments in GFP-FUS WT (induced and uninduced) and GFP-FUS R495X (uninduced) cells confirmed that an increase in mRFP-TIA-1 mobile fraction required the expression of mutant-FUS (Figure 3G). The increased mobile fraction for mRFP-G3BP and mRFP-TIA-1 indicates that these proteins bind more weakly to factors within GFP-FUS R495X positive stress granules compared to stress granules lacking mutant-FUS. As a result, there is increased exchange of mRFP-G3BP and mRFP-TIA-1 between the area that is photobleached and the area that is not photobleached, resulting in fluorescence recovery. Together, these data demonstrate that the incorporation of mutant-FUS into sodium arsenite-induced stress granules decreases the binding of other stress granule-associated proteins within these structures.

Because we and others observed that stress granules form as a result of G3BP overexpression [31,47], we examined whether their dynamic properties were different compared to those stress granules induced by sodium arsenite. mRFP-G3BP exhibited significantly weaker binding (i.e., larger mobile fraction, $P < 0.05$) within stress granules in GFP-FUS WT cells under conditions of G3BP over-expression compared to sodium arsenite stress, indicating that the dynamic properties of these stress granules are inherently different (Additional file 3). The most striking difference was the effect of mutant-FUS: GFP-FUS R495X significantly *increased* mRFP-G3BP binding within stress granules (i.e., smaller mobile fraction) under conditions of G3BP over-expression compared to all other conditions, which is the opposite trend in sodium arsenite-induced stress granules (Figure 3). Therefore, the effect of GFP-FUS R495X on the dynamic properties of stress granules

depends on the stressor and is consistent with observations that the source of stress influences the constituents within stress granules [48]. Irrespective of the stress, our results show that the incorporation of GFP-FUS R495X into stress granules alters the dynamic binding interactions of other well-characterized stress granule-associated proteins within in these structures.

Expression of mutant-FUS increases the size and abundance of stress granules

In addition to dynamics, stress granule size and abundance could also be altered by the presence of mutant-FUS. As such, both stress granule size and abundance were quantified in HEK-293 cell lines expressing either GFP-FUS (WT or R495X) after exposure to 0.5 mM sodium arsenite for 1 hr, at which point stress granules were fully formed (>95% of cells contain stress granules). In contrast to previous methods that measure the area of stress granules, which does not take into account the three-dimensional aspect of these structures, we developed a method to quantify the volume of stress granules based on fluorescence intensity measurements (see Materials and methods). Briefly, fixed cells were labeled with an anti-G3BP antibody and then optically sectioned by confocal microscopy. Three-dimensional reconstruction of these sections allowed us to quantify the volume of selected stress granules (Figure 4A). This analysis revealed that GFP-FUS R495X expressing cells produced significantly larger stress granules (3.8 ± 0.1 μm^3) compared to GFP-FUS WT cells (2.7 ± 0.2 μm^3; Figure 4B and C). This trend is consistent with ALS-linked TDP-43 mutants, which also show an increased stress granule size under conditions of hyperosmolar stress [49], suggesting that this may be a common disease-related characteristic.

Our quantitative analysis also revealed that mutant-FUS expressing cells contained 27% more stress granules per cell (8.8 ± 0.3) compared to WT-FUS (6.9 ± 0.4; Figure 4B and D). This result is consistent with a recent report demonstrating a greater abundance of stress granules within patient FUS (R521C and R514G) fibroblast lines under conditions of sodium arsenite relative to control lines [30]. Moreover, cells expressing ALS-linked TDP-43 also produce more stress granules compared to control cells under stress [25]. Therefore, disease-causing FUS and TDP-43 proteins appear to alter stress granules morphology by increasing their size and abundance.

The RGG domains play a key role in modulating the association of mutant-FUS with stress granules

In order to understand the factors modulating the incorporation of mutant FUS into stress granules, we engineered GFP-tagged FUS constructs lacking the functional domains of FUS and tested their ability to incorporate into stress granules. The functional domains of FUS are as follows: the prion-like QGSY-rich region (QGSY), a glycine-rich region (GLY), an RNA recognition motif (RRM), and two arginine-glycine-glycine-rich domains (RGG1 and RGG2) separated by a C2-C2 zinc finger motif (ZF) (Figure 5A). All of these domains have been shown to play a role in modulating the incorporation of other RNA binding proteins into stress granules [26,50-52] and thus each have the potential to influence the association of mutant-FUS with stress granules. The extent with which FUS mutants localize to arsenite-induced SGs correlates with their level of cytoplasmic expression (Figures 1, 2 and [13]). However, since transient transfection of highly cytoplasmic FUS mutants (e.g., R495X) has the potential to produce cytoplasmic protein aggregates that could confound our stress granule analysis [13], domain deletion constructs were engineered within the background of the less aggregation-prone R521G mutant.

Transient transfection of GFP-FUS R521G deletion constructs in HeLa cells resulted in varying degrees of GFP-FUS cytoplasmic expression: FL, ΔQGSY, ΔRGG1, ΔGLY and ΔRRM were predominately expressed in the nucleus, whereas relatively high cytoplasmic expression was observed for ΔRGG2, which lacks part of the signal used for nuclear import of FUS [5] (Figure 5B). Deletion of the zinc finger motif resulted in a construct that failed to express in mammalian cells (data not shown), possibly because this construct is unstable and/or structurally altered [53]. Although GFP-FUS R521G exhibits cytoplasmic expression upon transient transfection [2], the levels here were not sufficient for an accurate stress granule analysis. It was therefore necessary to increase the cytoplasmic expression of FUS-deletion constructs by co-transfection with maltose binding protein (MBP)-tagged M9M. M9M is a transportin/Kapβ2-specific nuclear import inhibitor that blocks the nuclear import of FUS [6,54]. Co-transfection with MBP-M9M increased cytoplasmic retention of GFP-FUS for all constructs, ensuring that each construct had equal potential to assemble into stress granules (Figure 5B).

Administration of 0.5 mM sodium arsenite for 1 hr induced stress granule formation (Figure 5B) in ~75% of cells for all constructs. A ratio of the GFP signal within stress granules relative to the diffuse GFP-FUS signal in the cytoplasm (stress granule/diffuse FUS signal) was used to quantify the incorporation of each construct within stress granules. Full length GFP-FUS R521G exhibited a robust localization to stress granules with a stress granule/diffuse FUS ratio of 4.75 +/− 0.97 (Figure 5B and C). As expected for a protein that does not associate with stress granules, analysis with free GFP as a negative control produced the lowest ratio of 1.13 +/− 0.11. GFP-FUS R521G ΔQGSY, ΔGLY, and ΔRRM were not significantly different from FL GFP-FUS R521G. In contrast, deletion of the RGG1

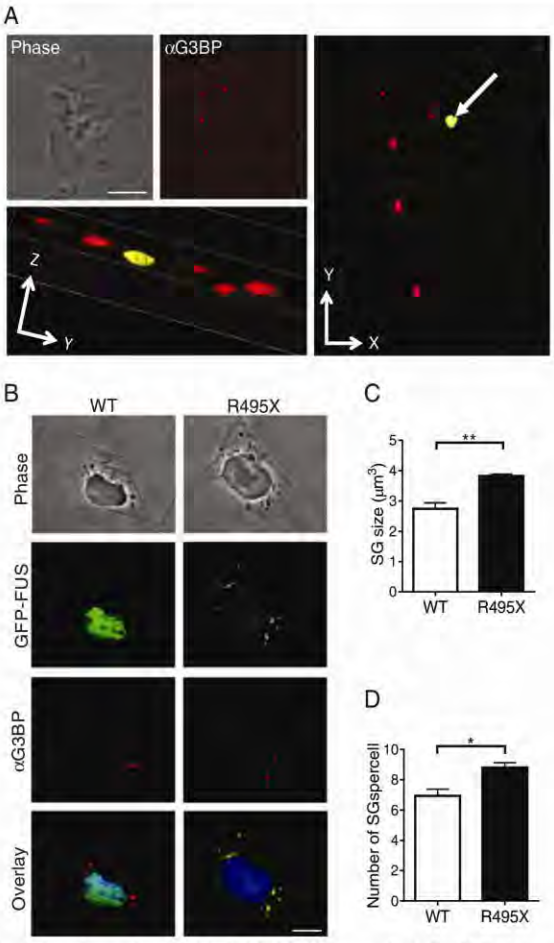

Figure 4 Stress granule size and number are increased in GFP-FUS R495X expressing cells. (A) Clockwise order: representative single-plane phase (top left) and anti-G3BP (stress granule marker; red) immunofluorescence (top middle) confocal images of an HEK-293 cell expressing GFP-FUS WT treated with 0.5 mM sodium arsenite for 1 hr. Three-dimensional (3D) reconstruction was used to quantify stress granule volume (see Materials and methods, and C within this figure). The *xy* (right) and *yz* (bottom; view along arrow in xy image) planes for this 3D reconstructed image are shown; the stress granule highlighted in yellow is marked for volume analysis. Scale bar = 10 μm. **(B)** Representative maximum projection confocal images of GFP-FUS WT and GFP-FUS R495X expressing cells treated as in **(A)** exemplify the size and number of stress granules for each line. Scale bar = 10 μm. **(C and D)** GFP-FUS R495X expressing cells contain stress granules with larger volume **(C)** and in greater abundance **(D)** relative to cells expressing GFP-FUS WT. Asterisks indicate statistically significant differences between cell lines as determined by the Student's t-test (**P < 0.01, *P < 0.05) on data from n=3 independent experiments. All error bars represent SEMs.

domain (ΔRGG1) significantly impaired the localization of FUS into stress granules (1.72 +/− 0.22), and deletion of the RGG2 domain (ΔRGG2) exhibited a similar impairment trend (2.23 +/− 0.48). We note that while distinct FUS-positive stress granules are observed for ΔRGG2, a comparatively high level of GFP-FUS signal remains diffuse, yielding a low stress granule/diffuse FUS ratio. All constructs were expressed at comparable levels (Figure 5D)

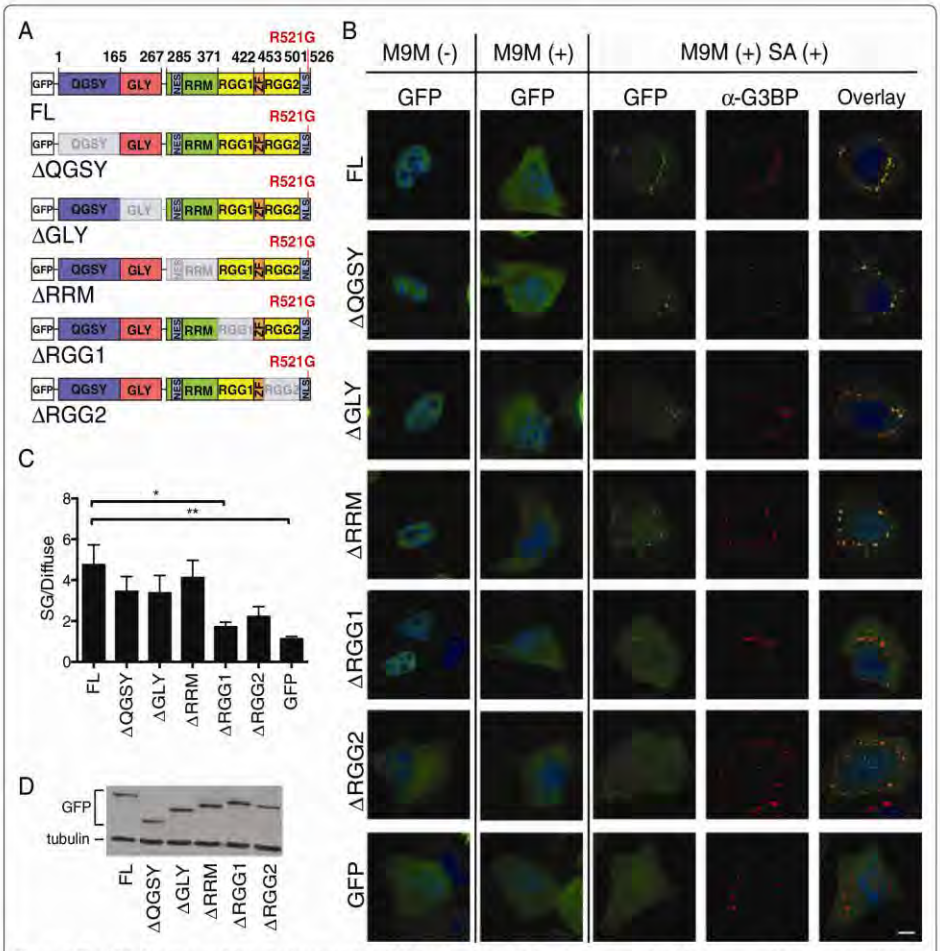

Figure 5 The RGG domains modulate the incorporation of FUS into arsenite-induced stress granules. (A) Illustration of full length (FL) GFP-FUS R521G and constructs lacking the following sequences: Gln-Gly-Ser-Tyr-rich (ΔQGSY), Gly-rich (ΔGLY), RNA recognition motif (ΔRRM), and Arg-Gly-Gly-rich (RGG) regions (ΔRGG1 and ΔRGG2). **(B)** Confocal images of HeLa cells transfected with GFP-FUS R521G constructs (green) alone (–) or co-transfected (+) with MBP-M9M, the transportin-1 inhibitor. Note the increased levels of cytoplasmic GFP-FUS in co-transfected cells (compare columns 1 and 2). Confocal fluorescence images of co-transfected cells treated with 0.5 mM sodium arsenite for 1 hr were used to assess the ability of GFP-FUS R521G constructs (green; column 3) to associate with stress granules (G3BP; red; column 4). The greatest degree of GFP and G3BP co-localization was observed in cells expressing FL GFP-FUS R521G, whereas there was minimal co-localization in control cells expressing free GFP (compare panels in column 5). **(C)** Quantitative analysis (see Materials and methods) of **(B)** reveals that constructs lacking RGG domains (ΔRGG1 and ΔRGG2) exhibit impaired localization to stress granules. Statistically significant comparisons include FL and ΔRGG1 (*$P < 0.05$), FL and GFP (**$P < 0.01$), and ΔQGSY and GFP (*$P < 0.05$; not shown on graph for clarity) by one-way ANOVA followed by a Dunnett's post-hoc test on n=3 independent experiments. All error bars represent SEMs. **(D)** Western blot analysis of HeLa cells in **(B)** demonstrates equivalent expression levels for all GFP-FUS R521G constructs.

and a threshold was applied (see Materials and methods) such that all cells included in this analysis expressed similar levels of FUS. Together, these data demonstrate that the RGG domains in FUS are the most important for mutant-FUS localization to stress granules.

Methylation of mutant-FUS is not required for its assembly into stress

In light of the 20 dimethylated arginine residues within the RGG domains of FUS [55], and the fact that arginine dimethylation dictates protein and RNA interactions as

well as protein subcellular localization [56], we explored the possibility that arginine dimethylation of mutant-FUS regulates its association with stress granules. While methylated FUS has been detected within stress granules in cell culture and pathological CNS inclusions from individuals harboring FUS mutations [5], it is not clear whether methylation is actually required for FUS incorporation into these structures. To investigate this question, HeLa cells were pre-treated with the global methyltransferase inhibitor adenosine 2,3-dialdehyde (AdOx) [57] prior to expression of the highly cytoplasmic GFP-FUS R495X mutant and sodium arsenite exposure. We note that conditions (see Materials and methods) were used to minimize GFP-FUS R495X aggregation in these experiments. Immunoprecipitation of GFP-FUS R495X using an anti-GFP antibody, followed by western analysis with the dimethyl-specific ASYM24 antibody, confirmed that GFP-FUS R495X is hypomethylated in the presence of AdOx (Figure 6A). Despite the significant degree of hypomethylation, GFP-FUS R495X maintains a robust association with stress granules under these conditions (Figure 6B and C). Conversely, the overall ASYM24 signal, including the signal within stress granules, is significantly attenuated. Similar results were seen in our stable HEK-293 GFP-FUS R495X line (data not shown). While the small population of methylated GFP-FUS R495X that remains after AdOx treatment (Figure 6A) could be sequestered into stress granules, the significant decrease in ASYM24 signal (i.e., the decrease in signal for methylated proteins) with no decrease in GFP-FUS signal argues against this possibility. Therefore, while methylated mutant-FUS can assemble into stress granules, this post-translational modification is not a prerequisite for its incorporation.

Discussion

The association of cytoplasmically mislocalized ALS-linked FUS mutants with stress granules is well established [5,6,13,26-30], but what affect does mutant-FUS have on the properties of stress granules? We sought to examine the effect of mutant-FUS on the physical properties of stress granules that are potentially linked to function. While there is no functional assay per se for stress granules, they are believed to represent sites of mRNA triage, which influences whether particular mRNA transcripts are retained within stress granules, translated on ribosomes or degraded within P-bodies [20]. There is also evidence that the signaling activity of proteins can be controlled by their sequestration and/or release from stress granules during stress [22]. Thus, the cellular response to stress is modulated, at least in part, by stress granules. Since mutant-FUS, but not WT-FUS, is incorporated into stress granules under various induced stressors, the mutant protein has the potential to disturb stress granules and impair cellular stress response in ways that could contribute to ALS pathogenesis [19].

Stress granules assemble in response to induced stress. Our results show that ALS-linked, cytoplasmic FUS R495X delays the assembly of stress granules in both HEK-293 (Figure 1) and neuronal NSC-34 (Figure 2) cells under conditions of acute oxidative stress. The predominantly nuclear FUS H517Q mutant also delays stress granule assembly, but to a lesser degree than FUS R495X (Figure 1). Therefore, the delay in stress granule assembly correlates with cytoplasmic levels of mutant-FUS, probably because the protein is poised to enter stress granules once stress is induced. Since over-expression of some ALS-FUS mutants reportedly induce the spontaneous formation of cytoplasmic inclusions that stain positively for stress granule markers [28,29], one might expect the expression of mutant-FUS to correlate with a faster rate of stress granule assembly. However, the properties of stress granules are influenced by the nature of the induced stressor [48], and we show that stress granules induced by protein over-expression exhibit different dynamic properties than those induced by sodium arsenite (Additional file 3). We also demonstrate that mutant-FUS accelerates the disassembly of stress granules (Figure 1D). Therefore, expression of mutant-FUS appears to disfavor the formation of and/or destabilizes stress granules, possibly by interfering with protein interactions within these structures (Figure 3). The effects of mutant-FUS on stress granule assembly and disassembly are reminiscent of effects seen during TDP-43 knock-down [37]. Considering that stress granule assembly is a regulated process [20], factors that either delay or accelerate stress granule assembly/disassembly may adversely affect cellular homeostasis.

Interestingly, once stress granules are formed, mutant-FUS exerts an effect on both stress granule morphology and abundance that may appear counterintuitive based on the effect of FUS during the processes of assembly and disassembly. While the expression of GFP-FUS R495X both disfavors stress granule assembly and weakens stress granule associated interactions, under conditions of persistent stress the size and abundance of stress granules is augmented by the expression of mutant-FUS (Figure 4). This increased size and abundance of stress granules does not necessarily mean these structures are held together more tightly, but rather is a likely consequence of the additional protein load associated with these structures from the GFP-FUS R495X protein itself. This rationale may also be relevant to the increased size of stress granules in ALS-linked TDP-43 mutants under conditions of hyperosmolar stress [49] and suggests that this phenotype may be part of a common disease pathway. An intriguing, but not mutually exclusive, possibility is that mutant-FUS and TDP-43 recruit additional protein partners and mRNA substrates into stress granules, thereby further increasing their size

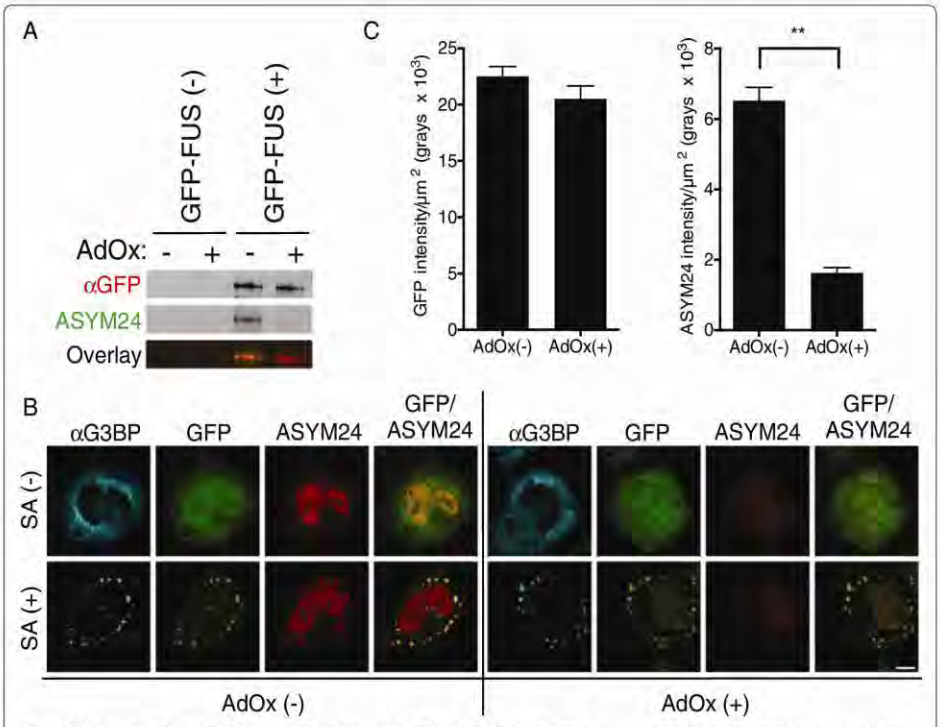

Figure 6 Methylation of mutant-FUS is not required for its assembly into stress granules. HeLa cells transfected with GFP-FUS R495X were pre-treated with the methyltransferase inhibitor adenosine-2,3 dialdehyde (AdOx) and then exposed to sodium arsenite to promote stress granule assembly. **(A)** GFP-FUS R495X was detected by western analysis only for immunoprecipitation (IP) reactions from transfected cells (GFP-FUS (+)). Anti-GFP was used for both IP and western analyses. The ASYM24 antibody revealed that GFP-FUS R495X was hypomethylated on arginine residues when cells were pre-treated with AdOx. **(B)** Confocal fluorescence images revealed a robust association of GFP-FUS R459X with sodium arsenite-induced (SA(+)) stress granules, both in the absence (left panels) and presence (right panels) of AdOx. Conversely, the ASYM24 signal within the same stress granule was dramatically attenuated when cells were pre-treated with AdOx. **(C)** Quantification of n=3 independent experiments from **(B)** further supports the conclusions above. Statistical significance was determined by a Student's t-test (** $P < 0.01$). All error bars represent SEMs.

and abundance (Figure 4 and [25,30]). Indeed, thousands of mRNA transcripts are bound by FUS [58,59] with many distinct mRNAs bound by cytoplasmic mutant-FUS but not WT FUS [59]. Therefore, mutant-FUS may inappropriately process mRNAs and/or facilitate aberrant cytoplasmic protein interactions during stress. The latter possibility is supported by our FRAP analyses, which showed that both mRFP-G3BP and mRFP-TIA-1 exhibit weaker binding and heightened dynamics within sodium arsenite-induced stress granules containing mutant-FUS (Figure 3). In fact, GFP-FUS R495X altered the dynamic properties of stress granules in all of our FRAP experiments, raising the possibility that mutant-FUS interferes with the sorting mechanisms [21,22] associated with these structures under stress.

If the association of mutant-FUS with stress granules does indeed represent a gain of toxic interaction, it will be important to identify factors that modulate this association. Although FUS contains multiple domains that contribute to FUS aggregation [60] and/or are homologous to sequences that direct other proteins into stress granules [26,50-52], our results show that the RGG domains are largely responsible for directing FUS into stress granules (Figure 5). Our results are in general agreement with a recent report by Bentmann et al., which also demonstrated a key role for the RGG domains in assembling FUS into stress granules [26]. However, our results do not support a role for the Gly-rich and RRM domains in this process, whereas the former study did. This discrepancy may be due to the difference in FUS constructs, stressor (sodium

arsenite versus heat shock [26]) and/or the FUS mutation (R521G versus P525L [26]) that were employed in these studies. Whether the RNA-binding ability of FUS is required for its localization to stress granules is not altogether clear [26,27]. Several domains within FUS exhibit RNA-binding capabilities, including the RMM, RGG, and zinc finger domains. Bentmann et al. demonstrated a correlation between cytoplasmic FUS constructs that bound RNA and were incorporated into stress granules, consistent with a role for RNA-binding in the assembly of mutant-FUS into stress granules [26].

That the RGG domains direct mutant-FUS to stress granules raises the possibly that this process is controlled by arginine dimethylation of RGG motifs [61]. Emerging evidence indicates that the RGG motifs within FUS are methylated by protein arginine N-methyltransferase-1 (PRMT1) [55,62,63], and that this post-translational modification can influence the subcellular localization of mutant-FUS [62,63]. While stress granules contain methylated proteins (Figure 6B), and methylated forms of mutant-FUS have been detected in both stress granules and diseased-tissues [5], our data suggests that methylation of FUS is not a prerequisite for its incorporation into stress granules (Figure 6).

How might the incorporation of mutant-FUS into stress granules alter cellular homeostasis under conditions of induced stress, and what are the implications for neurodegenerative disease? We show that mutant-FUS delays stress granule assembly (Figures 1 and 2), decreases the binding of stress granule-associated proteins within stress granules (Figure 3), and increases both size and abundance of stress granules (Figure 4). These physical and dynamic properties of stress granules are thought to be linked to stress granule function, and thus the effects of mutant-FUS may culminate in impaired stress response and, eventually, in neurodegeneration. Although there have been no reports of overt cytotoxicity in mutant-FUS cellular models exposed to sodium arsenite or other stressors, the effects of impaired stress response may appear more distinctly as a function of age, disease progression and/or chronic stress in the human disease [19]. In fact, stress granule marker proteins have been detected within the pathological inclusions of CNS tissues from patients with ALS and FTLD [6,25], supporting the notion that stress response factors are altered during the course of disease. Moreover, these observations raise the possibility that stress granules are precursors to the end-stage aggregates that are characteristic of these diseases [23]. Although our data show that mutant-FUS accelerates stress granule disassembly, under conditions of persistent stress these granules containing mutant-FUS are larger and more numerous and thus have the potential to coalesce into larger aggregates. Extending analyses of stress granules to other models systems, such as human iPS cells from individuals with ALS or ALS rodent models, may allow us to better address whether altered stress granule assembly plays a role in disease onset and/or progression, and whether the association of ALS-linked proteins with stress granules does in fact impact disease.

Conclusions

ALS-linked FUS mutants that mislocalize to the cytoplasm not only incorporate into stress granules under conditions of oxidative stress, but the presence of mutant-FUS in stress granules alters the properties of these structures. Expression of mutant-FUS delays the assembly and expedites the disassembly of stress granules. Furthermore, the morphology and dynamics of these structures is influenced by the presence of mutant-FUS. Therefore, our data are consistent with a gain of toxic function for mutant-FUS with respect to stress granule assembly and dynamics.

Materials and methods

Cell culture and drug treatments

Inducible GFP-FUS expressing FlpIn HEK-293 cells were maintained as described previously [13]. Human cervical carcinoma cells (HeLa) were maintained in Modified Eagle's medium (MEM, Gibco 10370) supplemented with 10% (v/v) heat inactivated fetal bovine serum (Sigma, F4135), 2 mM L-glutamine (Gibco, 25030), and 1% (v/v) penicillin and streptomycin solution (Gibco, 15140). Mouse motor neuron–like hybrid cell lines (NSC-34) [38] constitutively expressing untagged human FUS were maintained in Dulbecco's modified Eagle's medium (Invitrogen, 11965118) supplemented with 10% (v/v) tetracycline-tested fetal bovine serum (Sigma, F6178), and 2 μg/mL puromycin (Invitrogen, A11138-03).

NSC-34 cells constitutively expressing untagged human FUS constructs were generated by lentiviral transduction of the CSCW2-IRES-GFP lentivector (a generous gift from Dr. Miguel Esteves, University of Massachusetts Medical School) containing FUS (WT or mutant R495X). Flow cytometry was used to enrich for expression of the GFP reporter in each line. Cells with equivalent levels of exogenous FUS proteins were employed.

For drug treatments, the following stocks were prepared and stored at freezing temperatures: 50 mg/mL doxycycline (Sigma, D9891) in water (−80°C), 100 mM sodium arsenite (Sigma, 71287) in water (−20°C) and 20 mM adenosine-2,3 dialdehyde ("AdOx"; Sigma, A7154) in water (−20°C). FUS expression in the FlpIn HEK-293 lines was induced with the addition of 1 μg/mL doxycycline for 24 hrs unless otherwise noted. Cells were then exposed to sodium arsenite and/or AdOx as described below.

Plasmids and cloning

The pEmRFP-G3BP and mRFP-TIA-1 plasmids for FRAP analyses were generously provided by Drs. Nancy Kedersha and Paul Anderson (Brigham and Women's Hospital, Harvard Medical School). The mRFP-TIA-1 was subcloned into the low expression lentivirus vector CShPW2 (a gift from Miguel Estevez, UMMS) with NheI and Knp1 restriction sites using BP Clonase II (Invitrogen, 11789–020), thereby creating CShPW2-RFP-TIA-1. MBP-M9M was a kind gift from Dr. Yuh Min Chook (University of Texas Southwestern Medical Center).

GFP-FUS R521G deletion constructs were constructed as follows: PCR amplified full length GFP-FUS R521G, flanked by attB homologous sequences, was cloned into pDONR221 vector (Invitrogen, 12536–017) with BP Clonase II (Invitrogen, 11789–020) to generate the starting plasmid pDONR221:GFP-FUS R521G. To facilitate substitution of the full length gene with deletion/truncation variants, restriction sites for KpnI and XbaI were introduced upstream of the ATG start codon and downstream the TAA stop codon, respectively, using the following primers: **fwd**: GGGGACAAGTTTGTACAAAAAAGCAGGCTGG TACC**ATG**GCCTCAAACGATTATACCC, **rev**: GGGGA CCACTTTGTACAAGAAAGCTGGGTTCTAGA**TTA**AT ACGGCCTCTCCCTGC. To generate deletion constructs, the following primers were designed by joining the upstream and downstream sequences flanking the domain that was deleted: **ΔGLY_fwd**: AGAACCAGTACAACAG CAGCAGTACCATCTTTGTGCAAGGCC; **ΔGLY_rev**: ACTCAATTGTAACATTCTCACCCAGACTGCCAGA CAACAACACCCGGGCAGACTTTAATCGGG; **ΔRR M_rev**: CCACGACCATTGCCACCACCGTTGTTGTC TGAATTATCCTGTTCG; **ΔRGG1_fwd**: CAAGGTCT CATTTGCTACTCGCGCTGGTGACTGGAAGTGTCC; **ΔRGG1_rev**: CATATTCTCACAGGTGGGATTAGGCC GATTAAAGTCTGCCCGGC; **ΔRGG2_fwd**: CCAGTGT AAGGCCCCTAAACCAGATAAGATGGATTCCAGGGG TGAGCAC; **ΔRGG2_rev**: GTGCTCACCCCTGGAATC CATCTTATCTGGTTTAGGGGCCTTACACTGG; **Δ422-526_fwd**: GGGGACAAGTTTGTACAAAAAAGCAGGC TGGTACC**ATG**GCCTCAAACGATTATACCC; **Δ422-526_rev**: GGGGACCACTTTGTACAAGAAAGCTGG GTTCTAGA**TTA**TCGCTGCTGTCCTCCACC. The deletion reactions were performed using the pDONR221: FUS R521G plasmid as template and the QuikChange II Mutagenesis kit (Stratagene; 200523) according to the manufacturer's instructions. For the ΔQGSY truncation construct, PCR was performed using a reverse primer for the full-length R521G gene paired with a forward primer containing the 5'-end sequences of ΔGLY flanked by the restriction enzyme KpnI recognition sequence: **ΔQGSY_fwd**: CAGGCTGGTACCGGTGGTGGAGGTGGAGGT. All constructs were then sub-cloned into the expression vector pDEST-53 (Invitrogen) using Gateway cloning method with LR Clonase II (Invitrogen, 11791–100) according to the manufacturer's instructions.

Immunofluorescence

Standard immunofluorescence protocols were employed as described previously [13]. Briefly, cells were fixed with 4% paraformaldehyde for 10–15 min then blocked with PBSAT (1X PBS/1% BSA/0.5% Triton-X 100) for 30–60 min at ambient temperature. Primary antibodies described in each experiment were diluted in PBSAT and applied to cells at ambient temperature for 1 hr. Primary antibody dilutions were as follows: 1:2000 for mouse anti-G3BP (BD Transduction Labs, 611126), 1:1000 for rabbit anti-G3BP (Proteintech, 130-57-2AP), 1:1500 for rabbit anti-dimethyl arginine ("ASYM24"; Millipore, 07–414) and 1:200 mouse anti-FUS (Santa Cruz, SC-4771). Cells were then incubated with secondary antibodies diluted 1:1000–1:2500 in PBSAT for 45 min at ambient temperature. Secondary antibodies included Dylight 549 conjugated anti-mouse IgG (Jackson ImmunoResearch Labs, 715-505-151), Cy3 conjugated anti-mouse IgG (Jackson ImmunoResearch Labs, 715-165-151), Cy3 conjugated anti-rabbit IgG (Jackson ImmunoResearch Labs, 711-165-152), and Cy5 conjugated anti-mouse IgG (Jackson ImmunoResearch Labs, 715-175-151). GFP signal was enhanced by 1:1000 dilution of Alexa Fluor 488-conjugated rabbit anti-GFP (Invitrogen, A21311). Cells were stained with 34 ng/mL DAPI in dH_2O, and coverslips were mounted with ProLong Gold anti-fade reagent (Invitrogen, P36930).

Western blotting

Standard western blotting protocols were employed as described previously [13]. Primary antibodies described in each experiment were diluted as follows: 1:1000 for mouse anti-GFP (Living Colors; Clontech, 632380), 1:1000 for rabbit anti-dimethyl-arginine ("ASYM24"; Millipore, 07–414), 1:1000 for mouse anti-tubulin (Sigma, T9026), and 1:1000 for rabbit anti-FUS. Rabbit anti-FUS antibodies were generated by GenScript against a C-terminal epitope, using the peptide CKFGGPRDQGSRHDSEQDNSD. Blots were incubated with primary antibodies for 1 hr at ambient temperature or overnight at 4°C. Secondary antibodies, including anti-mouse IRDye 680 (Licor, 926–32220) or IRDye 800 (LiCor, 926–32210) and anti-rabbit IRDye 680 (LiCor, 926–32220) or IRDye 800 (Licor, 926–32211), were diluted 1:10000 and incubated with blots for 1–2 hrs at ambient temperature. Bands were visualized with an Odyssey Infrared Imager (LiCor, Model 9120), and densitometry measurements performed with the Odyssey Software (LiCor, V3.0).

Stress granule assembly and disassembly kinetics

Inducible GFP-FUS (WT, R495X and H517Q) HEK-293 cells were plated on coverslips at a density of 5×10^4

cells/coverslip. The next day, GFP-FUS expression was induced as described above. For stress granule assembly measurements, cells were treated with 0.25 mM sodium arsenite for 40 or 90 min. Coverslips were then fixed and processed for immunofluorescence (IF) with the mouse anti-G3BP and rabbit anti-GFP antibodies listed above. For stress granule disassembly measurements, cells were treated with 0.25 mM sodium arsenite for 60 min, at which time the media containing sodium arsenite was replaced with fresh media. After 90 min in fresh media, cells were processed for IF as described above. The percentage of cells with stress granules was determined as [(the number of cells containing at least one stress granule / total number of cells) × 100]. More than 2000 healthy, interphase, non-crowded cells were counted in multiple (between n=4 and n=11, depending on cell line and condition) independent experiments for both assembly and disassembly conditions. A one-way ANOVA with Tukey's multiple comparisons post-test was used to compare the induced and uninduced groups. Similar parameters were used for assembly kinetics in NSC-34 parent cells and cells expressing untagged human FUS proteins with the following changes: cells were treated with sodium arsenite for 1 hr, and immunofluorescence was performed with the rabbit anti-G3BP and mouse anti-FUS antibodies listed above. More than 2000 cells were counted in at least n=11 independent experiments per condition. Statistical significance was determined by one-way ANOVA with Tukey's multiple comparisons post-test.

Fluorescence recovery after photobleaching

GFP-FUS WT and GFP-FUS R495X HEK-293 cells were plated at a density of 8×10^4 cells/plate in 35 mm glass bottom dishes (MatTek Corp, P35GC-1.5-14-C), allowed to adhere for 48 hrs, then transfected with either CShPW2-RFP-TIA-1 or pEmRFP-G3BP expression plasmids using Lipofectamine 2000 (Invitrogen, 11668–019) according to the manufacturer's instructions with a 1.6 μl Lipo: 3.2 μg DNA ratio. Approximately 23 hr post-transfection, phenol red(−) growth media without (overexpression experiments) or containing 0.2 mM sodium arsenite (stress granule experiments) was applied to the cells for 1 hr prior to FRAP.

FRAP experiments were performed at 37°C as previously described [45]. Multiple cells were analyzed in each experiment over a 30 min period starting at 60 min of sodium arsenite exposure. Experiments were carried out on a Leica SP5 AOBS laser scanning confocal microscope using a 40× 1.3NA water immersion objective or a Leica SP1 system using a 40×, 1.25NA oil immersion objective. No more than two stress granules, from opposite sides of a cell, were individually bleached using a 1-3s laser pulse delivered by a 488 nm or 561 nm laser. A pre-bleach, immediate post-bleach and 16 additional post-bleach images spaced at 5 sec intervals were captured. Leica Confocal Software (Leica Microsystems, Exton, PA) was used to measure fluorescence intensity in the bleached region of interest (ROI), the whole cell, and in a background control area lacking cells at each time point. The data was analyzed and background fluorescence subtracted using Excel. The relative fluorescence intensity (I_{rel}) in the bleached area was calculated as previously shown [45]. Briefly, the following equation was used: $I_{rel,\ t} = (I_t \times (C_0/C_t))-(I_{pbl} \times (C_0/C_{bl}))/(I_0-(I_{pbl} \times (C_0/C_{pbl}))$, where C_0 is the total cellular fluorescence before bleaching, C_{pbl} is the total cellular fluorescence in the post-bleach image, C_t is the total cellular fluorescence at time t, I_0 is the pre-bleach ROI fluorescence intensity, I_t is the ROI fluorescence intensity at time t, and I_{pbl} is the post-bleach ROI fluorescence intensity. The data was normalized using this equation such that the post-bleach ROI fluorescence intensity was set to 0 and the pre-bleach ROI fluorescence intensity to 1. I_t was calculated as the percentage difference between the relative fluorescence asymptote of the recovery curve and a relative recovery of 1, a value that would reflect complete recovery without an immobile fraction. Recovery curves were drawn using Graphpad Prism 6 (Graphpad Software), with individual time points presented as means ± SEMs. Fluorescence recovery half times were calculated from exponential one-phase association curves best fit for the recovery graphs: $F(t) = F_{max}\ (1- e^{-kt})$. Mobile fractions were calculated from the plateau region from each curve, which was identified as the series of data points with < 2% change in slope over time.

At least two independent experiments were performed for all conditions. The total number of stress granules analyzed for each condition is shown in Figure 3. A two-way ANOVA was used to determine statistical significance between the mobile fractions for each of the experiments.

Morphology experiments

Stable GFP-FUS HEK-293 cells were plated and processed for immunofluorescence as described under 'stress granule assembly and disassembly kinetics' above, except that cells were treated with 0.5 mM sodium arsenite for 1 hr. Confocal stacked images (0.2 μm stack step, 4 μm range) were acquired using a Zeiss Axiovert 200 microscope with a PerkinElmer UltraView LAS spinning disc equipped with a 100× phase objective. Imaris analytical software (Bitplane Scientific Software) was used to construct 3D projections of image stacks. Volume measurements were taken of each stress granule with a G3BP fluorescence signal that was at least 2-fold above background. Because P-bodies had an average volume of 0.5 μm^3 (data not shown) by the same analysis, only stress granules with a volume > 0.5 μm^3 were included in the analysis. Data is averaged from three independent experiments per line, using approximately 30 stress granules per condition. Statistical significance was determined using the Student's t-test.

Analysis of FUS deletion constructs in stress granule assembly

HeLa cells were plated on coverslips at a density of 2.5 × 10^4 cells/coverslip and adhered at 37°C for 24 hrs, after which GFP-FUS R521G truncation constructs and MBP-M9M were transiently transfected into cells using Lipofectamine-2000 (Invitrogen, 11668) according to the manufacturer's instructions. Twenty-four hours post transfection, cells were subjected to media containing 0.5 mM sodium arsenite for 1 hr. Cells were processed immunofluorescence with mouse anti-G3BP as described above.

Confocal microscopy was performed using a Solamere Technology Group CSU10B spinning disk confocal system equipped with a Yokogawa CSU10 spinning disk confocal scan head. Image stacks (0.2 μm stack step; 13 stack range) were acquired using a 100× oil objective, a Roper Cool-snap HQ2 camera and MetaMorph V7.6.3 software. Background signal was subtracted by removing fluorescence from a dark-current image (acquired with the laser off) from each raw image. For the GFP images, variations in illumination and detection efficiencies at each pixel were corrected by dividing the dark-adjusted intensities by a normalized flat-field image of a uniformly green fluorescent slide (Chroma Technology, Rockingham, VT, USA) acquired using the same 525/50 nm band-pass filter. Four channels were imaged per cell: FITC for GFP-FUS, Cy3 for G3BP, DAPI for nuclei and phase for cell borders.

The extent of GFP-FUS incorporation into stress granules was analyzed with MetaMorph V7.6.3 software using the Integrated Morphometry Analysis tool. Since cells with a GFP signal brighter than 1.5 × 10^6 grays/μm^2 tended to form cytoplasmic aggregates *a priori* of arsenite treatment (data not shown), only transfected cells with GFP-FUS expression levels < 1.5 × 10^6 grays/μm^2 were selected for analysis. Stress granules were selected using the Cy3 (G3BP) channel as a reference. The slice corresponding to the center of the stress granule was selected from each image stack. Stress granules with an area of at least 0.5 μm^2 were selected. An outline was drawn around each G3BP granule, and this outline was then transferred to the corresponding FITC (GFP-FUS) image, such that the GFP-FUS signal intensity ("stress granules intensity") within that granule could be measured. GFP signal intensity measurements were also acquired in the region proximal to the stress granule, and was referred to as the "Diffuse intensity". The ratio of stress granule intensity (i.e., GFP-FUS inside the stress granule) to diffuse intensity (i.e., GFP-FUS outside the stress granule) was determined for a total of 75–150 stress granules per construct over three independent experiments. Statistical significance was determined by a one-way ANOVA followed by a Dunnett's post hoc test in Graphpad Prism 6 (Graphpad software).

Methyltransferase inhibition studies

HeLa cells were plated at a density of 2.5 × 10^4 cells/coverslip and adhered for 24 hrs, after which GFP-FUS R495X expression constructs were transiently transfected with Lipofectamine-2000 either with or without 25 μM AdOx for 24 hr. Cells were then exposed to 0.5 mM sodium arsenite for 1 hr, and coverslips were processed for immunofluorescence using the mouse anti-G3BP rabbit and ASYM24 antibodies as described above. For quantification, confocal images of 30 cells per condition across three independent experiments were taken, and the intensity of GFP-FUS and ASYM24 signal within stress granules was determined between AdOx-treated and untreated conditions using MetaMorph as described above. Statistical significance was determined using a Student's t-test.

For GFP immunoprecipitation (IP) reactions, cells were lysed for 15 min in IP buffer (400 μL 1% NP-40 (MP Biomedicals, 198596)/50 mM Tris–HCl (Sigma T3253-500G)/5 mM EDTA (Fisher E478-500)/150 mM NaCl and 10% v/v glycerol (Acros 15982–0010) in water; pH 7.5), and centrifuged at 13000 rpm for 15 min at 4°C. The supernatant was pre-cleared with 50 μL Biomag Protein G beads (Qiagen, 311812) for 2 hrs at 4°C. Anti-GFP-coated beads for each sample were prepared by incubating 0.5 μL of anti-GFP (Abcam, ab290) in 400 μL of IP buffer with 50 μL Biomag Protein G beads for 2 hrs at 4°C. IP reactions were performed at 4°C overnight with 100 μg of pre-cleared lysate. Protein elution was accomplished with 50 μL 1X SDS loading buffer (Boston Bioproducts BP11R) for 5 min at 95°C, and 20 μL of sample was subjected to western blot analysis with mouse anti-GFP, mouse anti-tubulin and ASYM24 as described above.

Additional files

Additional file 1: A minor fraction of GFP-FUS H517Q incorporates into stress granules in response to sodium arsenite. Images for the indicated GFP-FUS cell line (top 3 rows) were collected as described in Figure 1A. Antibody markers used for immunofluorescence are indicated on the left. Images overexposed for GFP detection (bottom row) reveal that a minor fraction of GFP-FUS H517Q (green) co-localizes with G3BP-positive stress granules (red). FUS H517Q containing stress granules are denoted by arrows. Conversely, GFP-FUS WT is not detected in stress granule (i.e., there is no GFP-positive signal that co-localized with G3BP), even with high exposure. Scale bar = 5 μm.

Additional file 2: NSC-34 cells expressing untagged human FUS WT and R495X exhibit similar transduction efficiencies. Fluorescent images of the GFP reporter (green) in NSC-34 cells transduced with lentivirus containing untagged human FUS WT or R495X. Transduction efficiencies of approximately 100% were determined for both lines. Cellular nuclei are stained with DAPI (blue). Scale bar = 20 μm.

Additional file 3: Sodium arsenite induced stressed granules display different dynamics compared to those induced by mRFP-G3BP over-expression. (A) Transfection of mRFP-G3BP was sufficient to induce G3BP positive stress granules in a subset of both GFP-FUS WT and GFP-FUS R495X cells as determined by live cell imaging. Scale bar = 20 μm. **(B)** The FRAP recovery curve for mRFP-G3BP inside the stress granule

in (A) was different depending on whether mRFP-G3BP was transfected into GFP-FUS WT (blue circle) or R495X (red square) expressing cells. Note the trend is opposite from sodium arsenite-induced stress granule in Figure 3. **(C)** Quantification of the mobile fraction from the recovery curves in (B) compared to those in Figure 3G revealed that expression of GFP-FUS R495X significantly increased mRFP-G3BP binding (i.e., smaller mobile fraction) to stress granules in the over-expression condition compared to all other conditions. Asterisks indicate statistically significant differences between cell lines as determined by two-way ANOVA (****$P < 0.0001$) on data from n=3 independent experiments. Additional significant comparisons include, but are not shown for clarity: WT in the overexpression versus WT in the sodium arsenite condition ($P < 0.05$); R495X in the overexpression versus R495X in the sodium arsenite condition ($P < 0.0001$); R495X in the overexpression versus WT in the sodium arsenite condition ($P < 0.05$). The total number (N) of stress granules analyzed is indicated. All error bars represent SEMs.

Competing interests
The authors declare that they have no competing interests.

Authors' contributions
DB, LK, and CW planned and performed the majority of experiments; DB, AJQ and JAN planned, performed and analyzed data for FRAP; RJC cloned deletion constructs for structure-function analyses; RRKS and KB contributed to the design and data interpretation for experiments; DB, LK and DAB wrote the paper. All authors read and approved the final manuscript.

Acknowledgements
We thank Dr. Zuoshang Xu for his critical review of the manuscript, Dr. John Landers for helpful discussion, Dr. Paul Furcinitti of the UMass Medical School Core Digital Imaging Facility for his assistance with the confocal microscopy, Dr. Miguel Esteves (University of Massachusetts Medical School) for the CSCW2-IRES-GFP lentivector and production of lentivirus, Drs. Nancy Kedersha and Paul Anderson (Brigham and Women's Hospital, Harvard Medical School) for the pEmRFP-G3BP and mRFP-TIA-1 plasmids, Dr. Yuh Min Chook (University of Texas Southwestern Medical Center) for the MBP-M9M plasmid, Drs. Zuoshang Xu and Stephen Doxsey (University of Massachusetts Medical School) for use of their microscopes, and Nathan Lemay for his assistance with experiments. We acknowledge financial support from the ALS Therapy Alliance-CVS Pharmacy (DAB), ALS Association (DAB), the Worcester Foundation (DAB), and the US National Institutes of Health/National Institute on Neurological Disorders and Stroke (R01NS067206-01 and R01NS078145-01; DAB).

Author details
[1]Department of Neurology, University of Massachusetts Medical School, Worcester, MA, USA. [2]Department of Cell and Developmental Biology, University of Massachusetts Medical School, Worcester, MA, USA. [3]Department of Biochemistry and Molecular Pharmacology, University of Massachusetts Medical School, Worcester, MA, USA.

Received: 16 April 2013 Accepted: 27 August 2013
Published: 31 August 2013

References

1. Calvio C, Neubauer G, Mann M, Lamond AI: **Identification of hnRNP P2 as TLS/FUS using electrospray mass spectrometry.** *RNA* 1995, **1**:724–733.
2. Kwiatkowski TJ Jr, Bosco DA, Leclerc AL, Tamrazian E, Vanderburg CR, Russ C, Davis A, Gilchrist J, Kasarskis EJ, Munsat T, *et al*: **Mutations in the FUS/TLS gene on chromosome 16 cause familial amyotrophic lateral sclerosis.** *Science* 2009, **323**:1205–1208.
3. Vance C, Rogelj B, Hortobagyi T, De Vos KJ, Nishimura AL, Sreedharan J, Hu X, Smith B, Ruddy D, Wright P, *et al*: **Mutations in FUS, an RNA processing protein, cause familial amyotrophic lateral sclerosis type 6.** *Science* 2009, **323**:1208–1211.
4. Bosco DA, Landers JE: **Genetic determinants of amyotrophic lateral sclerosis as therapeutic targets.** *CNS Neurol Disord Drug Targets* 2010, **9**:779–790.
5. Dormann D, Madl T, Valori CF, Bentmann E, Tahirovic S, Abou-Ajram C, Kremmer E, Ansorge O, Mackenzie IR, Neumann M, Haass C: **Arginine methylation next to the PY-NLS modulates Transportin binding and nuclear import of FUS.** *EMBO J* 2012, **31**:4258–4275.
6. Dormann D, Rodde R, Edbauer D, Bentmann E, Fischer I, Hruscha A, Than ME, Mackenzie IR, Capell A, Schmid B, *et al*: **ALS-associated fused in sarcoma (FUS) mutations disrupt Transportin-mediated nuclear import.** *EMBO J* 2010, **29**:2841–2857.
7. Andersson MK, Stahlberg A, Arvidsson Y, Olofsson A, Semb H, Stenman G, Nilsson O, Aman P: **The multifunctional FUS, EWS and TAF15 proto-oncoproteins show cell type-specific expression patterns and involvement in cell spreading and stress response.** *BMC Cell Biol* 2008, **9**:37.
8. Zinszner H, Sok J, Immanuel D, Yin Y, Ron D: **TLS (FUS) binds RNA in vivo and engages in nucleo-cytoplasmic shuttling.** *J Cell Sci* 1997, **110**(Pt 15):1741–1750.
9. Fujii R, Okabe S, Urushido T, Inoue K, Yoshimura A, Tachibana T, Nishikawa T, Hicks GG, Takumi T: **The RNA binding protein TLS is translocated to dendritic spines by mGluR5 activation and regulates spine morphology.** *Curr Biol* 2005, **15**:587–593.
10. Fujii R, Takumi T: **TLS facilitates transport of mRNA encoding an actin-stabilizing protein to dendritic spines.** *J Cell Sci* 2005, **118**:5755–5765.
11. Lagier-Tourenne C, Polymenidou M, Hutt KR, Vu AQ, Baughn M, Huelga SC, Clutario KM, Ling SC, Liang TY, Mazur C, *et al*: **Divergent roles of ALS-linked proteins FUS/TLS and TDP-43 intersect in processing long pre-mRNAs.** *Nature Neurosci* 2012, **15**:1488–1497.
12. Halliday G, Bigio EH, Cairns NJ, Neumann M, Mackenzie IR, Mann DM: **Mechanisms of disease in frontotemporal lobar degeneration: gain of function versus loss of function effects.** *Acta Neuropathol* 2012, **124**:373–382.
13. Bosco DA, Lemay N, Ko HK, Zhou H, Burke C, Kwiatkowski TJ Jr, Sapp P, McKenna-Yasek D, Brown RH Jr, Hayward LJ: **Mutant FUS proteins that cause amyotrophic lateral sclerosis incorporate into stress granules.** *Human Mol Genet* 2010, **19**:4160–4175.
14. Ishigaki S, Masuda A, Fujioka Y, Iguchi Y, Katsuno M, Shibata A, Urano F, Sobue G, Ohno K: **Position-dependent FUS-RNA interactions regulate alternative splicing events and transcriptions.** *Sci Rep* 2012, **2**:529.
15. Rogelj B, Easton LE, Bogu GK, Stanton LW, Rot G, Curk T, Zupan B, Sugimoto Y, Modic M, Haberman N, *et al*: **Widespread binding of FUS along nascent RNA regulates alternative splicing in the brain.** *Sci Rep* 2012, **2**:603.
16. Tan AY, Riley TR, Coady T, Bussemaker HJ, Manley JL: **TLS/FUS (translocated in liposarcoma/fused in sarcoma) regulates target gene transcription via single-stranded DNA response elements.** *Proc Natl Acad Sci U S A* 2012, **109**:6030–6035.
17. Wang X, Arai S, Song X, Reichart D, Du K, Pascual G, Tempst P, Rosenfeld MG, Glass CK, Kurokawa R: **Induced ncRNAs allosterically modify RNA-binding proteins in cis to inhibit transcription.** *Nature* 2008, **454**:126–130.
18. Da Cruz S, Cleveland DW: **Understanding the role of TDP-43 and FUS/TLS in ALS and beyond.** *Curr Opin Neurobiol* 2011, **21**:904–919.
19. Dormann D, Haass C: **TDP-43 and FUS: a nuclear affair.** *Trends Neurosci* 2011. http://www.ncbi.nlm.nih.gov/pubmed/21700347.
20. Anderson P, Kedersha N: **Stress granules: the Tao of RNA triage.** *Trends Biochem Sci* 2008, **33**:141–150.
21. Kedersha N, Anderson P: **Stress granules: sites of mRNA triage that regulate mRNA stability and translatability.** *Biochem Soc Trans* 2002, **30**:963–969.
22. Wippich F, Bodenmiller B, Trajkovska MG, Wanka S, Aebersold R, Pelkmans L: **Dual specificity kinase DYRK3 couples stress granule condensation/dissolution to mTORC1 signaling.** *Cell* 2013, **152**:791–805.
23. Wolozin B: **Regulated protein aggregation: stress granules and neurodegeneration.** *Mol Neurodegener* 2012, **7**:56.
24. Fujita K, Ito H, Nakano S, Kinoshita Y, Wate R, Kusaka H: **Immunohistochemical identification of messenger RNA-related proteins in basophilic inclusions of adult-onset atypical motor neuron disease.** *Acta Neuropathol* 2008, **116**:439–445.
25. Liu-Yesucevitz L, Bilgutay A, Zhang YJ, Vanderweyde T, Citro A, Mehta T, Zaarur N, McKee A, Bowser R, Sherman M, *et al*: **Tar DNA binding protein-43 (TDP-43) associates with stress granules: analysis of cultured cells and pathological brain tissue.** *PloS One* 2010, **5**:e13250.
26. Bentmann E, Neumann M, Tahirovic S, Rodde R, Dormann D, Haass C: **Requirements for stress granule recruitment of fused in sarcoma (FUS) and TAR DNA-binding protein of 43 kDa (TDP-43).** *J Biol Chem* 2012, **287**:23079–23094.

27. Daigle JG, Lanson NA Jr, Smith RB, Casci I, Maltare A, Monaghan J, Nichols CD, Kryndushkin D, Shewmaker F, Pandey UB: **RNA-binding ability of FUS regulates neurodegeneration, cytoplasmic mislocalization and incorporation into stress granules associated with FUS carrying ALS-linked mutations.** *Human Mol Genet* 2013.
28. Gal J, Zhang J, Kwinter DM, Zhai J, Jia H, Jia J, Zhu H: **Nuclear localization sequence of FUS and induction of stress granules by ALS mutants.** *Neurobiol Aging* 2010, **32**:2323.e27-40.
29. Ito D, Seki M, Tsunoda Y, Uchiyama H, Suzuki N: **Nuclear transport impairment of amyotrophic lateral sclerosis-linked mutations in FUS/TLS.** *Ann Neurol* 2011, **69**:152–162.
30. Vance C, Scotter EL, Nishimura AL, Troakes C, Mitchell JC, Kathe C, Urwin H, Manser C, Miller CC, Hortobagyi T, *et al*: **ALS mutant FUS disrupts nuclear localisation and sequesters wild-type FUS within cytoplasmic stress granules.** *Human Mol Genet* 2013, **22**:2676–2688.
31. Aulas A, Stabile S, Vande Velde C: **Endogenous TDP-43, but not FUS, contributes to stress granule assembly via G3BP.** *Mol Neurodegener* 2012, **7**:54.
32. Kedersha N, Cho MR, Li W, Yacono PW, Chen S, Gilks N, Golan DE, Anderson P: **Dynamic shuttling of TIA-1 accompanies the recruitment of mRNA to mammalian stress granules.** *J Cell Biol* 2000, **151**:1257–1268.
33. Rodriguez VM, Carrizales L, Jimenez-Capdeville ME, Dufour L, Giordano M: **The effects of sodium arsenite exposure on behavioral parameters in the rat.** *Brain Res Bull* 2001, **55**:301–308.
34. Tabocova S, Hunter ES 3rd, Gladen BC: **Developmental toxicity of inorganic arsenic in whole embryo: culture oxidation state, dose, time, and gestational age dependence.** *Toxicol Appl Pharmacol* 1996, **138**:298–307.
35. Sama RR, Ward CL, Kaushansky LJ, Lemay N, Ishigaki S, Urano F, Bosco DA: **FUS/TLS assembles into stress granules and is a prosurvival factor during hyperosmolar stress.** *J Cell Physiol* 2013, **228**:2222–2231.
36. Kedersha N, Anderson P: **Mammalian stress granules and processing bodies.** *Methods Enzymol* 2007, **431**:61–81.
37. McDonald KK, Aulas A, Destroismaisons L, Pickles S, Beleac E, Camu W, Rouleau GA, Vande Velde C: **TAR DNA-binding protein 43 (TDP-43) regulates stress granule dynamics via differential regulation of G3BP and TIA-1.** *Human Mol Genet* 2011.
38. Cashman NR, Durham HD, Blusztajn JK, Oda K, Tabira T, Shaw IT, Dahrouge S, Antel JP: **Neuroblastoma x spinal cord (NSC) hybrid cell lines resemble developing motor neurons.** *Dev Dyn* 1992, **194**:209–221.
39. Huang C, Zhou H, Tong J, Chen H, Liu YJ, Wang D, Wei X, Xia XG: **FUS transgenic rats develop the phenotypes of amyotrophic lateral sclerosis and frontotemporal lobar degeneration.** *PLoS Genet* 2011, **7**:e1002011.
40. Ju S, Tardiff DF, Han H, Divya K, Zhong Q, Maquat LE, Bosco DA, Hayward LJ, Brown RH Jr, Lindquist S, *et al*: **A Yeast Model of FUS/TLS-Dependent Cytotoxicity.** *PLoS Biol* 2011, **9**:e1001052.
41. Lanson NA Jr, Maltare A, King H, Smith R, Kim JH, Taylor JP, Lloyd TE, Pandey UB: **A Drosophila model of FUS-related neurodegeneration reveals genetic interaction between FUS and TDP-43.** *Human Mol Genet* 2011, **20**:2510–2523.
42. Guil S, Long JC, Caceres JF: **hnRNP A1 relocalization to the stress granules reflects a role in the stress response.** *Mol Cell Biol* 2006, **26**:5744–5758.
43. Kedersha N, Stoecklin G, Ayodele M, Yacono P, Lykke-Andersen J, Fritzler MJ, Scheuner D, Kaufman RJ, Golan DE, Anderson P: **Stress granules and processing bodies are dynamically linked sites of mRNP remodeling.** *J Cell Biol* 2005, **169**:871–884.
44. Nickerson JA: **The biochemistry of RNA metabolism studied in situ.** *RNA Biol* 2009, **6**:25–30.
45. Quaresma AJ, Sievert R, Nickerson JA: **Regulation of mRNA Export by the PI3 kinase / AKT Signal Transduction Pathway.** *Mol Biol Cell* 2013.
46. Buchan JR, Parker R: **Eukaryotic stress granules: the ins and outs of translation.** *Mol Cell* 2009, **36**:932–941.
47. Tourriere H, Chebli K, Zekri L, Courselaud B, Blanchard JM, Bertrand E, Tazi J: **The RasGAP-associated endoribonuclease G3BP assembles stress granules.** *J Cell Biol* 2003, **160**:823–831.
48. Buchan JR, Yoon JH, Parker R: **Stress-specific composition, assembly and kinetics of stress granules in Saccharomyces cerevisiae.** *J Cell Sci* 2011, **124**:228–239.
49. Dewey CM, Cenik B, Sephton CF, Dries DR, Mayer P, Good SK, Johnson BA, Herz J, Yu G: **TDP-43 is directed to stress granules by sorbitol, a novel physiological osmotic and oxidative stressor.** *Mol Cell Biol* 2010, **31**:1098–1108.
50. De Leeuw F, Zhang T, Wauquier C, Huez G, Kruys V, Gueydan C: **The cold-inducible RNA-binding protein migrates from the nucleus to cytoplasmic stress granules by a methylation-dependent mechanism and acts as a translational repressor.** *Experimental Cell Res* 2007, **313**:4130–4144.
51. Kedersha NL, Gupta M, Li W, Miller I, Anderson P: **RNA-binding proteins TIA-1 and TIAR link the phosphorylation of eIF-2 alpha to the assembly of mammalian stress granules.** *J Cell Biol* 1999, **147**:1431–1442.
52. Rajyaguru P, She M, Parker R: **Scd6 targets eIF4G to repress translation: RGG motif proteins as a class of eIF4G-binding proteins.** *Mol Cell* 2012, **45**:244–254.
53. Iko Y, Kodama TS, Kasai N, Oyama T, Morita EH, Muto T, Okumura M, Fujii R, Takumi T, Tate S, Morikawa K: **Domain architectures and characterization of an RNA-binding protein, TLS.** *J Biol Chem* 2004, **279**:44834–44840.
54. Cansizoglu AE, Lee BJ, Zhang ZC, Fontoura BM, Chook YM: **Structure-based design of a pathway-specific nuclear import inhibitor.** *Nat Struct Mol Biol* 2007, **14**:452–454.
55. Rappsilber J, Friesen WJ, Paushkin S, Dreyfuss G, Mann M: **Detection of arginine dimethylated peptides by parallel precursor ion scanning mass spectrometry in positive ion mode.** *Anal Chem* 2003, **75**:3107–3114.
56. Bedford MT, Clarke SG: **Protein arginine methylation in mammals: who, what, and why.** *Molecular cell* 2009, **33**:1–13.
57. Grant AJ, Lerner LM: **Dialdehydes derived from adenine nucleosides as substrates and inhibitors of adenosine aminohydrolase.** *Biochemistry* 1979, **18**:2838–2842.
58. Colombrita C, Onesto E, Megiorni F, Pizzuti A, Baralle FE, Buratti E, Silani V, Ratti A: **TDP-43 and FUS RNA-binding proteins bind distinct sets of cytoplasmic messenger RNAs and differently regulate their post-transcriptional fate in motoneuron-like cells.** *J Biol Chem* 2012, **287**:15635–15647.
59. Hoell JI, Larsson E, Runge S, Nusbaum JD, Duggimpudi S, Farazi TA, Hafner M, Borkhardt A, Sander C, Tuschl T: **RNA targets of wild-type and mutant FET family proteins.** *Nat Struct Mol Biol* 2011, **18**:1428–1431.
60. Sun Z, Diaz Z, Fang X, Hart MP, Chesi A, Shorter J, Gitler AD: **Molecular Determinants and Genetic Modifiers of Aggregation and Toxicity for the ALS Disease Protein FUS/TLS.** *PLoS Biol* 2011, **9**:e1000614.
61. Rajyaguru P, Parker R: **RGG motif proteins: modulators of mRNA functional states.** *Cell Cycle* 2012, **11**:2594–2599.
62. Tradewell ML, Yu Z, Tibshirani M, Boulanger MC, Durham HD, Richard S: **Arginine methylation by PRMT1 regulates nuclear-cytoplasmic localization and toxicity of FUS/TLS harbouring ALS-linked mutations.** *Human Mol Genet* 2012, **21**:136–149.
63. Yamaguchi A, Kitajo K: **The Effect of PRMT1-Mediated Arginine Methylation on the Subcellular Localization, Stress Granules, and Detergent-Insoluble Aggregates of FUS/TLS.** *PloS One* 2012, **7**:e49267.

doi:10.1186/1750-1326-8-30
Cite this article as: Baron *et al.*: Amyotrophic lateral sclerosis-linked FUS/TLS alters stress granule assembly and dynamics. *Molecular Neurodegeneration* 2013, **8**:30.

BIBLIOGRAPHY

1. Ackerley S, Grierson AJ, Banner S, Perkinton MS, Brownlees J, Byers HL, Ward M, Thornhill P, Hussain K, Waby JS, Anderton BH, Cooper JD, Dingwall C, Leigh PN, Shaw CE, Miller CC (2004) p38alpha stress-activated protein kinase phosphorylates neurofilaments and is associated with neurofilament pathology in amyotrophic lateral sclerosis. Mol Cell Neurosci 26:354-364.

2. Akhmedov AT, Bertrand P, Corteggiani E, Lopez BS (1995) Characterization of two nuclear mammalian homologous DNA-pairing activities that do not require associated exonuclease activity. Proc Natl Acad Sci U S A 92:1729-1733.

3. Alami NH, Smith RB, Carrasco MA, Williams LA, Winborn CS, Han SS, Kiskinis E, Winborn B, Freibaum BD, Kanagaraj A, Clare AJ, Badders NM, Bilican B, Chaum E, Chandran S, Shaw CE, Eggan KC, Maniatis T, Taylor JP (2014) Axonal Transport of TDP-43 mRNA Granules Is Impaired by ALS-Causing Mutations. Neuron 81:536-543.

4. Aletta JM, Hu JC (2008) Protein arginine methylation in health and disease. Biotechnol Annu Rev 14:203-224.

5. Alfieri RR, Petronini PG (2007) Hyperosmotic stress response: comparison with other cellular stresses. Pflugers Arch 454:173-185.

6. Anderson P, Kedersha N (2008) Stress granules: the Tao of RNA triage. Trends Biochem Sci 33:141-150.

7. Anderson P, Kedersha N (2009) Stress granules. Curr Biol 19:R397-398.

8. Andersson MK, Stahlberg A, Arvidsson Y, Olofsson A, Semb H, Stenman G, Nilsson O, Aman P (2008) The multifunctional FUS, EWS and TAF15 proto-oncoproteins show cell type-specific expression patterns and involvement in cell spreading and stress response. BMC Cell Biol 9:37.

9. Arai M, Iwakura M, Matthews CR, Bilsel O (2011) Microsecond subdomain folding in dihydrofolate reductase. J Mol Biol 410:329-342.

10. Aulas A, Stabile S, Vande Velde C (2012) Endogenous TDP-43, but not FUS, contributes to stress granule assembly via G3BP. Mol Neurodegener 7:54.

11. Baechtold H, Kuroda M, Sok J, Ron D, Lopez BS, Akhmedov AT (1999) Human 75-kDa DNA-pairing protein is identical to the pro-oncoprotein TLS/FUS and is able to promote D-loop formation. J Biol Chem 274:34337-34342.

12. Baker M *et al.* (2006) Mutations in progranulin cause tau-negative frontotemporal dementia linked to chromosome 17. Nature 442:916-919.

13. Barbeito AG, Mesci P, Boillee S (2010) Motor neuron-immune interactions: the vicious circle of ALS. J Neural Transm 117:981-1000.

14. Baron DM, Kaushansky LJ, Ward CL, Sama RR, Chian RJ, Boggio KJ, Quaresma AJ, Nickerson JA, Bosco DA (2013) Amyotrophic lateral sclerosis-linked FUS/TLS alters stress granule assembly and dynamics. Mol Neurodegener 8:30.

15. Bedford MT, Clarke SG (2009) Protein arginine methylation in mammals: who, what, and why. Mol Cell 33:1-13.

16. Beghi E, Logroscino G, Chio A, Hardiman O, Millul A, Mitchell D, Swingler R, Traynor BJ (2010) Amyotrophic lateral sclerosis, physical exercise, trauma and sports: results of a population-based pilot case-control study. Amyotroph Lateral Scler 11:289-292.

17. Belli S, Vanacore N (2005) Proportionate mortality of Italian soccer players: is amyotrophic lateral sclerosis an occupational disease? Eur J Epidemiol 20:237-242.

18. Bendotti C, Atzori C, Piva R, Tortarolo M, Strong MJ, DeBiasi S, Migheli A (2004) Activated p38MAPK is a novel component of the intracellular inclusions found in human amyotrophic lateral sclerosis and mutant SOD1 transgenic mice. J Neuropathol Exp Neurol 63:113-119.

19. Bendotti C, Bao Cutrona M, Cheroni C, Grignaschi G, Lo Coco D, Peviani M, Tortarolo M, Veglianese P, Zennaro E (2005) Inter- and intracellular signaling in amyotrophic lateral sclerosis: role of p38 mitogen-activated protein kinase. Neurodegener Dis 2:128-134.

20. Bentmann E, Haass C, Dormann D (2013) Stress granules in neurodegeneration - lessons learnt from TAR DNA binding protein of 43 kDa and fused in sarcoma. FEBS J 280:4348-4370.

21. Bentmann E, Neumann M, Tahirovic S, Rodde R, Dormann D, Haass C (2012) Requirements for stress granule recruitment of fused in sarcoma (FUS) and TAR DNA-binding protein of 43 kDa (TDP-43). J Biol Chem 287:23079-23094.

22. Bertrand P, Akhmedov AT, Delacote F, Durrbach A, Lopez BS (1999) Human POMp75 is identified as the pro-oncoprotein TLS/FUS: both POMp75 and POMp100 DNA homologous pairing activities are associated to cell proliferation. Oncogene 18:4515-4521.

23. Bevilacqua E, Wang X, Majumder M, Gaccioli F, Yuan CL, Wang C, Zhu X, Jordan LE, Scheuner D, Kaufman RJ, Koromilas AE, Snider MD, Holcik M, Hatzoglou M (2010) eIF2alpha phosphorylation tips the balance to apoptosis during osmotic stress. J Biol Chem 285:17098-17111.

24. Bilsel O, Yang L, Zitzewitz JA, Beechem JM, Matthews CR (1999) Time-resolved fluorescence anisotropy study of the refolding reaction of the alpha-subunit of tryptophan synthase reveals nonmonotonic behavior of the rotational correlation time. Biochemistry 38:4177-4187.

25. Bosco DA, Lemay N, Ko HK, Zhou H, Burke C, Kwiatkowski TJ, Jr., Sapp P, McKenna-Yasek D, Brown RH, Jr., Hayward LJ (2010a) Mutant FUS proteins that cause amyotrophic lateral sclerosis incorporate into stress granules. Hum Mol Genet 19:4160-4175.

26. Bosco DA, Morfini G, Karabacak NM, Song Y, Gros-Louis F, Pasinelli P, Goolsby H, Fontaine BA, Lemay N, McKenna-Yasek D, Frosch MP, Agar JN, Julien JP, Brady ST, Brown RH, Jr. (2010b) Wild-type and mutant SOD1 share an aberrant conformation and a common pathogenic pathway in ALS. Nat Neurosci 13:1396-1403.

27. Brady ST, Richards BW, Leopold PL (1993) Assay of vesicle motility in squid axoplasm. Methods Cell Biol 39:191-202.

28. Brocker C, Thompson DC, Vasiliou V (2012) The role of hyperosmotic stress in inflammation and disease. Biomol Concepts 3:345-364.

29. Brooke GN, Culley RL, Dart DA, Mann DJ, Gaughan L, McCracken SR, Robson CN, Spencer-Dene B, Gamble SC, Powell SM, Wait R, Waxman J, Walker MM, Bevan CL (2010) FUS/TLS is a novel mediator of androgen-dependent cell-cycle progression and prostate cancer growth. Cancer Res 71:914-924.

30. Brooks BR (1994) El Escorial World Federation of Neurology criteria for the diagnosis of amyotrophic lateral sclerosis. Subcommittee on Motor Neuron Diseases/Amyotrophic Lateral Sclerosis of the World Federation of Neurology Research Group on Neuromuscular Diseases and the El Escorial "Clinical limits of amyotrophic lateral sclerosis" workshop contributors. J Neurol Sci 124 Suppl:96-107.

31. Brooks BR, Miller RG, Swash M, Munsat TL (2000) El Escorial revisited: revised criteria for the diagnosis of amyotrophic lateral sclerosis. Amyotroph Lateral Scler Other Motor Neuron Disord 1:293-299.

32. Burg MB, Ferraris JD, Dmitrieva NI (2007) Cellular response to hyperosmotic stresses. Physiol Rev 87:1441-1474.

33. Cai Q, Ferraris JD, Burg MB (2005) High NaCl increases TonEBP/OREBP mRNA and protein by stabilizing its mRNA. Am J Physiol Renal Physiol 289:F803-807.

34. Calvio C, Neubauer G, Mann M, Lamond AI (1995) Identification of hnRNP P2 as TLS/FUS using electrospray mass spectrometry. RNA 1:724-733.

35. Calvo A, Moglia C, Balma M, Chio A (2010) Involvement of immune response in the pathogenesis of amyotrophic lateral sclerosis: a therapeutic opportunity? CNS Neurol Disord Drug Targets 9:325-330.

36. Cashman NR, Durham HD, Blusztajn JK, Oda K, Tabira T, Shaw IT, Dahrouge S, Antel JP (1992) Neuroblastoma x spinal cord (NSC) hybrid cell lines resemble developing motor neurons. Dev Dyn 194:209-221.

37. Chio A, Benzi G, Dossena M, Mutani R, Mora G (2005) Severely increased risk of amyotrophic lateral sclerosis among Italian professional football players. Brain 128:472-476.

38. Chio A, Calvo A, Dossena M, Ghiglione P, Mutani R, Mora G (2009) ALS in Italian professional soccer players: the risk is still present and could be soccer-specific. Amyotroph Lateral Scler 10:205-209.

39. Chio A, Mora G, Leone M, Mazzini L, Cocito D, Giordana MT, Bottacchi E, Mutani R (2002) Early symptom progression rate is related to ALS outcome: a prospective population-based study. Neurology 59:99-103.

40. Coffman CJ, Horner RD, Grambow SC, Lindquist J (2005) Estimating the occurrence of amyotrophic lateral sclerosis among Gulf War (1990-1991) veterans using capture-recapture methods. Neuroepidemiology 24:141-150.

41. Colclasure GC, Parker JC (1992) Cytosolic protein concentration is the primary volume signal for swelling-induced [K-Cl] cotransport in dog red cells. J Gen Physiol 100:1-10.

42. Colombrita C, Onesto E, Megiorni F, Pizzuti A, Baralle FE, Buratti E, Silani V, Ratti A (2012) TDP-43 and FUS RNA-binding proteins bind distinct sets of cytoplasmic messenger RNAs and differently regulate their post-transcriptional fate in motoneuron-like cells. J Biol Chem 287:15635-15647.

43. Correa SA, Eales KL (2012) The Role of p38 MAPK and Its Substrates in Neuronal Plasticity and Neurodegenerative Disease. J Signal Transduct 2012:649079.

44. Cox PA, Richer R, Metcalf JS, Banack SA, Codd GA, Bradley WG (2009) Cyanobacteria and BMAA exposure from desert dust: a possible link to sporadic ALS among Gulf War veterans. Amyotroph Lateral Scler 10 Suppl 2:109-117.

45. Cronin S, Hardiman O, Traynor BJ (2007) Ethnic variation in the incidence of ALS: a systematic review. Neurology 68:1002-1007.

46. Crozat A, Aman P, Mandahl N, Ron D (1993) Fusion of CHOP to a novel RNA-binding protein in human myxoid liposarcoma. Nature 363:640-644.

47. Cruts M *et al.* (2006) Null mutations in progranulin cause ubiquitin-positive frontotemporal dementia linked to chromosome 17q21. Nature 442:920-924.

48. Da Cruz S, Cleveland DW (2011) Understanding the role of TDP-43 and FUS/TLS in ALS and beyond. Curr Opin Neurobiol 21:904-919.

49. Dahl SC, Handler JS, Kwon HM (2001) Hypertonicity-induced phosphorylation and nuclear localization of the transcription factor TonEBP. Am J Physiol Cell Physiol 280:C248-253.

50. Daigle JG, Lanson NA, Jr., Smith RB, Casci I, Maltare A, Monaghan J, Nichols CD, Kryndushkin D, Shewmaker F, Pandey UB (2013) RNA-binding ability of FUS regulates neurodegeneration, cytoplasmic mislocalization and incorporation into stress granules associated with FUS carrying ALS-linked mutations. Hum Mol Genet 22:1193-205

51. de Jong SW, Huisman MH, Sutedja NA, van der Kooi AJ, de Visser M, Schelhaas HJ, Fischer K, Veldink JH, van den Berg LH (2012) Smoking, alcohol consumption, and the risk of amyotrophic lateral sclerosis: a population-based study. Am J Epidemiol 176:233-239.

52. De Leeuw F, Zhang T, Wauquier C, Huez G, Kruys V, Gueydan C (2007) The cold-inducible RNA-binding protein migrates from the nucleus to cytoplasmic stress granules by a methylation-dependent mechanism and acts as a translational repressor. Exp Cell Res 313:4130-4144.

53. Dejardin J, Kingston RE (2009) Purification of proteins associated with specific genomic Loci. Cell 136:175-186.

54. DeJesus-Hernandez M *et al.* (2011) Expanded GGGGCC hexanucleotide repeat in noncoding region of C9ORF72 causes chromosome 9p-linked FTD and ALS. Neuron 72:245-256.

55. del Aguila MA, Longstreth WT, Jr., McGuire V, Koepsell TD, van Belle G (2003) Prognosis in amyotrophic lateral sclerosis: a population-based study. Neurology 60:813-819.

56. Deng HX, Zhai H, Bigio EH, Yan J, Fecto F, Ajroud K, Mishra M, Ajroud-Driss S, Heller S, Sufit R, Siddique N, Mugnaini E, Siddique T (2010) FUS-immunoreactive inclusions are a common feature in sporadic and non-SOD1 familial amyotrophic lateral sclerosis. Ann Neurol 67:739-748.

57. Dewey CM, Cenik B, Sephton CF, Dries DR, Mayer P, 3rd, Good SK, Johnson BA, Herz J, Yu G (2010) TDP-43 is directed to stress granules by sorbitol, a novel physiological osmotic and oxidative stressor. Mol Cell Biol 31(5):1098-108.

58. Di Ciano-Oliveira C, Sirokmany G, Szaszi K, Arthur WT, Masszi A, Peterson M, Rotstein OD, Kapus A (2003) Hyperosmotic stress activates Rho: differential involvement in Rho kinase-dependent MLC phosphorylation and NKCC activation. Am J Physiol Cell Physiol 285:C555-566.

59. Dolzhanskaya N, Merz G, Aletta JM, Denman RB (2006) Methylation regulates the intracellular protein-protein and protein-RNA interactions of FMRP. J Cell Sci 119:1933-1946.

60. Dormann D, Haass C (2011) TDP-43 and FUS: a nuclear affair. Trends Neurosci 34:339-48.

61. Dormann D, Haass C (2013) Fused in sarcoma (FUS): An oncogene goes awry in neurodegeneration. Mol Cell Neurosci 56:475-86.

62. Dormann D, Madl T, Valori CF, Bentmann E, Tahirovic S, Abou-Ajram C, Kremmer E, Ansorge O, Mackenzie IR, Neumann M, Haass C (2012) Arginine methylation next to the PY-NLS modulates Transportin binding and nuclear import of FUS. EMBO J 31:4258-4275.

63. Dormann D, Rodde R, Edbauer D, Bentmann E, Fischer I, Hruscha A, Than ME, Mackenzie IR, Capell A, Schmid B, Neumann M, Haass C (2010) ALS-associated fused in sarcoma (FUS) mutations disrupt Transportin-mediated nuclear import. EMBO J 29:2841-2857.

64. Du K, Arai S, Kawamura T, Matsushita A, Kurokawa R (2011) TLS and PRMT1 synergistically coactivate transcription at the survivin promoter through TLS arginine methylation. Biochem Biophys Res Commun 404:991-996.

65. Emara MM, Fujimura K, Sciaranghella D, Ivanova V, Ivanov P, Anderson P (2012) Hydrogen peroxide induces stress granule formation independent of eIF2alpha phosphorylation. Biochem Biophys Res Commun 423:763-769.

66. Ferraris JD, Williams CK, Jung KY, Bedford JJ, Burg MB, Garcia-Perez A (1996) ORE, a eukaryotic minimal essential osmotic response element. The aldose reductase gene in hyperosmotic stress. J Biol Chem 271:18318-18321.

67. Fischer-Hayes LR, Brotherton T, Glass JD (2013) Axonal degeneration in the peripheral nervous system: implications for the pathogenesis of amyotrophic lateral sclerosis. Exp Neurol 246:6-13.

68. Fujii R, Takumi T (2005) TLS facilitates transport of mRNA encoding an actin-stabilizing protein to dendritic spines. J Cell Sci 118:5755-5765.

69. Fujii R, Okabe S, Urushido T, Inoue K, Yoshimura A, Tachibana T, Nishikawa T, Hicks GG, Takumi T (2005) The RNA binding protein TLS is translocated to dendritic spines by mGluR5 activation and regulates spine morphology. Curr Biol 15:587-593.

70. Gal J, Zhang J, Kwinter DM, Zhai J, Jia H, Jia J, Zhu H (2011) Nuclear localization sequence of FUS and induction of stress granules by ALS mutants. Neurobiol Aging 32(12):2323.

71. Gallop JL, McMahon HT (2005) BAR domains and membrane curvature: bringing your curves to the BAR. Biochem Soc Symp:223-231.

72. Gamba G (2005) Molecular physiology and pathophysiology of electroneutral cation-chloride cotransporters. Physiol Rev 85:423-493.

73. Garay-Arroyo A, Lledias F, Hansberg W, Covarrubias AA (2003) Cu,Zn-superoxide dismutase of Saccharomyces cerevisiae is required for resistance to hyperosmosis. FEBS Lett 539:68-72.

74. Garner MM, Burg MB (1994) Macromolecular crowding and confinement in cells exposed to hypertonicity. Am J Physiol 266:C877-892.

75. Gendron TF, Belzil VV, Zhang YJ, Petrucelli L (2014) Mechanisms of toxicity in C9FTLD/ALS. Acta Neuropathol 127(3):359-76.

76. Gijselinck I *et al.* (2011) A C9orf72 promoter repeat expansion in a Flanders-Belgian cohort with disorders of the frontotemporal lobar degeneration-amyotrophic lateral sclerosis spectrum: a gene identification study. Lancet Neurol 11:54-65.

77. Gitcho MA, Baloh RH, Chakraverty S, Mayo K, Norton JB, Levitch D, Hatanpaa KJ, White CL, 3rd, Bigio EH, Caselli R, Baker M, Al-Lozi MT, Morris JC, Pestronk A, Rademakers R, Goate AM, Cairns NJ (2008) TDP-43 A315T mutation in familial motor neuron disease. Ann Neurol 63:535-538.

78. Gitler AD, Shorter J (2011) RNA-binding proteins with prion-like domains in ALS and FTLD-U. Prion 5:179-187.

79. Goetz CG (2000) Amyotrophic lateral sclerosis: early contributions of Jean-Martin Charcot. Muscle Nerve 23:336-343.

80. Goodier JL, Zhang L, Vetter MR, Kazazian HH, Jr. (2007) LINE-1 ORF1 protein localizes in stress granules with other RNA-binding proteins, including components of RNA interference RNA-induced silencing complex. Mol Cell Biol 27:6469-6483.

81. Gordon PH (2013) Amyotrophic Lateral Sclerosis: An update for 2013 Clinical Features, Pathophysiology, Management and Therapeutic Trials. Aging Dis 4:295-310.

82. Guil S, Long JC, Caceres JF (2006) hnRNP A1 relocalization to the stress granules reflects a role in the stress response. Mol Cell Biol 26:5744-5758.

83. Han TW, Kato M, Xie S, Wu LC, Mirzaei H, Pei J, Chen M, Xie Y, Allen J, Xiao G, McKnight SL (2012) Cell-free formation of RNA granules: bound RNAs identify features and components of cellular assemblies. Cell 149:768-779.

84. Hardy J, Rogaeva E (2013) Motor neuron disease and frontotemporal dementia: sometimes related, sometimes not. Exp Neurol pii:S0014-4886(13)00330.

85. Hasler U, Jeon US, Kim JA, Mordasini D, Kwon HM, Feraille E, Martin PY (2006) Tonicity-responsive enhancer binding protein is an essential regulator of aquaporin-2 expression in renal collecting duct principal cells. J Am Soc Nephrol 17:1521-1531.

86. Haussinger D, Lang F (1992) Cell volume and hormone action. Trends Pharmacol Sci 13:371-373.

87. Henson JH (1999) Relationships between the actin cytoskeleton and cell volume regulation. Microsc Res Tech 47:155-162.

88. Hicks SW, Machamer CE (2005) Golgi structure in stress sensing and apoptosis. Biochim Biophys Acta 1744:406-414.

89. Hoell JI, Larsson E, Runge S, Nusbaum JD, Duggimpudi S, Farazi TA, Hafner M, Borkhardt A, Sander C, Tuschl T (2011) RNA targets of wild-type and mutant FET family proteins. Nat Struc Mol Biol 18:1428-1431.

90. Horner RD, Grambow SC, Coffman CJ, Lindquist JH, Oddone EZ, Allen KD, Kasarskis EJ (2008) Amyotrophic lateral sclerosis among 1991 Gulf War veterans: evidence for a time-limited outbreak. Neuroepidemiology 31:28-32.

91. Horner RD, Kamins KG, Feussner JR, Grambow SC, Hoff-Lindquist J, Harati Y, Mitsumoto H, Pascuzzi R, Spencer PS, Tim R, Howard D, Smith TC, Ryan MA, Coffman CJ, Kasarskis EJ (2003) Occurrence of amyotrophic lateral sclerosis among Gulf War veterans. Neurology 61:742-749.

92. Huang C, Zhou H, Tong J, Chen H, Liu YJ, Wang D, Wei X, Xia XG (2011) FUS transgenic rats develop the phenotypes of amyotrophic lateral sclerosis and frontotemporal lobar degeneration. PLoS Genet 7:e1002011.

93. Huisman MH, Seelen M, de Jong SW, Dorresteijn KR, van Doormaal PT, van der Kooi AJ, de Visser M, Schelhaas HJ, van den Berg LH, Veldink JH (2013) Lifetime physical activity and the risk of amyotrophic lateral sclerosis. J Neurol Neurosurg Psychiatry 84:976-981.

94. Hutton M *et al.* (1998) Association of missense and 5'-splice-site mutations in tau with the inherited dementia FTDP-17. Nature 393:702-705.

95. Ichikawa H, Shimizu K, Hayashi Y, Ohki M (1994) An RNA-binding protein gene, TLS/FUS, is fused to ERG in human myeloid leukemia with t(16;21) chromosomal translocation. Cancer Res 54:2865-2868.

96. Iervolino A, Santilli G, Trotta R, Guerzoni C, Cesi V, Bergamaschi A, Gambacorti-Passerini C, Calabretta B, Perrotti D (2002) hnRNP A1

nucleocytoplasmic shuttling activity is required for normal myelopoiesis and BCR/ABL leukemogenesis. Mol Cell Biol 22:2255-2266.

97. Ishigaki S, Masuda A, Fujioka Y, Iguchi Y, Katsuno M, Shibata A, Urano F, Sobue G, Ohno K (2012) Position-dependent FUS-RNA interactions regulate alternative splicing events and transcriptions. Sci Rep 2:529.

98. Ito D, Seki M, Tsunoda Y, Uchiyama H, Suzuki N (2010) Nuclear transport impairment of amyotrophic lateral sclerosis-linked mutations in FUS/TLS. Ann Neurol 69:152-62..

99. Juliano RL (2002) Signal transduction by cell adhesion receptors and the cytoskeleton: functions of integrins, cadherins, selectins, and immunoglobulin-superfamily members. Annu Rev Pharmacol Toxicol 42:283-323.

100. Kabashi E, Valdmanis PN, Dion P, Spiegelman D, McConkey BJ, Vande Velde C, Bouchard JP, Lacomblez L, Pochigaeva K, Salachas F, Pradat PF, Camu W, Meininger V, Dupre N, Rouleau GA (2008) TARDBP mutations in individuals with sporadic and familial amyotrophic lateral sclerosis. Nat Genet 40:572-574.

101. Kanai Y, Dohmae N, Hirokawa N (2004) Kinesin transports RNA: isolation and characterization of an RNA-transporting granule. Neuron 43:513-525.

102. Karamyan VT, Speth RC (2008) Animal models of BMAA neurotoxicity: a critical review. Life Sci 82:233-246.

103. Karve TM, Cheema AK (2011) Small changes huge impact: the role of protein posttranslational modifications in cellular homeostasis and disease. J Amino Acids 2011:207691.

104. Kasarskis EJ, Lindquist JH, Coffman CJ, Grambow SC, Feussner JR, Allen KD, Oddone EZ, Kamins KA, Horner RD (2009) Clinical aspects of ALS in Gulf War veterans. Amyotroph Lateral Scler 10:35-41.

105. Kato M, Han TW, Xie S, Shi K, Du X, Wu LC, Mirzaei H, Goldsmith EJ, Longgood J, Pei J, Grishin NV, Frantz DE, Schneider JW, Chen S, Li L, Sawaya MR, Eisenberg D, Tycko R, McKnight SL (2012) Cell-free formation of RNA granules: low complexity sequence domains form dynamic fibers within hydrogels. Cell 149:753-767.

106. Kedersha N, Anderson P (2002) Stress granules: sites of mRNA triage that regulate mRNA stability and translatability. Biochem Soc Trans 30:963-969.

107. Kedersha N, Anderson P (2007) Mammalian stress granules and processing bodies. Methods Enzymol 431:61-81.

108. Kedersha N, Cho MR, Li W, Yacono PW, Chen S, Gilks N, Golan DE, Anderson P (2000) Dynamic shuttling of TIA-1 accompanies the recruitment of mRNA to mammalian stress granules. J Cell Biol 151:1257-1268.

109. Kedersha N, Stoecklin G, Ayodele M, Yacono P, Lykke-Andersen J, Fritzler MJ, Scheuner D, Kaufman RJ, Golan DE, Anderson P (2005) Stress granules and processing bodies are dynamically linked sites of mRNP remodeling. J Cell Biol 169:871-884.

110. Kelstrup CD, Young C, Lavallee R, Nielsen ML, Olsen JV (2012) Optimized fast and sensitive acquisition methods for shotgun proteomics on a quadrupole orbitrap mass spectrometer. J Proteome Res 11:3487-3497.

111. Kim SH, Shanware NP, Bowler MJ, Tibbetts RS (2010) Amyotrophic lateral sclerosis-associated proteins TDP-43 and FUS/TLS function in a common biochemical complex to co-regulate HDAC6 mRNA. J Biol Chem 285:34097-34105.

112. Kino Y, Washizu C, Aquilanti E, Okuno M, Kurosawa M, Yamada M, Doi H, Nukina N (2011) Intracellular localization and splicing regulation of FUS/TLS are variably affected by amyotrophic lateral sclerosis-linked mutations. Nucleic Acids Res 39:2781-2798.

113. Ko BC, Ruepp B, Bohren KM, Gabbay KH, Chung SS (1997) Identification and characterization of multiple osmotic response sequences in the human aldose reductase gene. J Biol Chem 272:16431-16437.

114. Ko BC, Turck CW, Lee KW, Yang Y, Chung SS (2000) Purification, identification, and characterization of an osmotic response element binding protein. Biochem Biophys Res Commun 270:52-61.

115. Ko BC, Lam AK, Kapus A, Fan L, Chung SK, Chung SS (2002) Fyn and p38 signaling are both required for maximal hypertonic activation of the osmotic response element-binding protein/tonicity-responsive enhancer-binding protein (OREBP/TonEBP). J Biol Chem 277:46085-46092.

116. Ko KS, Arora PD, McCulloch CA (2001) Cadherins mediate intercellular mechanical signaling in fibroblasts by activation of stretch-sensitive calcium-permeable channels. J Biol Chem 276:35967-35977.

117. Kovar H (2011) Dr. Jekyll and Mr. Hyde: The Two Faces of the FUS/EWS/TAF15 Protein Family. Sarcoma 2011:837474.

118. Kuroda M, Sok J, Webb L, Baechtold H, Urano F, Yin Y, Chung P, de Rooij DG, Akhmedov A, Ashley T, Ron D (2000) Male sterility and enhanced radiation sensitivity in TLS(-/-) mice. EMBO J 19:453-462.

119. Kwiatkowski TJ, Jr. *et al.* (2009) Mutations in the FUS/TLS gene on chromosome 16 cause familial amyotrophic lateral sclerosis. Science 323:1205-1208.

120. Lagier-Tourenne C, Polymenidou M, Cleveland DW (2010) TDP-43 and FUS/TLS: emerging roles in RNA processing and neurodegeneration. Hum Mol Genet 19:R46-64.

121. Lagier-Tourenne C *et al.* (2012) Divergent roles of ALS-linked proteins FUS/TLS and TDP-43 intersect in processing long pre-mRNAs. Nat Neurosci 15:1488-1497.

122. Lakowicz JR (2006) Principles of fluorescence spectroscopy, 3rd Edition. New York: Springer.

123. Lang F, Busch GL, Ritter M, Volkl H, Waldegger S, Gulbins E, Haussinger D (1998) Functional significance of cell volume regulatory mechanisms. Physiol Rev 78:247-306.

124. Law WJ, Cann KL, Hicks GG (2006) TLS, EWS and TAF15: a model for transcriptional integration of gene expression. Brief Funct Genomic Proteomic 5:8-14.

125. Lawson SK, Dobrikova EY, Shveygert M, Gromeier M (2013) p38alpha mitogen-activated protein kinase depletion and repression of signal transduction to translation machinery by miR-124 and -128 in neurons. Mol Cell Biol 33:127-135.

126. Lee JK, Shin JH, Hwang SG, Gwag BJ, McKee AC, Lee J, Kowall NW, Ryu H, Lim DS, Choi EJ (2013) MST1 functions as a key modulator of neurodegeneration in a mouse model of ALS. Proc Natl Acad Sci U S A 110:12066-12071.

127. Lee TH, Linstedt AD (1999) Osmotically induced cell volume changes alter anterograde and retrograde transport, Golgi structure, and COPI dissociation. Mol Biol Cell 10:1445-1462.

128. Lerga A, Hallier M, Delva L, Orvain C, Gallais I, Marie J, Moreau-Gachelin F (2001) Identification of an RNA binding specificity for the potential splicing factor TLS. J Biol Chem 276:6807-6816.

129. Lewis SM, Veyrier A, Hosszu Ungureanu N, Bonnal S, Vagner S, Holcik M (2007) Subcellular relocalization of a trans-acting factor regulates XIAP IRES-dependent translation. Mol Biol Cell 18:1302-1311.

130. Li YR, King OD, Shorter J, Gitler AD (2013) Stress granules as crucibles of ALS pathogenesis. J Cell Biol 201:361-372.

131. Ling SC, Polymenidou M, Cleveland DW (2013) Converging mechanisms in ALS and FTD: disrupted RNA and protein homeostasis. Neuron 79:416-438.

132. Liu-Yesucevitz L, Bilgutay A, Zhang YJ, Vanderwyde T, Citro A, Mehta T, Zaarur N, McKee A, Bowser R, Sherman M, Petrucelli L, Wolozin B (2010) Tar DNA binding protein-43 (TDP-43) associates with stress granules: analysis of cultured cells and pathological brain tissue. PloS One 5:e13250.

133. Logroscino G, Traynor BJ, Hardiman O, Chio A, Couratier P, Mitchell JD, Swingler RJ, Beghi E (2008) Descriptive epidemiology of amyotrophic lateral sclerosis: new evidence and unsolved issues. J Neurol Neurosurg Psychiatry 79:6-11.

134. Mackenzie IR, Rademakers R, Neumann M (2010) TDP-43 and FUS in amyotrophic lateral sclerosis and frontotemporal dementia. Lancet Neurol 9:995-1007.

135. Magnus T, Beck M, Giess R, Puls I, Naumann M, Toyka KV (2002) Disease progression in amyotrophic lateral sclerosis: predictors of survival. Muscle Nerve 25:709-714.

136. Mao L, Hartl D, Nolden T, Koppelstatter A, Klose J, Himmelbauer H, Zabel C (2008) Pronounced alterations of cellular metabolism and structure due to hyper- or hypo-osmosis. J Proteome Res 7:3968-3983.

137. Mastrocola AS, Kim SH, Trinh AT, Rodenkirch LA, Tibbetts RS (2013) The RNA Binding Protein Fused In Sarcoma (FUS) Functions Downstream of PARP in Response to DNA Damage. J Biol Chem 288(34):24731-41.

138. Miller RG, Mitchell JD, Moore DH (2012) Riluzole for amyotrophic lateral sclerosis (ALS)/motor neuron disease (MND). Cochrane Database Syst Rev 3:CD001447.

139. Miyakawa H, Woo SK, Chen CP, Dahl SC, Handler JS, Kwon HM (1998) Cis- and trans-acting factors regulating transcription of the BGT1 gene in response to hypertonicity. Am J Physiol 274:F753-761.

140. Moeckel GW, Zhang L, Chen X, Rossini M, Zent R, Pozzi A (2006) Role of integrin alpha1beta1 in the regulation of renal medullary osmolyte concentration. Am J Physiol Renal Physiol 290:F223-231.

141. Moore MJ (2005) From birth to death: the complex lives of eukaryotic mRNAs. Science 309:1514-1518.

142. Morelli MJ, Allen RJ, Wolde PR (2011) Effects of macromolecular crowding on genetic networks. Biophys J 101:2882-2891.

143. Morfini GA, Burns M, Binder LI, Kanaan NM, LaPointe N, Bosco DA, Brown RH, Jr., Brown H, Tiwari A, Hayward L, Edgar J, Nave KA, Garberrn J, Atagi Y, Song Y, Pigino G, Brady ST (2009) Axonal transport defects in neurodegenerative diseases. J Neurosci 29:12776-12786.

144. Morfini GA, Bosco DA, Brown H, Gatto R, Kaminska A, Song Y, Molla L, Baker L, Marangoni MN, Berth S, Tavassoli E, Bagnato C, Tiwari A, Hayward LJ, Pigino GF, Watterson DM, Huang CF, Banker G, Brown RH, Jr., Brady ST (2013) Inhibition of fast axonal transport by pathogenic SOD1 involves activation of p38 MAP kinase. PloS One 8:e65235.

145. Morlando M, Dini Modigliani S, Torrelli G, Rosa A, Di Carlo V, Caffarelli E, Bozzoni I (2012) FUS stimulates microRNA biogenesis by facilitating co-transcriptional Drosha recruitment. EMBO J 31:4502-4510.

146. Morozova N, Weisskopf MG, McCullough ML, Munger KL, Calle EE, Thun MJ, Ascherio A (2008) Diet and amyotrophic lateral sclerosis. Epidemiology 19:324-337.

147. Munoz L, Ralay Ranaivo H, Roy SM, Hu W, Craft JM, McNamara LK, Chico LW, Van Eldik LJ, Watterson DM (2007) A novel p38 alpha MAPK inhibitor suppresses brain proinflammatory cytokine up-regulation and attenuates synaptic dysfunction and behavioral deficits in an Alzheimer's disease mouse model. J Neuroinflammation 4:21.

148. Nagata K, Hama I, Kiryu-Seo S, Kiyama H (2014) microRNA-124 is down regulated in nerve-injured motor neurons and it potentially targets mRNAs for KLF6 and STAT3. Neuroscience 256:426-432.

149. Nakaya T, Alexiou P, Maragkakis M, Chang A, Mourelatos Z (2013) FUS regulates genes coding for RNA-binding proteins in neurons by binding to their highly conserved introns. RNA 19:498-509.

150. Neumann M, Sampathu DM, Kwong LK, Truax AC, Micsenyi MC, Chou TT, Bruce J, Schuck T, Grossman M, Clark CM, McCluskey LF, Miller BL, Masliah E, Mackenzie IR, Feldman H, Feiden W, Kretzschmar HA, Trojanowski JQ, Lee VM (2006) Ubiquitinated TDP-43 in frontotemporal lobar degeneration and amyotrophic lateral sclerosis. Science 314:130-133.

151. Nielsen DK, Jensen AK, Harbak H, Christensen SC, Simonsen LO (2007) Cell content of phosphatidylinositol (4,5)bisphosphate in Ehrlich mouse ascites tumour cells in response to cell volume perturbations in anisotonic and in isosmotic media. J Physiol 582:1027-1036.

152. Nilius B, Prenen J, Voets T, Eggermont J, Droogmans G (1998) Activation of volume-regulated chloride currents by reduction of intracellular ionic strength in bovine endothelial cells. J Physiol 506 (Pt 2):353-361.

153. NINDS (2013) "Amyotrophic Lateral Sclerosis (ALS) Fact Sheet," NINDS, NIH Publication No. 13-916 In.

154. Niu C, Zhang J, Gao F, Yang L, Jia M, Zhu H, Gong W (2012) FUS-NLS/Transportin 1 complex structure provides insights into the nuclear targeting mechanism of FUS and the implications in ALS. PloS One 7:e47056.

155. O'Dea RF, Mirkin BL, Hogenkamp HP, Barten DM (1987) Effect of adenosine analogues on protein carboxylmethyltransferase, S-adenosylhomocysteine hydrolase, and ribonucleotide reductase activity in murine neuroblastoma cells. Cancer Res 47:3656-3661.

156. Panagopoulos I, Aman P, Fioretos T, Hoglund M, Johansson B, Mandahl N, Heim S, Behrendtz M, Mitelman F (1994) Fusion of the FUS gene with ERG in acute myeloid leukemia with t(16;21)(p11;q22). Genes Chromosomes Cancer 11:256-262.

157. Papadimitriou D, Le Verche V, Jacquier A, Ikiz B, Przedborski S, Re DB (2010) Inflammation in ALS and SMA: sorting out the good from the evil. Neurobiol Dis 37:493-502.

158. Papapetropoulos S (2007) Is there a role for naturally occurring cyanobacterial toxins in neurodegeneration? The beta-N-methylamino-L-alanine (BMAA) paradigm. Neurochem Int 50:998-1003.

159. Parker JC, Colclasure GC (1992) Macromolecular crowding and volume perception in dog red cells. Mol Cell Biochem 114:9-11.

160. Pasinelli P, Brown RH (2006) Molecular biology of amyotrophic lateral sclerosis: insights from genetics. Nat Rev Neurosci 7:710-723.

161. Pedersen SF, Nilius B (2007) Transient receptor potential channels in mechanosensing and cell volume regulation. Methods Enzymol 428:183-207.

162. Pedersen SF, Hoffmann EK, Mills JW (2001) The cytoskeleton and cell volume regulation. Comp Biochem Physiol A Mol Integr Physiol 130:385-399.

163. Perez-Losada J, Sanchez-Martin M, Rodriguez-Garcia MA, Perez-Mancera PA, Pintado B, Flores T, Battaner E, Sanchez-Garcia I (2000a) Liposarcoma initiated by FUS/TLS-CHOP: the FUS/TLS domain plays a critical role in the pathogenesis of liposarcoma. Oncogene 19:6015-6022.

164. Perez-Losada J, Pintado B, Gutierrez-Adan A, Flores T, Banares-Gonzalez B, del Campo JC, Martin-Martin JF, Battaner E, Sanchez-Garcia I (2000b) The chimeric FUS/TLS-CHOP fusion protein specifically induces liposarcomas in transgenic mice. Oncogene 19:2413-2422.

165. Perrotti D, Iervolino A, Cesi V, Cirinna M, Lombardini S, Grassilli E, Bonatti S, Claudio PP, Calabretta B (2000) BCR-ABL prevents c-jun-mediated and proteasome-dependent FUS (TLS) proteolysis through a protein kinase CbetaII-dependent pathway. Mol Cell Biol 20:6159-6169.

166. Peter BJ, Kent HM, Mills IG, Vallis Y, Butler PJ, Evans PR, McMahon HT (2004) BAR domains as sensors of membrane curvature: the amphiphysin BAR structure. Science 303:495-499.

167. Piazza O, Siren AL, Ehrenreich H (2004) Soccer, neurotrauma and amyotrophic lateral sclerosis: is there a connection? Curr Med Res Opin 20:505-508.

168. Qiu H, Lee S, Shang Y, Wang WY, Au KF, Kamiya S, Barmada SJ, Finkbeiner S, Lui H, Carlton CE, Tang AA, Oldham MC, Wang H, Shorter J, Filiano AJ, Roberson ED, Tourtellotte WG, Chen B, Tsai LH, Huang EJ (2014) ALS-associated mutation FUS-R521C causes DNA damage and RNA splicing defects. J Clin Invest 124:981-999.

169. Rabbitts TH, Forster A, Larson R, Nathan P (1993) Fusion of the dominant negative transcription regulator CHOP with a novel gene FUS by translocation t(12;16) in malignant liposarcoma. Nat Genet 4:175-180.

170. Rappsilber J, Friesen WJ, Paushkin S, Dreyfuss G, Mann M (2003) Detection of arginine dimethylated peptides by parallel precursor ion scanning mass spectrometry in positive ion mode. Anal Chem 75:3107-3114.

171. Ren G, Vajjhala P, Lee JS, Winsor B, Munn AL (2006) The BAR domain proteins: molding membranes in fission, fusion, and phagy. Microbiol Mol Biol Rev 70:37-120.

172. Renton AE, Chio A, Traynor BJ (2014) State of play in amyotrophic lateral sclerosis genetics. Nat Neurosci 17:17-23.

173. Renton AE *et al.* (2011) A hexanucleotide repeat expansion in C9ORF72 is the cause of chromosome 9p21-linked ALS-FTD. Neuron 72:257-268.

174. Riggi N, Cironi L, Suva ML, Stamenkovic I (2007) Sarcomas: genetics, signalling, and cellular origins. Part 1: The fellowship of TET. J Pathol 213:4-20.

175. Rogelj B, Easton LE, Bogu GK, Stanton LW, Rot G, Curk T, Zupan B, Sugimoto Y, Modic M, Haberman N, Tollervey J, Fujii R, Takumi T, Shaw CE, Ule J (2012) Widespread binding of FUS along nascent RNA regulates alternative splicing in the brain. Sci Rep 2:603.

176. Romero-Santacreu L, Moreno J, Perez-Ortin JE, Alepuz P (2009) Specific and global regulation of mRNA stability during osmotic stress in Saccharomyces cerevisiae. RNA 15:1110-1120.

177. Rosen DR, Siddique T, Patterson D, Figlewicz DA, Sapp P, Hentati A, Donaldson D, Goto J, O'Regan JP, Deng HX, *et al.* (1993) Mutations in Cu/Zn superoxide dismutase gene are associated with familial amyotrophic lateral sclerosis. Nature 362:59-62.

178. Rotunno MS, Bosco DA (2013) An emerging role for misfolded wild-type SOD1 in sporadic ALS pathogenesis. Front Cell Neurosci 7:253.

179. Rowland LP (2001) How amyotrophic lateral sclerosis got its name: the clinical-pathologic genius of Jean-Martin Charcot. Arch Neurol 58:512-515.

180. Rulten SL, Rotheray A, Green RL, Grundy GJ, Moore DA, Gomez-Herreros F, Hafezparast M, Caldecott KW (2013) PARP-1 dependent recruitment of the amyotrophic lateral sclerosis-associated protein FUS/TLS to sites of oxidative DNA damage. Nucleic Acids Res 42(1):307-14.

181. Rutherford NJ *et al.* (2008) Novel mutations in TARDBP (TDP-43) in patients with familial amyotrophic lateral sclerosis. PLoS Genet 4:e1000193.

182. Sama RR, Ward CL, Kaushansky LJ, Lemay N, Ishigaki S, Urano F, Bosco DA (2013) FUS/TLS assembles into stress granules and is a prosurvival factor during hyperosmolar stress. J Cell Physiol 228(11):2222-31.

183. Sanchez-Ramos C, Tierrez A, Fabregat-Andres O, Wild B, Sanchez-Cabo F, Arduini A, Dopazo A, Monsalve M (2011) PGC-1alpha regulates translocated in liposarcoma activity: role in oxidative stress gene expression. Antioxid Redox Signal 15:325-337.

184. Sasaki S, Iwata M (1996) Impairment of fast axonal transport in the proximal axons of anterior horn neurons in amyotrophic lateral sclerosis. Neurology 47:535-540.

185. Sasaki S, Warita H, Abe K, Iwata M (2005) Impairment of axonal transport in the axon hillock and the initial segment of anterior horn neurons in transgenic mice with a G93A mutant SOD1 gene. Acta Neuropathol 110:48-56.

186. Scarmeas N, Shih T, Stern Y, Ottman R, Rowland LP (2002) Premorbid weight, body mass, and varsity athletics in ALS. Neurology 59:773-775.

187. Schliess F, Reinehr R, Haussinger D (2007) Osmosensing and signaling in the regulation of mammalian cell function. FEBS J 274:5799-5803.

188. Shevchenko A, Tomas H, Havlis J, Olsen JV, Mann M (2006) In-gel digestion for mass spectrometric characterization of proteins and proteomes. Nat Protoc 1:2856-2860.

189. Shing DC, McMullan DJ, Roberts P, Smith K, Chin SF, Nicholson J, Tillman RM, Ramani P, Cullinane C, Coleman N (2003) FUS/ERG gene fusions in Ewing's tumors. Cancer Res 63:4568-4576.

190. Silani V, Messina S, Poletti B, Morelli C, Doretti A, Ticozzi N, Maderna L (2011) The diagnosis of Amyotrophic lateral sclerosis in 2010. Arch Ital Biol 149:5-27.

191. Smardo FL, Jr., Burg MB, Garcia-Perez A (1992) Kidney aldose reductase gene transcription is osmotically regulated. Am J Physiol 262:C776-782.

192. Song Y, Nagy M, Ni W, Tyagi NK, Fenton WA, Lopez-Giraldez F, Overton JD, Horwich AL, Brady ST (2013) Molecular chaperone Hsp110 rescues a vesicle transport defect produced by an ALS-associated mutant SOD1 protein in squid axoplasm. Proc Natl Acad Sci U S A 110:5428-5433.

193. Soto C, Estrada LD (2008) Protein misfolding and neurodegeneration. Arch Neurol 65:184-189.

194. Soufi B, Kelstrup CD, Stoehr G, Frohlich F, Walther TC, Olsen JV (2009) Global analysis of the yeast osmotic stress response by quantitative proteomics. Mol Biosyst 5:1337-1346.

195. Spencer PS, McCauley LA, Joos SK, Lasarev MR, Schuell T, Bourdette D, Barkhuizen A, Johnston W, Storzbach D, Wynn M, Grewenow R (1998) U.S. Gulf War Veterans: service periods in theater, differential exposures, and persistent unexplained illness. Portland Environmental Hazards Research Centre. Toxicol Lett 102-103:515-521.

196. Sreedharan J, Blair IP, Tripathi VB, Hu X, Vance C, Rogelj B, Ackerley S, Durnall JC, Williams KL, Buratti E, Baralle F, de Belleroche J, Mitchell JD, Leigh PN, Al-Chalabi A, Miller CC, Nicholson G, Shaw CE (2008) TDP-43 mutations in familial and sporadic amyotrophic lateral sclerosis. Science 319:1668-1672.

197. Storlazzi CT, Mertens F, Nascimento A, Isaksson M, Wejde J, Brosjo O, Mandahl N, Panagopoulos I (2003) Fusion of the FUS and BBF2H7 genes in low grade fibromyxoid sarcoma. Hum Mol Genet 12:2349-2358.

198. Stroud JC, Lopez-Rodriguez C, Rao A, Chen L (2002) Structure of a TonEBP-DNA complex reveals DNA encircled by a transcription factor. Nat Struct Biol 9:90-94.

199. Sun Z, Diaz Z, Fang X, Hart MP, Chesi A, Shorter J, Gitler AD (2011) Molecular Determinants and Genetic Modifiers of Aggregation and Toxicity for the ALS Disease Protein FUS/TLS. PLoS Biol 9:e1000614.

200. Takahama K, Oyoshi T (2013) Specific Binding of Modified RGG Domain in TLS/FUS to G-Quadruplex RNA: Tyrosines in RGG Domain Recognize 2'-OH of the Riboses of Loops in G-Quadruplex. J Am Chem Soc 135:18016-18019.

201. Takahama K, Arai S, Kurokawa R, Oyoshi T (2009) Identification of DNA binding specificity for TLS. Nucleic Acids Symp Ser (Oxf):247-248.

202. Takahama K, Takada A, Tada S, Shimizu M, Sayama K, Kurokawa R, Oyoshi T (2013) Regulation of telomere length by G-quadruplex telomere DNA- and TERRA-binding protein TLS/FUS. Chem Biol 20:341-350.

203. Tan AY, Manley JL (2009) The TET family of proteins: functions and roles in disease. J Mol Cell Biol 1:82-92.

204. Therrien M, Rouleau GA, Dion PA, Parker JA (2013) Deletion of C9ORF72 Results in Motor Neuron Degeneration and Stress Sensitivity in C. elegans. PLoS One 8:e83450.

205. Tortarolo M, Veglianese P, Calvaresi N, Botturi A, Rossi C, Giorgini A, Migheli A, Bendotti C (2003) Persistent activation of p38 mitogen-activated protein kinase in a mouse model of familial amyotrophic lateral sclerosis correlates with disease progression. Mol Cell Neurosci 23:180-192.

206. Tourriere H, Chebli K, Zekri L, Courselaud B, Blanchard JM, Bertrand E, Tazi J (2003) The RasGAP-associated endoribonuclease G3BP assembles stress granules. J Cell Biol 160:823-831.

207. Tradewell ML, Yu Z, Tibshirani M, Boulanger MC, Durham HD, Richard S (2012) Arginine methylation by PRMT1 regulates nuclear-cytoplasmic localization

and toxicity of FUS/TLS harbouring ALS-linked mutations. Hum Mol Genet 21:136-149.

208. Trojsi F, Monsurro MR, Tedeschi G (2013) Exposure to environmental toxicants and pathogenesis of amyotrophic lateral sclerosis: state of the art and research perspectives. Int J Mol Sci 14:15286-15311.

209. Uhlik MT, Abell AN, Johnson NL, Sun W, Cuevas BD, Lobel-Rice KE, Horne EA, Dell'Acqua ML, Johnson GL (2003) Rac-MEKK3-MKK3 scaffolding for p38 MAPK activation during hyperosmotic shock. Nat Cell Biol 5:1104-1110.

210. Vaccaro A, Tauffenberger A, Ash PE, Carlomagno Y, Petrucelli L, Parker JA (2012) TDP-1/TDP-43 regulates stress signaling and age-dependent proteotoxicity in Caenorhabditis elegans. PLoS Genet 8:e1002806.

211. van Blitterswijk M, Wang ET, Friedman BA, Keagle PJ, Lowe P, Leclerc AL, van den Berg LH, Housman DE, Veldink JH, Landers JE (2013) Characterization of FUS mutations in amyotrophic lateral sclerosis using RNA-Seq. PloS One 8:e60788.

212. Van Deerlin VM *et al.* (2008) TARDBP mutations in amyotrophic lateral sclerosis with TDP-43 neuropathology: a genetic and histopathological analysis. Lancet Neurol 7:409-416.

213. van der Houven van Oordt W, Diaz-Meco MT, Lozano J, Krainer AR, Moscat J, Caceres JF (2000) The MKK(3/6)-p38-signaling cascade alters the subcellular distribution of hnRNP A1 and modulates alternative splicing regulation. J Cell Biol 149:307-316.

214. Vance C *et al.* (2009) Mutations in FUS, an RNA processing protein, cause familial amyotrophic lateral sclerosis type 6. Science 323:1208-1211.

215. Veldink JH, Kalmijn S, Groeneveld GJ, Titulaer MJ, Wokke JH, van den Berg LH (2005) Physical activity and the association with sporadic ALS. Neurology 64:241-245.

216. Waibel S, Neumann M, Rosenbohm A, Birve A, Volk AE, Weishaupt JH, Meyer T, Muller U, Andersen PM, Ludolph AC (2012) Truncating mutations in FUS/TLS give rise to a more aggressive ALS-phenotype than missense mutations: a clinico-genetic study in Germany. Eur J Neurol 20:540-546.

217. Wang H, O'Reilly EJ, Weisskopf MG, Logroscino G, McCullough ML, Thun MJ, Schatzkin A, Kolonel LN, Ascherio A (2011) Smoking and risk of amyotrophic lateral sclerosis: a pooled analysis of 5 prospective cohorts. Arch Neurol 68:207-213.

218. Wang WY, Pan L, Su SC, Quinn EJ, Sasaki M, Jimenez JC, Mackenzie IR, Huang EJ, Tsai LH (2013) Interaction of FUS and HDAC1 regulates DNA damage response and repair in neurons. Nat Neurosci 16:1383-1391.

219. Wang X, Arai S, Song X, Reichart D, Du K, Pascual G, Tempst P, Rosenfeld MG, Glass CK, Kurokawa R (2008) Induced ncRNAs allosterically modify RNA-binding proteins in cis to inhibit transcription. Nature 454:126-130.

220. Welch WJ, Suhan JP (1985) Morphological study of the mammalian stress response: characterization of changes in cytoplasmic organelles, cytoskeleton,

and nucleoli, and appearance of intranuclear actin filaments in rat fibroblasts after heat-shock treatment. J Cell Biol 101:1198-1211.

221. Wippich F, Bodenmiller B, Trajkovska MG, Wanka S, Aebersold R, Pelkmans L (2013) Dual specificity kinase DYRK3 couples stress granule condensation/dissolution to mTORC1 signaling. Cell 152:791-805.

222. Wolozin B (2012) Regulated protein aggregation: stress granules and neurodegeneration. Mol Neurodegener 7:56.

223. Woo SK, Lee SD, Na KY, Park WK, Kwon HM (2002) TonEBP/NFAT5 stimulates transcription of HSP70 in response to hypertonicity. Mol Cell Biol 22:5753-5760.

224. Wu CH *et al.* (2012) Mutations in the profilin 1 gene cause familial amyotrophic lateral sclerosis. Nature 488:499-503.

225. Wu Y, Kondrashkina E, Kayatekin C, Matthews CR, Bilsel O (2008) Microsecond acquisition of heterogeneous structure in the folding of a TIM barrel protein. Proc Natl Acad Sci U S A 105:13367-13372.

226. Xie W, Denman RB (2011) Protein methylation and stress granules: posttranslational remodeler or innocent bystander? Mol Biol Int 2011:137459.

227. Yamaguchi A, Kitajo K (2012) The Effect of PRMT1-Mediated Arginine Methylation on the Subcellular Localization, Stress Granules, and Detergent-Insoluble Aggregates of FUS/TLS. PloS One 7:e49267.

228. Yasuda K, Zhang H, Loiselle D, Haystead T, Macara IG, Mili S (2013) The RNA-binding protein Fus directs translation of localized mRNAs in APC-RNP granules. J Cell Biol 203:737-746.

229. Yokoseki A, Shiga A, Tan CF, Tagawa A, Kaneko H, Koyama A, Eguchi H, Tsujino A, Ikeuchi T, Kakita A, Okamoto K, Nishizawa M, Takahashi H, Onodera O (2008) TDP-43 mutation in familial amyotrophic lateral sclerosis. Ann Neurol 63:538-542.

230. Zago S, Poletti B, Morelli C, Doretti A, Silani V (2011) Amyotrophic lateral sclerosis and frontotemporal dementia (ALS-FTD). Arch Ital Biol 149:39-56.

231. Zhang ZC, Chook YM (2012) Structural and energetic basis of ALS-causing mutations in the atypical proline-tyrosine nuclear localization signal of the Fused in Sarcoma protein (FUS). Proc Natl Acad Sci U S A 109:12017-12021.

232. Zhou Y, Liu S, Liu G, Ozturk A, Hicks GG (2013) ALS-Associated FUS Mutations Result in Compromised FUS Alternative Splicing and Autoregulation. PLoS Genet 9:e1003895.

233. Zimmerberg J, McLaughlin S (2004) Membrane curvature: how BAR domains bend bilayers. Curr Biol 14:R250-252.

234. Zinszner H, Albalat R, Ron D (1994) A novel effector domain from the RNA-binding protein TLS or EWS is required for oncogenic transformation by CHOP. Genes Dev 8:2513-2526.

235. Zinszner H, Sok J, Immanuel D, Yin Y, Ron D (1997) TLS (FUS) binds RNA in vivo and engages in nucleo-cytoplasmic shuttling. J Cell Sci 110 (Pt 15):1741-1750.

236. Zoccolella S, Beghi E, Palagano G, Fraddosio A, Guerra V, Samarelli V, Lepore V, Simone IL, Lamberti P, Serlenga L, Logroscino G (2007) Riluzole and amyotrophic lateral sclerosis survival: a population-based study in southern Italy. Eur J Neurol 14:262-268.

237. Zulys M (2008) Mitochondrial Remodeling During Hyperosmotic Stress. (Master's thesis) Retrived from University of Tornoto Research Repository http://hdl.handle.net/1807/17240.